Universität Rostock Traditio et Innovatio

Aus der Professur für Bodenphsik
der Agrar- und Umweltwissenschaftlichen Fakultät

Groundwater quality and submarine groundwater discharge from rewetted coastal fen peatlands

Dissertation

zur Erlangung des akademischen Grades
Doktor der Agrarwissenschaften (Dr. agr.)

an der Agrar- und Umweltwissenschaftlichen Fakultät der Universität Rostock

vorgelegt von
M.Sc. Erwin Don R. Racasa
Geb. Am 07.04.1989 in Lucban, Quezon, Philippines
Wohnaft in Rostock

Rostock, 15 September 2023

https://doi.org/10.18453/rosdok_id00004902

Gutachter

1. **Dr. Manon Janssen**
   Bodenphysik, Agrar- und Umweltwissenschaftliche Fakultät
   Universität Rostock

2. **Prof. Dr. Gerald Jurasinski**
   Moorforschung, Institut für Botanik und Landschaftsökologie
   Universität Greifswald

3. **Prof. Dr. Fernando Siringan**
   The Marine Science Institute, College of Science
   University of the Philippines Diliman

4. **Prof. Dr. Gudrun Massmann**
   Hydrogeologie und Landschaftswasserhaushalt
   Institut für Biologie und Umweltwissenschaften
   Carl von Ossietzky Universität Oldenburg

Eingereicht am: **15 September 2023**
Verteidigt am: **21 Juni 2024**

Table of Contents

List of Tables

List of Figures

List of Supplementary Tables

List of Supplementary Figures

List of Symbols and Abbreviation

ANC	Acid neutralizing capacity	LS	Lowers sands
Br^-	Bromide	m	Meter
BH	Borehole	masl	Meters above sea level
BP	Before present	Mg^{2+}	Magnesium
BS	Baltic Sea	MP	Measuring Point (station)
Ca^{2+}	Calcium	Mt	Metric ton
CH_4	Methane	N_2O	Nitrous oxide
Cl^-	Chloride	Na^+	Sodium
Cm	centimeter	NH_4^+	ammonium
CO_2	Carbon dioxide	NO_2^-	Nitrite
CO_3^{2-}	Carbonate	NO_3^-	Nitrate
d	Day	P	Phosphorus; Peat groundwater, if written with a number preceding it (e.g. 7P)
DD	Drammendorf	PO_4^{3-}	Phosphate
DIC	Dissolved Inorganic Carbon	S	Surface water (if written with a number preceding it, e.g., 7S)
DIN	Dissolved Inorganic Nitrogen	SC	Specific conductivity
DIP	Dissolved Inorganic Phosphorus	SGD	Submarine groundwater discharge
DO	Dissolved Oxygen	SM	Supplementary material
DOC	Dissolved Organic Carbon	SO_4^{2-}	Sulfate
DON	Dissolved Organic Nitrogen	SOM	Soil organic matter
DS	Dune sands	STE	Subterranean estuary
GHG/s	Greenhouse gas/es	SW	Surface water
GW	Groundwater	SWI	Seawater intrusion
F^-	Fluoride	T	Temperature
H^+	Hydrogen	TDN	Total Dissolved Nitrogen
H2O	Water level	TDS	Total Dissolved Solids
HCO_3^-	Bicarbonate	yr	Year
HM	Hütelmoor		
hr	Hour		
K^+	Potassium		
K_1, K_2	Equilibrium constants		
km	kilometer		
K_s	Hydraulic conductivity		

Dedication

“I learned that courage was not the absence of fear, but the triumph over it. The brave man is not he who does not feel afraid, but he who conquers that fear.”
- Nelson Mandela

I dedicate this dissertation to our younger selves who did not believe we could make it. We can and we will–one paper at a time.

Acknowledgements

I started my Ph.D. journey in 2019 by packing my life in a backpack and a piece of luggage, leaving my family and friends in the Philippines, and moving halfway across the world. I did not know what to expect but I was armed with grit and determination. Little did I know that it would be more than challenging as the coronavirus pandemic in 2020 changed the world as we know it. For getting me through my doctoral studies and through these difficult times, I would like to acknowledge the support of the following people:

Dr. Manon Janssen, my Ph.D. supervisor, for teaching me the skills and knowledge I needed, for exhibiting unparalleled patience and understanding, and for guiding me throughout this dissertation. I am grateful for everything.

Prof. Dr. Bernd Lennartz, my Ph.D. co-supervisor, for the technical guidance and support to this dissertation.

Dr. Haojie Liu, for always being supportive and for the random nuggets of wisdom whenever I see him.

Jakob Kienzler, Luis Zambrano, and Yousief Dawit, my student assistants, for your hard work and help with the field campaigns, even during harsh conditions.

Tilo Hartwig, Evelyn Bolzmann, Dr. Stefan Köhler, and Karin Eckelt, for your field, laboratory, and administrative support.

Matthias Naumann and Enrico Daum, for field elevation survey support and for handling computer-related problems.

Dr. Fernando Siringan, my M.Sc. supervisor, for introducing me to the world of SGD, for training me to be a good researcher, and for the passion you have shown us. Thank you for being a source of inspiration, and believing that I can pursue a Ph.D.

The Baltic TRANSCOAST 2nd cohort and associate PhDs, thank you for all the help and support. Thank you to *Anna Jenner, Cheryl Batistel, Cordula Gutekunst, Miaorun Wang, Sate Ahmad, Simeon Choo, Werna Werna* and those I fail to mention for helping me out during my numerous field campaigns. I also want to thank my Rostock constants for helping me keep my sanity throughout the pandemic. I am ecstatic that I got to share this journey with you.

My friends from all over Europe, US, Australia, and the Philippines, thank you for the support as always. You don't know how your simple and random messages have uplifted me through all these years.

For Gab, my number one supporter, for giving me something to look forward to at the end of each day.

My family, especially *my Nanay*, who is the reason why I try to better myself every day.

To the *Baltic TRANSCOAST Program* and the *German Research Foundation (DFG)* for the financial support and for allowing me to pursue a Ph.D. in Germany.

Thanks to everyone who has helped me in one way or another.

Erwin

Summary

Coastal peatlands, and mires and peatlands in general, have immense potential for climate change mitigation. Despite covering a tiny fraction of the world's land area, they play a significant role in the global carbon cycle, with terrestrial carbon stores exceeding the total carbon pool of the world's forest. However, most peatlands in Europe, and ~95% in Germany, have been drained and diked for various agricultural purposes, turning them from carbon sinks into sources. Rewetting drained peatlands involves restoring their previous hydrological levels, which, for coastal peatlands, also restores the positive hydraulic gradient from the land to the sea. As a result, submarine groundwater discharge (SGD) could be expected and could be an important pathway for materials from carbon-rich peatlands to its coastal environments. Along the brackish Baltic Sea are several low-lying coastal peatlands, which are perfect candidates for rewetting with seawater. Freshwater rewetting can successfully curb carbon dioxide (CO_2) emissions, but potent methane (CH_4) emissions may arise. In contrast, rewetting with seawater could restore sulfate (SO_4^{2-}) pools and provide an alternative electron acceptor for microbial degradation, thus preventing CH_4 emissions. Nevertheless, seawater also introduces other materials, e.g., sodium (Na^+) and chloride (Cl^-), that can lead to a potential export of carbon and other materials from the peatland to their coastal environments. Given that the impacts of rewetting coastal peatlands are mainly understudied, this dissertation aims to (1) quantify the magnitude of terrestrial SGD from rewetted coastal peatlands and determine the factors contributing to it, (2) unravel the processes behind the spatial and temporal dynamics of terrestrial and total SGD, (3) determine the impact of a storm surge event to SGD fluxes, and lastly, (4) understand the effects of seawater on surface and groundwater quality of brackish-rewetted and seawater-rewetted fen coastal peatlands.

Two-dimensional steady-state groundwater flow numerical simulations were conducted using the HYDRUS modeling package with a diked, brackish-rewetted fen as the reference coastal peatland. Field-gathered properties of the reference peatland were used, characterized by a peat layer extending underneath the beach. Soil physical properties, hydraulic gradients, geological stratifications, and topography were varied to depict a realistic range of properties found in coastal peatlands. The simulations revealed that the extending peat layer acts as a barrier and determines the location of terrestrial SGD. A two-discharge region was observed with average seepage rates of 1.05 cm d^{-1} and 0.16 cm d^{-1} near- and offshore, respectively. One-third of the terrestrial SGD comes from precipitation at the dune dike. The scenario simulations yielded 0.008 – 0.293 m^2 d^{-1} terrestrial SGD fluxes. Among the factors, the hydraulic gradient (groundwater level) and the hydraulic conductivity (K_s) of the geological layers primarily drive the magnitude of terrestrial SGD.

The same brackish-rewetted fen, but with updated boundaries based on newer information, was used to assess the short- and long-term temporal dynamics of SGD. Transient simulations were applied, and extended groundwater and sea level data (five years) were employed. Due to its sensitivity to water flow and terrestrial SGD, K_s of the geological layers were optimized against observed groundwater levels through inverse modeling. In addition, manual seepage meters were deployed to measure direct seepage rates and to take SGD samples for water quality analyses. The existence of the two-discharge region, due mainly to the peat layer extension, was reinforced. Along the

transect, the highest mean discharge at the nearshore is 10.2 cm d^{-1}, while offshore discharge reached a mean of 1.1 cm d^{-1}. Groundwater level controls the seasonal variability of terrestrial SGD, but sea level dictates the daily hydraulic gradient and the resulting total SGD. The total SGD is highest in winter due to a stronger sea level variability, while it is lowest in summer because of calmer sea conditions, less seawater intrusion (SWI) and low groundwater levels. Terrestrial SGD is highest in spring, but the relative contribution to total SGD is the same for spring and summer. Estimated fluxes of Dissolved Organic Carbon (DOC), Dissolved Inorganic Carbon (DIC), and ammonium (NH_4^+) were comparable to other environments from the Baltic Sea, demonstrating their potential impact on local biogeochemistry and marine ecosystems.

The storm surge event of January 2019 resulted in the most considerable SWI flux at the peatland's coastal side, which eventually discharged as recirculated SGD a few days later. The rapid flux of seawater could flush out remineralized carbon and other materials at the groundwater-seawater interface. In addition, the storm surge flooded the peatland and rapidly raised the groundwater level by 0.36 m, thereby increasing the hydraulic gradient directed towards the sea.

In the same brackish-rewetted fen and another recently seawater-rewetted fen, it was found that seawater influx either through storm surge events or by seawater rewetting could significantly affect surface waters and notably impact groundwater quality, specifically DOC and NH_4^+ concentrations. An increase in specific conductivity (SC) and pH was observed from surface waters of both sites. However, it was highly significant for the seawater-rewetted fen since the peatland was converted into a lagoon-like environment. In the brackish-rewetted fen, increased DOC concentrations were observed in the peat layer under high SC and decreased pH conditions, contradicting some laboratory-based studies. In the seawater-rewetted fen, an initial decrease in DOC concentrations were observed, but additional sample at a later time also showed an increase in concentration under the same conditions of increasing SC and decreasing pH. Though the processes were not explicitly determined, the DOC mobilization was likely related to the anion exchange of organic acids with SO_4^{2-}. Cation exchange of NH_4^+ and Na^+ also possibly occurred. Prior to the current seawater influence, the hydrogeochemistry of surface and groundwater of coastal peatlands revealed past variable marine influence likely dependent on distance from the coast, peat thickness, and possibly drainage networks. Depending on local settings, the ditches may act as a hydrological barrier to seawater intrusion or as a conduit for transporting seawater.

In conclusion, this dissertation highlights the occurrence of SGD from rewetted coastal peatlands and the various factors and drivers affecting its temporal and spatial dynamics. Submarine groundwater discharge from these environments can potentially contribute to local biogeochemistry and impact marine ecological systems. Meanwhile, the impacts of seawater influx on coastal peatland groundwater still need to be further studied. Although rewetting could reduce greenhouse gas (GHG) emissions, it remains to be seen whether its impacts to marine ecosystems and water quality – groundwater and connected streams and rivers – will be beneficial or harmful.

Zusammenfasung

Torfgebiete an der Küste sowie Moore und Torfgebiete im Allgemeinen haben ein immenses Potenzial für die Abschwächung des Klimawandels. Obwohl sie nur einen winzigen Bruchteil der weltweiten Landfläche bedecken, spielen sie eine bedeutende Rolle im globalen Kohlenstoffkreislauf, wobei die terrestrischen Kohlenstoffspeicher den gesamten Kohlenstoffpool der Wälder der Welt übersteigen. Die meisten Moore in Europa und ~95 % in Deutschland wurden jedoch für verschiedene landwirtschaftliche Zwecke entwässert und eingedeicht, wodurch sie von Kohlenstoffsenken zu Kohlenstoffquellen wurden. Die Wiedervernässung entwässerter Moore beinhaltet die Wiederherstellung des früheren Wasserstandes, was für Moore an der Küste auch die Wiederherstellung des positiven hydraulischen Gradienten vom Land zum Meer bedeutet. Infolgedessen ist ein submariner Grundwasserabfluss (SGD) zu erwarten, der ein wichtiger Weg für Stoffe aus kohlenstoffreichen Torfgebieten in die Küstengebiete sein könnte. Entlang der brackigen Ostsee gibt es mehrere niedrig gelegene Küstentorfgebiete, die sich perfekt für die Wiedervernässung mit Meerwasser eignen. Die Wiedervernässung mit Süßwasser kann die Kohlendioxid (CO_2)-Emissionen erfolgreich sequestrieren, aber es kann zu starken Methan (CH_4)-Emissionen kommen. Im Gegensatz dazu könnte die Wiedervernässung mit Meerwasser die Sulfat (SO_4^{2-})-Pools wiederherstellen und einen alternativen Elektronenakzeptor für den mikrobiellen Abbau bieten, wodurch CH_4-Emissionen verhindert werden. Allerdings führt das Meerwasser auch andere Stoffe ein, z. B. Natrium (Na^+) und Chlorid (Cl^-), die zu einem potenziellen Export von Kohlenstoff und anderen Stoffen aus dem Moor in die Küstengebiete führen können. Da die Auswirkungen der Wiedervernässung von küstennahen Torfgebieten bisher nur unzureichend erforscht sind, zielt diese Dissertation darauf ab, (1) das Ausmaß des terrestrischen SGD aus wiedervernässten küstennahen Torfgebieten zu quantifizieren und die Faktoren zu bestimmen, die dazu beitragen, (2) die Prozesse hinter der räumlichen und zeitlichen Dynamik des terrestrischen und des gesamten SGD zu entschlüsseln, (3) die Auswirkungen einer Sturmflut auf die SGD-Flüsse zu bestimmen und schließlich (4) die Auswirkungen des Meerwassers auf die Oberflächen- und Grundwasserqualität von brackisch- und meerwasserbenetzten Küstentorfgebieten zu verstehen.

Es wurden zweidimensionale numerische Simulationen der stationären Grundwasserströmung mit dem HYDRUS-Modellierungspaket durchgeführt, wobei ein eingedämmtes, mit Brackwasser benetztes Niedermoor als Referenzküstentorfgebiet diente. Es wurden die vor Ort gesammelten Eigenschaften des Referenzmoores verwendet, das durch eine Torfschicht gekennzeichnet ist, die sich unterhalb des Strandes erstreckt. Die physikalischen Eigenschaften des Bodens, die hydraulischen Gradienten, die geologische Schichtung und die Topografie wurden variiert, um eine realistische Bandbreite von Eigenschaften abzubilden, die in Küstenmooren vorkommen. Die Simulationen ergaben, dass die sich ausdehnende Torfschicht als Barriere wirkt und die Lage der terrestrischen SGD bestimmt. Es wurde eine Region mit zwei Abflüssen mit durchschnittlichen Versickerungsraten von 1,05 cm d^{-1} und 0,16 cm d^{-1} in Küstennähe bzw. vor der Küste beobachtet. Ein Drittel des terrestrischen SGD stammt aus Niederschlägen am Dünendeich. Die Szenariosimulationen ergaben 0,008 - 0,293 m^2 d^{-1} terrestrische SGD-Flüsse. Unter den Faktoren bestimmen vor allem der hydraulische Gradient (Grundwasserstand) und die hydraulische Leitfähigkeit (Ks) der geologischen Schichten das Ausmaß der terrestrischen SGD.

Dasselbe brackig-vernässte Niedermoor, jedoch mit aktualisierten Grenzen auf der Grundlage neuerer Informationen, wurde verwendet, um die kurz- und langfristige zeitliche Dynamik von SGD zu bewerten. Es wurden instationäre Simulationen durchgeführt, und es wurden erweiterte Grundwasser- und Meeresspiegeldaten (fünf Jahre) verwendet. Aufgrund ihrer Empfindlichkeit gegenüber dem Wasserfluss und dem terrestrischen SGD wurden die Ks der geologischen Schichten durch inverse Modellierung gegenüber den beobachteten Grundwasserständen optimiert. Darüber hinaus wurden manuelle Sickerwasserzähler eingesetzt, um die direkte Sickerwassermenge zu messen und SGD-Proben für Wasserqualitätsanalysen zu entnehmen. Das Vorhandensein einer Region mit zwei Abflüssen, die hauptsächlich auf die Ausdehnung der Torfschicht zurückzuführen ist, wurde bestätigt. Entlang des Transekts beträgt der höchste mittlere Abfluss im küstennahen Bereich 10,2 cm d-1, während der mittlere Abfluss im küstenfernen Bereich bei 1,1 cm d^{-1} liegt. Der Grundwasserspiegel steuert die jahreszeitliche Variabilität des terrestrischen SGD, während der Meeresspiegel den täglichen hydraulischen Gradienten und den daraus resultierenden Gesamt-SGD bestimmt. Der Gesamt-SSD ist im Winter aufgrund der stärkeren Schwankungen des Meeresspiegels am höchsten, während er im Sommer aufgrund des ruhigeren Seegangs, der geringeren Meerwasserintrusion (SWI) und der niedrigen Grundwasserstände am niedrigsten ist. Terrestrischer SGD ist im Frühjahr am höchsten, aber der relative Beitrag zum Gesamt SGD ist im Frühjahr und im Sommer gleich. Die geschätzten Flüsse von gelöstem organischem Kohlenstoff (DOC), gelöstem anorganischem Kohlenstoff (DIC) und Ammonium (NH_4^+) waren mit anderen Umgebungen der Ostsee vergleichbar, was ihre potenziellen Auswirkungen auf die lokale Biogeochemie und die marinen Ökosysteme zeigt.

Das Sturmflutereignis im Januar 2019 führte zum größten SWI-Fluss an der Küstenseite des Torfgebiets, der schließlich einige Tage später als rezirkulierter SGD abfloss. Der rasche Zustrom von Meerwasser könnte remineralisierten Kohlenstoff und andere Materialien an der Grenzfläche zwischen Grundwasser und Meerwasser ausspülen. Darüber hinaus überflutete die Sturmflut das Moor und hob den Grundwasserspiegel rasch um 0,36 m an, wodurch sich das hydraulische Gefälle zum Meer hin erhöhte.

In demselben mit Brackwasser benetzten Niedermoor und in einem anderen, kürzlich mit Meerwasser benetzten Niedermoor wurde festgestellt, dass der Zufluss von Meerwasser entweder durch Sturmfluten oder durch Wiederbenetzung mit Meerwasser die Oberflächengewässer erheblich beeinträchtigen und die Qualität des Grundwassers, insbesondere die DOC- und NH_4^+-Konzentrationen, spürbar beeinflussen kann. In den Oberflächengewässern beider Standorte wurde ein Anstieg der spezifischen Leitfähigkeit (SC) und des pH-Werts beobachtet. Im meerwasserbenetzten Niedermoor war dies jedoch besonders ausgeprägt, da das Moor in eine lagunenartige Umgebung umgewandelt wurde. Im brackig-vernässten Niedermoor wurden in der Torfschicht unter hohen SC- und niedrigeren pH-Bedingungen erhöhte DOC-Konzentrationen beobachtet, was im Widerspruch zu einigen Laborstudien steht. Im meerwasserbenetzten Niedermoor wurde zunächst ein Rückgang der DOC-Konzentration beobachtet, doch eine zusätzliche Probe zu einem späteren Zeitpunkt zeigte ebenfalls einen Anstieg der Konzentration unter den gleichen Bedingungen wie steigendem SC und sinkendem pH-Wert. Obwohl die Prozesse nicht explizit bestimmt wurden, war die DOC-Mobilisierung wahrscheinlich mit dem Anionenaustausch von organischen Säuren mit SO_4^{2-} verbunden. Möglicherweise fand auch ein Kationenaustausch von NH_4^+ und Na^+ statt. Die Hydrogeochemie des

Oberflächen- und Grundwassers von Küstentorfgebieten zeigte, dass es in der Vergangenheit einen variablen marinen Einfluss gab, der wahrscheinlich von der Entfernung zur Küste, der Torfdicke und möglicherweise von Entwässerungsnetzen abhing. Je nach den örtlichen Gegebenheiten können die Gräben als hydrologische Barriere gegen das Eindringen von Meerwasser oder als Kanal für den Transport von Meerwasser dienen.

Zusammenfassend lässt sich sagen, dass diese Dissertation das Auftreten von SGD aus wiedervernässten Küstentorfgebieten und die verschiedenen Faktoren und Triebkräfte aufzeigt, die ihre zeitliche und räumliche Dynamik beeinflussen. SGD aus diesen Gebieten kann potenziell zur lokalen Biogeochemie beitragen und sich auf marine Ökosysteme auswirken. In der Zwischenzeit müssen die Auswirkungen des Meerwasserzustroms auf das Grundwasser von Küstenmoorgebieten noch weiter untersucht werden. Obwohl die Wiedervernässung die Treibhausgasemissionen verringern könnte, bleibt abzuwarten, ob ihre Auswirkungen auf die marinen Ökosysteme und die Wasserqualität - Grundwasser und angeschlossene Bäche und Flüsse - nützlich oder schädlich sein werden.

1. INTRODUCTION

1.1 Background

Climate change is the defining issue of our time (United Nations, 2018). The recent human-induced climate change is projected to impact low-lying, terrestrial, and ocean ecosystems (Pörtner et al., 2022) as the rising concentration of greenhouse gases (GHGs) is directly linked to the increase in the average global temperature on Earth (United Nations, 2023). As such, the Paris Agreement was entered into by governments around the world to reduce GHG emissions and limit the increase of global average temperature to 1.5 ^{0}C (United Nations Climate Change, 2023).

Restoring peatlands could help mitigate the increase in GHG emissions. Peatlands cover about 3% of the world's area but store large amounts of organic carbon (Limpens et al., 2008; Mitra et al., 2005). However, due to past anthropogenic activities such as diking and draining, many of the peatlands in Europe are degraded (Tanneberger et al., 2021). This degradation has turned peatlands from carbon sinks to carbon sources (Holden, 2005; Kreyling et al., 2021; Leifeld et al., 2019). Thus, rewetting drained peatlands can reduce GHG emissions by preventing further peat mineralization. As a nature-based solution, this management strategy could be the most cost-effective mitigation measure (Leifeld & Menichetti, 2018). However, its impact on the hydrology, biogeochemistry, and flora and fauna of peatlands still needs to be fully understood. For instance, freshwater rewetting may curb carbon dioxide (CO_2) emissions but also induce methane (CH_4) emissions (Hahn et al., 2015) or mobilize remineralized forms of organic matter (Zak & Gelbrecht, 2007). For coastal peatlands, which could be rewetted with seawater, restoration could either be beneficial when the addition of sulfate suppresses methane emissions (Gutekunst et al., 2022) or harmful when higher salinity stresses plants causing plant growth retardation (Batistel et al., 2022). Furthermore, raising water levels to previous hydrologic levels increases the potential for submarine groundwater discharge (SGD) to adjacent peatland coastal waters, likely increasing the mobilization of organic carbon and export of solutes from the peatland to the sea. Moreover, climate change raises the risk of sea level rise and storm flooding events (Sterr, 2008). In addition to coastal peatland rewetting with seawater, storm surge inundations in the short term and sea level rise in the long term could also impact the hydrology and hydrochemistry of coastal peatlands.

The "*Baltic TRANSCOAST – The German Baltic Sea Coast as Terrestrial- Marine Interface of Water and Matter Fluxes"* is an interdisciplinary research training program between the University of Rostock and the Leibniz Institute for Baltic Sea Research that seeks to enhance the knowledge of the shallow coasts at the transition of land and sea. This dissertation is conducted under the framework of this program and investigates submarine groundwater discharge from rewetted coastal peatlands and the impact on surface and groundwater quality of rewetting with seawater and storm surge inundations.

1.2 Baltic Sea

The Baltic Sea in northern Europe is one of the largest brackish water basins worldwide, encompassing a surface area of 420,000 km^2 (Figure 1.1A) (HELCOM, 2018). With a

drainage area that is four-fold larger than the sea itself and a very narrow connection to the North Sea and Atlantic Ocean, the Baltic Sea is an almost land-locked sea with an average surface water salinity of 7.5 psu (Szymczycha & Pempkowiak, 2016). The smaller sub-basins have salinities ranging from 20–25 psu near its North Sea entrance and 0–2 psu in its northern and eastern sections (HELCOM, 2009, 2018). Geologically, the Baltic Sea is young, having been formed 7800 years ago during the Littorina transgression due to rapid sea level rise (Lampe, 2005). The transition to its current brackish state only started around 2000 years ago (HELCOM, 2018).

The Baltic Sea is facing a multitude of challenges and problems. It suffers from severe eutrophication, making it one of the worst-affected bodies of water in this regard (Malone & Newton, 2020). The primary driver behind this is the high catchment population density and its unique physiographic characteristics (HELCOM, 2018; 2009). Intensifying phytoplankton blooms and increasing spatiotemporal extent of hypoxic areas have been reported because of eutrophication. Additionally, climate change is warming the Baltic Sea region and will have a variety of effects on the terrestrial and marine ecosystems (BACC II Author Team, 2014). Apparent changes in the hydrological cycle are expected in the coming decades (BACC II Author Team, 2014), while relative sea level rise in the 21st century is projected at ~0.70 m in Copenhagen and Gdansk (Grinsted et al., 2015). The southern coast of the Baltic Sea (specifically Kiel and Mecklenburg Bays sub-basin) is especially vulnerable to storm surges and negative storm surges due to the prevailing northwestern and northeastern wind systems (Wolski & Wisniewski, 2020). On an annual average, the German town of Warnemünde (Rostock) experiences 4.4 and 1.2 storm surges with heights of ≥0.7 masl and ≥1.0 masl, respectively (Wolski & Wisniewski, 2020).

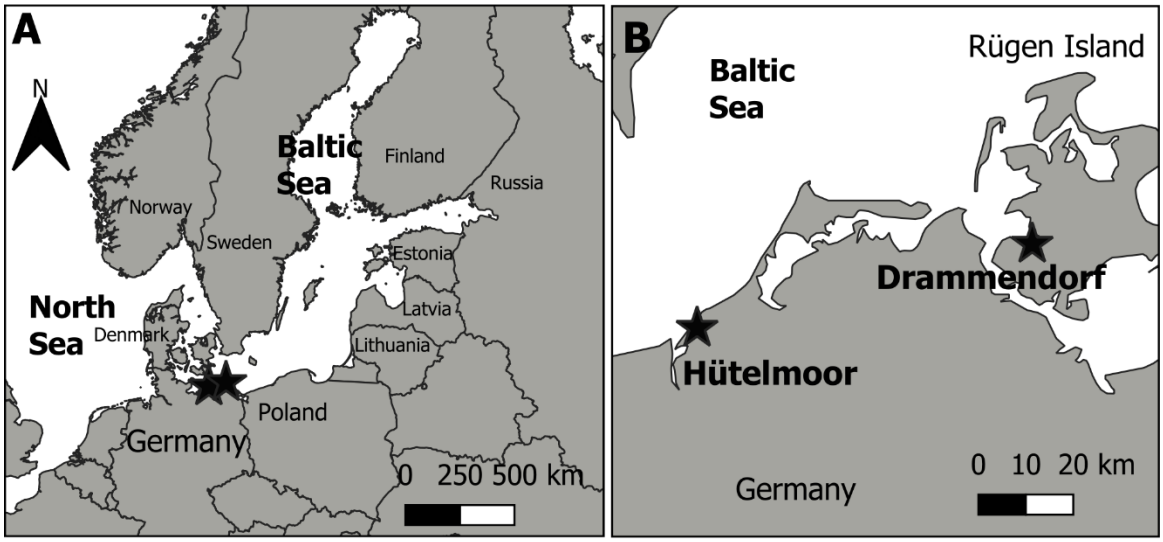

Figure 1.1. Baltic Sea and location of study sites. A) Location of the Baltic Sea in northern Europe showing the surrounding countries and the location of the study sites along the German coast. B) Magnified map of the location of the study sites "Hütelmoor" and "Drammendorf" in northeast Germany.

1.3 Coastal Peatlands

1.3.1 Basic Concepts

Wetlands are defined as “land areas that are saturated or flooded with water either permanently or seasonally” (Ramsar Convention Secretariat, 2014). They are immensely important ecosystems often associated with waste, decay, and something to be re-purposed. However, coastal wetlands provide various ecosystem services such as carbon sequestration, natural coast protection, fisheries support, and water quality improvement and are valued at US$ 194,000 ha^{-1} yr^{-1} (Schuerch et al., 2018).

One type of wetlands is peatlands, which naturally accumulate peat at the surface (Joosten et al., 2017; Tanneberger et al., 2021). Peat is *in situ* accrued material of at least 30% dead organic matter (Joosten et al., 2017). Meanwhile, mire is a term used for a “living peatland” or peatlands with vegetation that forms peat. Hence, all mires are both peatlands and wetlands. However, not all peatlands are wetlands since their severe drainage would exclude them as wetlands (Joosten et al., 2017).

The definition of peat and peatland varies across many countries. In Germany, “Moor” is generally used for all natural or semi-natural wetlands. Several peatland typologies also exist, but the German soil classification system defines Moor/ peatlands with soil layers characterized by 30% organic matter/ humus content and a minimum of 30 cm depth. Peatlands are also differentiated into “Hochmoor” and “Niedermoor” to refer to bogs and fens, respectively. Bog soils are formed by plants under ombrotrophic conditions (rainwater-fed) and are described as having a lower groundwater pH and lower plant species diversity. They are located mostly in high northern latitudes, with *Sphagnum* mosses dominating the plant community. Fens, in contrast, are formed by plants growing under minerotrophic conditions (groundwater-fed) and have higher groundwater pH and plant species diversity. Large numbers of fens are in floodplains with plant communities dominated by alder trees, *Phragmites*, or brownmoss sedges. Further definitions and classifications are discussed by Joosten et al. (2017).

Along the German Baltic coast, low-lying coastal areas with peatlands are abundant (Jurasinski et al., 2018), with some expected to continue underwater beyond the current coastline (Kreuzburg et al., 2018). Approximately 40,000 ha of coastal peatlands are found along the German state of Mecklenburg-Western Pomerania (Jurasinski et al., 2018), which also has the highest percentage of peatlands among the country’s states (~ 13%) (Joosten et al., 2017). Two of these coastal peatlands – the Hütelmoor and Drammendorf – are the subject of this dissertation (Figure 1.1B). They are discussed in detail in the succeeding chapters.

1.3.2 Why are Peatlands Important?

Peatlands provide a wide range of ecosystem services classified into four groups: provisioning, regulating, cultural, and supporting (Joosten & Clarke, 2002; Kimmel & Mander, 2010). Some examples of provisioning services include 1) peat extraction for horticulture, agriculture, domestic heating and energy generation; 2) wild plants and animals for food, fur and medicine; 3) and freshwater sourced from reservoirs draining peatlands. Regulating services include 1) climate regulation through regulation of

greenhouse gases and climatic processes; 2) water regulation by serving as water storage and source of groundwater; 3) water purification and waste treatment retention, recovery, and removal of excess nutrients and pollutants; 4) and erosion protection of underlying soils by peat blanket. Additionally, cultural services include opportunities for recreation and tourism, personal feeling and well-being, religious significance, and opportunities for training and research. Finally, supporting services include biodiversity, soil formation, and nutrient cycling functions.

Among these various ecosystem services, regulating services are highly relevant as humanity grapples against the impacts of climate change. Peatlands play a major role in moderating climate due to their long-term ability to absorb carbon dioxide: peat accumulation of a few meters could take several millennia (Holden, 2005). Although peatlands cover a tiny fraction of the world's land area, they store 10% of all freshwater and 30% of land-based organic carbon (Limpens et al., 2008; Mitra et al., 2005). In Europe, when all organic soils are considered (peat is >0 cm), peatlands amount to 1,000,000 km^2 or about 10% of the total land area (Tanneberger et al., 2021). Peatlands are the largest long-term carbon store in the terrestrial biosphere (Joosten et al., 2016), exceeding the total carbon pool of the world's forest (Schwieger et al., 2021).

1.3.3 Drainage Impacts and Hydrologic Restorations

Many peatlands in Europe have been diked, ditched, drained, and dredged for agricultural use, causing several environmental problems. An estimated 50% of peatland-rich countries in Europe have been drained (Figure 1.2) (Tanneberger et al., 2021). In Germany, almost all peatlands were drained (95%). The long history and the large scale of peatland drainage cause emissions of greenhouse gases, i.e., carbon dioxide (CO_2) and nitrous oxide (N_2O), reduction in water quality due to discharge of nutrients, land subsidence of 1-2 cm yr^{-1}, and biodiversity loss (Kreyling et al., 2021; Tanneberger et al., 2021). Drainage drastically alters peat physical properties, leading to increased bulk density and decreased porosity, hydraulic conductivity (K_s), and storativity (Kreyling et al., 2021). Drained peatlands in Europe can contribute ~220 Mt CO_2eq yr^{-1} or about 5% of total EU GHG emissions (Tanneberger et al., 2021).

Rewetting drained peatlands can address problems of biodiversity and greenhouse gas emissions. Hydrologic restoration efforts directly and indirectly affect emergent vegetation, soils, flora, and fauna (Turner & Lewis, 1996). Raising water levels near to the surface, i.e., ditch closing, can provide habitat for rare and threatened biodiversity and induce establishment of graminoid wetland plants (Kreyling et al., 2021; Tanneberger et al., 2021). In addition, GHG emissions can be curbed by decreasing CO_2 and N_2O emissions and preventing DOC losses (Tanneberger et al., 2021). Although CH_4 emissions re-establishes after freshwater rewetting, the short-lived but strong CH_4 radiative forcing does not undermine the long-term climate change mitigation potential of peatland rewetting (Günther et al., 2020). Yet, impacts of disturbance in peat may be irreversible (Holden, 2005) and may not return from their old selves (Kreyling et al., 2021).

Coastal peatlands, which are at the interface between the land and sea, are perfect candidates for seawater rewetting. Restoring the natural connection of coastal peatlands with the sea could replenish sulfate pools and prevent methane emissions by providing an alternative electron acceptor in the form of sulfate (Gutekunst et al., 2022; Knorr & Blodau,

2009; Pönisch & Breznikar, 2004). Storm surges can also bring seawater and other salts and inundate the low-lying coastal peatlands. As the impacts of climate change further intensify, the average number of storm surges, the maximum annual sea levels, and the duration of high sea levels are expected to increase, as has been documented in the last 60 years (Wolski & Wisniewski, 2021).

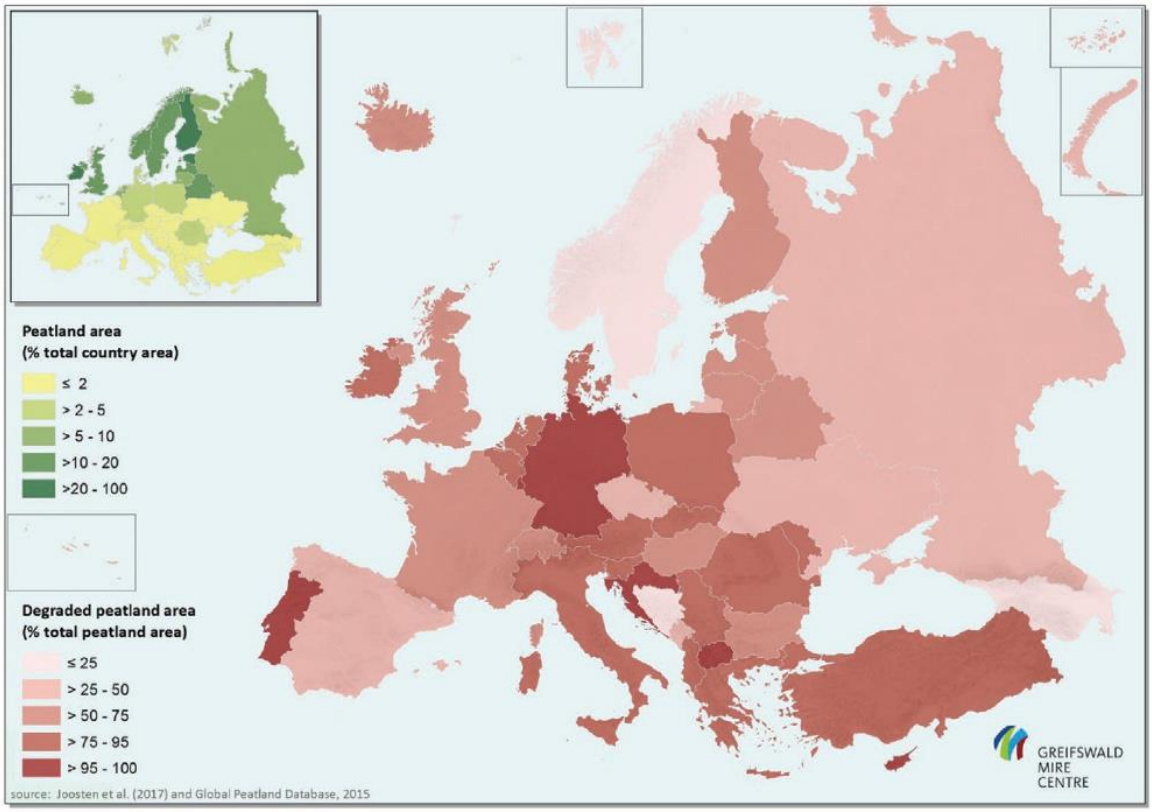

Figure 1.2. Percentage of degraded peatlands and percentage of peatland cover per country in Europe (from Tanneberger et al., 2021).

1.4 Submarine Groundwater Discharge

1.4.1 Basic Concepts

Submarine groundwater discharge (SGD) is an important land-ocean pathway for water and materials (Burnett et al., 2003, 2006; Moore, 2010; Taniguchi et al., 2019). It is defined as “the flow of water through continental and insular margins from seabed to the coastal ocean, regardless of fluid composition or driving force” (Burnett et al., 2003; Taniguchi et al., 2019). However, before its current definition, confusion in the terminology was common in the early days of SGD owing to its multidisciplinary nature. Hydrogeologists use “groundwater” to refer exclusively to land-derived water, while oceanographers use the term for any subsurface water, including recirculated seawater (Jiao & Post, 2019). Another common term used in literature is “subterranean estuary (STE),” which refers to the mixing zone between groundwater and seawater within a coastal aquifer (Moore, 1999). Recently, porewater exchange (<m and <hr) was differentiated from SGD (>m and >hr) (Taniguchi et al., 2019) based on spatial and temporal scales. Here, the term SGD

refers to any water that comes out of the seafloor – regardless of the salinity. Furthermore, in the following chapters, the terms “total SGD,” “terrestrial SGD,” and “recirculated SGD” refer to the sum of land-derived groundwater and recirculated seawater, the land-derived groundwater, and recirculated seawater, respectively. In addition, to put things into perspective, Bratton’s (2010) spatial scale for SGD will be loosely followed in this dissertation. According to this definition, the nearshore scale spans 0–10 m offshore, the embayment scale refers to a distance of 10 m up to 10 km offshore, and the shelf scale spans the whole length of the continental shelf (Bratton, 2010). This dissertation is limited to the nearshore (from shoreline to ~35 m) and offshore (>~35 m to 245 m) scales.

1.4.2 Importance

Although rivers are the traditional pathway for water and material transport to the oceans, several global and local studies have established the volumetric and chemical importance of SGD. Submarine groundwater discharge is ubiquitous and has been found in all types of shorelines – sandy, muddy, and rocky (Santos et al., 2021). Global estimates of fresh SGD vary widely, ranging from 0.01% to 10% of surface-water runoff (Burnett et al., 2001; Church, 1996; Slomp & Van Cappellen, 2004). Luijendink et al. (2020) estimated that fresh groundwater discharge is ~0.6% of the total freshwater input but exceeds 25% of the river flux in 26% of estuaries, 17% of salt marshes, and 14% of coral reefs. Moreover, the global total SGD estimate, including recirculated seawater, is three to four times greater than rivers (Kwon et al., 2014) which has also been observed in local settings (Hwang et al., 2005, 2010; Lee & Kim, 2007).

Chemical inputs from SGD into the oceans are important since groundwater usually has higher concentrations of solutes. Submarine groundwater discharge is known to have high concentrations of nutrients, trace metals, and other contaminants (Moore, 2010; Zhang & Mandal, 2012). In a study conducted by Cho et al. (2018), global total SGD was found to contribute 1.4-, 1.6-, and 0.7-fold of Dissolved Inorganic Nitrogen (DIN), Dissolved Inorganic Phosphorus (DIP), and Dissolved Silica (DSi), respectively, in comparison to river fluxes to the global ocean. Additionally, SGD surpasses river fluxes in 60% of the 200 global study sites, with median total SGD fluxes of 6.0 mmol m^{-2} d^{-1} DIN, 0.1 mmol m^{-2} d^{-1} DIP, and 6.5 mmol m^{-2} d^{-1} DSi (Santos et al., 2021).

As early as the pre-1980s, SGD has been observed to impact ecosystems in relation to productivity, biomass, species composition, and biozonation (Johannes, 1980). Since then, SGD studies have revealed that it affects the water quality of diverse coastal ecosystems such as estuaries, coral reefs, coastal embayments and lagoons, and intertidal wetlands, including mangroves and salt marshes (Moore, 2010; Mulligan & Charette, 2006; Santos et al., 2021). The impact could be beneficial (e.g., increased primary productivity, enhanced growth rates of mussels, oysters and abundance of fish, and partial buffering against ocean acidification) or harmful (e.g., harmful algal blooms, decreased herbivory in macrophytes, and stress in coral reefs). Moreover, the economic, historical, and cultural relevance of SGD has been documented worldwide (Moosdorf & Oehler, 2017; Taniguchi et al., 2019). For instance, historical records have indicated that humans have been using submarine springs for thousands of years, as evidenced by references to “Dilmun”, the paradise island with overflowing freshwater, and the Christian Garden of Eden (Taniguchi et al., 2019). Despite decades of research proving the

importance of SGD in a variety of ecosystems, it is still often ignored in coastal nutrient budget studies (Santos et al., 2021).

1.4.3 Drivers and Factors

Submarine groundwater discharge is driven by several terrestrial and marine physical drivers (Figure 1.3). Topographic/ hydraulic gradient and the oscillation of groundwater levels are the main terrestrial drivers of SGD (Santos et al., 2012; Michael et al., 2005) but local factors such as sediment hydraulic conductivity, geological stratifications and heterogeneities, complex coastal morphology, and thickness of aquifers (Luijendijk et al., 2020; Racasa et al., 2021; Robinson et al., 2018) also influence the magnitude and location of SGD. Groundwater discharges along the coast as long as there is a positive hydraulic gradient towards the sea (Santos et al., 2012). The fresh SGD component is primarily controlled by the flow capacity of coastal aquifers as determined by the topographic gradient, aquifer thickness, and permeability (Luijendijk et al., 2020). However, the seasonal oscillation of hydraulic heads leads to the movement of the groundwater-seawater interface and the recirculation and discharge of seawater (Michael et al., 2005). The resulting saline discharge could be higher than freshwater discharge.

Marine drivers include tides, waves, water density differences, and sea level changes (Santos et al., 2012; Robinson et al., 2018). Tides bring in large amounts of seawater and solutes, which infiltrate coastal aquifers during flow tide and induce seawater recirculation at ebb tide (Robinson et al., 2018). Waves also bring seawater into the aquifer, but the effect is highly irregular and occurs on multiple time scales (Robinson et al., 2018). Wave setup flushes shallower layers in shorter times (in cm and min range), while tidal pumping flushes deeper depths and longer times (in m and hr-d range) (Santos et al., 2012). Density differences between porewater and the overlying seawater may lead to convection with spatiotemporal scales spanning from centimeters to kilometers and hours to years (Santos et al., 2012).

The multiple sources of water from various driving forces is the primary reason SGD can generate extensive chemical fluxes into the sea (Moore, 1999; Jiao & Post, 2019). High microbial activity in the STE, due to the different water sources, makes it a unique biogeochemical reactor (Moore, 1999). As an illustration, anoxic and terrestrially sourced SGD have higher proportions of ammonium, while large quantities of marine organic matter from recirculated SGD can be remineralized into phosphate (PO_4^{3-}), nitrate (NO_3^-), NH_4^+, CH_4, and CO_2 (Robinson et al., 2018). Further, even if there is no net SGD water flux, such as during tidal pumping, the chemical mass that goes back into the sea could be much higher. Radium in groundwater could be desorbed by higher salinity water during high tide and transported to the sea during low tide (Moore, 1996).

Since most shorelines are exposed to multiple forcings from the land and sea, the interactions among these drivers are generally non-linear and not a sum of independent terms (Robinson et al., 2018). Aside from the mentioned forcings, other small-scale drivers of porewater exchange and groundwater flow include ripple migration, bioirrigation, gas bubbles, and sediment compaction (Santos et al., 2012). For a more comprehensive understanding of this topic, the review papers by Moore (2010), Santos et al. (2012), Robinson et al. (2018), and Taniguchi et al. (2019) should be referenced.

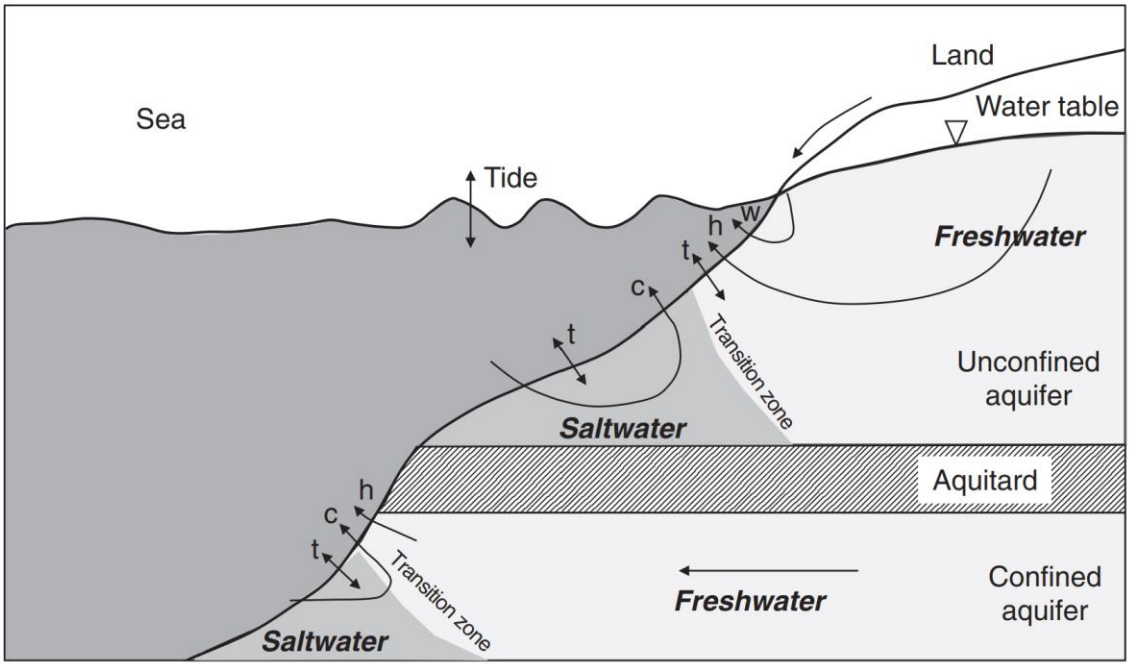

Figure 1.3 The driving forces of SGD: w=wave setup, h=hydraulic gradient, t=tidal pumping, c=convection (from Jiao & Post, 2019 based on Taniguchi et al., 2002).

1.4.4 Methods for Measuring SGD

Measuring SGD is challenging because of its spatial and temporal variability, thus often requiring multidisciplinary methods. A five-year study by the International Atomic Energy Agency and the United Nations Educational, Scientific and Cultural Organization compared multiple methods. It came up with the most common approaches, including seepage meters, piezometers, natural tracers, water balance, hydrograph separation techniques, and theoretical analysis and numerical simulations (Burnett et al., 2006). Taniguchi et al. (2019) noted that SGD studies apply multiple techniques, including geochemical tracers, geophysical approaches, direct measurements, and hydrological modeling. Among these, the seepage meter remains the only device to directly quantify the exchange between groundwater and surface water across the sediment-water interface (Rosenberry et al., 2020). However, seepage meters can only be used on a limited spatial scale. In contrast, enriched geochemical tracers in groundwater, like radium, radon, and methane isotopes, are often used to quantify regional SGD (beach/ embayment scale) estimates (Burnett et al., 2006; Taniguchi et al., 2019). In a review of 239 SGD case studies, 27% and 45% used radon and radium approaches to quantify SGD (Santos et al., 2021). With the direct seepage meters and the natural tracers, a significant gap remains between the two approaches that can be bridged qualitatively using geophysical methods like thermal infrared sensing, electrical ground conductivity mapping, and seafloor mapping and seismic profiling (Taniguchi et al., 2019). In this dissertation, SGD was quantified using seepage meters and numerical simulations, which are further discussed in the following paragraphs.

One of the earliest seepage meters that is still the basis of many seepage meters used today was designed by Lee (1977). The device was developed from one end of a 208 L steel drum with a small water outlet connected to a plastic collection bag (Lee, 1977)

(Figure 1.4). Groundwater discharge or recharge is measured by inserting the drum open end into the sediment and noting the water's volume change in the bag over a known period. Using seepage meters is labor intensive since it requires multiple drums to cover the natural spatial and temporal variability of SGD. Aside from this, measurement artifacts could arise from resistance or wave effects on the seepage bag (Burnett et al., 2006). Seepage bag resistance could be addressed by using the correct diameter of the connection tubes, while wave effects could be avoided by extending connection tubes and using a "box shelter" for the bags (Duque et al., 2020; Rosenberry et al., 2020). Automated seepage meters were also developed to address the labor demands of using seepage meters (Burnett et al., 2006). Seepage meters are a powerful tool for measuring direct SGD from the seafloor when properly used.

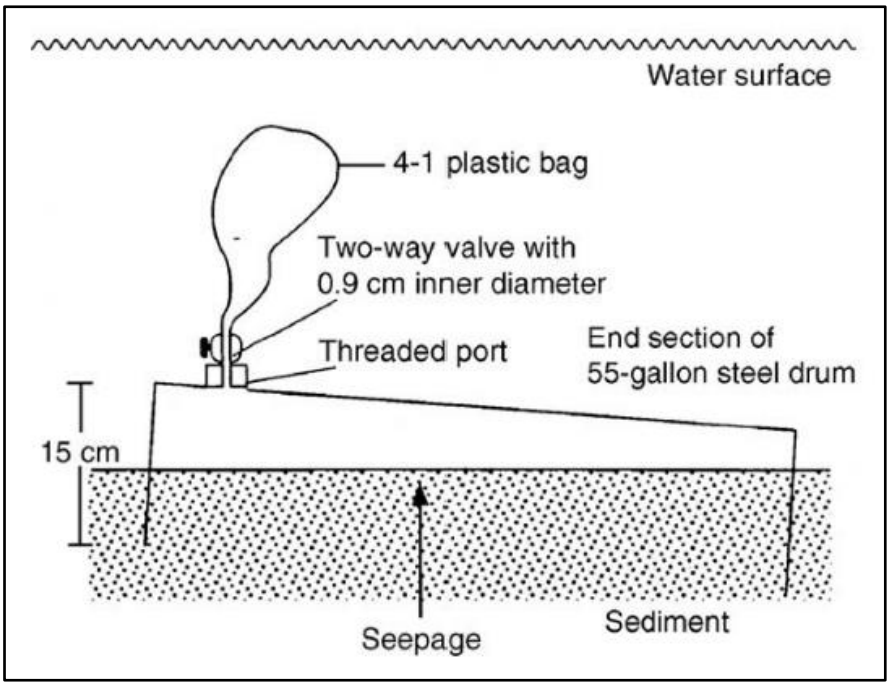

Figure 1.4. Diagram of a seepage meter showing the open end drum and the seepage bag (collection bag). Seepage from the seafloor is measured by measuring the change in volume in the seepage bag over a known period of time (from Burnett et al., 2006).

The first to use mathematical models to measure seepage rates were McBride and Pfannkuch (1975), Fukuo and Kaihotsu (1988), and Bokuniewicz (1992) (Burnett et al., 2006). Initially, offshore seepage rates were described to be exponentially decreasing through lakebeds using numerical models (McBride & Pfannkuch, 1975). Then, using analytical solutions, SGD was determined to mostly flow through the nearshore interface between groundwater and surface water (Fukuo & Kaihotsu, 1988). In addition, SGD decreases exponentially from the coast, with the rate of decrease greater in environments with gentler slopes. Later, it was determined that a single exponential function underestimated SGD in both nearshore and offshore areas and overestimated SGD at intermediate distances (Bokuniewicz, 1992; Burnett et al., 2006). Unlike analytical models, which use simpler forms of the governing equation and require simpler geometry and boundary conditions, numerical models use an approximate form of the governing

equation under complex geometries (3D) and boundary and initial conditions (Anderson et al., 2015). Numerical models are powerful tools for forecasting or hindcasting groundwater discharge, describing physical flow patterns, and estimating regional or global discharge groundwater fluxes. For example, large seasonal saline discharge measured directly and inferred from geochemical tracers was found to be a result of seasonal groundwater level oscillations using numerical modeling (Michael et al., 2005). Groundwater-seawater mixing in the subterranean estuary was visualized, revealing the occurrence of an “upper saline plume” and “fresh discharge tube” in addition to the classical salt wedge view of the groundwater-seawater interface (Robinson et al., 2006, 2007). Finally, numerical modeling was also used to establish a global estimate of the freshwater component of SGD (Luijendijk et al., 2020). The disadvantage of using hydrological models is that, on average, SGD estimates are a factor of two lesser than geochemical tracers but are otherwise effective in quantifying specific driving forces and components of fresh and saline SGD (Santos et al., 2021).

1.4.5 Fresh and Recirculated SGD

Numerous SGD studies differentiate between fresh and recirculated (saline) SGD, especially when interpreting nutrient fluxes to the coastal ocean (Santos et al., 2021). Fresh and recirculated SGD are different: fresh SGD is a source of new water and high concentration dissolved species, while recirculated SGD flushes out remineralized nutrients from organic matter and entrained nutrients from the mixing of fresh-saline waters (Santos et al., 2021). In addition, in terms of volumetric contribution, the fresh SGD component is only a tiny fraction of the total SGD (Burnett et al., 2001; Church, 1996; Luijendijk et al., 2020; Slomp & Van Cappellen, 2004). Meanwhile, recirculated SGD, which exceeds fresh SGD at most sites except for rocky coastlines, has a net zero water volume exchange over multiple timescales (Santos et al., 2021). As an example, Santos et al. (2021) proposed the expected SGD from different coastal systems and their associated nitrogen fluxes: sandy – brackish SGD, NH_4^+ ~ Dissolved Organic Nitrogen (DON) > NO_3^-; muddy – saline SGD>>fresh SGD, DON + NH_4^+; rocky – fresh SGD> saline SGD, NO_3^- > DON ~ NH_4^+. Regarding uncertainties in regional and global estimates, fresh SGD has large uncertainties, but saline SGD is further less understood (Santos et al., 2021). Seawater infiltration and subsequent discharge as recirculated SGD can have timescales of days to weeks (tide- or storm-driven) or seasons to years (convection or sea level oscillations), thus complicating SGD estimations.

1.4.6 SGD in the Baltic Sea and Wetland Ecosystems

There have been a number of SGD studies conducted in the Baltic Sea, particularly in the last decade. A literature search in SCOPUS with the search terms “submarine groundwater discharge” AND “Baltic Sea” shows 53 documents (Figure 1.5), with several studies coming from Poland and Germany. Previous SGD studies were conducted in known groundwater discharge areas such as the Bay of Puck in Poland (Kłostowska et al., 2020; Szymczycha et al., 2012, 2020; Szymczycha & Pempkowiak, 2016) and in Eckernförnde Bay, Germany (Kreuzburg et al., 2023; Müller et al., 2011; Schlüter et al., 2004).

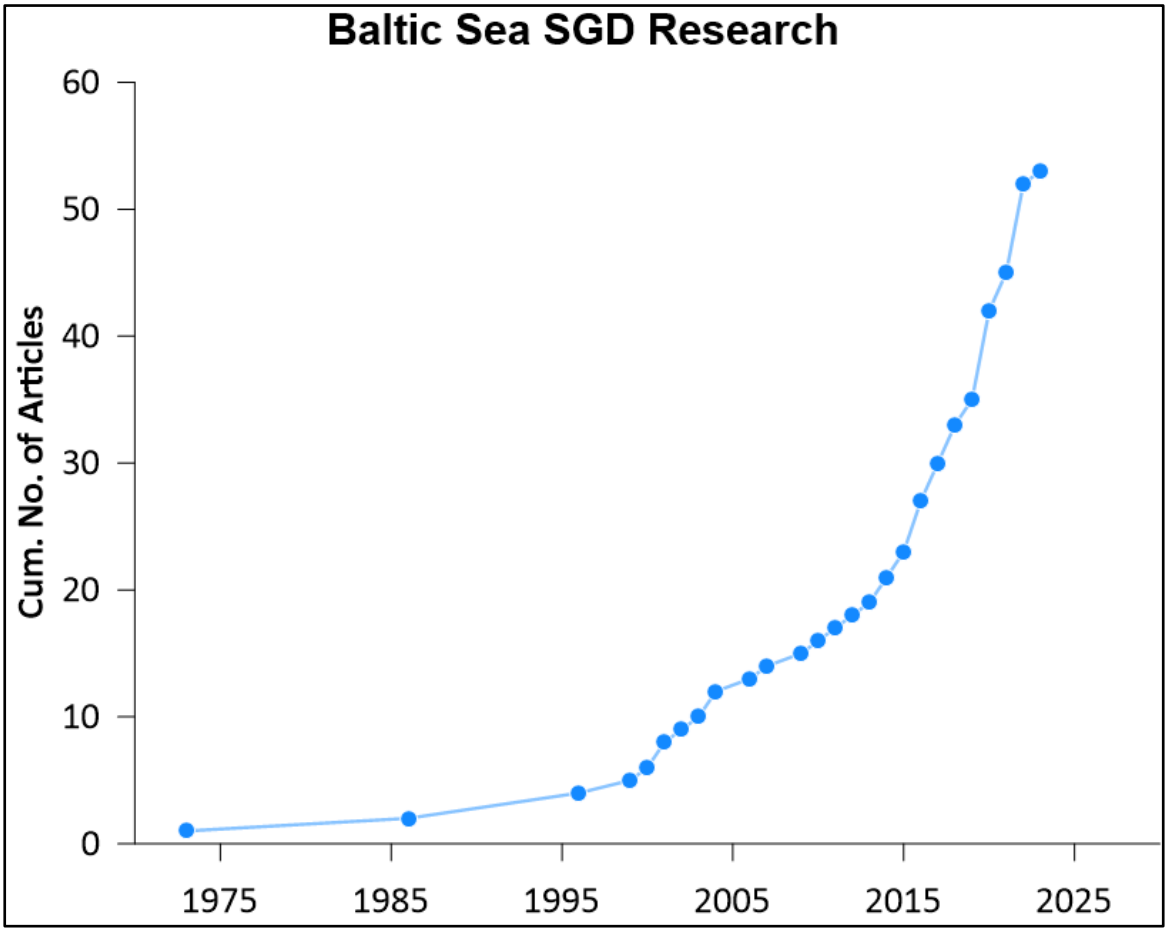

Figure 1.5. Cumulative number of SGD research articles in the Baltic Sea based on SCOPUS search terms "submarine groundwater discharge" AND "Baltic Sea".

1.5 Coastal Peatland Knowledge Gaps on Submarine Groundwater Discharge, Storm Surge Impacts, and Rewetting with Seawater

Most information on SGD was generated from sandy shorelines. Limited research has been conducted on muddy shorelines like salt marshes, mangroves (Taniguchi et al., 2019), and coastal peatlands abundant along the Baltic Sea. With the search terms "submarine groundwater discharge" AND "wetlands," SCOPUS lists 75 articles, book chapters, review papers, and editorials. Based on SCOPUS, no SGD research has been done from coastal peatlands except for the related recent articles by the Baltic TRANSCOAST group (Jurasinski et al., 2018; Kreuzburg et al., 2018, 2020; Racasa et al., 2021; Toro et al., 2022). In addition to this literature, although SGD was not the focus of their research, terrestrial groundwater discharge estimates from the Hütelmoor peatland to the Baltic Sea were presented by Miegel et al. (2016) and Schreiber et al. (2021). The low hydraulic conductivity of peat layers, particularly those extending to the sea (Kreuzburg et al., 2018), could significantly impact water and solute flow and transport from peatland to the sea.

Submarine groundwater discharge from coastal peatlands could be different from other coastal environments because of their brackish surface and groundwaters and the non-

tidal nature of the Baltic Sea. In the Hütelmoor peatland, past inundations have been recorded, and one-third of the groundwater is sourced from the Baltic Sea based on chloride concentrations and sulfur isotopes (Koebsch et al., 2019; Toro et al., 2022). As such, coastal peatlands along the Baltic Sea are expected to have brackish groundwaters and, eventually, brackish SGD due to the long history of seawater influence. Additionally, tides may have little impact on SGD in the Baltic Sea. Many studies focused on nearshore tidally driven SGD with semi-diurnal, diurnal, or fortnightly variations (Santos et al., 2021). In contrast, tides in the semi-enclosed basin have a maximal height of 23 cm for the whole region and 6 cm in the southwestern region near the Danish straight (Medvedev et al., 2016). Spatial and temporal dynamics arising from the rewetting of coastal peatlands are unknown, although marine forcings, such as density-driven convection and tidal pumping, may have limited impact on SGD from coastal peatlands.

Wind-driven sea levels and storm surges could be relevant to spatial and temporal SGD dynamics. Wind direction and monthly precipitation were found to be important short-term factors for SGD in the Bay of Puck, Baltic Sea (Kłostowska et al., 2020). Moreover, the location of the study sites is vulnerable to storm surges and negative storm surges, as has been shown by Wolski & Wiśniewski (2020), with at least one storm surge of ≥1.0 masl expected annually. On January 2, 2019, a storm surge of 1.69 masl height flooded the Hütelmoor study site with seawater, followed by another storm surge of 1.17 masl height a week later.

Large fluxes of remineralized forms of organic matter can potentially arise from high carbon wetland environments, including coastal peatlands. Mangroves contributed >70% of total DOC and DIC input into a bay from SGD-derived fluxes (Chen et al., 2018). Salt marsh carbon export exceeds sediment carbon burial rates (Correa et al., 2022), while wetland-drained coastal canals export DOC and free CO_2 from SGD (Davis et al., 2020). High SGD-derived carbon fluxes were estimated from the Baltic Sea (Szymczycha & Pempkowiak, 2016) and the Gulf of Mexico (Santos et al., 2009a) comparable to river sources. In coastal peatlands with very high organic matter and remineralized species, SGD fluxes to their local adjacent water bodies may have higher fluxes of DOC, DIC, NH_4^+, among others. Coastal peatlands in northeast Germany are expected to play a pivotal role in buffering the exchange of water and dissolved particulate compounds between the land and sea (Jurasinski et al., 2018), but implications to coastal nutrient budgets and primary productivity could also be relevant.

Storm surges bring salts such as sodium, chloride, and sulfate to coastal peatlands. Likewise, coastal peatland rewetting with seawater will bring these salts to the peatlands. Competitive adsorption of Na^+ with NH_4^+ in peat samples has been noted (McCarter et al., 2018), leading to NH_4^+ release in saline water during short-term leaching experiments (Liu & Lennartz, 2019b). Increasing salinity and chloride concentration also affect the DOC release from peat since high ionic strength and low pH will cause a solubility reduction (Liu & Lennartz, 2019b). However, differing relationships between salinity and DOC have been reported in the literature. Tiemeyer et al. (2017) showed decreasing DOC with increasing electrical conductivity in laboratory experiments while revealing increasing DOC with increasing electrical conductivity in field measurements. The decline in DOC concentrations and reduced annual export of DOC were also reported from a mature and forested wetland (Ardón et al., 2016). Meanwhile, DOC concentrations and Total Dissolved

Nitrogen (TDN) increased with increasing SO_4^{2-} levels (Gosch et al., 2019). Furthermore, peat degradation complicates flow, storage, and transport of water and solutes in peatlands.

The impact of storm surge flooding and seawater rewetting on coastal peatlands' surface and groundwater quality and the indirect effects of greenhouse gas emissions still need to be fully understood. The storm surge in 2019 and the drought in the preceding year increased sulfate availability to the peatland and overall decrease in CH_4 and CO_2 concentrations after seawater inflow, although microbial analysis in peat soils point to CH_4 decline in other compartments of the peat-water-atmosphere continuum (Gutekunst et al., 2022). Rewetting potentially releases large amounts of phosphorus (P), NH_4+, and DOC into surface waters (Zak & Gelbrecht, 2007), as has been observed after seawater rewetting of the Drammendorf peatland for Dissolved Inorganic Nitrogen (DIN), P, and CH_4, at least in the first year of rewetting (Pönisch & Breznikar, 2004). Further studies are required to fully understand the impacts of seawater on coastal peatlands. Moreover, most laboratory and field studies are limited in terms of temporal scale and the depth of peat soils in consideration, usually the upper 50 cm depths. The long-term impacts of seawater on the hydrochemistry of groundwater in deeper depths (>50 cm depth) are not studied.

1.6 Objectives and Hypotheses

The overall objective of this dissertation is to gain a comprehensive understanding of the processes involved in submarine groundwater discharge and the long-term impact of seawater on the surface and groundwater quality of rewetted coastal peatlands within the context of the Baltic TRANSCOAST Research Training Group. The specific objectives and the related hypotheses were formulated as follows:

i. Terrestrial SGD: The objectives of this work package were to quantify the magnitude and location of terrestrial SGD flux from a rewetted coastal peatland located along the Baltic Sea; and determine the factors that govern terrestrial SGD from low-lying coastal peatlands by assessing the impact of soil hydraulic properties, hydraulic gradient, and geological stratification, and topography.
It was hypothesized that SGD occurs from coastal peatlands with groundwater level and hydraulic conductivity of peatland geological layers determining the magnitude of terrestrial SGD. In addition, more terrestrial SGD occurs at the coast.

ii. Seasonal dynamics of SGD: The objectives of this work package were to describe groundwater flow pathways from a rewetted coastal peatland to the Baltic Sea; determine the magnitudes of total, terrestrial, and recirculated SGD on different temporal scales; and estimate solute fluxes.
It was hypothesized that the terrestrial and total SGD seasonal magnitudes depend on the hydraulic gradient, subject to the groundwater and sea level interaction.

iii. Impact of storm surge on SGD: The objective of this additional work package (included in Chapter 3) was to investigate the impact of a 2019 storm surge event on water exchange on a rewetted, diked coastal peatland.

It was hypothesized that storm surge increases SWI fluxes, which leads to an eventual increase in SGD fluxes.

iv. Seawater impact on surface- and groundwater quality: This work package aimed to understand the seawater's impact on water quality after a storm surge flooded a brackish-rewetted fen and upon rewetting of a drained fen with seawater.
It was hypothesized that seawater input significantly changes the surface and groundwater chemistry of coastal peatlands. Moreover, additional input of sodium, chloride, and sulfate decreases DOC/DIC and increases ammonium concentrations of surface and groundwaters of coastal peatlands.

1.7 Structure of This Dissertation

This dissertation consists of five chapters, with **Chapter 1** introducing the Baltic Sea, coastal peatlands, and submarine groundwater discharge. This chapter provides an overview of the environmental significance of peatlands in general and discusses anthropogenic impacts on peatlands and their current restoration efforts. In addition, the chapter provides an overview of submarine groundwater discharge, including its definition and role in coastal nutrient budgets. The reader is also introduced to physical drivers that influence SGD, along with the existing various methods used to study it, with a particular focus on numerical simulations and seepage meters. Finally, the knowledge gaps in understanding SGD from coastal peatlands and the impact of seawater on surface and groundwater quality were identified. The objectives and hypotheses are also listed in this chapter.

Chapter **2** determines terrestrial SGD magnitude and location from the brackish-rewetted Hütelmoor coastal peatland, using long-term groundwater and sea level data and field-measured soil physical properties. To understand the controlling factors of terrestrial SGD, steady-state numerical simulations were conducted, incorporating realistic soil physical properties, hydraulic gradients, geological stratifications, and topography commonly observed in coastal peatlands. The findings of this chapter were published in Frontiers in Earth Science entitled "Submarine groundwater discharge from non-tidal coastal peatlands along the Baltic Sea" (Racasa et al., 2021). Table format in this chapter maybe different from the original publication but the contents were not changed. Moreover, since the references from this publication are integrated into the whole dissertation, suffix identifiers maybe added to the original in-text citation. For example, Liu & Lennartz, 2019 was changed to Liu & Lennartz, 2019a.

In Chapter **3**, five-year transient numerical simulations are analyzed to reveal important SGD and seawater intrusion (SWI) processes at different temporal scales from the Hütelmoor coast. This chapter explores the importance of sea level in a coastal area with low elevation, albeit non-tidal. Fluxes of DOC, DIC, and NH_4^+ are initially estimated to assess their potential relevance to local biogeochemistry. Additionally, it explores water fluxes at the coast preceding, during, and following a storm surge in 2019. This chapter is a full paper to be submitted to a journal publication.

Chapter **4** investigates the effect of storm surge inundation and rewetting with seawater on both surface water and groundwater quality. The study primarily centers on the Hütelmoor and Drammendorf peatlands, which experienced seawater flooding and rewetting, respectively. The investigation emphasizes DOC, DIC, and NH_4^+ since these

parameters are known to have elevated levels in peatlands. This chapter is another full paper which will be submitted for publication.

The final chapter, Chapter **5**, serves as a culmination and synthesis of the entire dissertation. This chapter underscores the novel contribution of this research to the understanding of submarine groundwater discharge from coastal peatlands, and its land-derived groundwater quality. Furthermore, this chapter allows the dissertation to provide more context into the broader perspective of peatland management and its potential impacts on the local environment.

2. SUBMARINE GROUNDWATER DISCHARGE FROM NON-TIDAL COASTAL PEATLANDS ALONG THE BALTIC SEA

Erwin Don Racasa[1*], Bernd Lennartz[1], Miriam Toro[1,2], Manon Janssen[1]

[1]Soil Physics, Faculty of Agricultural and Environmental Sciences, University of Rostock, Rostock, Germany

[2]Landesamt für Landwirtschaft, Umwelt und ländliche Räume, Flintbek, Germany

Published in **Frontiers in Earth Science (2021) 9:665802**

Abstract

Submarine groundwater discharge (SGD) is an important pathway for water and materials within the land-ocean transition zone that can impact coastal environments and marine life. Although research from sandy shorelines has rapidly advanced in recent years, there is very little understanding of coastal areas characterized by a low hydraulic conductivity (K_s), such as carbon-rich coastal peatlands. The objective of this study was to determine the magnitude and location of terrestrial SGD to be expected from a non-tidal low-lying coastal peatland located along the Baltic Sea and to understand the controlling factors using numerical modeling. We employed the HYDRUS-2D modeling package to simulate water movement under steady-state conditions in a transect that extends from the dune dike-separated rewetted fen to the shallow sea. Soil physical properties, hydraulic gradients, geological stratifications, and topography were varied to depict the range of properties encountered in coastal peatlands. Our results show that terrestrial SGD occurs at the study site at a flux of 0.080 $m^2\ d^{-1}$, with seepage rates of 1.05 cm d^{-1} (upper discharge region) and 0.16 cm d^{-1} (lower discharge region above submerged peat layer). These calculated seepage rates compare to observations from other wetland environments and SGD sites in the Baltic Sea. The groundwater originates mainly from the dune dike – recharged by precipitation and infiltration from ponded peatland surface water – and to a lesser extent from the sand aquifer. The scenario simulations yielded a range of potential SGD fluxes of 0.008 to 0.293 $m^2\ d^{-1}$. They revealed that the location of terrestrial SGD is determined by the barrier function of the peat layer extending under the sea. However, it has little impact on volume flux as most SGD occurs near the shoreline. Magnitude of SGD is mainly driven by hydraulic gradient and the hydraulic conductivity of peat and beach/ dune sands. Anisotropy in the horizontal direction, aquifer and peat thickness, and peatland elevation have little impacts on SGD. We conclude that SGD is most probable from coastal peatlands with high water levels, large K_s and/or a dune dike or belt, which could be an essential source for carbon and other materials via the SGD pathway.

Keywords: *coastal wetlands, HYDRUS-2D, terrestrial SGD, hydraulic conductivity (K), non-tidal shorelines, dune dike, rewetted peatlands*

2.1 Introduction

Submarine groundwater discharge has been recognized as an important land-ocean route for water and materials (Burnett et al., 2006; Burnett et al., 2003; Moore, 2010; Taniguchi et al., 2019) and often has higher concentrations of carbon, nutrients, and metals than river waters (Moore, 2010). Along the German coast of the southern Baltic Sea, low-lying coastal areas with peatlands (<1 masl elevation) have been abundantly documented (Jurasinski et al., 2018), some with submerged peat extending beyond the coastline (Kreuzburg et al., 2018). The vast majority of these coastal peatlands are degraded due to a long history of drainage for agricultural usage (Baird, 1997) and bordered by coastal protection measures (Bollmann, et al. 2010). They are thus characterized by a low hydraulic conductivity (K_s) and low hydraulic gradients. In organic-rich subterranean estuaries, high concentrations of remineralized forms of organic matter have been reported (Taniguchi et al., 2019). Coastal peatlands with their large stores of carbon, organic matter, and nutrients from decaying plants could thus be a potentially overlooked source of water and materials for the Baltic Sea via the SGD pathway.

The occurrence of SGD – sourced from terrestrial groundwater or recirculated seawater and usually a mixture of both – depends on several factors. Soil hydrological properties, such as hydraulic conductivity, anisotropy, and preferential flow pathways, can affect the magnitude and location of terrestrial SGD. Real-world complexities such as geological heterogeneities, non-uniform and evolving alongshore and cross-shore morphology (Robinson et al., 2018), topographic differences, and anthropogenic structures can also be important factors. Global coastal groundwater discharge is predominantly controlled by the flow capacity of aquifers - a product of permeability, topographic gradient, and thickness of coastal aquifers (Luijendijk et al., 2020). In contrast, SGD from recirculated seawater or 'recirculated SGD' is driven by currents, waves, tides, and density differences (Taniguchi et al., 2019). In this research, we focus only on terrestrial SGD.

Although SGD studies have rapidly advanced in recent years, most information was generated from sandy shorelines. Very little research has been conducted on muddy shorelines such as salt marshes, mangroves (Taniguchi et al., 2019), and even coastal peatlands. Previous SGD studies in the Baltic Sea have focused on known and expected groundwater discharge areas (Szymczycha et al., 2014; 2016a; 2016b; 2020) but new sources, such as submarine terraces (Jakobsson et al., 2020) and pockmarks (Idczak et al., 2020), have also been proposed. Total groundwater discharge in the Baltic Sea was estimated at 1% of total river runoff but phosphorus and carbon SGD fluxes were calculated to be 86% and 30%, respectively, of rivers (Szymczycha & Pempkowiak, 2016b). The measured annual average concentrations of dissolved organic carbon (DOC) in the Bay of Puck is 5.8 mg C L^{-1} (Szymczycha et al., 2014). However, in coastal peatlands, DOC and other materials concentrations can be much more relevant.

Our study seeks to address the lack of data for SGD from coastal peatlands using numerical simulations. The main objectives are to 1) quantify magnitude and location (distance from coast) of terrestrial SGD flux from a coastal peatland located along the Baltic Sea and 2) determine the factors that govern terrestrial SGD from peatlands in low-lying coastal environments by assessing the impact of soil hydraulic properties, sea- and groundwater levels, and geological stratification and topography. With the current trend

on restoring extensively modified coastal peatlands to mitigate greenhouse gas emissions, understanding how groundwater flows and how materials are transported is ever more imperative.

2.2 Materials and Methods

2.2.1 Study Site

The reference peatland for simulating groundwater flow and discharge in this study is based on a coastal peatland near the city of Rostock, northeast Germany, the Hütelmoor Nature Reserve ("Naturschutzgebiet Heiligensee und Hütelmoor"; 54.2139^0N 12.1725^0E) (Figure 2.1). This coastal peatland borders the Baltic Sea along a 3-km long shoreline, but is physically separated by a 40-m wide dune dike that thins out in its northern part. The area was shaped by the Weichselian ice age. The glacial till is covered by glacio-fluvial sands with 2.5 to 15 m thickness, which now form a shallow aquifer (Ibenthal, 2020 and references therein). During the Littorina transgression 8000—1200 BP, the rising groundwater level resulted in the development of a paludification fen from 7000 BP onwards (Kreuzburg et al., 2018). Peat thickness is up to 3 m in the central peatland and near the coast, while it thins out towards the forest. A special feature is the outcropping of the peat at the coastline and in the shallow Baltic Sea. Strongly decomposed sedges and reed make up the peat. Elevation of the peatland is -0.15—0.75 masl (meters above sea level) with a total area of 350 ha (Ibenthal, 2020). Annual precipitation, annual evapotranspiration, and average daily temperature are 693 mm, 604 mm (1951—2010; Miegel et al., 2016), and 9.7 ^{0}C (at Warnemünde, ~7 km away, 1990—2019; DWD, 2020), respectively.

The Hütelmoor, similar to many coastal peatlands in the southern Baltic Sea region, has been artificially drained, diked, and utilized as pasture. Initial drainage started in the 18th century and extensive pumping from 1976 to 1991 led to degradation and compaction of the peat's upper decimeters (Jurasinski et al., 2018). In December 2009, the construction of a ground sill with an elevation of 0.4 masl at the outlet of the peatland's ditch system enabled rewetting and renaturation of the peatland. Since then, most of the peatland is flooded with surface waters. The ditches still drain the peatland when the water level exceeds the groundsill, they affect local groundwater flow fields and divert water inflow from the forest (Ibenthal, 2020). The peatland is still separated from the Baltic Sea by a dune dike, that is not maintained anymore. The electrical conductivity (EC) in ground- and surface water in the peatland ranged from 4-13 mS/cm and thus revealed brackish waters, originating from earlier inundations and occasional seawater inflow via the dike system during storms (Ibenthal, 2020). In comparison, several EC measurements from the nearshore waters in front of the Hütelmoor ranged from 18 to 27 mS/ cm, corresponding to a salinity of 11–15 psu. Due to the brackish nature of groundwater in the peatland, we name the submarine groundwater discharging from land "terrestrial" (and not fresh) SGD in this study.

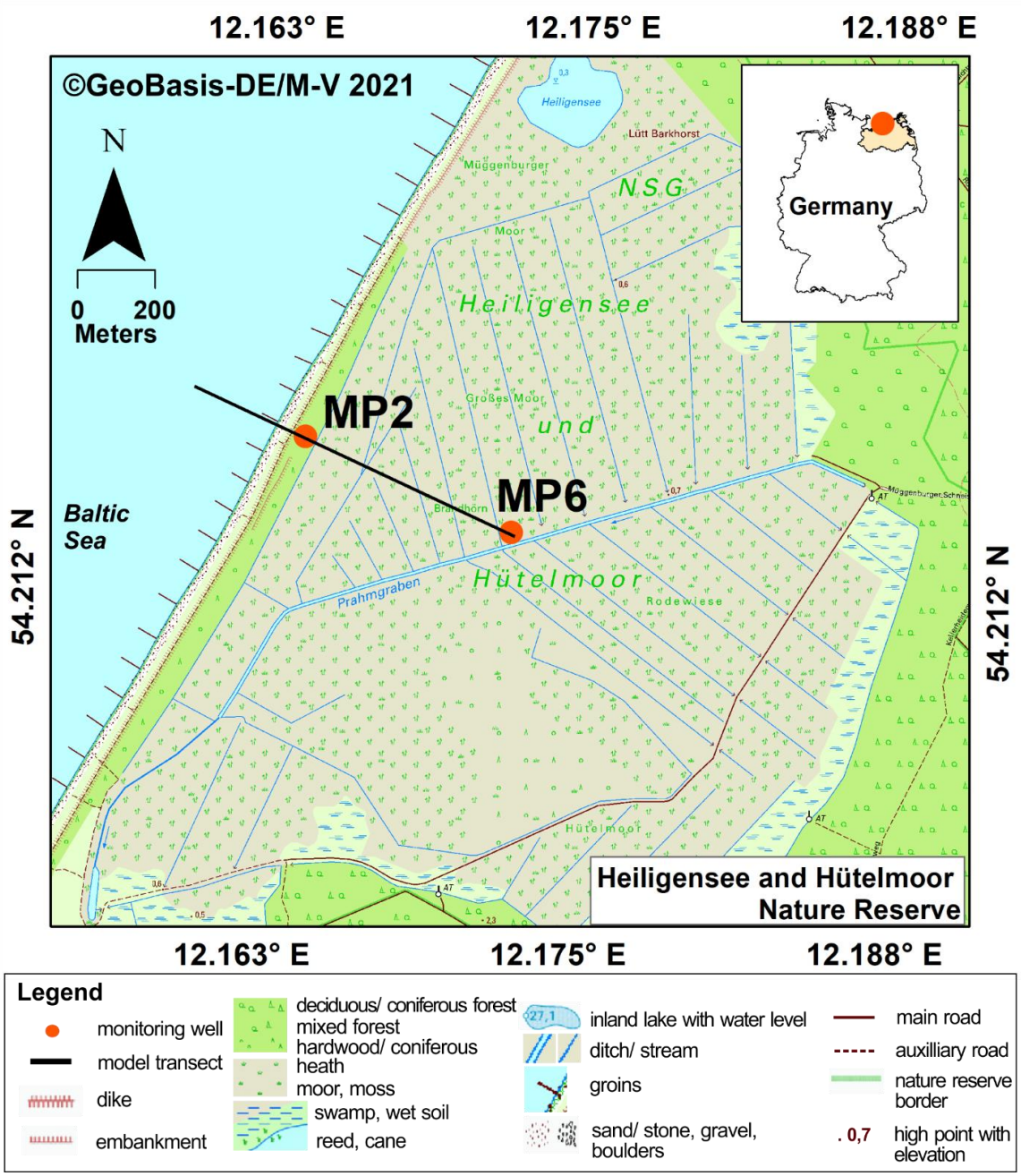

Figure 2.1. The nature reserve „Heiligensee und Hütelmoor", in Mecklenburg-Western Pomerania, Germany. The black line indicates the transect for the 2D groundwater model. MP2 and MP6 are groundwater observation wells. A groundsill was installed at the outlet of the ditch system in December 2009, restricting the drainage function of the ditches to high water levels. The background topographical map was taken from https://www.laiv-mv.de/Geoinformation/Karten/Topographische-Karten/.

2.2.2 Approach for Modelling Terrestrial SGD

We simulated terrestrial submarine groundwater discharge in the Hütelmoor using the HYDRUS-2D modeling package. HYDRUS simulates water movement in variably saturated media by solving the Richards equation for Darcian water flow:

Equation 2.1

$$\frac{\partial \theta}{\partial t} = \frac{\partial}{\partial x_i}\left[K\left(K_{ij}^{A}\frac{\partial h}{\partial x_j} + K_{iz}^{A}\right)\right] - S$$

where θ is the volumetric water content, h is pressure head, x_i are spatial coordinates, t is time, S is the sink term, K_{iz}^{A} are components of anisotropy tensor $K_{\square}^{A}$, and K is unsaturated hydraulic conductivity (Šimůnek, et al., 2018). The equations are solved using the Galerkin-type linear finite elements method which can be discretized spatially and temporally. An iterative process is used to solve the equations due to the non-linear nature of the Richards equation (Šimůnek et al., 2018).

HYDRUS can simulate the flow of water both in the unsaturated dune dike and the fully saturated peatland. The reference scenario comprises a 2D cross-section reaching from the central part of the Hütelmoor Nature Reserve peatland into the shallow Baltic sea (Figures 2.1 and 2.2). The topography, geological stratification, material properties, and boundary conditions were based on measured data, and steady-state groundwater fluxes were simulated to yield a long-term average of terrestrial SGD. Fluxes originating from aquifer, peat, and dune were quantified separately. In subsequent model runs, these factors were changed one by one based on actual and realistic predicted conditions, to determine their respective impacts on SGD.

Water inflows (Figure 2.2 - blue arrows) into the coastal peatland system come from 1) the ponded surface waters above the peat, 2) precipitation at dune dike and beach, 3) recharge from recirculated SGD at the seafloor (corresponding to Constant Pressure Head 2), and 4) lateral groundwater inflow from the landside. Outflows (orange arrows) from the system occur as evapotranspiration in the dune and the total SGD from the seafloor. Uncertainty in water flow from the sea-submerged aquifer sands (left boundary) makes it either an inflow or outflow region. Infiltration from ponded peatland surface waters is also expected into the dune dike.

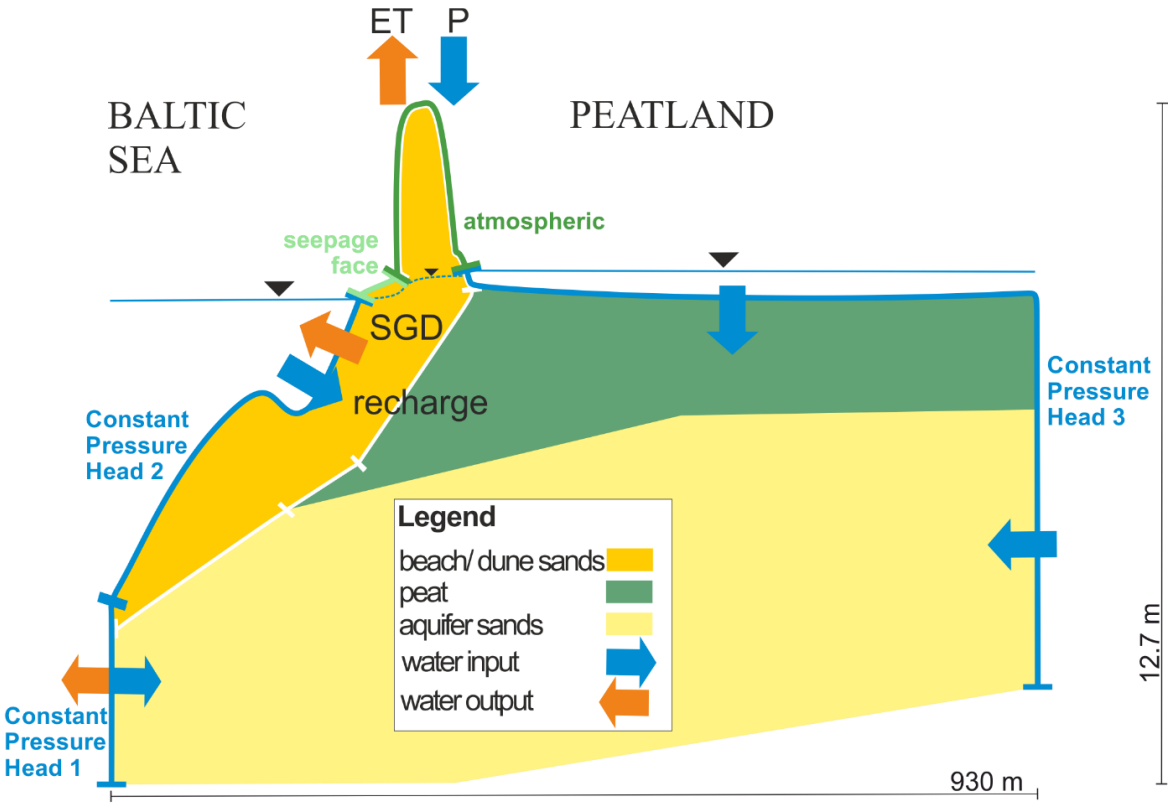

Figure 2.2. Coastal peatland system with water in- and outflows and model boundary conditions. White lines at the boundary of the beach/ dune sands are mesh lines used to calculate water fluxes. The peat extension layer is also depicted here. Note the vertical exaggeration of the cross-section.

2.2.3 Modeling Domain

We established the modeling domain (SM Figure 2.1) using published and available data. It extends from the shallow Baltic Sea to the central peatland (Figure 2.1). Elevation measurements at the groundwater observation wells (Ibenthal, 2020) and seawater level were used as reference points of the domain, while ground heights in between these reference points were obtained from a Digital Elevation Map (provided by Landesamt für innere Verwaltung Mecklenburg-Vorpommern, Schwerin, Germany) using the 3D Analyst Toolbox of ARCMap. The materials were distributed following the geological profile constructed based on sediment cores (Ibenthal, 2020; Jurasinski et al., 2018). Bathymetric data from marine surveys (Kreuzburg et al., 2018) completed the model geometry, taking note of the longshore bar mound 100 m from the coast. The modeling domain's total length is 930 m, of which 245 m extend into the sea. In the vertical direction, it extends from 3.7 masl at the top of the dune dike to -9 masl at the aquifer bottom. The bottom boundary follows the surface of the glacial till.

The modeling domain's discretization was carefully scrutinized and yielded a final target size of 1.0 m, x-direction stretching factor of 25, and a smoothing factor of 1.8. To account for the highly non-linear water flow in the unsaturated zone of the dune dike, a surface mesh refinement of 0.05 m was applied in the upper beach/dune sands. Surface refinements of 0.2 m and 0.5 m were also applied at the lower beach/ dune sands and

peat materials, respectively. A total of 3,454 nodes resulted from this configuration with 351 nodes and 351 elements on the domain boundary.

2.2.4 Model Runtime

The maximum model runtime was set at 360 days. All simulations achieved steady-state in the given runtime except for the minimum beach/ dune K_s scenario, where runtime was increased to 720 days. Initial, minimum, and maximum time steps were set at 0.01 d, 0.001 d, and 5 d, respectively.

2.2.5 Soil Hydraulic Parameters

We applied the single-porosity van Genuchten-Mualem model. Soil hydraulic properties of the reference scenario (Table 2.1) were derived from soil data gathered previously at the study site. For soil texture of the aquifer sands and beach/ dune sands, average particle size distributions were calculated from 34 and 6 soil samples, respectively. The resulting composition of aquifer sands was 89.4% sand, 7.5% silt and 3.1% clay. The beach/ dune sands were sandier with 98.3 % sand, 0.9% silt and 0.8% clay. Soil hydraulic parameters were then generated using the neural network prediction "Rosetta" incorporated into the HYDRUS software (Schaap et al., 2001). Peat hydraulic parameters were calculated with the pedotransfer functions for sedge bulk density of ≤ 0.2 g cm^{-3} proposed by Liu & Lennartz (2019a), based on measured bulk density ranging from 0.12 to 0.15 g cm^{-3} in the peatland (L. Gosch, personal communication, August 23, 2019) and 0.17 g cm^{-3} in the peat exposed at the coastline (Gosch et al., 2019). The residual water content for peat was assigned a value of 0.2. For the tortuosity and pore-connectivity parameter (l), a value of 0.5 is acceptable for degraded fen peat under wet or saturation conditions (Dettmann et al., 2014; Liu & Lennartz, 2019a) as well as for sands, as this is the average value for most soils based on calculations by Mualem (1976) (Simunek et al., 2018). For the peat and aquifer sands, saturated hydraulic conductivities, values determined with slug tests at the study site were used (Ibenthal, 2020); the resulting K_s values (geometric means) are 8.64 x 10^{-3} m d^{-1} for the peat (n = 4) and 1.73 m d^{-1} for the aquifer sands (n = 4). Dune K_s of 11.8 m d^{-1} (n = 8) was laboratory-determined on samples taken in the northern part of the dune and was adapted from a previous study (Mohawesh et al., 2017).

Table 2.1. Soil hydraulic parameters used in the standard scenario.

Name	Q_r (m^3 m^{-3})	Q_s (m^3 m^{-3})	α (m^{-1})	N	K_s (m d^{-1})	l
Beach/ Dune Sands	0.05150	0.37662	3.39265	4.04174	11.8100	0.5
Peat	0.20000	0.88000	2.90000	1.22000	0.00864	0.5
Aquifer Sands	0.04644	0.38180	3.72309	2.52943	1.73000	0.5

Q_r = residual water content; Q_s = saturated water content; α and n = parameters in the soil water retention function; K_s = saturated hydraulic conductivity; l = tortuosity parameter in the conductivity function

2.2.6 Boundary and Initial Conditions

The model boundary conditions (BC) were set as follows (see also Figure 2.2): Atmospheric BC was applied to the dune surface wherein long-term averages of meteorological variables were used (average precipitation: 1.90 mm d^{-1}; average

evapotranspiration: 1.65 mm d^{-1}) (Rostock-Warnemünde 1951-2010; Miegel et al. 2016). At the beach, a seepage face BC was applied which switches to atmospheric BC in the absence of seepage. However, no seepage was observed across the seepage face in any of the simulations. In HYDRUS, 'seepage face' refers to the boundary condition applied in surfaces where water leaves the saturated part of the flow domain. Constant head BCs in hydrostatic equilibrium were set on the left side (Constant Pressure Head 1) and at the seafloor (Constant Pressure Head 2), the pressure head corresponds to the average sea water level at Warnemünde, Rostock (2005-2015) of 0.091 masl (ITZBund, 2020). Likewise, the right-side boundary (Constant Pressure Head 3), which continues to the peatland surface, was assigned a constant BC in hydrostatic equilibrium, corresponding to the average peatland water level of 0.357 masl (September 2016 to October 2018; derived from 73,735 individual 15-min interval measurements; converted to equivalent freshwater heads). No flux was assumed at the bottom as the glacial till was considered impermeable.

Initial pressure heads were set to correspond with the constant head boundary conditions. As such, the initial bottom pressure head amounted to 9.357 m. A slight slope (0.05˚, x-direction) from the sea up to behind the dike was added because of pressure head differences. The peatland's ponded conditions have a higher pressure head compared to the seawater on the left side. The angular slope was not applied in sea level scenarios as the hydraulic gradient's difference was only 0.001 m.

2.2.7 Uncertainty Analysis

Most groundwater bodies are heterogeneous with hydraulic conductivity variability influencing groundwater transport (Peña-Haro et al., 2011). In peat soils, it has been shown that a heterogeneous hydraulic conductivity distribution can lead to complex groundwater flow patterns (Beckwith et al., 2003). Since our simulations are based on homogenous hydraulic conductivities in the three materials considered, uncertainty of the model outcome resulting from the variability of K_s cannot be assessed. To address this, we performed 100 extra simulation runs with random K_s values (SM Table 2.1). The number of replicates of the K_s measurements was too small to derive distributions (aquifer, peat), or samples were only taken from a single site (beach/dune K_s). We therefore additionally analyzed K_s values calculated from particle size distributions following Beyer (1964) both for the aquifer (n = 34) and the beach/dune sands (n = 6). The geometric means were close to the ones of the measured K_s values. All K_s values were then $\log_{10}$-transformed. Random numbers were drawn from normal distributions with means based on the measured values, and the standard deviations of the Beyer-derived values.

For the peat K_s, the coefficient of variation reported by Baird (1997) for a degraded peat was used to calculate the SD. Other published datasets for fen peat (Liu et al., 2016; Wang et al., 2021) were not considered because of much higher K_s values. The $\log_{10}$ mean and SD were then used to generate the random K_s values. In SM Table 2.1, a descriptive statistics summary of the random K_s values is listed.

2.2.8 Scenarios

To investigate the factors that affect the magnitude and location of terrestrial SGD from coastal peatlands, three clusters of scenarios were analyzed: 1) soil physical properties,

2) hydraulic gradients and, 3) geological stratification and topography (Table 2.2). The parameters were changed one at a time to better determine their individual impacts on SGD.

Soil physical properties

We investigated the effects of different magnitudes of material K_s and peat anisotropy. The peat K_s in the reference scenario is similar to mesic-humic peat in a peatland-pond system (Ferone & Devito, 2004) but lower than the average K_s for peatland sedges compiled in a meta-study (2.24 x 10^{-1} m d^{-1}; Liu & Lennartz, 2019a). To picture a realistic range of potential peat K_s in coastal peatlands, the minimum, maximum and geometric mean of sedge peat K_s reported by Liu & Lennartz (2019a) was used as well as mean ± one standard deviation of the log-transformed K_s. For the aquifer and beach/dune sands, K_s values were estimated from particle size distributions described previously. For the beach/ dune sands, though, the aquifer sand K_s value of the reference scenario (1.73 m d^{-1}) was used as the minimum value.

Anisotropy of K_s has been reported repeatedly in peat (Wang et al., 2020), with fen peats showing a higher K_s either in vertical or horizontal direction depending on peat type (Liu et al., 2016). Wang et al. (2020) reported anisotropy in two fens with K_s in the vertical direction being larger than the horizontal direction ($K_{sv} > K_{sh}$) by a factor of six. Liu et al. (2016) described anisotropy with the higher flow in the horizontal direction by factors of up to seven. However, vertical flow was higher by a factor of 14 in one sample. Therefore, we examined the anisotropy's effect in both the vertical and horizontal direction, with factors ranging from three to fourteen.

Hydraulic gradients

To analyse the effect of changing water levels in peatlands on terrestrial SGD, we used the minimum and maximum values measured during a three-year well monitoring period. The mean ± one standard deviation was also used to depict intermediate peat water levels. Furthermore, a 0.090 masl peat water level, similar to sea level, was simulated.

Investigated seawater levels were based on sea-level rise scenarios (BACC II Author Team, 2014; Grinsted et al., 2015). A global mean sea level rise mid-range estimate of +0.70 m is expected. We took this as the maximum value and divided it into five equal increments. We assumed that the peatland water level will rise in response to rising sea levels, so that the peatland water level was set equal to the sea level (hydraulic head = 0.001 m).

Geological stratification and topography

Geological stratifications, changing profiles, and the topography could also influence the magnitude and location of groundwater across the seafloor. Changing the thickness of the peat and aquifer sands layers plays a major role in water transport due to their relation to hydraulic conductivity. Here, the original peat thickness of 2.2 m was varied from 0.3 m up to 5 m - from the minimum peat depth for soils to be considered a mire based on the German soil classification system (Trepel et al., 2017), to thick fen peats. On average, peat layers are often assumed to be between 1.5 – 2 m (Zauft et al., 2010). As a response

to the changing peat thickness, the upper limit of the aquifer sands also changed, while the lower limit was kept constant. However, to determine the impact of the aquifer sands thickness alone, simulations of 1 – 5 m thick aquifer sands with a constant peat thickness were also performed.

In the Hütelmoor and other coastal peatlands, it has been observed that the peat layer extends below the dune dike and beyond the shoreline, sometimes with outcropping peat in shallow waters. To examine the impact of varying seaward peat extension, the peat layer ended under the shoreline in the minimum scenario and was extended until the left border of the modeling domain in the maximum scenario. We also simulated scenarios of various seafloor depths ranging from -4.1 to 0.0 masl to represent coastal areas with broader and shallower nearshore zones. An additional scenario of the same seafloor geometry as the reference scenario without the longshore bar at 100 m from the shore was also simulated.

Scenarios for changing the topography of the study area were conducted by altering the man-made dike height and the peat elevation. The dike height was incrementally decreased by 0.7 m from 3.7 m up to 0.8 masl. Concurrently, peat elevation was raised from its current height of 0.0 masl in the middle of the peatland to 0.5 masl, which is a realistic value for more natural peatlands. The 0.357 masl peat water level was kept constant in this set of simulations to determine the effect of the topography alone.

Table 2.2. Steady-state scenarios used in the modeling.

Scenario Cluster	Specific Scenario	Values Used
Soil Physical Properties	Peat hydraulic conductivity (K_s) (m d^{-1})	**0.00864** (0.000408, 0.0339, 0.224, 1.48, 17.4)
	Aquifer Sand K_s (m d^{-1})	**1.73** (0.429, 2.20, 3.94, 7.06, 10.7)
	Beach/ Dune Sands K_s (m d^{-1})	**11.8** (1.73, 6.90, 19.8, 56.5, 66.1)
	Anisotropy of K_s (K_{sh}/ K_{sv})*	**1.00** (3.00, 5.75, 8.50, 11.2, 14.0)
	Anisotropy of K_s (K_{sv}/ K_{sh})	**1.00** (3.00, 5.75, 8.50, 11.2, 14.0)
Hydraulic Gradients	Peatland water level (masl)	**0.36** (-0.40, 0.09, 0.12, 0.59, 0.82)
	Sea level (masl)	**0.09** (0.23, 0.37, 0.51, 0.65, 0.79)
Geological Stratification and Topography	Thickness of peat layer and aquifer sands (m; mid-peatland)	**2.2+6.0** (0.3+7.9, 1.0+7.2, 3.0+5.2, 4.0+4.2, 5.0+3.2)
	Thickness of aquifer sands# (m; mid-peatland)	**6.0** (1.0, 2.0, 3.0, 4.0, 5.0)
	Seafloor depth (masl)	**-5.5** (0.0, -1.4, -2.7, -4.1, -5.5 (without longshore bar))
	Seaward peat extension (m)	**90** (0, 45, 135, 180, 245)

	Peatland surface elevation (masl; mid-peatland)	**0.0** (0.1, 0.2, 0.3, 0.4, 0.5)
	Dike height (masl)	**3.7** (3.0, 2.3, 1.5, 0.8, 0.1)

*K_{sv} = hydraulic conductivity in the vertical direction, K_{sh} = hydraulic conductivity in the horizontal direction; #changed by raising the lower boundary of the aquifer, while the boundary to the peat remained constant

2.2.9 Quantification of Terrestrial SGD

HYDRUS calculates flow velocities for each of the nodes and reports integrated fluxes across boundaries. Terrestrial SGD was assumed to be equal to the flux across the Constant Pressure Head 2 boundary, which extends across the entire seafloor (Figure 2.2). The net flux of recirculated seawater across this boundary is zero under steady-state conditions. The terrestrial SGD comprises all the water from the peat, aquifer sands, and beach/ dune sands that come out as submarine groundwater discharge. Water fluxes from each of the different materials were determined using mesh lines in the material boundaries (Figure 2.2); fluxes across mesh lines are calculated by HYDRUS in the same way as those across the boundary conditions.

Discharge and recharge regions in the seafloor were identified by looking at velocity vectors and streamlines, both of which are outcomes of HYDRUS graphic user interface post-processes. After identification of discharge and recharge regions, we added meshlines to these regions to quantify water fluxes separately. Discharge determined from these regions can be defined as “total SGD”, since it includes both terrestrial and recirculated SGD. However, caution should be taken when interpreting total and recirculated SGD as the model does not consider marine forcings such as waves. The calculated fluxes across boundaries or mesh lines are reported in $m^2\,d^{-1}$. To determine the seepage rate from the seafloor ($m\,d^{-1}$), the fluxes were divided by the total length of the respective boundary or mesh line.

2.3 Results

2.3.1 Flow Patterns and Location of SGD in Coastal Peatlands

Reference Peatland

Submarine groundwater discharge has been observed in two separate areas of the seafloor in the reference simulation (Figure 2.3A). Firstly, SGD is released in the upper 0.6 m water depth over a distance of 10 m from the shoreline into the sea (upper discharge region). Here, water originates from (1) atmospheric input to the dune and the beach and (2) peatland surface water that infiltrated into the dune base, as deduced from velocity vectors. Water flows from the dune base into the beach sands and towards the Baltic Sea, following the hydraulic gradient. The underlying peat acts as an aquitard due to its low hydraulic conductivity, limiting the infiltration of surface water and groundwater flow.

The lower discharge region is located at 1.4 – 1.7 m depth (length ~ 15 m), with water coming from the sand aquifer. Flowing particles (user-defined particles showing trajectory and position through time) were observed to cross from the aquifer sands through the

thinly buried peat layer and to the beach/ dune sands (SM Figure 2.2A). In between the two described discharge regions, areas with seawater recharge are found, contributing to the overall SGD flux. No seepage from the beach occurred.

Scenarios

Among all scenario simulations, two different patterns of SGD were observed with either two discharge regions (as in the reference peatland) or one discharge region (Figure 2.3B, 3C). However, most submarine groundwater appears to discharge in the upper 0.6 m of the seafloor based on velocity vectors.

The two-discharge-region pattern seems to form when there is considerable water flow from the aquifer (due to higher aquifer K_s than minimum value, increased aquifer thickness) or when the hydraulic gradient is large. The pattern is maintained when beach/dune K_s, peat K_{sh}/K_{sv} ratio, seafloor depth, peat elevation, and dike height are varied. In all those scenarios, the general groundwater discharge pattern remains similar to the reference peatland mainly due to the strong impact of the peat layer extending towards the sea. However, the lengths of the discharge regions may differ between the simulations. For example, the upper discharge region is smallest for the shallowest seafloor scenario, where SGD is limited to a few meters near the shore.

The single discharge region, located in the upper seafloor, occurs whenever the influence of the peat layer extending to the sea to act as a barrier is either diminished (upper and lower discharge regions merge) or amplified (development of lower discharge region is impeded). For instance, larger peat K_s than the reference (Figure 2.3B) or peat K_{sv}/K_{sh} ratios > 3 reduce the barrier effect of the peat extension layer. Thus, both the dune and aquifer flow pathways merge in the beach sands to a one-discharge area. In contrast, increasing peat thickness and continuing the peat layer (Figure 2.3C) farther under the Baltic Sea magnify the barrier effect of the peat layer, and upflow of water from the aquifer to the seafloor is prevented. Furthermore, a decrease in aquifer flow due to a decrease in aquifer thickness leads to a single discharge-region flow pattern.

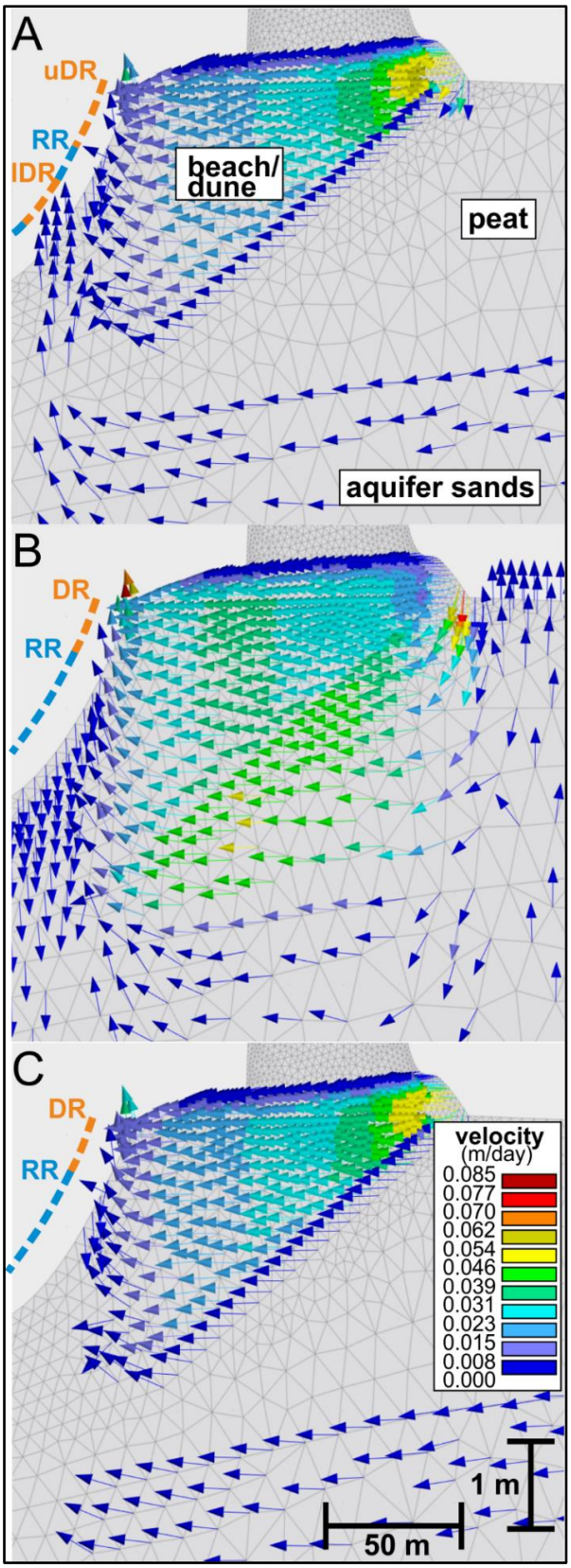

Figure 2.3. Groundwater flow paths of the reference and selected scenarios illustrated using velocity vectors, in subset of the modelling domain. From top to bottom: (A) reference, (B) peat K_s max, (C) peat extension max. Discharge (DR) and recharge regions (RR) are indicated with orange and blue dashed lines, respectively. The upper (uDR) and lower (lDR) discharge regions are shown in panel 3A.

2.3.2 SGD Fluxes from Coastal Peatlands

Reference Peatland

Water inputs into the modelling domain mainly originate from infiltration at the dune dike base and peat surface and the lateral groundwater inflow (these latter two cannot be distinguished), while atmospheric input at dune and beach is less important (Figure 2.4). Outputs are terrestrial SGD across the seafloor and a minimal groundwater outflow through the sea-submerged aquifer sands on the left boundary of the modeling domain.

Looking at the simulated terrestrial SGD flux across the seafloor, our long-term average SGD is 0.080 $m^2\ d^{-1}$ (0.056 L $min^{-1}\ m^{-1}$) (Figure 2.5). Upscaled total terrestrial SGD for the entire 3-km coastline of the Hütelmoor is estimated to be 240 $m^3\ d^{-1}$, or 168 L min^{-1}. We evaluated the uncertainty of the reference scenario's SGD based on the combination of random K_s for the three materials, due to its high variability in nature. The boxplot in Figure 2.5 presents the uncertainty analysis results (see also SM Table 2.1). The median SGD of the 100 simulation runs is 0.083 $m^2\ d^{-1}$ and thus close to the value of the reference scenario. The lower and upper bounds are 0.038 $m^2\ d^{-1}$ and 0.195 $m^2\ d^{-1}$.

The seepage rate calculated separately for both observed discharge regions revealed that discharge is distinctly higher near the shore. Most SGD flows out in the upper discharge region with a flux of 0.106 $m^2\ d^{-1}$ and a corresponding seepage rate of 0.0105 m d^{-1} (Table 2.3). An additional but vitally lower flux of 0.023 $m^2\ d^{-1}$ (seepage rate: 0.0016 m d^{-1}) is found in the lower discharge region. The seafloor's average seepage rate is 0.0033 m d^{-1} based on the terrestrial SGD flux of the whole seafloor and the lengths of the discharge regions. Average discharge flux (0.128 $m^2\ d^{-1}$) and seepage rate (0.0052 m d^{-1}) calculated from the two discharge regions are slightly higher than the terrestrial SGD flux across the seafloor, which is due to the additional input of recirculated SGD from the recharge regions. Still, we are able to show here that most terrestrial SGD occurs in the upper seafloor with minor flux arising from the thin section of the peat extension.

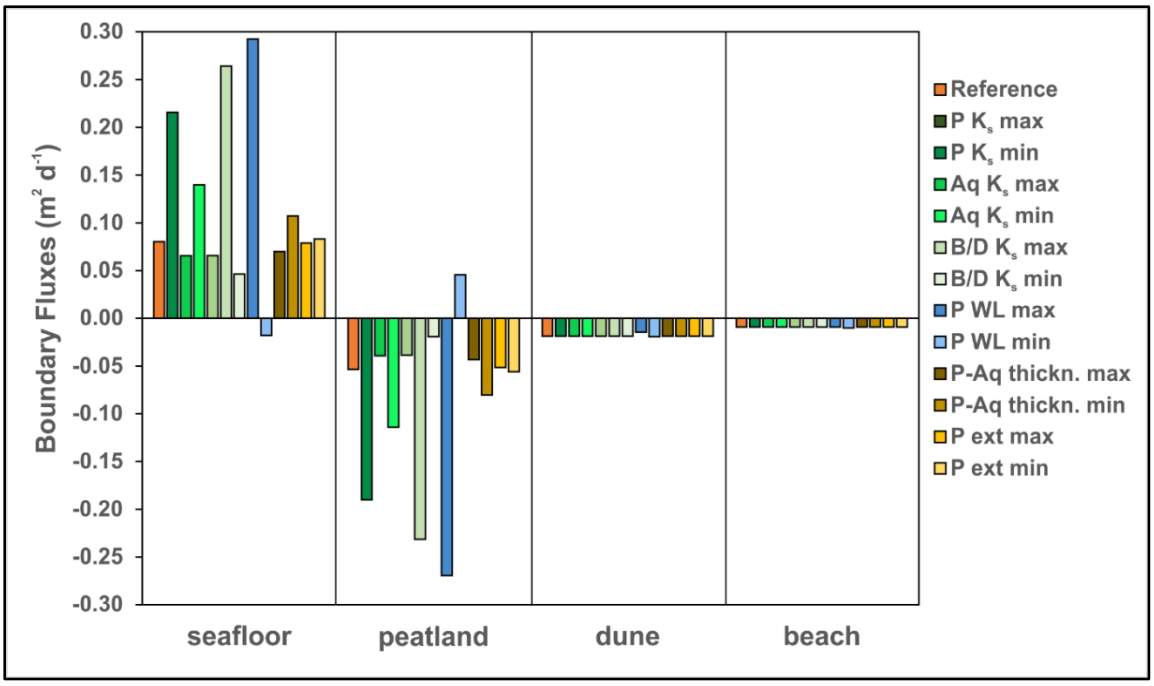

Figure 2.4. Net boundary fluxes of the reference scenario (orange) and selected scenarios of soil physical properties (green shades), hydraulic gradients (blue shades), and geological stratifications (yellow shades). For location of boundaries, see Figure 2.2 (seafloor ≙ Constant Pressure Head 2; peatland ≙ Constant Pressure Head 3; dune ≙ atmospheric; beach ≙ seepage face). Fluxes from the left boundary (Constant Pressure Head 1) were not included due to low values (10^{-4} to 10^{-6} m^2 d^{-1}). Notations: P: peat, Aq: aquifer, B/D: beach/dune, WL: water level, ext: extension.

Table 2.3. Fluxes across specific discharge and recharge regions.

	Flux (m^2 d^{-1})	**Length (m)**	**Seepage rate (m d^{-1})**
Upper Discharge Region	0.106	10.0	0.0105
Lower Discharge Region	0.023	14.6	0.0016
Total Discharge	**0.128**	**24.6**	**0.0052*** **0.0033#**
Upper Recharge Region	-0.036	12.0	-0.0030
Lower Recharge Region	-0.017	208.5	-0.0001
Total Recharge	**-0.053**	**220.5**	**-0.0002**

*based on SGD flux of discharge regions

#based on terrestrial SGD flux of total seafloor

Range of SGD Expected from Coastal Peatlands

In nearly all scenarios, the majority of the water inputs come from the peatland with only minor atmospheric inputs from the dune and beach (Figure 2.4). The water input through the peatland increases with large hydraulic conductivity or gradient, while the atmospheric input remains constant.

The SGD fluxes simulated in the various scenarios range from 0.008 to 0.293 m^2 d^{-1}, corresponding to 10 to 360% of the reference scenario's flux (Figure 2.5). In one scenario

– with low peatland water level – a flow reversal was observed, i.e., seawater intrudes with a flux of -0.019 m^2 d^{-1}. The largest SGD flux is observed in the maximum water level scenario, and also the maximum K_s for peat and beach/ dune sands yield large fluxes (270 and 330% of reference, respectively). The effect of the aquifer sand K_s is less pronounced, with SGD fluxes amounting to 80–170% of the reference, but still considerably more than that of the other factors. All sea level rise simulations recorded minimal SGD fluxes (0.008–0.048 m^2 d^{-1}; 10– 60%). Peat anisotropy (0.081–0.104 m^2 d^{-1}; 101–130%), peat-aquifer thickness (0.070–0.107 m^2 d^{-1}; 87–134%), aquifer thickness (0.059–0.075 m^2 d^{-1}; 73–94%), seafloor depth (0.079–0.081 m^2 d^{-1}; 98–101%), peat extension (0.079–0.083 m^2 d^{-1}; 98–104%), and dike height (0.081–0.091 m^2 d^{-1}; 100–113%) have little impact on the SGD flux. Most of the simulated SGD fluxes fall within the range of values obtained from the K_s-based uncertainty analysis, where a minimum and maximum SGD flux of 0.038 m^2 d^{-1} and 0.493 m^2 d^{-1} were determined, respectively. The beach/ dune sands K_s is highly linearly correlated with SGD (R^2 = 0.9837) in the uncertainty analysis, while peat K_s (R^2 = 0.016) and aquifer sands K_s (R^2 = 0.0356) are not (Figure 2.7).

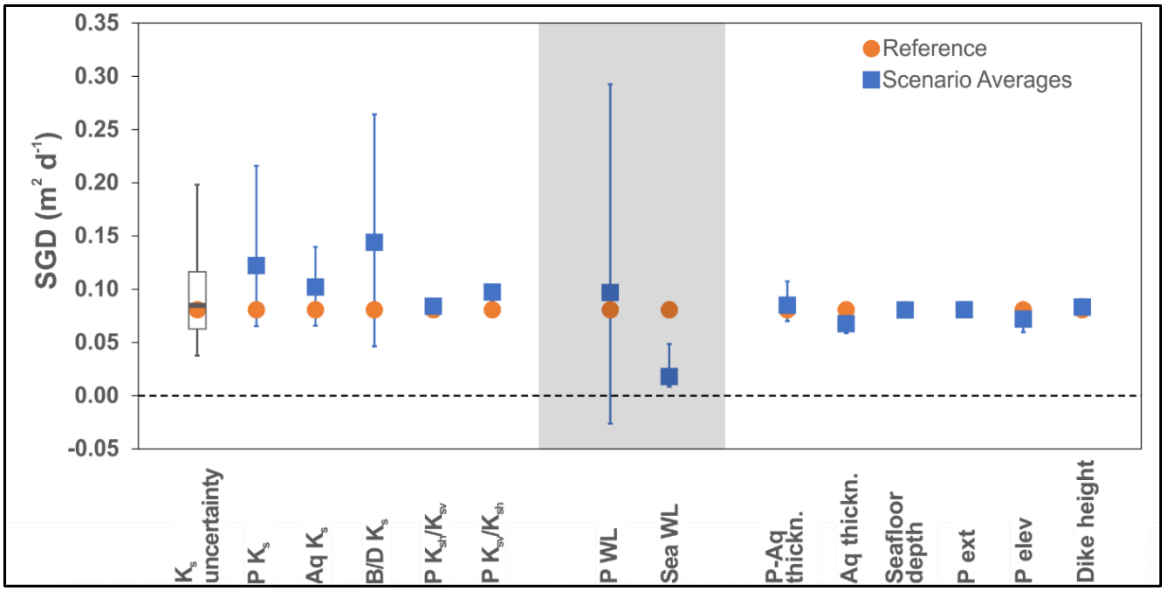

*Figure 2.5. Range of submarine groundwater discharge in different scenarios with results of K_s uncertainty analysis (boxplot). Blue boxes are averages of the scenario simulations and the error bars represent the range. Error bars of uncertainty analysis represent the upper and lower bounds based on ±1.5*Interquartile Range. The reference scenario flux is represented here in orange dots. The shaded area separates the three groups of properties. Notations: P: peat, Aq: aquifer, B/D: beach/dune, WL: water level, ext: extension.*

Origin of SGD Flux

To better understand the SGD flow and magnitude patterns in a coastal peatland system, we determined the source of terrestrial SGD (Figure 2.6). For this purpose, fluxes from different subsections of the materials (dune, beach, main peat body, thin peat extension, aquifer) to the beach sands were quantified in selected scenarios using meshlines (Figure 2.2). Positive fluxes are inputs and contributors to the beach sands while negative fluxes represent outflow of water (Figure 2.6). The sum of these fluxes should be equal to the terrestrial SGD determined at the seafloor boundary. The reference peatland has a 2.4%

accuracy. However, we observed deviations ranging from -13 to 9 % in other scenarios. This can be attributed to the fact that nodes at the edges of meeting meshlines are considered for flux calculations across both meshlines.

In the reference peatland, most of the terrestrial SGD comes from the dune dike (0.054 m^2 d^{-1}; 63%), recharged by precipitation (1/3) and infiltrating peatland surface waters (2/3), and the beach (0.0092 m^2 d^{-1}; 11%). The remaining part of the SGD originates from the aquifer, but flows upward through the thin, buried peat extension layer under the seafloor (0.022 m^2 d^{-1}; 26%). No discharge was observed from the main peat body, or directly from the aquifer into the marine sediments.

In the scenarios, the relative contributions of dune, beach, and aquifer to the terrestrial SGD vary as a function of soil properties and hydraulic gradient: With a high aquifer K_s, the aquifer (via the peat extension) gains in importance, while a low peatland water level or low K_s of peat or aquifer enhance the contribution from the dune. The relative contributions only increased/ decreased by 3% for the peat extension scenarios compared to the reference scenario. The share of the dune and beach varies from 41 to 89%.

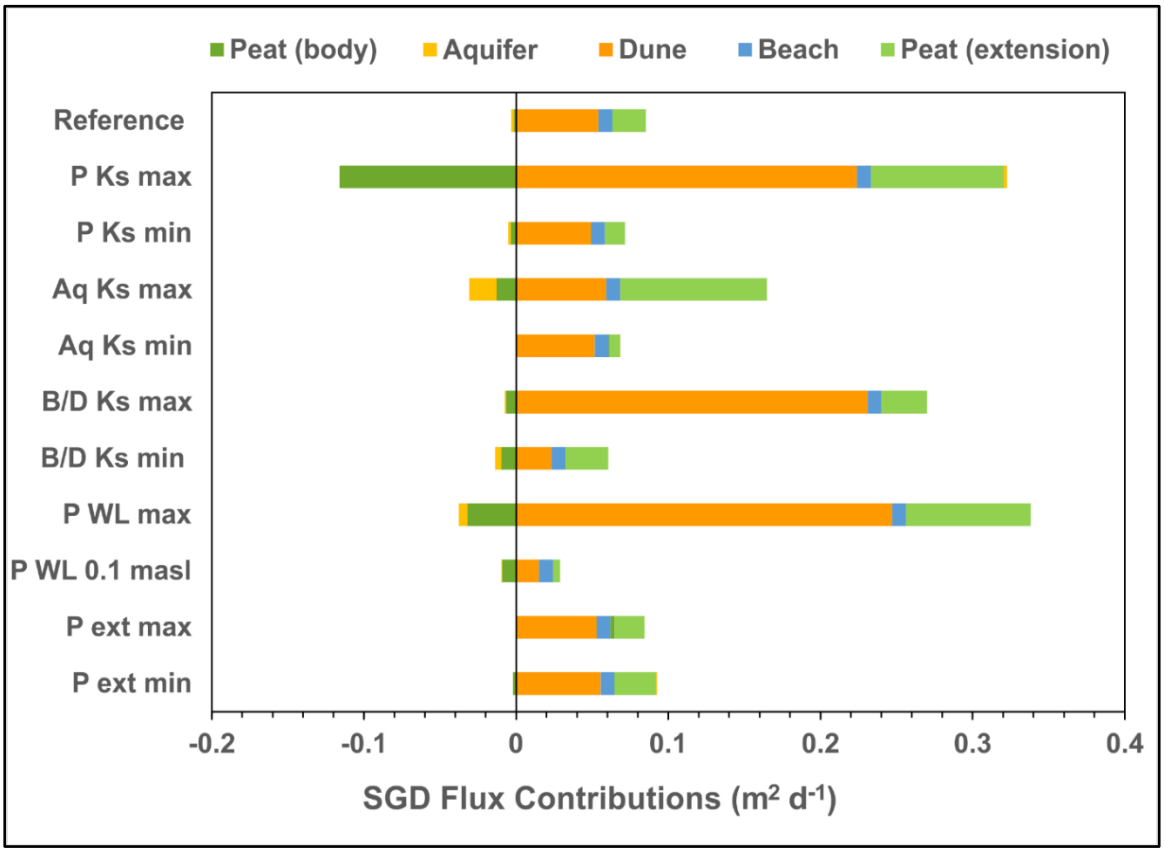

Figure 2.6. Contributions from the dune, beach, peat body, peat extension, and aquifer sands to the submarine groundwater discharge for selected scenarios. Positive fluxes are inputs while negative fluxes represent output of water from the beach sands. In P K_s max scenario, a large volume of water infiltrated the dune dike and then, water flowed down to the peat body.

2.4 Discussion

2.4.1 SGD Flux from Coastal Peatland

The upscaled total terrestrial SGD for the entire 3-km coastline of the Hütelmoor is 240 m^3 d^{-1}. Lower and upper limits of estimates based on K_s uncertainty are 114 m^3 d^{-1} and 596 m^3 d^{-1}, respectively. The results are slightly higher than previous terrestrial SGD estimates from the same study site with 15–164 m^3 d^{-1} (Miegel et al., 2016) and 180 m^3 d^{-1} (Ibenthal, 2020), which were calculated using water balance equations of the contribution of peat and aquifer sands (Miegel et al., 2016) and MODFLOW 3D numerical simulations including the dune sands (Ibenthal, 2020).

Comparing with other wetland environments, our average seepage rate of 0.33 cm d^{-1} is comparable in magnitude to a mudflat in China (Qu et al., 2017) and lower estimates of a tide-dominated coastal wetland in Taiwan (Hsu et al., 2020) (Table 2.4). However, it is expectedly lower than seepage rates from crab burrows-influenced tropical mangrove systems in Australia due to preferential flow pathways (Tait et al., 2017) and from a subtropical estuarine creek adjacent to a dune-wetland system (Sadat-Noori et al., 2015). The seepage rate near the shore (1.05 cm d^{-1}) is comparable to rates observed in sandy beaches (Kotwicki et al., 2014; Qu et al., 2017) and a sandy pockmark (Virtasalo et al., 2019) in the Baltic Sea. This result may be explained by the fact that terrestrial SGD could also be generated from small dune dike systems with additional inputs from infiltrating peatland surface waters. However, it should be noted that our average seepage rate represents terrestrial SGD only while seepage rate near the shore has contributions from recirculated SGD. Fresh SGD contributes 0.01-10% of surface water runoff (Church, 1996), with recent global estimates of 0.6% (Luijendijk et al., 2020). In tide-dominated systems, a conservative estimate of fresh SGD contribution is ~5% of the total flux (Li et al., 2009; (Santos et al., 2009a): Hsu et al., 2020). Total SGD flux estimates could thus be larger with possible large inputs from recirculated SGD.

Table 2.4. Seepage rates of SGD studies from wetland environments (shaded rows) and different locations in the Baltic Sea (non-shaded).

Environment	Seepage Rate (cm d^{-1})	Time period	Remarks	Location	Method Used	Reference
Fen peatland	0.330 (0.154–0.807) 1.053	Long-term average	Terrestrial SGD only; discharge regions 0.6 m depth incl. recirc. SGD	Rostock, Germany, Baltic Sea	HYDRUS 2D simulation	This study
Wetlands with… **Sandy beach** **Mud flat** **Estuarine intertidal zone** **Tidal marsh**	7.600 0.710 0.058 0.004			Jiaozhou Bay, China	Darcy's Law	Qu et al., 2017
Tide-dominated coastal wetland	0.200–25.000 0.100–47.000	Dry season Wet season		Gaomei Wetland, Westen Taiwan	Ra, Rn, H, O isotopes	Hsu et al., 2020
Mangrove creeks	1.500–30.900	Short term	From temperate to tropics	Australia (several)	Ra tracer	Tait et al., 2017
Estuarine creek adjacent to a dune-wetland	18±5, 20±6 65±18, 84±48	Dry season Wet season	Subtropical	New South Wales, Australia	Ra tracers	Sadat-Noori et al. 2015
Muddy sediments, subseafloor aquifers	0.054 >0.900	Long-term average	Maximal discharge	Eckernförde Bay, Germany, Baltic Sea	Cl^- tracer	Schlüter et al., 2004
Sandy beach	1.000–4.000 5.000–15.000	Winter/ spring Summer/ autumn		Puck Bay, Poland, Baltic Sea	Lee-type seepage meters	Kotwicki et al., 2014
Sandy pockmark	0.400–1.200	Short term	SGD concentrated in active pockmarks	Hanko Peninsula, Finland	Rn tracer	Virtasalo et al., 2019

2.4.2 Factors Controlling SGD from Coastal Peatlands

Importance of Peat Extension Layer to SGD Flow

The prevailing two-discharge region flow pattern in the reference peatland is due to the strong impact of the peat layer extending underneath the beach. In sandy lakeshores

(Fukuo & Kaihotsu, 1988; McBride & Pfannkuch, 1975) and coastal areas (Bokuniewicz, 1992), the concentration of terrestrial SGD at the interface of land and water body is expected with groundwater discharge rapidly decreasing as the distance from the shore increases. The distribution is affected, though, by aquifer heterogeneity and sediment hydraulic conductivity, which may vary over several orders of magnitude (Taniguchi et al., 2003). In this study, the occurrence of a lower SGD region is due to the barrier function of the peat extension layer, interrupting the flow field because of its hydraulic properties. This parallels offshore SGD originating from aquifers that have been confined by a low permeability material (Kooi & Groen, 2001; V. E. A. Post et al., 2013), which can extend several kilometers into the sea. In Sweden and Finland, groundwater has been observed to discharge from submarine terraces in siltier, more permeable portions of glacial clay at water depths of ~12 m (Jakobsson et al., 2020).

The barrier function of the peat layer interplays with its K_s, K_s anisotropy, and geological stratifications. It diminishes with larger peat K_s and K_{sv}/K_{sh} anisotropy values but is magnified with increasing peat thickness and longer extension of the peat into the sea. In a similar way that the peat extension and the main peat body restrict groundwater discharge to the sea, our model shows that the low-conductivity peat layer also hinders seawater intrusion towards the peatland. Scenarios with higher sea level did not result in the formation of a seawater wedge but rather in landward discharge behind the dune dike (SM Figure 2.2B). This pattern may be unique to ponded coastal peatlands and muddy shorelines. Thus, the peat may serve as a barrier for both groundwater discharge and seawater intrusion.

In terms of SGD magnitude, however, the peat extension layer is not important. Compared to the reference peatland, the SGD flux only decreased by 2% when the peat was extended to the left border of the modelling domain and only increased by 3% when it ended under the shoreline. Nonetheless, more peat material extending into the sea in the groundwater-seawater mixing zone may still be significant for material transport and biogeochemical processes (see below).

K_s and Hydraulic Gradient

While the peat extension layer determines the discharge patterns, the hydraulic conductivity and hydraulic gradient are the main controls of the magnitude of SGD from coastal peatlands. The peat K_s influences the infiltration of surface waters into the peat and subsequent SGD generation. A low peat K_s reduces the infiltration of surface water into the peat and limits the contribution of peat and underlying aquifer to SGD. However, it might prolong ponding under transient conditions, enabling infiltration into the dune dike base that eventually flows out as terrestrial SGD. For the aquifer sands K_s, a low K_s restricts discharge from the aquifer, resulting in a single SGD region related to the dune. Meanwhile, the beach/ dune sands K_s only affects the SGD flux magnitude and not the location. The high positive correlation of the beach/dune K_s with SGD (Figure 2.7) emphasizes the role of the coastal sediments for SGD generation in coastal peatlands.

The peat and the underlying aquifer sands' properties thus affect not only groundwater flow in the peatland (Quillet et al., 2017), but also SGD magnitude and location. Large hydraulic conductivities are typically found in pristine peat, while lower values are

characteristic of degraded peatlands (Lennartz & Liu, 2019) and are related to a decrease in macroporosity due to disintegration of plant materials (Liu et al., 2016). Peat can have macropores; a single-large pore space may take up 94–99% (Rezanezhad et al., 2016), which may dominate water and solute transport (Baird & Gaffney, 2000). In marine sediments, bioturbator bivalves such as *Mya arenaria,* found in most of the Baltic Sea (Forster & Zettler, 2004), may distinctly increase K_s. A direct correlation between hydraulic conductivity and SGD rates has been observed in a study of four different types of wetlands in China (Qu et al., 2017). Moreover, it has been shown that the bottleneck for coastal groundwater discharge is the flow capacity, which is a function of permeability, thickness of permeable units, and topographic gradient (Luijendijk et al., 2020).

The peatland's water level is the most sensitive factor determining the magnitude of terrestrial SGD (Figure 2.5). While Luijendijk et al. (2020) assumed the topographic gradient as the maximum possible hydraulic gradient, the average hydraulic gradient is larger than the topographic one at our study site. This is due to the ponded peatland surface waters maintained after rewetting by a groundsill, combined with the low peat K_s and the dune dike. We can assume that the resulting hydraulic gradient is similar to pristine conditions since subsidence and peat degradation after drainage lowered surface elevation of up to 1 m at the study site. However, it is expected that sea level rise will reduce the hydraulic gradient in the future. According scenarios have shown that the water flow direction even reverses and is directed towards the peatland inside the dune body if the sea level rises above the average peatland water level, while simultaneously SGD occurs underneath (SM Figure 2.2B). This results in a decreased SGD as a function of reduced hydraulic gradients.

The data presented here is from steady-state conditions depicting long-term averages, neglecting temporal dynamics of the hydraulic gradient. In reality, both seasonal and short-term variations occur (Ibenthal 2020). For example, larger gradients in winter due to rising ground- and surface water levels will induce higher SGD rates than in summer when evaporation is high (Miegel et al., 2016). In the short term, storms and changing seawater levels cause a high variability of hydraulic gradients. These variations will not affect the average SGD but will have an important impact on solute transport in the transition zone between land and sea.

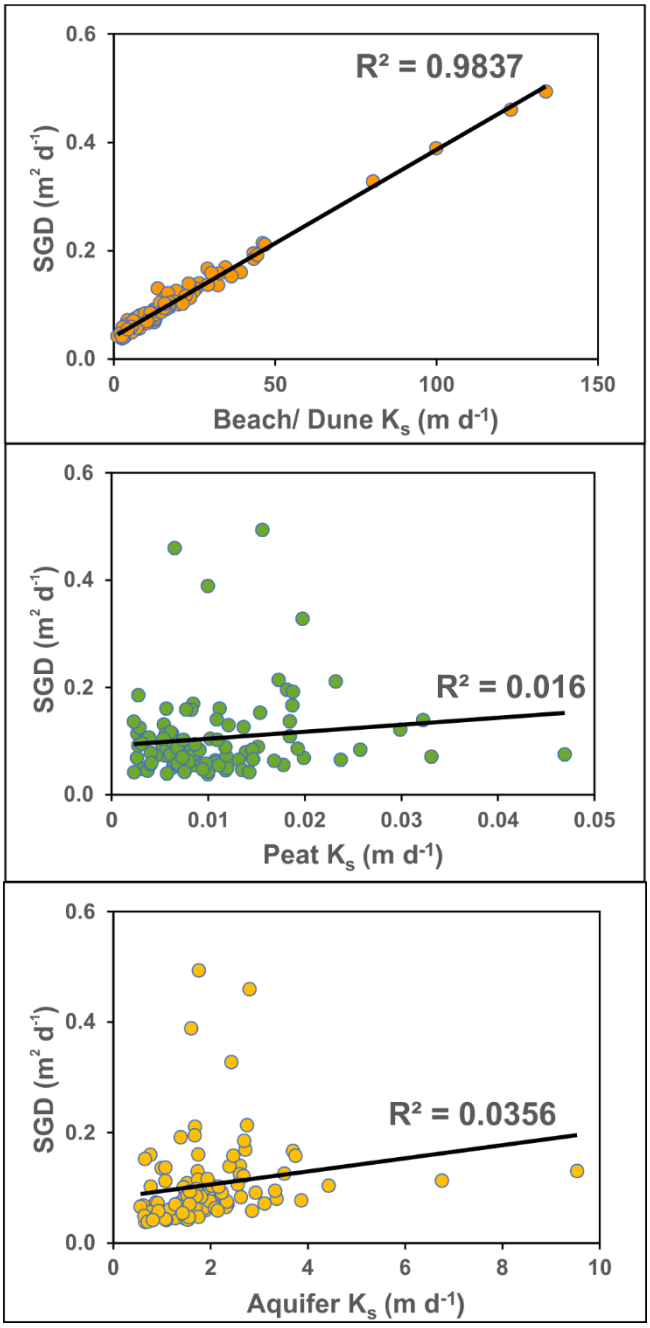

Figure 2.7. Linear regressions of SGD and material K_s, K_s data generated for uncertainty analysis. Beach/ dune sands K_s is highly correlated with SGD.

Other Factors

The remaining factors studied in this work have little impact on SGD flow and magnitude. Anisotropy of K_s, peat and aquifer thickness, and peat elevation have a relatively small impact compared to K_s and hydraulic gradient. Large peat K_{sh}/K_{sv} may only slightly enhance water flow into the peat extension but not strong enough to cancel its barrier function. Our findings are consistent with Beckwith et al. (2003), who showed that anisotropy has a smaller influence on groundwater flow patterns in peat than geological heterogeneity. Anisotropy also appeared to have a minor effect on phosphate transport than peat soil heterogeneity (Wang et al., 2020). The anisotropic angle was shown to be

highly significant for determining the landward extent of seawater in a high hydraulic conductivity homogenous aquifer (Costall et al., 2020). However, such saltwater wedge has not been observed at the study site neither in drillings nor in our simulations. Material thickness can – depending on its inherent K_s – impact SGD positively or negatively (Smith & Nield, 2003).

The impact of peat and aquifer thickness on flow and magnitude in our system is small compared to K_s and hydraulic gradient. However, we only simulated peat and aquifer sands thickness of 0.3 – 5.0 m and 1.0 – 5.0 m, respectively, typical of German coastal peatlands. In other peatlands, peat (Habicht et al., 2017) and aquifer sands (Vilumaa et al., 2017) might be thicker and may have a higher impact on SGD. Scenarios of higher peat elevation, expected in less degraded peatlands, resulted in slightly decreasing SGD because less surface water is available that can freely infiltrate into the dune dike base. However, it is also expected that less degraded peatlands will have larger K_s and thus will allow a larger volume of groundwater flow. To illustrate, a simulation of 0.4 masl peat elevation and K_s of 17.4 m d^{-1} resulted in 0.215 m^2 d^{-1} SGD flux, similar to the flux calculated from the scenario with the same peat K_s value.

Dike height and the seafloor depth do not have any distinct impact on either SGD magnitude nor location. With a shallower seafloor, only the water depth at which SGD occurs decreases, with implications for mixing into the water column. These results may be explained by the fact that the source of terrestrial SGD remains unaffected by the changes.

2.4.3 Model Limitations

This is the first time that HYDRUS-2D was used to determine SGD from a coastal peatland system, and it was able to address our objectives. The model has performed reasonably well – all scenarios have less than 1% relative mass balance error, the prescribed rate for water flow simulations. The lowest and highest relative errors were 0.01% and 0.89%, respectively.

A drawback of the model for applications at the coast is that it does not account for density-driven flow. We assume, however, that density effects can be neglected at our study site due to small density difference between the Baltic Sea and the peatland's groundwater. While the salinity of the Baltic Sea is comparably low near the study site with 11.4 psu (IOW, accessed 2020), high electrical conductivities and chloride concentrations have been recorded in the groundwater of the peatland (Ibenthal, 2020). They are rather homogeneously distributed in the peat and the underlying aquifer and are attributed to former floodings of the peatland with seawater, as has been proven with sulfur isotopes (Koebsch et al., 2019). The groundwater in the aquifer of the considered transect is decades old, as has been revealed by tritium-helium dating (Ibenthal, 2020). The densities of water samples collected between 2019—2020 from the groundwater peatland (n = 32) and dune (n = 3), from surface water (n = 15) and Baltic Sea (n = 5) were calculated for the long-term average temperature of 9.7^0 C, following Millero & Poisson (1981). Likewise, density from salinity measurements by IOW (n = 169; 1996–2018) was also calculated (SM Table 2.2). A density difference of 0.006 g cm^{-3} between Baltic Sea waters (IOW, accessed 2020) and groundwater in the Hütelmoor is more than four times lower than the

value used by Robinson et al. (2007) to simulate variable-density flow experiments. As such, less convective mixing is expected due to the lower density difference of groundwater and seawater.

The effect of density on the sea level pressure head and SGD was tested by calculating the equivalent freshwater head for a water depth of 1.0 m, where most of the SGD comes out. The calculated head difference between the reference scenario and the density-corrected head is 0.01 m, with discharge flux decreasing by only 0.002 m^2 d^{-1} (2%). We, therefore, assume that the model results are reliable despite neglecting density effects.

Furthermore, tides were not accounted for by the model, as they are assumed to be minimal at the study site. The Baltic Sea is an enclosed basin with a maximal tidal height of 23 cm (100-year period estimate) for the whole region and 6 cm in the nearby Danish straight (Medvedev et al., 2016).

2.4.4 Proposed Mechanisms for SGD Occurrence

Based on our simulations, it can be suggested that terrestrial SGD occurs more in peatlands that are (1) rewetted and diked with low peat K_s and (2) lowly-degraded peatlands with higher K_s and elevation. Future investigations on matter fluxes are thus recommended to focus on these environments.

Most coastal peatlands along the Baltic Sea are assumed to have low peat hydraulic conductivity as a result of draining and diking activities arising from agricultural use and coastal protection measures. Many of these peatlands may be rewetted in the future like the Hütelmoor since the restoration of peatlands by increasing the height of the water table is a cost-effective measure to cut down on greenhouse gas emissions (Leifeld & Menichetti, 2018). Low K_s and diking result in less infiltration of surface waters and ponding in the peatland. This water infiltrates the dune and eventually flows out as SGD. One interesting finding of this study is that most waters that come out as SGD are from the ponded surface waters.

Conversely, we can also expect SGD in peatlands that have higher elevation and are less degraded. In this setting, the peatlands have higher K_s allowing more water to infiltrate the ground, flowing into the dune and out of the seafloor as SGD. The peat extension, likely compacted due to pressure, may still hinder upflow from the aquifer sands. However, the upper peat layer will allow more groundwater to flow to the beach. Less degraded peat will also have a higher percentage of macroporosity, leading to preferential flow pathways. These observations point out the importance of land use in the past and land management activities in the future.

In both mechanisms, we have demonstrated that even a narrow dune can be important for groundwater recharge and subsequent SGD generation, as reported earlier for larger dune belts (Stieglitz, 2004; Röper et al., 2012). These results have consequences not only for the quantity but also for the quality of the discharged water, emphasizing the role of the dune and beach in total SGD flux. Taken together, our findings suggest that the dune is important for recharge and infiltration of peatland surface waters.

2.4.5 Implications for Carbon and Material Transport

It is now well-known that groundwater often has higher concentrations of carbon and materials (Moore, 2010) than its receiving body of water where it discharges. Over the last few years, organic-rich subterranean estuaries have been shown to have higher concentrations of remineralized components of organic matter, including nutrients, DOC, DIC, DOM, trace elements, reduced species such as ammonium and iron (II), and lower pH (Taniguchi et al., 2019). At our study site, DOC concentrations measured in groundwater in peat and aquifer amount to 48–490 mg C $L^{-1}$and 12–99 mg C L^{-1}, respectively, and to 38–380 mg C L^{-1} in the peatland's surface water. Our values are much higher than the previously mentioned DOC average from SGD (Szymczycha et al., 2014). While DOC may undergo several biogeochemical transformations before it is discharged to the sea, the high concentrations in peatland surface and groundwaters offer a glimpse of potential large DOC inputs via SGD. In addition, the absence of large rivers in the southern Baltic Sea could increase the importance of SGD as pathways for water and material transport.

Our study showed that a peat layer extending to the sea, and potentially cropping out, hardly influences the quantity of water fluxes. However, the peat could still be important biogeochemically. Peat from the study site has been shown to release DOC in contact with saline water (Gosch et al., 2018) and low-saline groundwater (Kreuzburg et al., 2020). Exposure of peat to water with changing salinity can promote the release of DOC and remineralized components such as CO_2 and DIC (Kreuzburg et al. 2020). As such, peat deposits along coastal zones could be potential hot spots of increased release of these materials and may be important to the release of climate-relevant gases (Kreuzburg et al., 2020). Moreover, additional geological complexities such as marine sediment bulldozing by bivalves and other groups in marine environments (Santos et al., 2012) and peat degradation and preferential solute transport on land (Liu et al., 2017) can enhance material export from coastal peatlands. Given the knowledge gaps in material transport and its abundance in the Baltic Sea, coastal peatlands warrant further scientific investigation to address their potential as an overlooked source of water and materials for the Baltic Sea via the SGD pathway, characterized by low hydraulic conductivity and low hydraulic gradient.

2.5 Conclusions

Coastal peatlands are widespread along the German Baltic Sea coast. They have often been drained and diked but are increasingly rewetted. This study aimed at assessing whether terrestrial submarine groundwater discharge is likely to occur from such a low-lying, low hydraulic conductivity coastal peatland using 2D numerical modelling of water flow, and at evaluating the factors that determine the magnitude and pattern of SGD from coastal peatlands presuming a range of realistic properties. Our simulations show that terrestrial SGD can originate from a low K_s and low gradient coastal peatland, although the SGD flux at our study site is in the lower range of other wetland environments and Baltic Sea SGD sites. The terrestrial SGD is sourced primarily from the dune dike, recharged from the ponded peatland surface waters and precipitation, and to a lesser extent from the shallow aquifer underlying the peat. As the peatland's surface and groundwater are typically enriched in remineralized organic matter, SGD is a potential

source of these materials with consequences for marine geochemical budgets and ecosystems, and matter fluxes need to be quantified.

A specific feature of coastal peatlands is that the peat layer may continue underneath the sea. Scenario simulations reveal that this extending peat layer has a barrier function and mainly determines the location of SGD in interplay with K_s and geological stratification. It is thus assumed to play a crucial role in how the marine ecosystem is affected locally. However, it has little effect on the SGD magnitude, which is mainly controlled by the hydraulic gradient and Ks, especially of beach/dune and peat. The high positive correlation between beach/dune Ks and SGD underlines the importance of even a small dune belt for SGD generation.

We conclude that SGD is most probable from those coastal peatlands with (i) high water levels, (ii) large Ks and/or (iii) a dune dike or belt, irrespective of the specific geologic setup or topography. This is assumed to be the case for rare, lowly-degraded peatlands, typically characterized by high permeability and water level, and for rewetted (formerly drained) peatlands, where the K_s of the degraded peat is small, but a high water level is maintained artificially and ponded water constitutes a unique water source for SGD. While current efforts of rewetting coastal peatlands are thus expected to increase their contribution to SGD, the expected sea level rise will counteract this development in the future.

2.6 Acknowledgements

We thank the Stadtforstamt Rostock for their support in the conduct of this research in the Naturschutzgebiet Heiligensee und Hütelmoor. We also thank editor and the reviewers for their valuable inputs which greatly improved this article. The authors would also like to thank Haojie Liu for his help in identifying the hydraulic properties of the peat soils.

Supplementary Material to Chapter 2

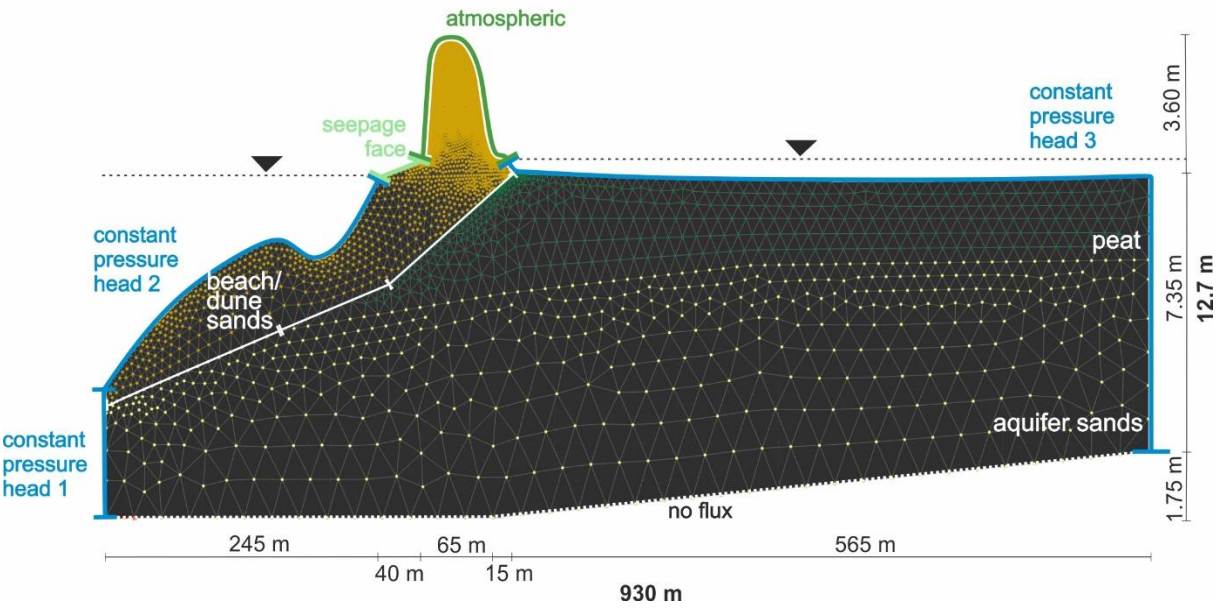

SM Figure 2.1. Modeling domain of the reference peatland with finite element mesh, geological materials, and boundary conditions. Meshlines (white lines) line the boundary of the beach/ dune sands to determine material groundwater contributions. Note the vertical exaggeration of the cross-section.

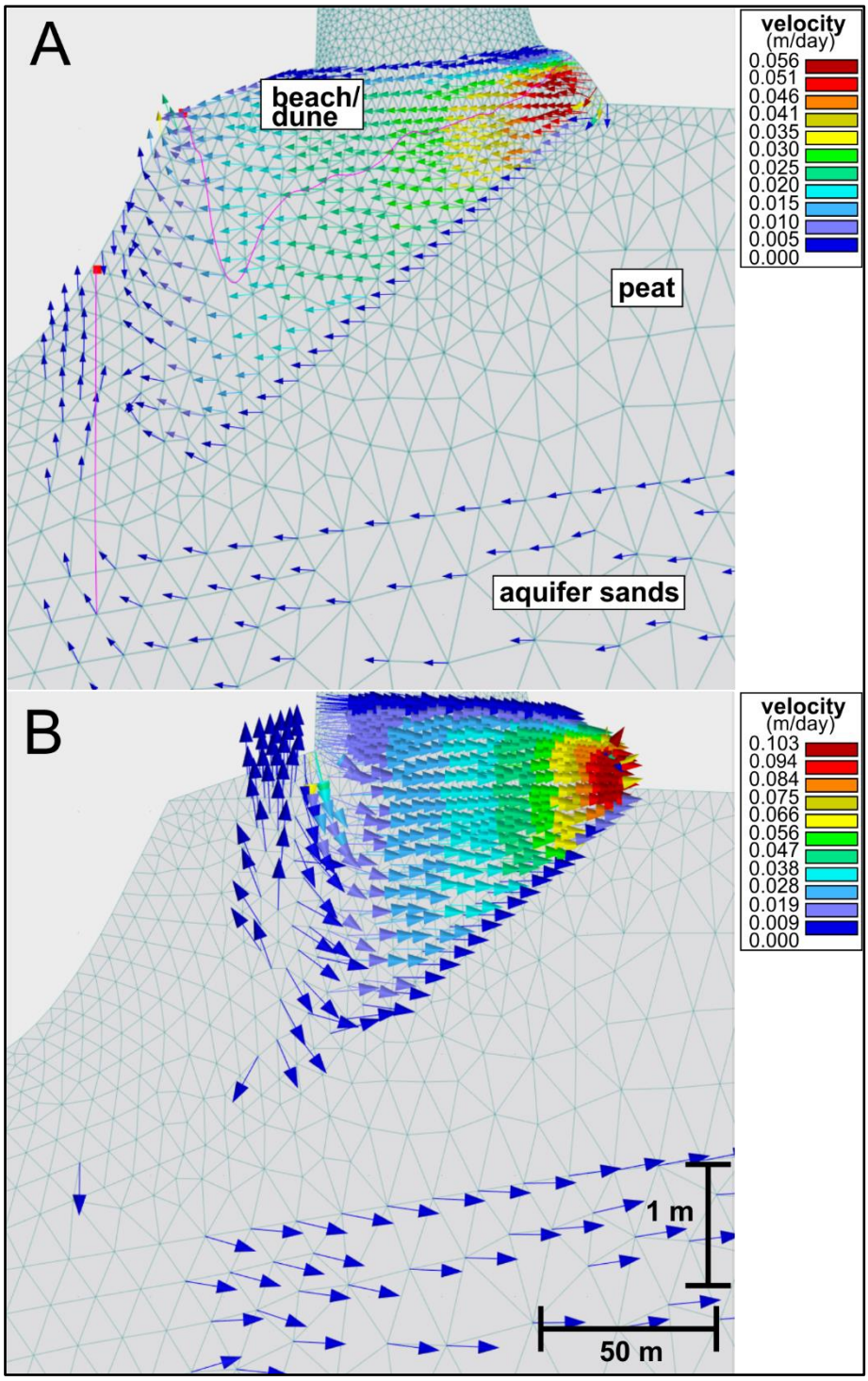

SM Figure 2.2. A) Reference peatland simulation with tracked path of two flowing particles (red dot with pink lines) – one infiltrating from the peatland and another flowing from the aquifer thru the peat extension layer and out of the seafloor. B) High sea level simulation (0.650 masl) results to seawater discharging landwards behind dune dike but no seawater infiltration at the peat extension layer.

SM Table 2.1. Descriptive statistics summary of the generated random log K_s values and subsequent SGD simulation results of the uncertainty analysis.

	Beach/ Dune log K_s (K_s in m d^{-1})	**Peat log K_s (K_s in m d^{-1})**	**Aquifer log K_s (K_s in m d^{-1})**	**SGD (m^2 d^{-1})**
Arithmetic Mean	1.069	-2.059	0.227	0.105
Median	1.087	-2.073	0.230	0.083
Standard Deviation	0.406	0.278	0.224	0.077
Kurtosis	-0.016	-0.239	0.731	11.7
Skewness	0.166	0.054	0.213	3.11
Minimum	0.080	-2.637	-0.251	0.0379
Maximum	2.127	-1.329	0.979	0.493
Count	100	100	100	100

SM Table 2.2. Density of waters from Hütelmoor peatland (2019–2020) and the Baltic Sea (1996–2018) corrected to a long-term average temperature of 9.7^0 C following Millero & Poisson (1981). The average difference in density between Baltic Sea and groundwater is 0.006 g cm^{-3} while difference of 0.007 g cm^{-3} and 0.006 g cm^{-3} were calculated for dune groundwater and surface water, respectively. For locations of groundwater wells, see Ibenthal (2020).

Type of Water	**Location**	**ρ (kg m^{-3})**	**ρ difference Baltic Sea down to -2.2 m (g cm^{-3})**	**Count**	**Collection Period**	**Reference**
Groundwater	Hütelmoor – Peat, aquifer, dune wells	1002.43	0.006	32	2019-2020	This study
Groundwater	Hütelmoor – Dune wells only	1001.25	0.007	3	2019-2020	This study
Surface water	Hütelmoor	1003.15	0.005	15	2019-2020	This study
Baltic Sea water	In front of Hütelmoor	1010.09	-0.002	5	2019-2020	This study
Baltic Sea water	From cruises in vicinity of the study site; down to -2.2 m depth	1008.47	n.a.	169	1996-2018	IOW, accessed 2020

3. SEASONAL DYNAMICS OF SUBMARINE GROUNDWATER DISCHARGE FROM A REWETTED COASTAL PEATLAND

Abstract

Most research on submarine groundwater discharge (SGD) focuses on sandy beaches. Fewer studies have investigated environments with low hydraulic conductivity (K_s) such as coastal peatlands, which are abundant along the southern Baltic Sea coast. In this study, we simulated groundwater flow from a coastal rewetted fen with a peat layer extending out into the sea to understand the short- and long-term dynamics of SGD, quantify SGD water and matter fluxes, and assess the impact of a storm surge on SGD and seawater intrusion (SWI). Five-year (2016–2021) daily 2D numerical simulations of groundwater flow were based primarily on monitored groundwater and sea level data and field-gathered soil hydraulic parameters. Hydraulic conductivities of three geological layers (aquifer sands, peat, beach+dune sands) were optimized against measured groundwater levels. In addition, manual seepage meter measurements were conducted and water samples collected. The modelled groundwater levels and seepage rates fitted the measured ones well. Our results reveal that the low-K_s peat layer determines the location and flow pathways of SGD, while sea level primarily determines the hydraulic gradient and SGD fluxes as a function of weather conditions. Two concentrated submarine discharge areas were observed: 1) nearshore (up to ~35 m from shore) where highest mean seepage rate reach up to 10.2 cm d^{-1} with waters originating from the dune dike and recirculated seawater; 2) offshore (50–75 m from shoreline) with the highest mean discharge rate of 1.1 cm d^{-1} at ~60 m distance. The groundwater-seawater interface below the dune dike moves between the beach and the central dune dike on daily to weekly basis. However, the spatial extent of the interface changes on a seasonal scale. Higher total SGD (= terrestrial SGD + recirculated seawater) fluxes occur in winter while terrestrial SGD contribution is highest in spring and summer. Higher seawater intrusion fluxes were observed during storm surges, while low sea levels cause higher SGD fluxes. Groundwater level and quality might be affected during storm events. The mean terrestrial SGD is 0.15 m^2 d^{-1} (range: -6.12–1.63 m^2 d^{-1}) while mean total SGD is 0.47 m^2 d^{-1} (range: 0.01–2.71 m^2 d^{-1}). Dissolved Organic and Inorganic Carbon (DOC, DIC) and ammonium (NH_4^+) fluxes from the diked peatland are comparable to other environments and other sources from the Baltic Sea demonstrating potential impact of SGD on local biogeochemistry. For the first time, our findings indicate that SGD from rewetted coastal peatlands and from similar low lying, low K_s wetlands could substantially contribute to carbon and nitrogen coastal budgets. In the future, the expected increase in sea level and storm surge events will impact groundwater and SGD from coastal peatlands.

Keywords: *HYDRUS, numerical modeling, wetlands, mire, storm surge, DOC, DIC, ammonium, fen*

3.1 Introduction

Over the last two centuries, the large increase in nitrogen (N) and phosphorus (P) release due to increasing human activities has caused eutrophication of water bodies, posing a threat to many coastal ecosystems worldwide (Pearl et al., 2014; Smith et al., 1999). One of the worst affected is the Baltic Sea (Malone & Newton, 2020) due to its high catchment population density and physiographic characteristics (HELCOM, 2018; 2009), resulting in intensifying phytoplankton blooms and increasing spatiotemporal extent of hypoxic areas. While most of the nutrients are transported from land to the Baltic sea through rivers, an increasing number of studies have documented submarine groundwater discharge (SGD) in e.g., Germany (Racasa et al., 2021; von Ahn et al., 2021), Poland (Szymczycha et al., 2014; Kotwicki et al., 2014), and Sweden and Finland (Jakobsson et al., 2020), which could also contribute to persistent coastal water quality issues (Santos et al., 2021).

Submarine groundwater discharge is an important pathway for nutrients and other materials from land to sea (Burnett et al., 2003; Burnett et al., 2006; Moore, 2010; Taniguchi et al., 2019), yet is often ignored in coastal nutrient budget studies (Santos et al., 2021). The term SGD refers to any water flow out across the seafloor regardless of fluid composition or driving force (Burnett et al., 2003; Taniguchi et al., 2019). “Groundwater” in this context can be freshwater, recirculated seawater, or a mixture of both and can be considered synonymous with porewater (Taniguchi et al., 2019). In many cases, the total flow is dominated by recirculated seawater going out of the mixing zone between groundwater and seawater in a coastal aquifer, also named subterranean estuary (Taniguchi et al., 2019). While fresh groundwater discharge accounts for ~0.6% of global freshwater input, it makes up more than 25% of the river flux in 26% of estuaries, 17% of salt marshes, and 14% of coral reefs (Luijendijk et al., 2020).

Several terrestrial and marine physical drivers affect SGD resulting in large temporal and spatial variabilities and affecting its composition. Main terrestrial drivers include hydraulic gradients and seasonal oscillations of groundwater levels (Santos et al., 2012; Michael et al., 2005) but factors like sediment hydraulic conductivity, geological stratifications and heterogeneities, complex coastal morphology, and thickness of aquifers (Racasa et al., 2021; Robinson et al., 2018; Luijendijk et al., 2020) can also influence magnitude and location of SGD. In any coastal environment, groundwater discharges as long as there is a positive hydraulic gradient towards the sea (Santos et al., 2012). The fresh groundwater discharge component is controlled by the flow capacity of coastal aquifers, determined by topographic gradient, aquifer thickness and permeability (Luijendijk et al., 2020). Meanwhile, seawater recirculation happens due to the movement of the groundwater-seawater interface in response to seasonal oscillation of hydraulic heads (Michael et al., 2005). This resulting saline discharge could be higher than freshwater discharge. Marine drivers, on the contrary, include tides, waves, water density differences, and sea level changes (Santos et al., 2012; Robinson et al., 2018).

Despite unfavorable conditions for water flow, submarine groundwater discharge also occurs in low-lying coastal peatlands with low hydraulic gradients and hydraulic conductivity as recently indicated by steady state numerical modeling (Racasa et al., 2021). Coastal peatlands, similar to inland peatlands, are important ecosystems that hold high amounts of carbon and nitrogen. In addition, peatlands provide several ecosystem

services: regulating (climate regulation, erosion protection), supporting (biodiversity, nutrient cycling), provisioning (food, public water supply), and cultural (spiritual, recreational) (Kimmel & Mander, 2010; Joosten & Clarke, 2002). However, many of these peatlands in Germany and Europe have been drained for agriculture (Baird, 1997), leading to high greenhouse gas emissions (Leifeld et al., 2019), and potentially exacerbating climate change. Rewetting strategies are currently being implemented as a countermeasure (Leifeld & Menichetti, 2018) and to support biodiversity (Tanneberger et al., 2021). Yet, rewetting also raises the risk of releasing substantial amounts of carbon and nitrogen to surface waters, at least in the subsequent months and years (Zak & Gelbrecht, 2007; Holden, 2005; Pönisch & Breznikar et al., 2023). Raising water levels together with high carbon and nitrogen groundwater concentrations from these organic-rich environments warrant a systemic understanding of water flow and solute transport from coastal peatlands to the sea through the SGD pathway.

This paper attempts to unravel the seasonal water exchange dynamics between a low-lying, diked and rewetted coastal fen and the Baltic Sea using HYDRUS-2D soil hydrological modeling, long-term groundwater level monitoring, and seepage meter measurements. The objectives of the study are 1) to describe groundwater flow pathways, 2) to determine daily, monthly, and seasonal SGD, seawater intrusion (SWI), and net (SGD+SWI) fluxes, 3) to estimate solute concentrations and SGD material fluxes and, 4) to investigate the impact of a 2019 storm surge event on water exchange in a rewetted, low-lying, diked coastal peatland.

3.2 Materials and Methods

3.2.1 Study Site

The present study focuses on a rewetted coastal fen peatland near Rostock, Germany called the Hütelmoor Nature Reserve (“Naturschutzgebiet Heiligensee und Hütelmoor”; 54.21390N 12.17250E), hereafter referred to as Hütelmoor (Figure 3.1). The coastal peatland is only separated from the Baltic Sea by an artificial 40-m wide dune dike that thins out in the northern part of the 3-km shoreline. The peatland is underlain by sands forming a shallow aquifer and a glacial till at the bottom. At the coast, beach/ dune sands overlie the up to 3 m thick peat (Figure 3.2; SM Figure 3.1). A detailed description of the geology of the peatland and its adjacent coastal area is presented in Toro et al. (2022) and Kreuzburg et al. (2018). The peatland’s notable feature is the outcropping peat deposits in the northern coastal area, and a submerged peat layer extending into the Baltic Sea (middle area) (Kreuzburg et al., 2018; Toro et al., 2022). Outcropping peat in very shallow waters has been observed in other coastal peatlands, and the peat layer can be expected to be a regional characteristic for Baltic Sea peatlands (Toro et al., 2022).

Like many coastal peatlands along the southwestern Baltic Sea, the Hütelmoor has been altered – drained, diked, and utilized for agriculture (for details, see Toro et al., 2022). It was rewetted in December 2009 via installation of a ground sill (height = ~0.40 masl: Toro et al., 2022) at its main water outlet. Currently, most of its area is flooded with surface waters. Seawater inundations occurred regularly (1872, 1904, 1913/14, 1949, and 1954) before construction of a dike in 1903 and its reinforcement in 1963 (Kolp, 1957). Afterwards, seawater inundations only happened during the storm surge events in 1995

and 2019. However, entry of seawater via the ground sill during storm flood events may occur more frequently (Schreiber et al., 2021). The long-term influence of seawater has turned the ground- and surface waters of the peatland brackish (Ibenthal, 2020).

The study area and the Western Baltic Sea in general (Kiel and Mecklenburg Bays) are particularly susceptible to storm surges and negative storm surges due to the prevailing northwestern and northeastern wind systems (Wolski & Wiśniewski, 2020). An average of 4.4 and 1.2 storm surges with heights of ≥0.7 masl and ≥1.0 masl, respectively, hit Warnemünde every year (Wolski & Wiśniewski, 2020). On January 2, 2019, a storm surge (sea level peak = 1.69 masl) destroyed part of the northern dune dike at the study site, which is not maintained any longer. A week later, another storm surge of 1.17 masl height occurred.

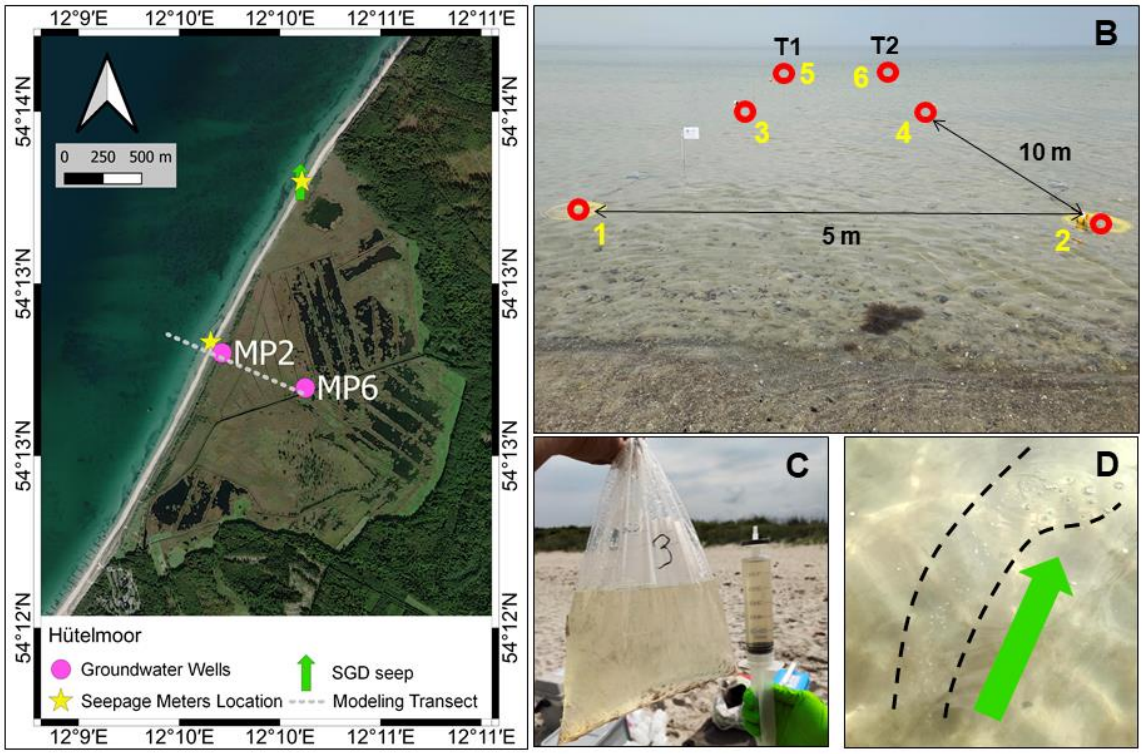

Figure 3.1. Study site Hütelmoor Nature Reserve and field set-up. A) Location of groundwater wells, seepage meter measurements, discovered groundwater seeps, and modeling transect. Lake Heiligensee can be seen in the northern side near the location of the discovered SGD seep; B) field set-up of seepage meter measurements during Jun/Jul 2021 fieldwork – red circles denote location of seepage meters (during the Sept 2021 fieldwork, distance between seepage meters perpendicular to the shore has been reduced to 5 m); C) Collected water sample from seepage meter from Jun-Jul 2021; D) Seeps discovered in Jul 2021 showing bubbles rising from seafloor to the sea surface.

3.2.2 Groundwater Monitoring and Sea Level

Groundwater levels were derived from 15-minute resolution pressure transducer loggers (Dipper-PTEC, SEBA Hydrometrie, Kaufbeuren, Germany) installed in observation wells at MP6 and MP2 (Figure 3.1A) in September 2016 and January 2017 respectively and deployed until October 2021. Wells at MP2 had filter screens at 0.13 to -0.38 masl (dune sands; MP2DS), -1.14 to -2.14 masl (peat; MP2P) and -3.00 to -4.20 masl (aquifer sands;

MP2LS), while at MP6, the filter screens were positioned at -0.41 to -1.41 masl (peat; MP6P) and -2.57 to -3.70 masl (aquifer; MP6LS). Barometric compensation and data cleaning (i.e., invalid data points after logger read out) were performed. Since head measurement errors can significantly increase the uncertainty of groundwater flow rate calculations (Rau et al., 2019), additional corrections were undertaken based on manual water level measurements, which were taken using an electric gauge about three to four times per year. For the loggers not showing a drift (MP2DS, MP2P, MP6P, MP6LS), a linear regression of logger measurements vs. manual measurements was performed and the logger data corrected following Ahmad et al. (2020) ($R^2 > 0.93$; SM Figure 3.2). The MP2LS logger exhibited a drift; the difference between manual and logger measurements increased with time. Here, the measurement error for a specific time was determined using a linear regression equation between timestamp and corresponding difference between manual and logger measurements. This measurement error was then added to the logger measurement to get the final water level. After correction, these point water head groundwater levels were transformed to equivalent freshwater heads to eliminate variable density effects (Post et al., 2007). Sea levels were gathered on an hourly (2016-2020) and minute (2020-2021) resolutions at the nearest tide gauge station at the Warnow River mouth (Rostock-Warnemünde; BSH, 2021). Both water level data sets were processed to daily/hourly values using the dplyr package (Wickham & Müller, 2022) in R (RStudio, 2022).

Water samples were collected from ground- and surface waters from the abovementioned wells as well as from the nearby shallow Baltic Sea from Apr 2019 – Apr 2022 (total water sampling campaigns = 9). All samples were filtered *in situ* using 0.20 µm Rotilabo (R) cellulose acetate membrane syringe filters (Carl Roth, Karlsruhe, Germany) for major ions and nutrients and 0.45 µm Filtropur S polyethersulfone membrane filters (Sarstedt, Nümbrecht, Germany) for DOC/DIC/TDN analyses. For the cation samples, 1 M nitric acid was added for sample preservation. Samples were chilled during transport using a cooler bag filled with frozen gel packs. Samples were stored in -20^{0}C freezers until laboratory analysis except for DOC samples which were temporarily stored at 4^{0}C and immediately analyzed.

3.2.3 Meteorological Data

Daily precipitation data was retrieved for Rostock-Warnemünde (DWD-CDC, 2021a), located at the coast at a distance of ~6.7 km from the study site, and were corrected following a Zone III, Type B classification for slightly protected rain gauges based on Richter (1995). Average precipitation from 2016-2021 (1.92 mm d^{-1}) is similar to the long-term average precipitation of 1.90 mm d^{-1} (1951-2010; Miegel et al., 2016). Reference evapotranspiration (ET_0) was estimated using the Penman-Monteith method following Allen et al. (1998). The calculations were based on wind speed and maximum and minimum temperature data from Rostock-Warnemünde (DWD-CDC, 2021b; 2021c; 2021d) and were carried out using the program “ETo-PM” (Lupia, 2013). Average wind speed at 10 m height was corrected to 2 m height (Allen et al., 1998) to match maximum and minimum temperatures also measured at 2 m height. The reference evapotranspiration was then multiplied with the factor 0.8, which had been determined by Miegel et al. (2016) by comparing field evaporation rates from the study site with calculated ET0 for Warnemünde. The five-year average (1.67 mm d^{-1}) is also similar to the long-term

estimate from 1951-2010 (1.65 mm d^{-1}; Miegel et al., 2016). For hourly modeling, hourly precipitation sums were also determined from DWD-CDC, while hourly ET_0 was calculated by dividing the daily values by 24.

3.2.4 Seepage Meter Measurements

Seepage meters were installed to determine local fluxes and obtain samples for solute analyses. There were two field campaigns: on June 29–July 2, 2021 (summer) in the northern part of the coast and on September 13–15, 2021 (fall) in front of the MP2 wells (Figure 3.1A). For each field campaign, a total of six manual seepage meters with diameters of 0.58 m were deployed in two transects (Figure 3.1B). Transect 1 (T1), consisting of three seepage meters (1, 3, 5), was for measuring seepage rates using 3 L seepage bags pre-filled with 1 L of seawater collected during sampling (based on Rosenberry et al., 2020; Duque et al., 2020). Transect 2 (T2) was deployed similar to T1 with empty seepage bags for water sampling. The empty seepage bags will fill with water even during SWI conditions. Four seepage chambers were traditionally fabricated (based on Lee, 1977), while two chambers were modified (based on Rosenberry et al., 2020; Duque et al., 2020) with a side hole and a seepage bag shelter for expectedly shallower water depths at 5 m distance from the shore (SM Figure 3.3). For the Jun/Jul sampling, the seepage meters were deployed at 5 m, 15 m, and 25 m distance from the shore and inserted 11–13 cm into the seafloor. On July 2, strong waves displaced seepage meters at -5 m and -25 m. The distances were changed to 5 m, 10 m, and 15 m for the September sampling considering local water depths at the time. Further, seepage meters were inserted only 4-11 cm into the seafloor due to the stony characteristic of the beach. All seepage meters were installed one day before sampling to allow the meters to equilibrate.

Sampling was performed every 1.75–2 hours during daytime for two (Sept) and three (Jun/Jul) days due to administrative and logistics limitations in the study area. Sample volume of T1 samples was measured using a 1 L graduated plastic cylinder. For T2 samples, subsamples were collected in © Falcon tubes for DOC/DIC/TDN (40 mL), nutrients (15 mL), and major ions (15 mL). Samples were treated as described in Section 3.2.2.

3.2.5 Laboratory Analyses

Samples for DOC/DIC/TDN were analyzed using a Analytik Jena Multi N/C 2100s analyzer (Jena, Germany). Samples for DOC were burned at 750^0C, while DIC samples were injected in phosphoric acid following manufacturer protocols. Blank samples from filtered distilled water were also analyzed. Ammonium (NH_4^+), and phosphate (PO_4^{3-}) were measured using a AA3 Continuous Flow Analyzer (Seal Analytical, Norderstedt, Germany). Major cations (NH_4^+, K^+, Ca^{2+}, Mg^{2+}, Na^+) and anions (SO_4^{2-}, Cl^-, Br^-) were analyzed using ion chromatography (Metrohm 930 Compact IC Flex; Herisau, Switzerland).

3.2.6 Numerical Modeling

Modeling Approach

To simulate groundwater flow in the Hütelmoor coastal peatland and quantify temporal fluxes of SGD and SWI, the HYDRUS model (ver. 3.04.0140, PC Progress, Prague, Czech

Republic) was used to describe water movement based on the Richard's equation for Darcian water flow (Simunek et al., 2018). The governing equations are numerically solved in HYDRUS using the Galerkin-type linear finite elements method. A steady-state water flow model was first developed based on averages of groundwater and sea level data for Sep 23 - Oct 31, 2016. The results of the steady-state simulation (running for 300 days to reach equilibrium) were then used as initial conditions for transient daily simulations for five hydrological years (HY) from Nov 1, 2016 – Oct 31, 2021. The first half was used for calibration (Nov 1, 2016 – Apr 30, 2019) while the second half was used for validation (May 1, 2019 – Oct 31, 2021).

Additional transient simulations were undertaken for the duration of the seepage meters fieldwork in September 2021 (see section 3.2.4) and for a storm surge on January 2, 2019. Averages of the five days prior to these events were used to establish the steady-state models that ran for 300 days. Like before, the final time layer of these steady-state models was used as initial conditions to their corresponding transient models.

Modeling Domain: Spatial and Time Discretization

Based on published and gathered field data, Racasa et al. (2021) previously established a steady-state HYDRUS model for the same transect (Figure 3.1A). The topography of the shallow beach in front of MP2 (where seepage meters were emplaced in Sept 2021) as well as the outer dune dike were updated using new high-resolution elevation measurements (± 3 cm), obtained using a Leica CS20 with Leica GS07 GNSS receiver and Leica Captivate collecting software on September 13, 2021. The current modeling domain extends landward by 675 m from a reference shoreline (water line on September 13, 2021; height = 0.32 masl) and 245 m seawards (total length = 920 m) (Figure 3.2; SM Figure 3.1). Three geological layers were assigned – peat, aquifer sands, and beach/dune sands. Spatial discretization was repeatedly reworked and triangular elements were constructed as small as possible, with trial simulations achieving water flux mass balance errors of less than 1% (the considered threshold for good water flow models). A final target size of 1.0 m, x-direction stretching factor of 25, and smoothing factor of 1.8 were used. Surface refinements of 0.04 m, 0.075 m, and 0.5 m were applied to the unsaturated beach/dune sands, saturated beach/dune sands, and peat layers, respectively. A total of 5496 nodes and 568 nodes on the domain boundary resulted from the applied configurations.

In terms of time discretization, minimum, maximum, and initial time steps of 1E-5 days, 5 days and 0.001 days were used, respectively. The first 300 days of simulation time used average steady-state values, which yielded the resulting distributions of hydraulic heads and the initial conditions for the transient simulations. The total transient simulation time is 1826 days corresponding to the five-year simulation period previously mentioned.

Soil Hydraulic Parameters

Soil hydraulic parameters were adapted from Racasa et al. (2021) (Table 3.1). The parameters were based on 1) field-gathered soil texture data for beach/ dune and aquifer sands transformed using "Rosetta" incorporated in HYDRUS (Schaap et al., 2001); 2) peat bulk density transformed using equations by Liu & Lennartz (2019a) and; 3) field-measured hydraulic conductivity using slug tests (Ibenthal, 2020). A problem with non-

convergence of the simulations was resolved by changing the van Genuchten parameter "n" of the beach/dune sands layer to 3.1 through manual optimization using reasonable values and considering the smallest relative mass balance errors. Hydraulic conductivities K_s compiled in Racasa et al. 2021 for the three layers were used as initial values for parameter estimation. The final optimized K_s values are also given in Table 3.1.

Table 3.1. Soil hydraulic parameters used in the HYDRUS model, with both initial and fitted K_s values given. Data were mostly adapted from Racasa et al. (2021).

	Q_r (m^3 m^{-3})	**Q_s (m^3 m^{-3})**	**α (m^{-1})**	**n**	**l**	**K_s (m d^{-1}) - initial**	**K_s (m d^{-1}) - final**
Beach/ Dune Sands	0.05150	0.37662	3.39265	3.1	0.5	11.8100	6.552
Aquifer Sands	0.04644	0.38180	3.72309	2.52943	0.5	1.73000	4.869
Peat	0.20000	0.88000	2.90000	1.22000	0.5	0.00864	0.00346

Boundary Conditions (BC)

Model boundary conditions (BC) are Variable Heads (VH) for the seafloor, left boundary, and peatland (VH1, VH2, and VH3, respectively), and atmospheric BC for the dune dike (Figure 3.2). For VH1 and VH2, the processed daily/hourly seawater levels were used. The extent of VH1 towards the beach/dune corresponded to the highest measured seawater level during the modelling period. VH1 changes to atmospheric BC when the nodal pressure head is negative. Meanwhile, for VH3, the daily/hourly processed groundwater level from MP6P was used to represent water level conditions in the peatland. Daily/hourly precipitation and ET_o were applied for the atmospheric BC. No flux was assigned to the glacial till bottom which is considered impermeable. Lastly, in the time-variable boundary conditions records, hCritA, which represents the minimum allowed pressure head at the soil surface with an atmospheric BC, was assigned a value of -10 m.

For the storm surge event simulation, no flux was assigned to the dune dike due to non-convergence and the assumed negligible influence of precipitation and evapotranspiration on water contents and water flow. All other BCs were kept the same.

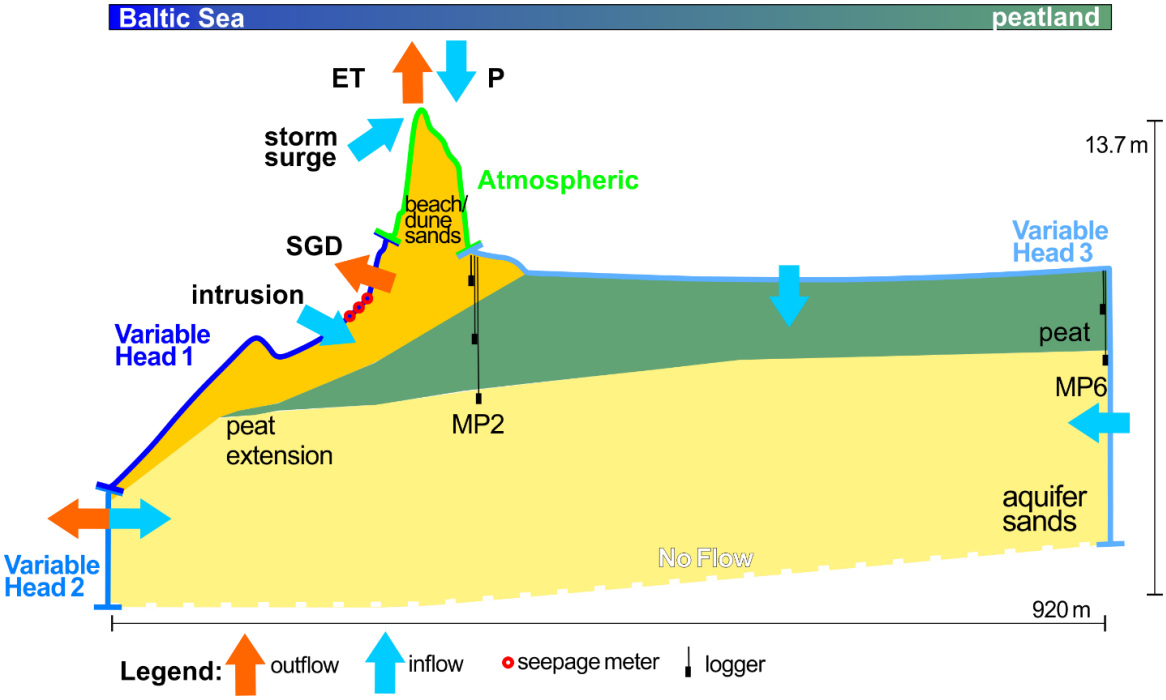

Figure 3.2. Schematic diagram of an anthropogenically-influenced coastal peatland system with geological layers, water inflows/outflows and boundary conditions of modelling domain. An important feature is the presence of a seaward submerged peat extension. Water inflows are precipitation (P) at the beach/dune, seawater inflow during storm surge and from recirculation of seawater, and lateral groundwater flow into the peatland. Outflows are from evapotranspiration (ET) at the dune dike and SGD. Both inflow and outflow can occur on the left-side boundary. Note: figure was compressed horizontally.

Model Calibration and Validation

Model calibration was conducted for the first half of the simulation period, while validation was performed using the latter half. To calibrate the model, we used the inverse solution function of HYDRUS to optimize the K_s values of the three geological layers (Table 3.1). The K_s is a sensitive parameter which could have a large influence on SGD (Racasa et al., 2021). The optimized parameters were determined by comparing the observed heads of the three MP2 data loggers (Figure 3.2) with the simulated ones. No internal weighting was assigned for the inverse solution. HYDRUS uses the Marquardt-Levenberg Optimization Algorithm, a weighted least-squares approach of the Marquardt's maximum neighborhood method, to minimize the objective functions (Šimunek et al., 2018).

To evaluate the goodness-of-fit of the model, we used the HYDRUS-determined Root Mean Square Weighted Error (RMSE), the regression coefficient r^2 of the observed and simulated heads (Equation 3.1) as well as the Kling Gupta Efficiency index (KGE, Gupta et al., 2009; Equation 3.2). The Nash-Sutcliffe Efficiency index (NSE) (Nash & Sutcliffe, 1970), which is the more traditional choice of metric, was not considered due to its low level of predictive skill in systems wherein the mean is not representative of strong seasonal regimes (Knoben et al., 2019). The KGE is based on a decomposition of the NSE considering correlation, variability bias, and mean bias.

Equation 3.1

$$r^2 = \frac{[\sum w_i \hat{y}_i y_i - \frac{\sum \hat{y}_i \sum y_i}{\sum w_i}]^2}{\left[\sum w_i \hat{y}_i^2 - \frac{(\sum \hat{y}_i)^2}{\sum w_i}\right]\left[\sum y_i^2 - \frac{(\sum y_i)^2}{\sum w_i}\right]}$$

where w_i is the weight associated with the observed head, $\hat{y}_i$ is the observed head, and y_i is the simulated head.

Equation 3.2

$$KGE = 1 - \sqrt{(r-1)^2 + \left(\frac{\sigma_s}{\sigma_o} - 1\right)^2 + \left(\frac{\mu_s}{\mu_o} - 1\right)^2}$$

where r is the linear correlation between observed and simulated heads, σ_s is the standard deviation in simulated heads, σ_o is standard deviation in observed heads, μ_s is the mean of simulated heads, and μ_o is the mean of observed heads.

Modeling results were also compared with seepage rates measured using seepage meters (see Section 3.2.4) by retrieving nodal velocities for the locations of the seepage meters.

3.2.7 Data Post-processing and Calculation of Material Fluxes

The magnitude of daily, monthly, and seasonal SGD/SWI/net fluxes was assessed by looking at nodal flows ($m^2\ d^{-1}$) at the seafloor. Here, the SGD flux is the total SGD or all the groundwater (terrestrial, recirculated, or mixed) that discharges to the sea. The daily SGD flux was determined by adding all nodal fluxes directed out of the modeling domain for each day (*Q (n)* of the Boundary.out output file). Meanwhile, the SWI is the seawater that intrudes into the seafloor and was determined by adding all the *Q(n)* fluxes directed into the modelling domain. Since no net water input is expected from marine drivers (Santos et al., 2012) as the SWI recirculates back to the sea, the SWI flux can be equated to the recirculated SGD. However, caution should be taken when using this definition since sea level measured from a nearby tidal gauge was used and actual marine drivers, i.e., wave setup flushing shallow layers in a shorter time scale, were not considered in this study. The net flux is the sum of SGD and SWI and – when positive – represents the terrestrial SGD from the peatland. The term terrestrial SGD was chosen since SGD from the peatland is expected not to be fresh, but brackish due to previous seawater inundations as shown in Toro et al., 2022.

SGD/SWI/net fluxes were only considered within 100 m from the coast. This seepage face distance was chosen since simulated SGD rates beyond this were <0.0002 m d^{-1}; and since the occurrence of terrestrial SGD rapidly decreases as the distance from the shore increases (McBride and Pfannkuch, 1975, Bokuniewicz, 1992). Furthermore, the chosen distance allows us to capture the influence of the submerged peat extension to groundwater flow. A similar distance perpendicular to the coast (150 m) has been considered for studying SGD from an unconfined, heterogenous aquifer (Li et al., 2009).

For the mean, minimum, and maximum flow velocities along the transect, the nodal velocities from the Boundary.out file was used. For nodes without SGD/ SWI during the five-year simulation, e.g., intermittent SGD/ SWI in upper beach areas and foot of dune dike, zero fluxes were considered when calculating the mean flow velocities. The dplyr (Wickham et al., 2022) and lubridate (Grolemund & Wickham, 2011) packages of R were used to post-process the data.

Material fluxes (mg m^{-2} d^{-1}) were estimated by getting the product of the total SGD flux and the solute concentrations (Equation 3.3):

Equation 3.3

$$Material\ Flux\ \left(\frac{mg}{m^2\ d}\right) = SGD\ (Water)\ Flux\ \left(\frac{m^2}{d}\right) * Solute\ Conc\ \left(\frac{mg}{L}\right) * \frac{1}{Seepage\ Face\ (m)}$$

where the material flux (mg m^{-2} d^{-1}) is the estimated flux of different solutes such as DOC, DIC, NH_4^+, and others; SGD flux (m^2 d^{-1}) is the average simulated SGD for 2016–2021, solute concentration (mg L^{-1}) is the average solute (DOC, DIC, NH_4^+, and others) concentration and; seepage face is the distance from the shore considered for the SGD flux simulation (100 m). The total material loads (mg d^{-1}) from the Hütelmoor coastal peatland can then be calculated by multiplying the material fluxes with the coastline length (3000 m) and seepage face (100 m).

3.3 Results

3.3.1 Seepage Rates and Salinity Measurements from Seepage Meters

Submarine groundwater discharge (Figure 3.1C: SGD waters collected from seepage meters) and seawater intrusion were both observed in the study site, with SGD occurring mostly in the June/July 2021 (summer) and SWI in the September 2021 (fall) measurements (Figure 3.3). In the summer sampling, the highest discharge rates were observed from -15 m (3.86 cm d^{-1}) and -25 m (3.47 cm d^{-1}) seepage meters measured at different days (Figure 3.3A). The lowest discharge rates as well as the two SWI rates observed (down to -1.12 cm d^{-1}) were seen at the -5 m seepage meter which was closest to the shore. Meanwhile, for the fall sampling, most seepage rate measurements were SWI with only a single discharge measurement (0.16 cm d^{-1}) recorded at -10 m distance from the shore (Figure 3.3B). The highest SWI was recorded at -5 m distance (-2.96 cm d^{-1}). For both sampling campaigns located at two different coastal areas of the Hütelmoor, measured seepage rates varied both temporally and spatially despite the small distances between the seepage meters. Flow direction changed generally from SGD in summer to SWI in fall attributed to lower groundwater levels (difference based on daily means: <0.16 m), higher sea levels (difference based on daily means: up to 0.52 m) and strong waves. Further, a discrete SGD site was discovered in July 2021 in the vicinity of the study area a few days after the fieldwork (Figure 3.1D).

Salinity of SGD waters differs between the two field campaigns. During the summer sampling, salinity of SGD waters had a limited range from 11.00 psu to 11.56 psu (Figure

3.3C). A much wider range but lower values (9.20 – 10.54 psu) were observed in fall (Figure 3D). However, ambient seawater salinity was always lower than the salinity measured in the seepage meters. In addition, temporal salinity variations of SGD waters from the same seepage meters are more pronounced in fall than in summer.

Mean daily SGD and salinity vary spatially (Figure 3.3E & 3.3F). Seepage (in summer) was lowest close to the shore, while SWI (in fall) was highest there. Mean daily salinity was lowest at mid-distance during the summer sampling while it decreased with distance from the shore in fall.

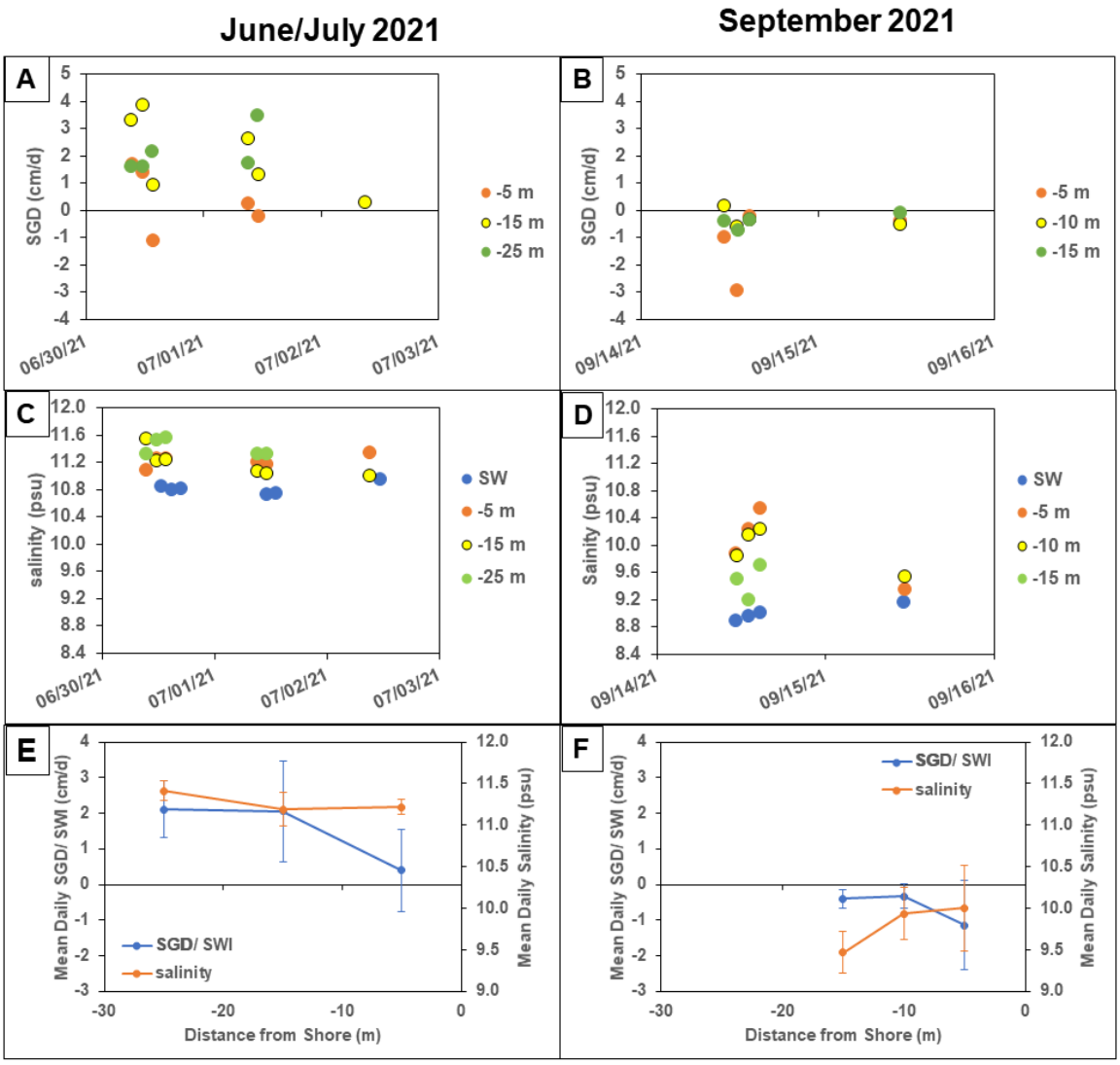

Figure 3.3. Submarine groundwater discharge field measurements gathered using manual seepage meters in June/July (summer; at northern part of coast) and September (fall; at middle part of coast) 2021 (for locations, see Figure 3.1). A, B) Submarine groundwater discharge (SGD). C, D) Salinity of SGD and ambient seawater (SW). E, F) Spatial distribution of mean daily SGD and mean daily salinity. Seepage meters at -5 m and -25 m (T1) were displaced by strong waves on July 2, 2021.

3.3.2 Model Calibration and Validation

K_s Optimization and Model goodness of fit

The inverse solution yielded optimized K_s values of 6.552 m d^{-1}, 4.869 m d^{-1}, and 0.003456 m d^{-1} for the beach/dune, aquifer, and peat layers, respectively. A low mass balance error of 0.096% was achieved in the final time step of the calibration period (Table 3.2). Simulated groundwater levels in the dune sands, peat, and aquifer sands match very well with the observed levels (Figure 3.4C-E). Calculated metrics of simulated vs. measured groundwater levels were satisfactory with RMSE and R^2 value of 0.103 and 0.992, respectively. High Kling-Gupta Efficiency indeces were recorded for all three geological layers, particularly when considering that the value should be higher than a benchmark of -0.41 (Knoben et al., 2019). Validation of the optimized parameters also reveal low MBE and RMSE values accompanied with high R^2 and KGE values for all the geological layers.

Table 3.2. Metrics for model calibration (Nov 2016 – Apr 2019 and validation (May 2019-Oct 2021) periods. MBE: mass balance error, RMSE: root mean square error, R: correlation coefficient, KGE: Kling-Gupta Efficiency index, MP2DS: dune sands, MP2P: peat, MP2LS: aquifer sands. MBE, RMSE and R^2 were retrieved from HYDRUS.

	MBE (%)	**RMSE**	**R^2**	**KGE**
Calibration	0.096	0.103	0.992	MP2DS: 0.626 MP2P: 0.713 MP2LS: 0.800
Validation	0.103	0.067	0.997	MP2DS: 0.659 MP2P: 0.501 MP2LS: 0.923

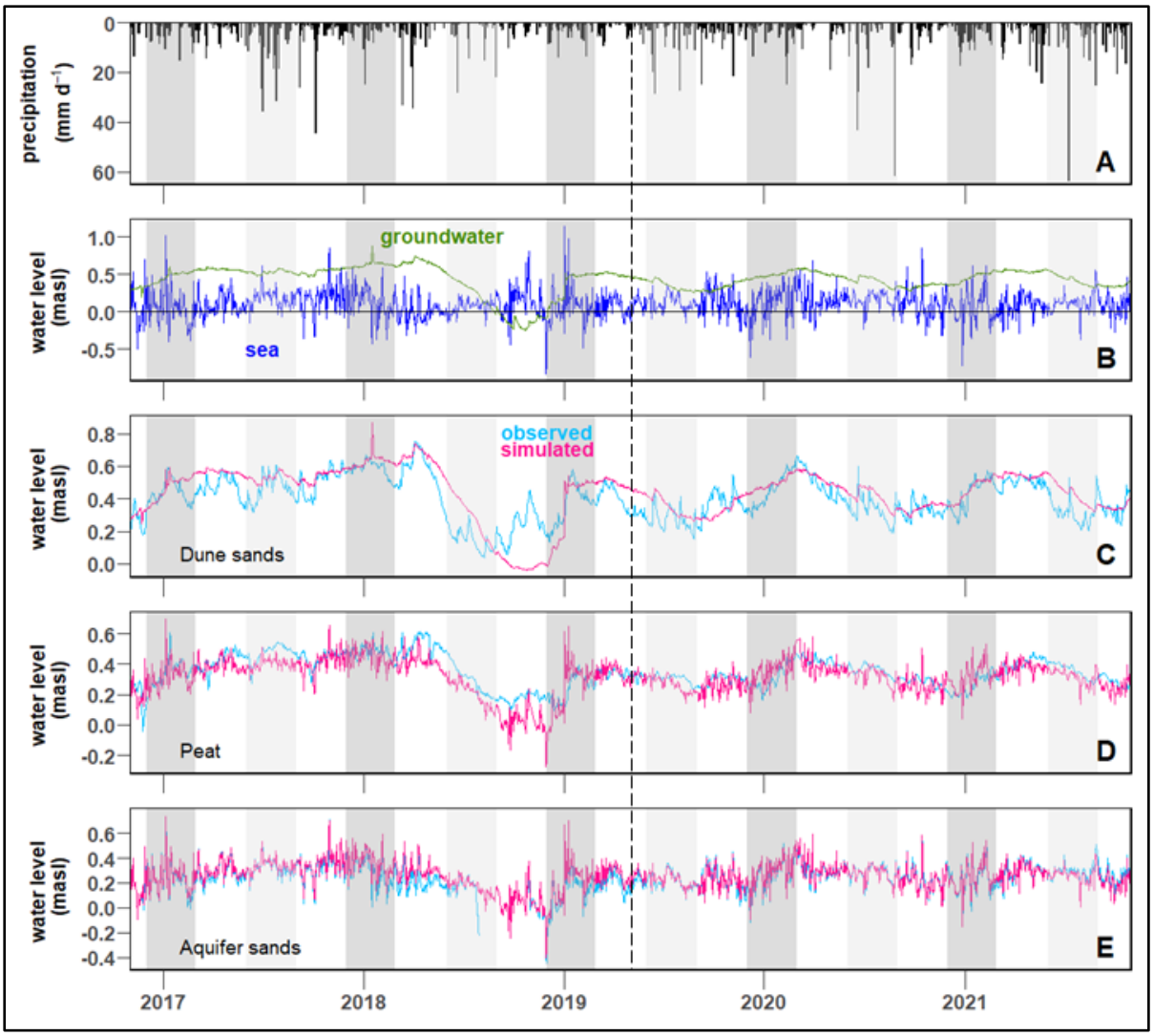

Figure 3.4. Precipitation (A), sea and groundwater (measured at MP6P) levels (B), and observed and simulated groundwater levels for the dune sands (MP2DS; C), peat layer (MP2P; D) and aquifer sands (MP2LS; E). Dark gray and light gray shades represent winter (Dec- Feb) and summer (Jun-Aug), respectively. The dashed line divides the panels into the calibration (left side) and the validation (right side) periods. Note that the extent of the y-axis differs between panels C, D and E.

Comparison of measured and simulated seepage rates

Aside from comparing observed and simulated water levels, we compared the simulated seepage rates with field measured ones in Sep 2021: the simulated seepage rates generally agree well with our limited data from seepage meters (Figure 3.5). The simulated seepage rates are in the same order of magnitude as the measured ones at -10 m and -15 m distance from the shore. However, simulated rates at -5 m have higher discharge/SWI magnitude than measured ones. Simulated seepage rates at -5 m distance from the shore vary inversely with SW level; GW level was stable during the field survey. On the contrary, simulated rates follow the trends of sea level change for the -10 m and -15 m seepage meters.

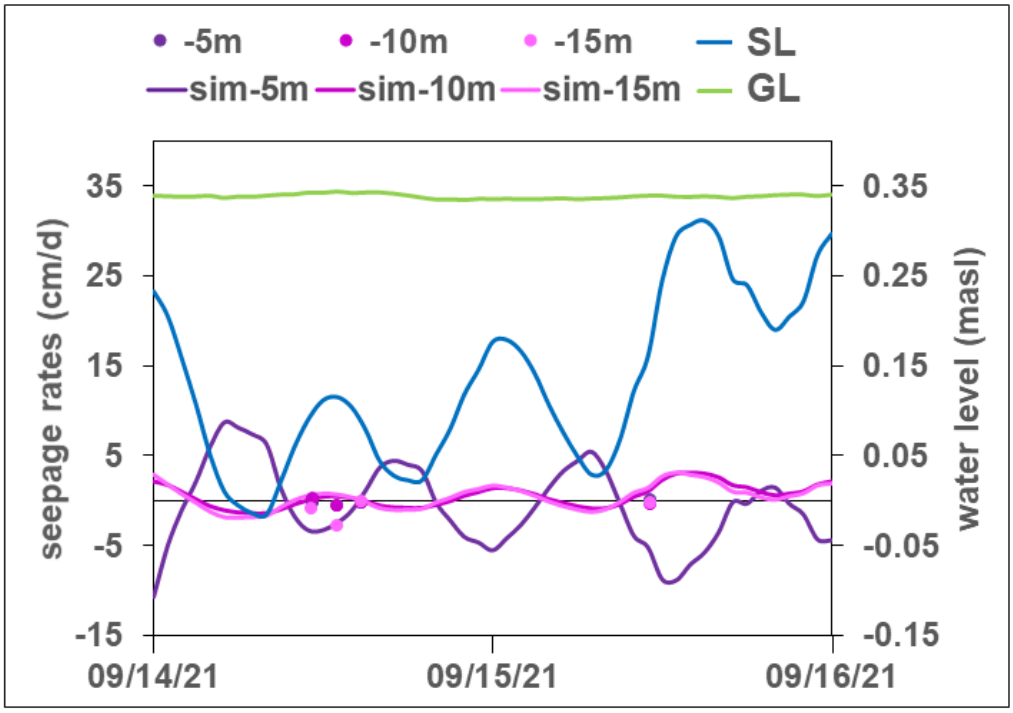

Figure 3.5. Simulated seepage rates (lines) compared with measured seepage rates (dots) using manual seepage meters at -5, -10 and -15 m distance from the coastline (September 14 – 15, 2021). SW: seawater level, GW: groundwater level measured behind dune dike.

3.3.3 Flow Pathways

The groundwater flow pathways and the origin of the groundwater discharging from the Hütelmoor peatland to the Baltic Sea can be deduced from flow velocity vectors (Figure 3.6). The general water flow direction is towards the sea, but seawater intrusion into the sea floor occurs depending on the sea level. Two concentrated SGD zones from the rewetted coastal peatland were detected: the first one nearshore (within ~-35 m; Figure 3.6), and the second one where the peat layer extending underneath the sea gets thinner (-50 to -75 m; Figure 3.6B, C and D). Groundwater discharging in the nearshore SGD zone originates either from 1) precipitation infiltrating into the dune dike and beach, 2) peatland surface waters infiltrating the dune dike, and/or 3) seawater recirculating back to the sea (see according numbers in Figure 3.6). The second SGD zone, an advective flow zone, appears to have mainly terrestrial origin – from the aquifer sands beneath the peat layer.

In between these two SGD zones and beyond the second discharge region, SGD and SWI may also occur (see 3.3.5 for magnitudes).

The first SGD zone is highly dynamic with contributions from both terrestrial SGD and recirculated SGD. Relatively more terrestrial SGD contribution is expected in spring (not shown) and summer (Figure 3.6C) with SGD expected to occur nearer to the shoreline. Meanwhile, recirculated SGD, usually in winter and fall (Figure 3.6A, D), occurs between ~-20 to -35 m from the shoreline. For the second SGD zone, discharge fairly occurs during most of the year (Figure 3.6B, C, D) though this zone is also susceptible to SWI. In spring and summer, more water outflows were recorded. In fall and winter, flow from the aquifer sands is considerably weaker and alternating SGD and SWI may occur.

The position of the groundwater-seawater interface oscillates throughout the year. We looked through five years of daily flow vectors, to determine the behavior of this most important interface located underneath the dune dike and immediate beach area (Figure 3.6). The interface is located where the velocity vectors coming from the terrestrial and marine sides meet. The position of the interface is highly dynamic and may oscillate seawards and landwards on a daily basis. At a seasonal scale, the following pattern is typical: – December–February (winter): stormy winter conditions albeit increasing groundwater levels moves the interface towards the peatland and reaches its maximum position under the dune dike (at ~35 m on January 5, 2021; Figure 3.6A); March–May (spring): highest groundwater levels moves interface back towards the seaside but stormy conditions still infiltrate seafloor but with less intensity (Figure 3.6B); June–August (summer): declining groundwater levels but calmer climatic conditions moves interface further towards the sea and reaches its outermost position near to the water line (Figure 3.6C); September–November (fall): high sea level from stormy conditions moves interface back towards the peatland (Figure 3.6D), atmospheric input is more pronounced due to low groundwater and seawater. The mentioned patterns last only for a few days before the interface resumes a seawards flow direction. Further groundwater-seawater interfaces can be described where the aquifer flow meets SWI (Figure 3.6).

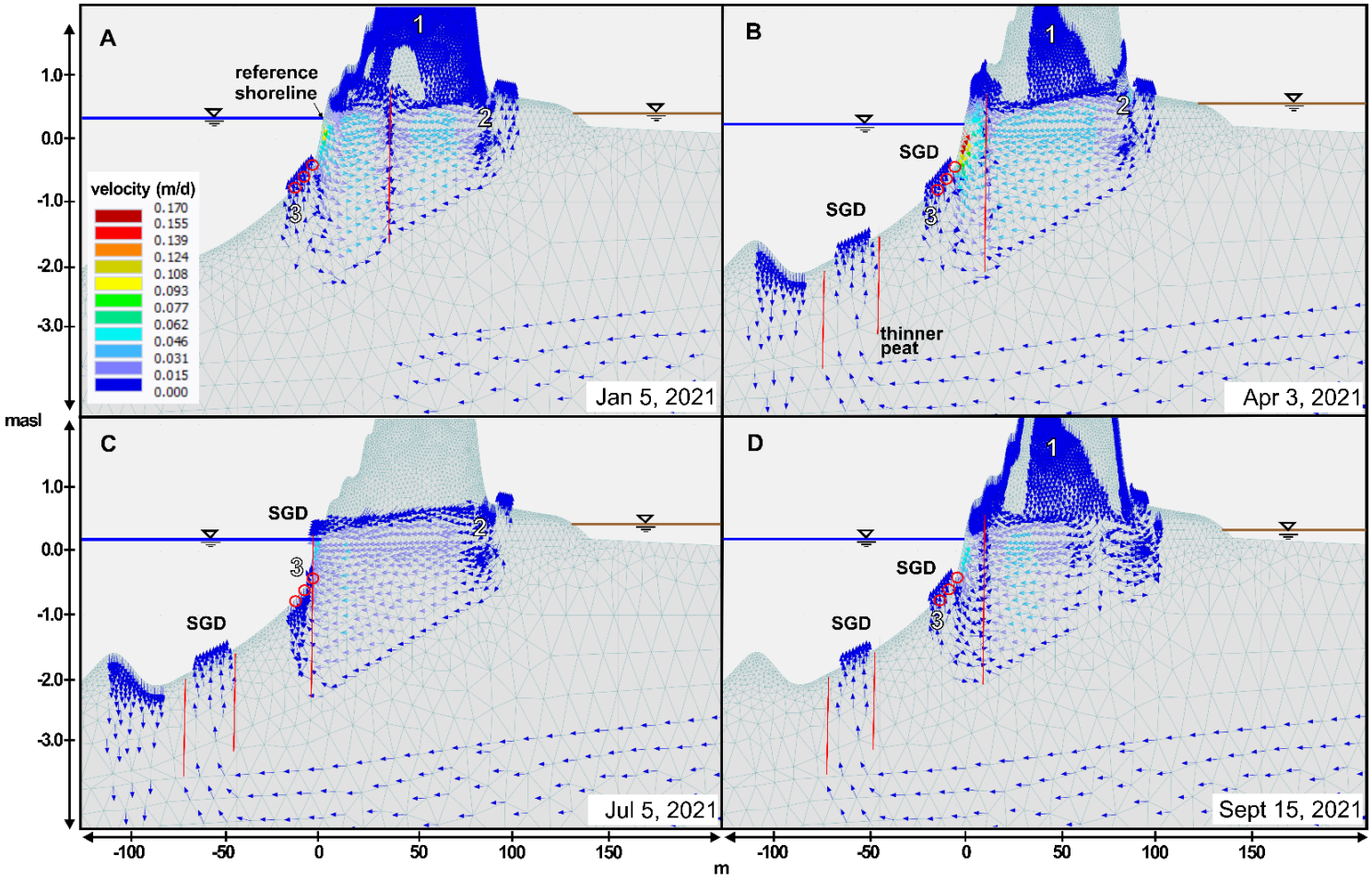

Figure 3.6. Velocity vectors of groundwater flow in a 2D transect between the Baltic Sea and the Hütelmoor peatland. The images are subsections of the modelling domain taken from HYDRUS simulations. Four dates were chosen, which are representative for the season stated in brackets. A) Jan 5, 2021 (Dec-Feb). B) Apr 3, 2021 (Mar-May). C) Jul 5, 2021 (Jun-Aug). D) Sept 15, 2021 (Sept-Nov). Red lines illustrate groundwater-seawater interfaces. Red circles indicate location of seepage meters. Blue line: seawater level, brown line: surface water level in peatland. Numbers represent the source of SGD in the nearshore SGD zone: 1 – precipitation at the dune dike, 2 – infiltrating peatland surface water at the base of the dune dike, 3 – recirculated seawater.

3.3.4 Daily, Monthly, and Seasonal SGD, SWI, and Net Fluxes

The meteorological conditions varied between the studied hydrological years. Hydrological Year (HY) 1 (Nov 2016–Oct 2017) was considered the wettest year with an annual precipitation of 833 mm. The driest years were HY2 (Nov 2017–Oct 2018) and HY3 (Nov 2018–Oct 2019) with annual precipitations of 600 mm and 579 mm, respectively. The climatic water balance of both years was negative (-43 mm a^{-1}). During the study period, daily precipitation reached up to 63.36 mm d^{-1}(Figure 3.4A), extremely high compared to a mean of 1.92 mm d^{-1}.

Mean daily sea level during the study period was 0.11 masl with an amplitude of 1.96 m (-0.82 to 1.14 masl; Figure 3.4B). However, sea levels showed a larger range at an hourly resolution (-1.12 masl to 1.69 masl). The highest sea level occurred during the January 2, 2019 storm surge. Mean daily groundwater level at the central peatland is 0.43 masl with an amplitude of 1.11 m (-0.24 masl to 0.87 masl). The lowest groundwater levels occurred during autumn 2018 (Figure 3.4B). The years of 2018 and 2019 were characterized by summer droughts which saw the normally ponded sites in the Hütelmoor drying up particularly in 2018.

The mean daily net flux is 0.15 m^2 d^{-1} ranging from -6.12 m^2 d^{-1} to 1.63 m^2 d^{-1} (Figure 3.6A). The highest daily net flux occurred on January 7, 2017, two days after a 1.02 masl (daily mean) storm surge. It was the result of a large hydraulic gradient (0.64 m) due to high groundwater level (0.47 masl) and low sea level (-0.17 masl). Similarly, high net fluxes were observed after the twin storm surges in January 2019. On the contrary, the lowest daily net flux (-6.12 m^2 d^{-1}) happened during the Jan 2, 2019 storm surge. Mean daily SGD flux (Figure 3.7B) is 0.47 m^2d^{-1} while mean daily SWI flux (Figure 3.7C) is -0.32 m^2d^{-1} (Table 3.3).

Based on cumulative net fluxes (Figure 3.7D), a general and steady terrestrial groundwater discharge can be observed in 2017 and 2019–2021. In summer and autumn 2018, though, the net terrestrial discharge stopped and turned negative, indicating a flow reversal. Net fluxes started to increase again from Nov 2018 with a momentary drop during the Jan 2019 storm surges. Since then, cumulative net flux steadily increased generally with daily and monthly changes visible in the plot.

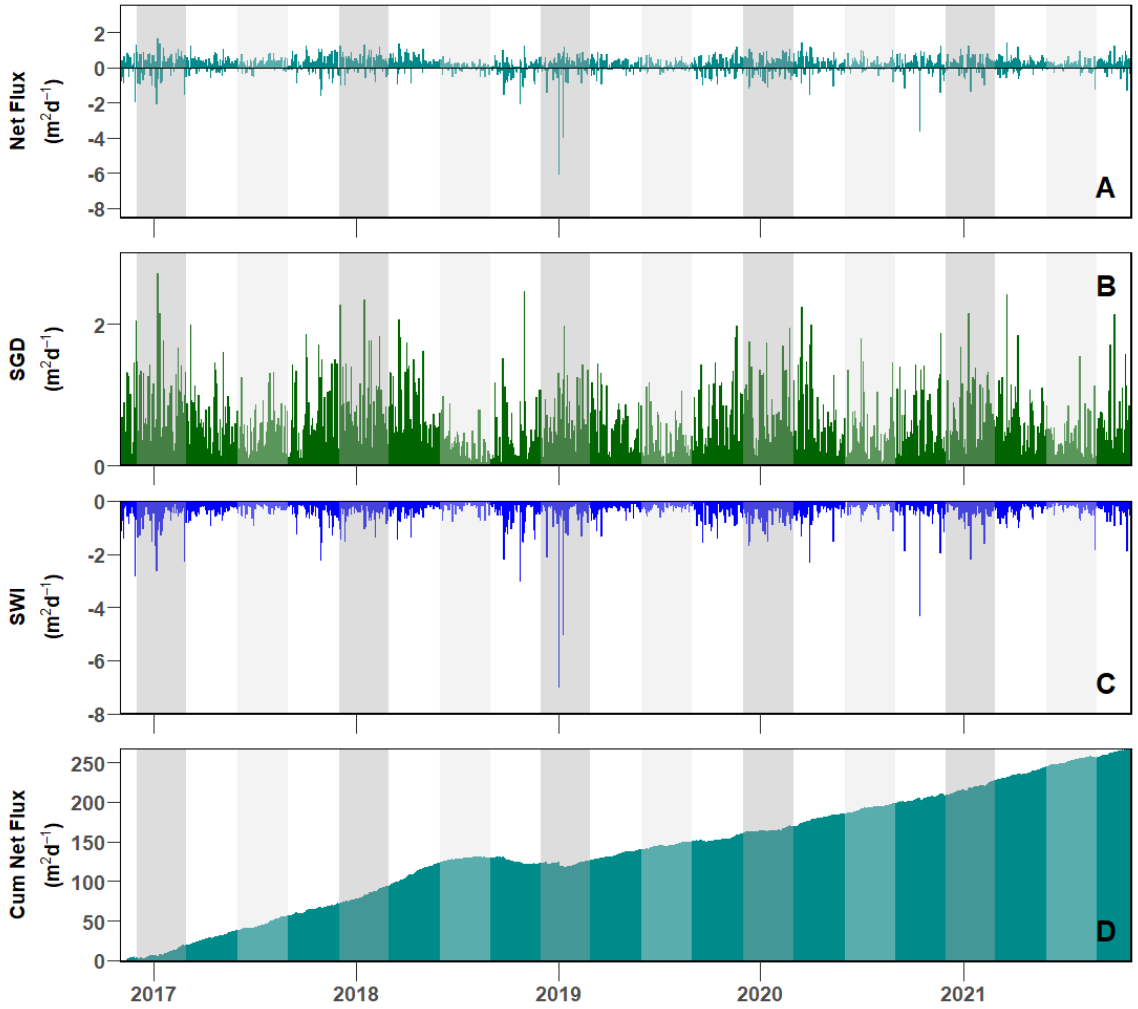

Figure 3.7. Simulated daily net flux (A), daily SGD flux (B), daily SWI flux (C), and cumulative net flux (D) at the coastal peatland Hütelmoor from Nov 2016 to Oct 2021. Alternating dark and light gray shades represent winter (Dec-Feb) and summer (Jun-Aug), respectively.

Looking at monthly scales, the climatic water balance is positive from October to March while negative values occur from April to September (Figure 3.8A). Most waters enter the system in winter, peaking in January (mean monthly sum: 42 ± 23 mm month^{-1}). By spring, waters leave the system with highest negative water balance in May (mean monthly sum: -34 ± 44 mm month^{-1}). In summer, a mostly negative water balance occurs and in fall, water balance starts to be positive again. Mean monthly groundwater level, meanwhile, peaks in March (0.57 ± 0.04 masl), two months after the maximum of the climatic water balance (Figure 3.8B). Groundwater level is lowest during the month of September (0.27 ± 0.20 masl). Mean monthly sea level ranges from 0.06 masl to 0.16 masl but variability, reflected by standard deviation, is higher than mean sea levels and changes for different months (Figure 3.8C). The highest mean monthly sea level happens in July but variability is also smaller during the summer (0.16 ± 0.11 masl). On the contrary, the monthly mean sea level in January is slightly smaller but standard deviation is much higher in winter (0.15 ± 0.24 masl). From October to February, standard deviation in mean sea level is ≥ 0.21 m while it drops to 0.11 masl in late spring and summer.

In terms of monthly means of net fluxes, peak terrestrial groundwater discharge occurs in February (0.23 ± 0.46 m^2d^{-1}) and March (0.23 ± 0.47 m^2d^{-1}) (Figure 3.8D). The discharge starts to decrease in April until October (0.06 ± 0.61 m^2d^{-1}) before increasing to a relatively constant mean discharge from November to January (0.12 – 0.14 m^2d^{-1}). It should be noted, though, that high standard deviations have been observed especially during the months of January and October. Lesser variations in the daily net fluxes are observed as the months progress from late spring to summer. This can also be seen in the probability distribution plot of the daily net fluxes (SM Figure 3.4). More positive and less varied daily net fluxes occur in spring and summer while the probability of negative daily net fluxes increases in fall and winter. In addition, spring daily net flux appears to be more positive in comparison to the other seasons.

Total SGD appears to be highest during Jan-Mar with mean daily SGD flux of ≥ 0.61 m^2 d^{-1} (Figure 3.8E). The standard deviation is also highest during these months (0.43–0.51 m^2 d^{-1}). Total SGD is expected to be lowest during Aug where mean daily SGD flux is 0.30 ± 0.28 m^2 d^{-1}. The least variability in total SGD occurs during May–Aug. Relative monthly contributions of terrestrial and recirculated SGD changes due to mainly changing contributions of recirculated SGD (Figure 3.8F). Despite not having the highest absolute terrestrial SGD, the month of May exhibited the highest % terrestrial SGD contribution. In Feb and Mar, when terrestrial SGD peaks (Figure 3.8D), total SGD also peaks during these months (Figure 3.8E), equating to high recirculated SGD contribution. The lowest terrestrial SGD contribution was recorded in October due to both low terrestrial SGD and high recirculated SGD.

The long-term contributions of recirculated and terrestrial SGD to total SGD amount to 69% and 31%, respectively (Table 3.3). During the drought year HY3, contribution of terrestrial SGD decreased to 22%. On the contrary, the largest percentage of terrestrial contribution was 36% during HY5. The highest total SGD was recorded during HY1 where total output reached a mean of 0.53 m^2 d^{-1} with 34% terrestrial and 66% marine contributions.

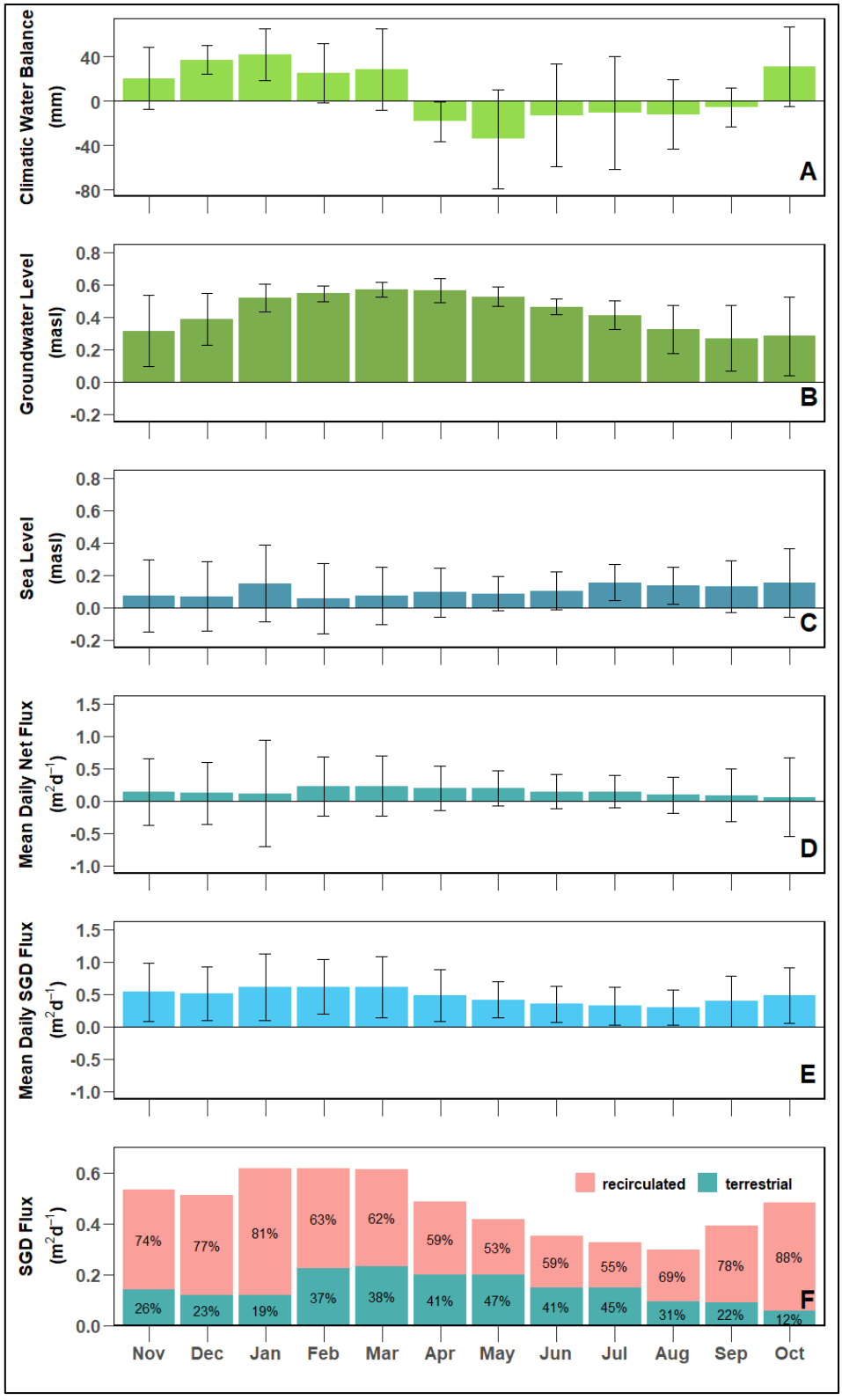

Figure 3.8. Monthly means of climatic water balance, groundwater level and net fluxes across the seafloor at the study site Hütelmoor in the study period Nov 2016–Oct 2021. A) Climatic water balance. B) Groundwater level (MP6P). C) Daily net flux. D) Mean daily net (terrestrial SGD) flux for each month. E) Mean daily (total) SGD flux for each month. F) Relative contribution of recirculated and terrestrial SGD to total SGD flux for each month. Error bars depict standard deviation based on daily values (A-E).

Table 3.3. Annual means of water fluxes in the coastal zone of the study site Hütelmoor. The Hütelmoor coastal zone extends from the base of the dune dike (+11 m) to 100 m seaward of the reference shoreline. The recirculated SGD is assumed to be equal to the absolute value of seawater intrusion.

	Water Fluxes					
	HY 1	HY2	HY3	HY4	HY5	All
Total output from the seafloor						
Submarine Groundwater Discharge (Total SGD; m^2 d^{-1})	0.53	0.48	0.40	0.47	0.46	0.47
Total input into the seafloor						
Seawater Intrusion (Recirculated SGD; m^2 d^{-1})*	-0.35	-0.33	-0.31	-0.33	-0.29	-0.32
% Recirculated SGD of Total SGD	66	69	78	70	64	69
Net output from the seafloor						
Net Flux (Terrestrial SGD; m^2 d^{-1})	0.18	0.15	0.09	0.14	0.17	0.15
% of Total SGD	34	31	22	30	36	31
Groundwater Level (masl)	0.51	0.41	0.34	0.45	0.45	0.43
Sea Level (masl)	0.12	0.10	0.10	0.13	0.09	0.11

HY = Hydrological Year

*Seawater intrusion has a negative sign, while terrestrial SGD has a positive sign.

3.3.5 Flow Velocity Along the Modeling Transect

Based on mean nodal flow velocities for the study period, we were able to quantitatively characterize the SGD and SWI zones along the transect. Positive and negative mean flow velocities are analogous to groundwater discharge and seawater intrusion, respectively. SGD dominated in two zones nearshore and above the end of the peat layer (Figure 3.9), similar to the zones identified from the flow velocity vectors (Section 3.3.3). The nearshore SGD zone has larger flow velocities that peaks at -2 m from the shore with a mean discharge of 10.2 cm d^{-1} (Figure 3.9A). Based on the mean and maximum flow velocities (Figure 3.9B), nearshore SGD may occur between +4 m to -35 m from the shoreline. Positive mean velocities, potentially corresponding to more terrestrial SGD, are restricted to -1 m to -7.5 m from the shoreline, though (inside green dashed lines). In the remaining nearshore area, SGD was observed, but SWI dominates. Meanwhile, the farther SGD zone extends from -50 m to -75 m from the shoreline (Figure 3.9) with peak mean flow velocity of 1.1 cm d^{-1} at -59 m from the shoreline. This also corresponds to potential terrestrial SGD (inside green dashed lines). In between the SGD zones and beyond the second discharge region, SGD with mean flow velocities of < 0.02 cm d^{-1} occur, otherwise, SWI areas prevail. In the usually unsaturated beach area near the base of the dune dike SWI occurs with extremely high flow velocities during storm surges (Figure 3.9C).

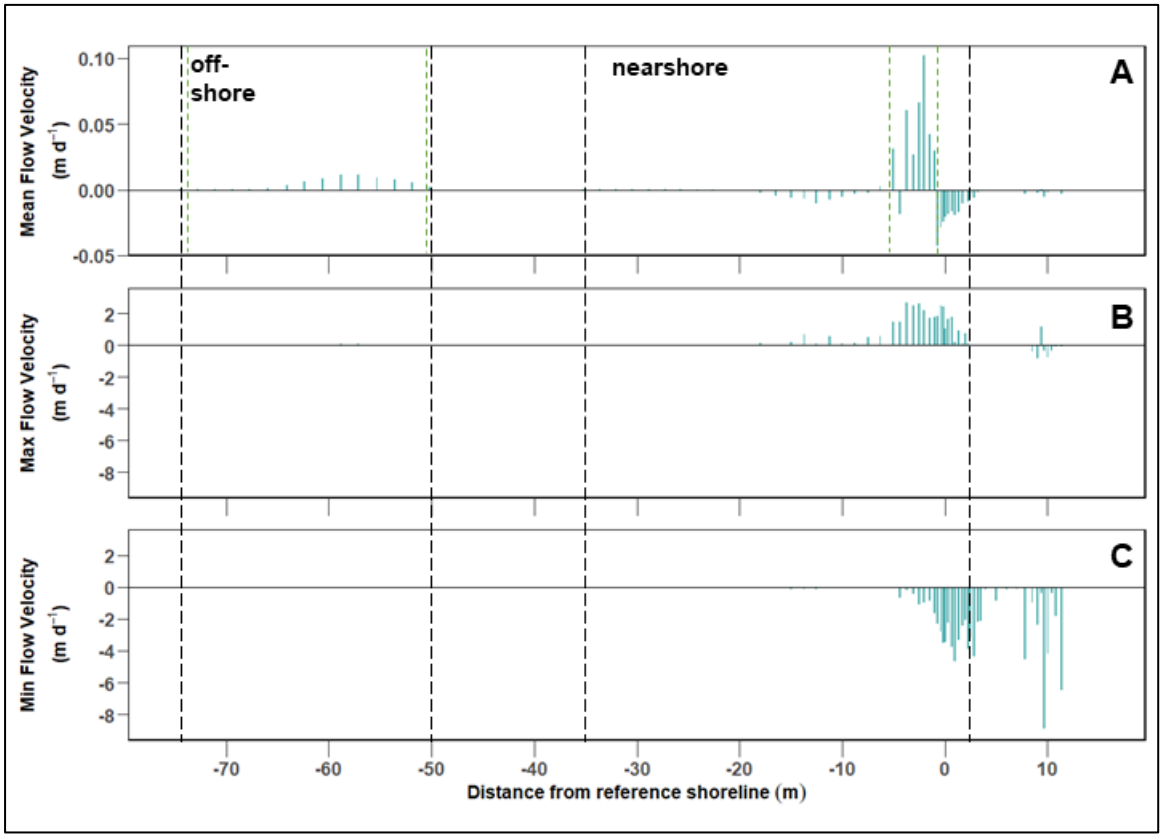

Figure 3.9: Mean (A), maximum (B), and minimum (C) flow velocities with respect to distance from the reference shoreline (X=0 m) at the study site Hütelmoor. Values were determined for each node of the modeling domain within the considered section for the entire simulation period 11/2016-10/2021. Beyond -75 m distance, flow velocities were extremely small and not visible in the plots. Positive velocities indicate groundwater discharge while negative values indicate seawater intrusion. Black dashed lines mark the maximum extent of the SGD zones as derived from distribution of mean and maximum flow velocities. Green dashed lines show where most terrestrial SGD potentially occurs.

3.3.6 Storm Surge in Jan 2019

The twin storm surge in early Jan 2019 destroyed the northern part of the dune dike, allowing seawater to flow into the peatland. In addition, seawater flooded the peatland via the groundsill, which is connected to the Warnow River and the Baltic Sea. Here, we show velocity vectors from one day before, during (peak), and until a day after the storm surge on January 2, 2019 (Figure 3.10).

One day before the peak storm surge (Jan 1, 2019 15:00), low groundwater (0.17 masl) and sea levels (-0.35 masl) resulted in limited groundwater discharge at the coast (Figure 3.10A). Twelve hours before the peak of the storm surge (Jan 2, 2019 2:00), the sea level (0.38 masl) started to increase while groundwater level stayed about the same (0.18 masl). Intrusion of seawater into the unsaturated beach can be seen which also led to discharge of seawater a few meters from the intrusion site (Figure 3.10B). During the peak of the storm surge (Jan 2, 2019 15:00), sea level height reached 1.69 masl but groundwater level was still the same (0.18 masl) (Figure 3.10C). The seawater reached and intruded the base of the unsaturated dune dike. A “circulation” cell can be observed where discharge

occurs a few meters (~5 m or less) from the location of the highest seawater intrusion velocity (or 552 cm d^{-1}) during the highest sea level. The highest seawater intrusion velocity was 1399 cm d^{-1} noted six hours before the peak storm surge at the foot of the dune dike. Six hours after the peak surge (Jan 2, 2019 21:00), groundwater level rapidly rose by 9 cm to 0.27 masl with peatland surface waters starting to infiltrate the base of the dune dike at its backside (Figure 3.10D). This groundwater level rise can be attributed to the seawater that flooded the peatland through the northern dike breach and the groundsill. After 12 hours (Jan 3. 2019 3:00; Figure 3.10E) until 24 hours (Jan 3, 2019 15:00; Figure 3.10F) from the peak surge, groundwater level further rose to 0.54 masl and then stayed the same. Meanwhile, sea level started to decrease until 0.32 masl 24 hours after the surge. The seawater that intruded the dune dike flowed both towards the sea (exfiltration via submarine groundwater discharge) and the peatland (Figure 3.10E, F). Intrusion depth of the seawater, visually determined from velocity vectors, was until ~2 m below the beach or until the beach dune-peat layer boundary. Furthermore, seawater flow into the aquifer sands was also observed up to four hours after the peak sea level (SM Figure 3.5).

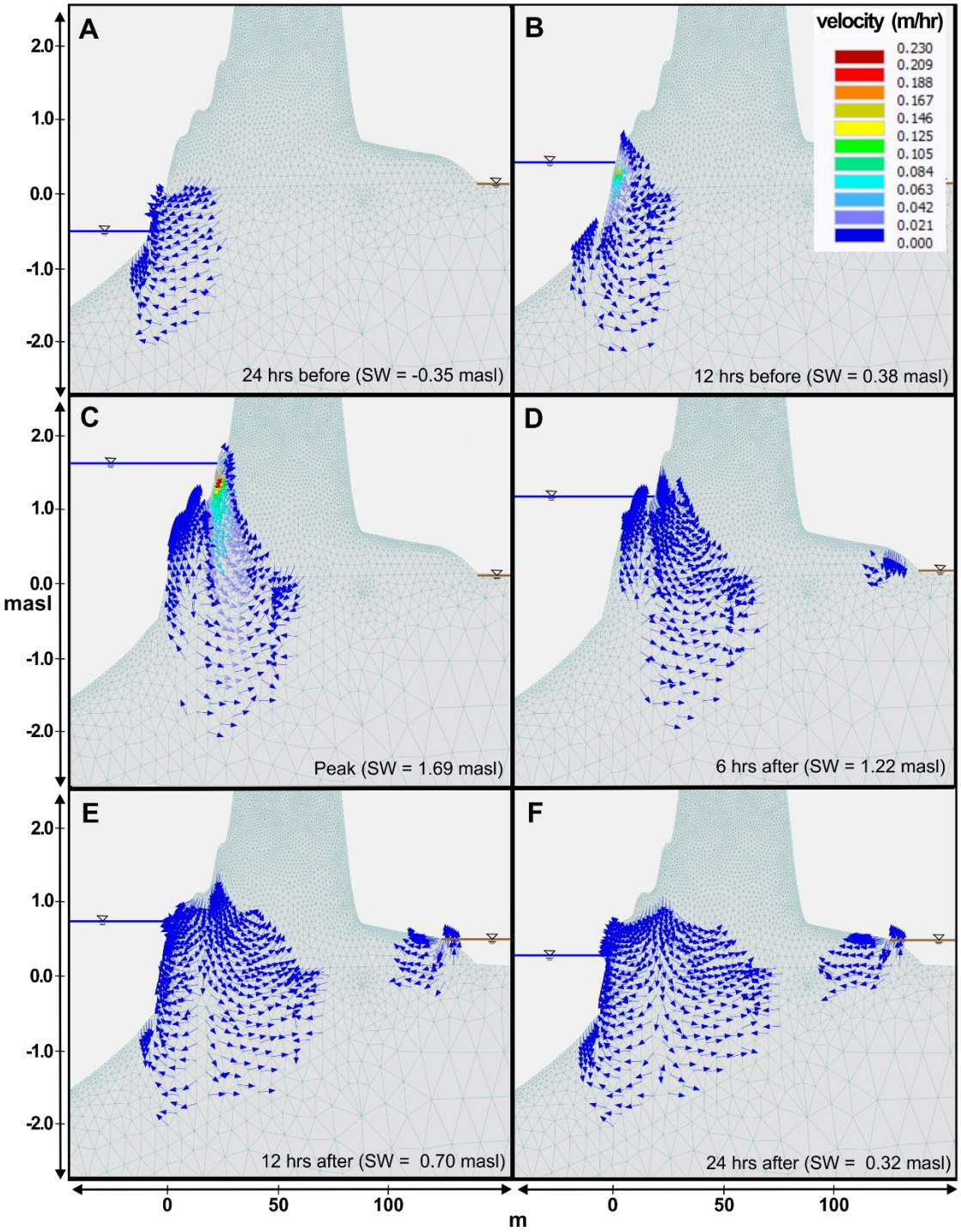

Figure 3.10. Velocity vectors taken from HYDRUS simulations showing the progression of the Jan 2, 2019 storm surge and indicating areas with submarine groundwater discharge and seawater intrusion.

3.3.7 Material Flux Estimates

Submarine groundwater discharge sampled with seepage meters exhibited higher solute concentrations than ambient seawater in both sampling periods, except for SO_4^{2-} and Br^- in September. Between the seepage meter field surveys, SGD solute concentrations were higher during the Jun/Jul sampling than in Sept 2021 (Table 3.4). Mean concentrations of DOC, DIC, ammonium, and TDN in SGD were substantially higher than ambient seawater

concentrations, although groundwater samples still had higher concentrations by one order of magnitude. On the contrary, SO_4^{2-} groundwater concentrations in the dune sands, peat, and aquifer sands are all on the lower end despite relatively high concentrations of Na^+ and Cl^-. Groundwater and surface samples from earlier field campaigns in 2017–2018 were taken from Toro et al. (2022).

In terms of SGD-derived material fluxes, based on seepage meter measurements, general discharge of materials has mostly been observed in summer while SWI was noted in fall. However, when modelled fluxes are used instead of measured seepage rates, discharge conditions prevailed and hence material fluxes were positive. Using the five-year mean total SGD flux for a seepage face distance of 25 m (the same distance for seepage meters deployed in summer) from the coast, year-round, long-term average fluxes of DOC, DIC, TDN, and NH_4^+ are 148.3±158.8 mg m^{-2} d^{-1}, 595.0±768.9 mg m^{-2} d^{-1}, 37.1±62.9 mg m^{-2} d^{-1}, and 28.3±44.4 mg m^{-2} d^{-1}, respectively. Although our SGD water sampling is limited, we have provided here the first estimates of SGD material fluxes from a rewetted coastal peatland.

Table 3.4. Material concentrations and SGD-derived material fluxes based on field (seepage meters) and modeling estimations for the coastal peatland Heiligensee and Hütelmoor. Material concentrations of ambient seawater and groundwater are also provided. Note that samplings in June/July and September occurred at different locations.

	Concentrations (mg L^{-1})			**SGD-derived Material Flux (mg m^{-2} d^{-1})**	
	SGD[1] Jun/Jul '21 (n=17) Sept '21 (n=12) Jun/Jul+Sept '21 (n=29)	**SW** Jun/Jul '21 (n=5) Sept '21 (n=4) 2019-2021 (n=12)	**Coastal GW** (2017-22)[2] MP2DS (N=6) MP2P (N=6) MP2LS (N=6)	**SM** Jun/Jul '21[3]	**Model** 2016-2021[4]
DOC	9.0±0.8 6.3±0.9 7.9±1.6	6.8±1.6 5.5±0.4 6.1±1.3	65.1±23.8 78.9±20.2 83.7±29.1	144±140	148±159
DIC	40.9±9.6 18.6±3.2 31.7±13.5	17.7±0.2 14.2±0.1 16.6±2.5	52.3±18.8 98.3±15.4 178.5±25.7	654±154	595±769
TDN	3.1±1.2 0.4±0.4 2.0±1.6	0.5±0.1 0.1±0.1 0.3±0.2	4.5±0.8 21.2±4.9 12.3±2.4	49.2±19.6	37.1±62.9
NH_4^+	2.1±0.9 0.7±0.7 1.5±1.1	<0.1±0.1 <0.1±0.1 0.3±0.6	1.9±0.6 158±2.1 10.3±2.8	33.5±14.2	28.3±44.4
Na^+	2920±441 2186±336 2616±539	2065±311 2020±200 2770±1133	433±205 781±102 943±254	46721±7056	49172±52731
K^+	102.3±20.0 78.7±14.0 92.5±21.1	69.8±18.7 70.0±14.0 97.9±44.1	18.5±4.5 27.4±4.3 29.8±5.5	1637±320	1739±1903
Ca^{2+}	140.5±28.7 101.6±17.3 124.4±31.1	82.7±22.7 88.3±16.9 117.8±50.8	88.8±54.1 36.3±9.3 155.3±52.9	2247±460	2338±2610
Mg^{2+}	338.7±71.3 254.4±43.2 303.8±73.7	238.5±80.5 228.4±43.7 325.3±147.8	52.9±28.6 82.7±10.2 84.6±23.8	5419±1142	5710±6331
PO_4^{3-}	0.9±1.3 0.6±0.7 0.7±0.8	b.d.l. b.d.l. b.d.l	5.5±n.a. 1.9±n.a. 1.3±n.a.	14.8±21.4	12.9±26.1
SO_4^{2-}	658.4±74.6 564.0±73.4 619.3±86.8	678.2±60.6 539.3±39.2 722.2±239.3	1.0±n.a. 25.7±21.1 12.1±n.a.	10534±1194	11639±1171
Cl^-	4816±676 4029±647 4490±762	4360±784 4010±345 5033±1745	854±520 1133±174 1520±342	77062±10817	84399±87440
Br^-	14.1±2.1 11.3±1.7 13±2.4	12.4±2.2 11.4±1.0 15.2±6.2	4.0±1.5 6.1±1.2 6.7±1.1	226±34	244±255

SGD = submarine groundwater discharge; SW = sea water; GW = groundwater; SM = seepage meter; b.d.l. = below detection limit; n.a. = not applicable; MP2DS = MP2-dune sands (filter depth: 0.13 to -0.38 masl); MP2P = MP2-peat (filter depth: -1.14 to -2.14 masl); MP2LS = MP2-aquifer sands (filter depth: -3.0 to 4.2 masl). The MP2 data loggers are located on the backside of the dune dike at 88 m from the reference shoreline. The detection limits are 0.5 mg L^{-1} and 0.1 mg L^{-1} for anions and cations, respectively.

[1]Ammonium and phosphate concentrations of some samples were below detection limit.

[2]Groundwater concentrations from 22.08.2017 and 30.04.2018 were taken from Toro et al., 2018. No DOC/DIC analyses were conducted on 22.08.2017. No TDN analysis was performed on 22.08.2017 and 30.04.2018. Ammonium, phosphate, and sulfate concentrations of some samples were below detection limit.

[3]Seepage rates were based only on the area covered by the seepage meters.

[4]Model net flux was based on a 100-m seepage face for Nov 2016–Oct 2021.

3.4 Discussion

3.4.1 Model Performance

The performance of the model was evaluated by comparing observed and simulated groundwater levels. In addition, measured and simulated seepage rates from September 2021 were compared. The low MBE and RMSE as well as high r^2 and KGE values both in the calibration and validation phases confirm the goodness of fit of the model to the observed water levels in all three geological layers. Similarly, for comparison with seepage meters, the difference between modelled and measured values could have risen from uncertainty in the depiction of the near-shore geology, especially depth and thickness of the peat layer, as well as wind and wave conditions. Stones and pebbles were observed at the seafloor surface during seepage meter measurements but were not accounted for in the model. The surface sediments at this part of the coast vary in time. Changing wind and wave conditions have been observed during the fieldwork, and two seepage meters were even displaced due to strong waves during the June/July sampling. A 24-hour seepage meter sampling cycle might have explained the variation of seepage rates with respect to the dynamic sea level, but could not be pursued because of administrative reasons. Nevertheless, simulated SGD/ SWI rates generally agree with measured rates. Overall, the model is able to predict SGD and SWI with high confidence based on mass balance errors, field data comparison, and performance metrics.

The model is limited by its non-inclusion of density-driven flow. However, due to the brackish nature of both the Baltic Sea and peatland groundwaters, little convective mixing of waters is expected. Thus, we assume that density effects can be neglected at our study site. The seawater salinity is comparably low at the study site at 11.4 psu while high specific conductivities and chloride concentrations were reported for the peatland groundwater due to previous Baltic Sea inundations (Racasa et al., 2021; Toro et al., 2022). Racasa et al. (2021) calculated the densities of groundwater and surface water of the peatland and the Baltic Sea using a long-term average temperature of 9.7^0C, following Millero & Poisson (1981). The density difference between the Baltic Sea and peatland groundwater is just ~0.006 g cm^{-3} while density difference between freshwater and higher salinity waters (35 psu) is more than four-fold. The details of the density difference calculation are provided by Racasa et al. (2021).

3.4.2 General Flow Patterns and Location of SGD zones

The general groundwater flow and location of SGD zones along the cross-shore transect are primarily a result of the submerged peat layer with low K_s that appears to limit water exchange between the Baltic Sea and the coastal peatland. Two dominant SGD zones were found: nearshore (up to -35 m from reference shoreline) and offshore above the thinner submerged peat layer (-50 m to -75 m from reference shoreline). Surface waters from the peatland that infiltrate into the dune dike base merge with infiltration from precipitation before flowing as SGD into the nearshore zone. Recirculated seawater also contributes to SGD there (number 3 in Figure 3.6B–D). The mean flow velocities indicate that SWI will most likely occur from +1.7 m to <-1 m (-1.1 to -4.3 cm d^{-1}) while terrestrial SGD possibly from -1 m to -7.5 m from the reference shoreline with a peak at - 2 m (10.2 cm d^{-1}). Beyond this point up to ~-21 m, SWI was dominant although SGD, most likely from recirculated seawater, has also been noted from this region. Submarine groundwater

discharge was still observed until -35 m (mean flow velocities =0.01 – 0.07 cm d^{-1}), which hence could be argued as the extent of the nearshore SGD zone. This SGD area is potentially discharging recirculated SGD too, originating from the SWI area previously mentioned.

The second SGD zone has a distinctly lower magnitude and peaks at ~-59 m (mean flow velocity = 1.1 cm d^{-1}) from the shoreline (e.g., Figure 3.6B with thinner peat extension labeled; see Figure 3.2 for geological layers) with maximum SGD flow velocity up to 5.03 cm d^{-1} at a water depth corresponding to ~-1.91 m. Based on the mean flow velocity and the velocity vectors, this SGD zone could be argued to be mainly of terrestrial origin with waters coming from the aquifer sands beneath the peat layer. This implies that other SGD zones can be expected along the Hütelmoor coastline wherever the submerged peat layer is thin (<~50 cm) or discontinuous. The peat layer has been eroded by storm surges in the northern part of the study site's coast (near lake Heiligensee) (Toro et al., 2022; Kreuzburg et al., 2018) and outcropping peat that has been washed ashore can still be seen occasionally. Groundwater seeps were recently found there (Figure 3.1D), which could have been the reason for the temperature, salinity, and bottom water CH_4 anomalies previously described by Jurasinski et al. (2018).

Our results show that SGD occurs from coastal peatlands and is concentrated at the nearshore interface and where a confining layer thins out. The high groundwater discharge nearshore is consistent with results of Bokuniewicz (1992) and Fukuo and Kaihotsu (1988) who showed that most groundwater discharge flows through the nearshore interface of land and ocean in an unconfined aquifer. Costall et al. (2020) have also shown faster groundwater velocities at the nearshore interface. However, here, we have shown that SGD also occurs offshore from a thin aquifer that has been confined by a peat layer extending out into the sea, similar to offshore groundwater discharging from submarine terraces (Jakobsson et al., 2020) and from continental shelves (Post et al., 2013). Michael et al. (2005; Supplementary Information) hypothetically predicted that concentrated offshore discharge occurs when the confining unit outcrops at the seafloor. Further, we have shown here regions of both SGD and SWI areas along the cross-shore transect potentially identifying terrestrial and recirculated SGD zones.

3.4.3 Magnitude of SGD Fluxes

The magnitude of groundwater discharge from the peatland to the Baltic Sea may not be as minor as previously thought. Previous studies (Miegel et al., 2016; Selle et al., 2016) from the same study site estimated that terrestrial groundwater discharge is negligible due to low permeability of the peat. However, our five–year mean net flux (0.15 m^2 d^{-1}; corresponding to 5.1 L s^{-1} along the peatland's coastline) and annual estimates (0.09–0.18 m^2 d^{-1}; 3.1– 6.2 L s^{-1}) show substantial terrestrial SGD from the coastal fen. The results compare well with groundwater flow estimates by Schreiber et al. (2021) where 4.5 L s^{-1} (2016) and 6.3 L s^{-1} (2010-2011) contribute to 4.8% and 5.5% of total water outflow from the peatland, respectively. Our values are higher than previous estimates by Ibenthal (2020; 2.1 L s^{-1}), Miegel et al. (2016; 0.2–1.9 L s^{-1}); and our steady-state simulations (Racasa et al., 2021: 2.9 L s^{-1}) but within the range of the previous study's estimated uncertainty (1.3–6.8 L s^{-1}). Moreover, the net fluxes only represent the terrestrial component of the total SGD.

The simulated maximum daily SGD flux of 2.7 m^2 d^{-1} (94.2 L s^{-1}) also reveals the extent of total SGD from the coastal peatland. Seawater intrusion at the beach could be a major contributor to SGD. The maximum daily SWI flux of -7.0 m^2 d^{-1} (-243.6 L s^{-1}) (Figure 3.9) indicates the potential extent of seawater intrusion. Saline SGD has often exceeded the volume of fresh SGD at sites where it has been measured (Santos et al., 2021; Taniguchi et al., 2019; Burnett et al., 2006). Globally, the magnitude of fresh SGD compared to surface runoff has been estimated to be 0.01% - 10% (Burnett et al., 2001; Church, 1996) and, more recently, to ~0.6% (Luijendik et al. 2020). For muddy coasts such as saltmarshes and mangroves, saline SGD is expected to be greater than fresh SGD as seawater infiltrates these ecosystems through secondary permeability from burrowing organisms, root structures, and buried vegetation (Santos et al., 2021). Moreover, global total SGD estimate is said to be three to four times greater than river discharge (Kwon et al., 2014). Furthermore, most modeling studies yield SGD estimates that are two orders of magnitude lower than those from field isotope measurements (Santos et al., 2021). Here, our model estimates are two orders of magnitude lower than other wetland environments which used Rn-222 isotopes. Hence, the total SGD estimates and recirculated seawater contribution presented in this study may be grossly underestimated.

3.4.4 Temporal variability of SGD

Submarine groundwater discharge in the coastal peatland system described here is highly variable in time. In shorter time scales of hours and days, the variability of SGD depends mainly on the sea level, which influences the hydraulic gradient. Winds, waves, tides, and storm surges (see section 3.4.5) affect sea level. Winds and waves coming from west-northwest, directed towards the shore, will lead to higher sea level and lower SGD fluxes. On the contrary, a lower sea level resulting from southeasterly winds and waves will increase SGD fluxes. In the nearby Bay of Puck (Poland, southern Baltic Sea), wind direction and sea level conditions, in addition to increased precipitation, significantly increased SGD rates (Kłostowska et al., 2020). Tides are expected to have little effect on SGD since the southern Baltic Sea has minimal tidal heights (Medvedev et al., 2016). However, based on our limited sampling, even small, localized tidal heights with amplitudes of 13–28 cm (Figure 3.5) might be important in low-lying coastal peatlands when the hydraulic gradient is low, such as in late summer and fall. Still, in comparison to amplitudes of sea level and groundwater level, tidal height in the Baltic Sea possibly has less impact to SGD rates. Furthermore, a time-series cross-correlation analysis of groundwater- and sea level with hydraulic gradient and SGD shows that sea level is the main determinant for mean daily SGD. Groundwater level (r=0.71, 95% confidence level) and sea level (r=-0.72, 95% confidence level) are both highly correlated with hydraulic gradient at zero lag, but sea level correlation with hydraulic gradient sharply decreases at other time lags (SM Figure 3.6). With SGD, correlation with sea level is also highest at zero lag (r=-0.53, 95% confidence level) with rapid decline in correlation values in other time lags. In contrast, SGD correlation with groundwater level is weak and broadly distributed from lag = 0 d (r=0.18, 95% confidence level) to peaking at time lags of 36 to 60 days (r=0.25, 95% confidence level). Taken together, these findings point out that sea level is a greater determinant of short-term variations in SGD flux rather than groundwater level. These results corroborate findings by Gonneea et al. (2013) where sea level dominated over groundwater heads as contributor to variability in the hydraulic gradient and possibly with SGD (not analyzed) in Waquiot Bay, USA.

Seasonal variability of SGD can be attributed to changing climatic water balance, groundwater level and prevailing weather conditions (Figure 3.8). Seasonal mean precipitation is highest in summer (77±37 mm month^{-1}) but is rather consistent during the other seasons (47 – 55 mm month^{-1}). The climatic water balance is positive from Dec to May with the highest value in January, while the most negative value is encountered in May (Figure 3.8). Meanwhile, mean monthly groundwater level peaks in March (0.57 masl) but is ≥0.52 masl between January and May. Groundwater levels have been shown to lag peak recharge by 0–3 months in sandy aquifers because percolation takes time and recharge continues after the peak recharge (Michael et al., 2005). The mean daily net flux is highest in February and March and has a strong coefficient of determination with mean monthly groundwater levels (R^2=0.74, 95% confidence level) indicating a strong influence of groundwater level on terrestrial SGD at a seasonal scale.

Sea level is affected by seasonal meteorological conditions which then affects seasonal variability of SGD. Mean monthly sea level ranges from 0.06 masl to 0.16 masl only but variability is key to understanding how SGD might be influenced. In May and June, relatively fair weather conditions are expected while stormy weather conditions prevail from October to February. This is reflected in the monthly sea level variability with high standard deviations (Figure 3.8D). Localized winds may affect the SGD processes. Wave set-up at reflective beaches (steep with coarse sediments) results in increased groundwater discharge with increased wave height (Santos et al., 2012; de Sieyes et al., 2011). Larger waves lead to larger wave setup and larger wave-pumped SGD (de Sieyes et al., 2011). In terms of average monthly total SGD flux, the highest fluxes occur in winter (Jan, Feb) and early spring (Mar) while the discharge is lowest during summer (Jun–Aug).

The seasonal variability of SGD also influences the nearshore general flow patterns (see Section 3.3.3) and the position of the groundwater-seawater interface. During winter, seawater intrusion is greatest due to winter storms, as can be deduced from flow patterns (Figure 3.6) and recirculated SGD contribution to total SGD (Figure 3.8F). Hence, the groundwater-seawater interface at the dune dike is at its most landward extent. As months progress to summer, the interface moves seawards despite the lowering groundwater level due to calmer sea conditions. However, it should be noted that the interface is not stable and can change its direction of movement within days because of sea level variability particularly in fall and winter. In addition, the vertical oscillation of the groundwater-seawater interface in unconfined coastal aquifers described in detail by Michael et al. (2005) has not been seen in this paper. Instead, oscillation of the groundwater-seawater interface in the horizontal direction has been observed. The Ghyben-Herzberg relation does not apply in our coastal peatland system due to brackish nature of both ground- and seawaters and the presence of a confining peat layer that extends seawards.

In summary, the seasonal variability of SGD in a low-lying diked and rewetted coastal peatland in the southern Baltic Sea depends on groundwater-sea level interactions but it is mainly sea level-dominated. During winter, the highest SGD flux occurs due to both increasing groundwater level and seawater intrusion brought about by increasing precipitation and winter storms, respectively. Seawater intrusion contributes about 74% to the SGD flux (Table 3.5). In spring, maximum groundwater level (March) coupled with decreasing sea level variability (least variability in May) also lead to high SGD flux with the highest terrestrial SGD contribution (41%). In summer, the lowest SGD flux occurs as low

groundwater levels and low seawater intrusion are observed because of low climatic water balance and more stable sea level conditions, respectively. The terrestrial SGD contribution remains high in summer (40%) even though groundwater level is declining, a further proof that the system is sea level dominated. In addition, the high precipitation in summer could also drive terrestrial SGD contribution coming from atmospheric inputs at the dune dike. The dune dike contributes about a third to the total terrestrial SGD (Racasa et al., 2021). Lastly, in fall, the SGD flux rises again due to higher variability in sea level, and therefore higher seawater intrusion, while groundwater level keeps on declining leading to a 20% contribution of land-derived SGD. In a similar tideless, semi-enclosed embayment in Obama Bay, Japan, the highest terrestrial SGD was observed in spring due to melting heavy snow and low sea level where seasonal increase in sea level also suppresses fresh SGD rates (Sugimoto et al., 2016). Similar high freshwater contribution in spring (May) and summer (July) and high recirculated seawater in fall (September) was seen in an intertidal flat in Korea (Waska & Kim, 2011).

Table 3.5. Groundwater level, sea level, submarine groundwater discharge (total SGD), and net flux (terrestrial SGD) during winter (Dec-Feb), spring (Mar-May), summer (Jun-Aug), and fall (Sep-Nov) from 11/2016 – 10/2021.

	Winter	**Spring**	**Summer**	**Fall**
Groundwater Level (masl)	0.48 ± 0.13	0.55 ± 0.06	0.40 ± 0.12	0.29 ±0.22
Sea Level (masl)	0.09 ± 0.23	0.08 ± 0.15	0.13 ± 0.12	0.12 ± 0.20
Submarine Groundwater Discharge Flux (m^2 d^{-1})	0.58 ± 0.46	0.51 ± 0.40	0.32 ± 0.28	0.47 ± 0.43
Net Flux (m^2 d^{-1})	0.15 ± 0.62	0.21 ± 0.37	0.13 ± 0.26	0.09 ± 0.52
% Terrestrial SGD	26	41	40	20

Interannual variation is a consequence of differing climatic water balances year-to-year: changing water input will change the water outputs including SGD. The high precipitation during HY1 naturally led to higher groundwater levels (Figure 3.4B) and terrestrial SGD contribution (Table 3.3). Only during HY5, the second highest annual precipitation, terrestrial SGD contribution was even higher, attributed to below-average seawater intrusion (Table 3.3). During the 2018 drought, a more negative climatic water balance resulted in more SWI as captured by cumulative net fluxes (Figure 3.7D). However, the 2019 drought could not be observed. No decrease in cumulative net flux was observed even though a negative annual climatic balance was recorded. This will be further explored in the next section.

3.4.5 Impact of Storm Surges, and Sea Level Rise

Storm surges impact SWI and SGD, and these impacts are expected to increase in the future. Over the past 60 years, the Baltic Sea has experienced more frequent storm surges that last longer and have higher sea levels (Wolski & Wiśniewski, 2021). The largest storm

surge during the study period intruded the unsaturated dune dike resulting in SWI and subsequent SGD from recirculated seawater. After a storm surge, there is typically a positive net flux and large SGD a few days later (Figure 3.7, 2.10). The study area is known for having the deepest negative storm surges and most frequent and longest-lasting low and very low sea levels (Wolski & Wiśniewski, 2020). Every year, the sea level goes down below ≤-0.7 masl and ≤-1.0 masl for approximately 32.5 hrs and 3.8 hrs, respectively. These storm surges, including negative storm surges, will affect both SGD and SWI water flux as well as the SGD composition.

High sea level due to storm surges can also impact the Hütelmoor peatland surface and groundwaters, and thus eventually SGD.Storms and wind events only slightly influenced SGD in a salt marsh compared to spring-neap tidal cycles (Wilson et al., 2015). However, when storm surge amplitude is large compared to tidal fluctuations (Wilson et al., 2015), such as in the Baltic Sea, the impact of storms could be greater. Moreover, storm surges also have the potential to influence groundwater and SGD for weeks and months (Cardenas et al., 2015; Nordio et al., 2023; Xin et al., 2014) to decadal scales (Anderson & Lauer, 2008). Legacy effects of seawater on groundwater quality have been seen in the Hütelmoor (Toro et al., 2022).

The 2019 storm surges replenished the depleted groundwaters in the Hütelmoor peatland. Groundwater level declined to as much as -0.24 masl during the 2018 drought. At the onset of the Jan 2 storm surge, groundwater levels rapidly rose from 0.18 masl to 0.54 masl within 12 hours. The following summer 2019, there was another drought in Eastern Germany and Poland (Boergens et al., 2020) but its impact on groundwater levels was less severe than in summer 2018. This is likely due to higher precipitation levels during summer 2019 despite similar annual climatic water balance for HY2 and 3. Additionally, the seawater flooding during storm surge may have contributed to the additional water in the peatland. Peatlands are known to store water and mitigate flooding. Ahmad et al. (2020) suggest that hydrological buffer function of drained fens can be restored through long-term rewetting. The seawater must have been retained in the peatland by the groundsill and contributed to the relatively higher groundwater levels compared to 2018. An overall downward-directed flow was deduced for the peat layer based on $^{4}He_{rad}$ isotope distributions and prevailing hydraulic gradients (Toro et al., 2022). Further, Koebsch et al. (2019) and Gutekunst et al. (2022) showed the infiltration of freshwater and brackish inflow, respectively, in porewater profiles taken from the study site. Flooding seawater can thus be expected to recharge groundwater and eventually discharge as SGD. However, flow velocities are very low and a delay of years or decades can be expected according to Toro et al. (2022).

Finally, sea level rise related to climate change will reduce hydraulic gradients and intensify seawater intrusion into the aquifer (Robinson et al., 2018). Increase in tide- and wave-induced seawater recirculations could have more pronounced impacts on the geochemical composition of the discharging groundwater especially with longer residence times (Tamborski et al., 2017). Large episodic wave events like storm surges could also have a lasting effect on water flow and salinity distribution (Robinson et al., 2018; Anderson & Lauer, 2008).

3.4.6 Geochemical Implications of Flow Dynamics

Like in sandy beach aquifers (Heiss & Michael, 2014), biogeochemical reactivity of submarine groundwater discharge from coastal peatlands must be closely linked to water flow and solute transport processes. In the first SGD zone, the nearshore mixing zone of brackish Baltic Sea waters and Hütelmoor groundwaters and the highly dynamic groundwater-seawater interface is expected to create an important reaction zone which can alter geochemical conditions along the discharge pathway (Robinson et al., 2007). As seawater intrudes the beach/ dune layer, it brings in oxidized waters which will mix with groundwater. Redox and pH transitions at the mixing zone have been shown to affect the distribution of metals and nutrients in nearshore aquifer and SGD (Robinson et al., 2007). The release of iron due to GW-SW mixing leads to accumulation of iron and the so-called "iron curtain" which also retains other materials (Charette et al., 2005; Charette & Sholkovitz, 2002). Since seawater infiltration into the dune dike varies temporally and spatially, distribution of solutes will also vary in both time and space.

In the second discharge region farther from the coast, this SGD zone could be a potential DOC hotspot as peat has been shown to release DOC in contact with both saline water (Gosch et al., 2018) and low saline groundwater (Kreuzburg et al., 2020). Seawater mixing with pore water has been reported to alter DOC reactivity and elevate DOC concentrations by 0.4 to 6.6 μmol L^{-1} (Goodridge, 2018). In addition, Tiemeyer et al. (2017) showed that field DOC concentrations increase with higher SC and low porewater velocities. Transient groundwater-seawater regimes will impact materials released from seaward, eroded, and exposed peat layers This has important regional implications since outcropping and extending peat layers are aplenty along the German Baltic coast.

Storm surges, high sea levels, and droughts will affect groundwater and eventual SGD chemical composition. Seasonal storm surge events and high sea levels may bring marine sulfate to the peatland through breaches in the dune dike and the groundsill. During droughts, if seawater intrusion in the peatland occurs, sulfate addition from seawater may enhance sulfate enrichment due to low water table. Drought and seawater inundation have been shown to increase sulfate availability in surface and pore waters from the Hütelmoor which has implications to microbial communities and greenhouse gas fluxes (Gutekunst et al., 2022). Ammonium may be released by seawater inundation as Na^+ and K^+ could compete with NH_4^+ adsorbed in peat soils (McCarter et al., 2018).

3.4.7 SGD-derived Material Fluxes and Loads

Groundwater sampled from seepage meters revealed seasonality of SGD originating from the peatland. Summer concentrations of SGD were higher than fall concentrations, e.g., DOC (1.4-fold), DIC (two-fold), TDN (eight-fold) and ammonium (four-fold). This matches with the decreasing contributions of terrestrial SGD from summer to fall (Figure 3.8F) and potentially lead to higher SGD-derived material fluxes in summer. Higher summer SGD nutrient and carbon fluxes have been shown in the Gulf of Mexico (Santos et al., 2008) and Obama Bay, Japan (Sugimoto et al., 2016). Further, the higher SGD solute concentrations compared to ambient seawater in both summer and fall (Table 3.4) signify the influence of terrestrial SGD to the total discharging groundwater from the seafloor.

Higher salinity of SGD compared to ambient seawater were reported for both sampling campaigns (Figure 3.3C). Unlike most coastal ecosystems where the adjacent seas have high salinity, Baltic Sea is brackish with an average surface water salinity of 7.5 psu (Szymczycha & Pempkowiak, 2016). The surface and groundwater of the Hütelmoor is also brackish (Racasa et al. 2021; Toro et al., 2022) and has been influenced continuously in the past by Baltic Sea inundations, with one-third of its groundwater originating from the sea (Toro et al., 2022). Therefore, the groundwater continuously discharging from the low-lying peatland is brackish. Particle tracking reveal that water flow from the dune and from the peatland could take from several months to years before groundwater discharges to the sea (SM Figure 3.7). Hence, discharging terrestrial groundwater from the coast could have originated from the peatland after several months or years. Moreover, seawater that intruded by wave setup possibly from months before and then, recirculates as SGD could have possibly caused the higher SGD salinity than the ambient seawater. The average seawater salinity near the study site is 11.4 psu which is higher than ambient seawater salinity during the sampling campaigns (Figure 3.3C, D).

The rewetted peatland is an unaccounted source of carbon and nitrogen to the Baltic Sea. Mean DOC and DIC fluxes estimated using SGD rates from seepage meters and simulated SGD compare to values reported for other environments (Table 3.6). Mean DOC and DIC flux for -2 m from the reference shoreline is in the same order of magnitude with fluxes from other carbon-rich environments, i.e., mangroves and coastal canal draining a wetland. Further, our DOC and DIC fluxes are comparable, if not higher, with values estimated from the Bay of Puck, southern Baltic Sea (Szymczycha et al. 2014). In addition, it should be noted that the peatland study site is a diked environment unlike with other open ecosystems where exchange of water and solutes occur freely. Between DIC and DOC fluxes, higher DIC flux is possibly due to remineralization of DOC in the STE. Remineralized carbon components (DIC, CO_2) have been released from peat exposed to waters with changing salinity (Kreuzburg et al., 2018). In addition, cabonate lacustrine sediments have been found in front of the lake Heiligensee causing enrichment of DIC in groundwater (Toro et al., 2018).

Calculated SGD-derived nutrient and carbon loads from rewetted coastal peatlands are important for the Baltic Sea. Area-normalized ammonium and phosphate loads of the Hütelmoor coastal peatland are 224% and 75% of the Upper Warnow Load (data from von Ahn, 2023; Table 3.7). Moreover, the area-normalized long-term (2012-2021) Warnow River ammonium load of 2.2 mol d^{-1} km^{-2} (HELCOM, 2022) pales in comparison to SGD ammonium load (fifteen-fold) although oxidized nitrate is the dominant form of nitrogen in the river. DOC and DIC loads are just 6% and 8% of the Upper Warnow River load. However, considering that coastal peatlands cover about 400 km^2 in the northeast German state of Mecklenburg-Wester Pomerania and that no other major rivers discharge to the sea, the role of SGD in delivering carbon and nitrogen loads from coastal peatlands to local coastal waters become highly relevant. Though, carbon and nutrient load estimates should be taken cautiously as they are based on limited field campaigns.

Table 3.6. Comparison of Dissolved Organic Carbon (DOC), Dissolved Inorganic Carbon (DIC), Total Dissolved Nitrogen (TDN), and ammonium (NH_4^+) fluxes from the Hütelmoor coastal peatland to other environments.

Environment	Seepage (cm d^{-1})	DOC Flux (mg m^{-2} d^{-1})	DIC Flux (mg m^{-2} d^{-1})	TDN Flux (mg m^{-2} d^{-1})	$NH4^+$ Flux (mg m^{-2} d^{-1})	Method	Reference
Coastal peatland*							This study
SM (summer)	1.6± 1.4	145 ± 140	654 ± 154	49 ± 20	34 ± 14	Seepage Meters	
Modeling (-25 m)	1.9 ± 1.6	148 ± 159	595 ± 769	37 ± 63	28 ± 44	HYDRUS Modeling	
Modeling (-2m)	10 ± 37	804 ± 3067	3226 ± 13023	201 ± 893	153 ± 662	HYDRUS Modeling	
Mangroves							Chen et al., 2018
Wet	36 ± 33	3723 ± 3603	8408 ± 9849	--		Rn-222	
Dry	20 ± 18	3003 ± 2763	3003 ± 2883	--			
Mangroves	14 ± 6.3	1285 ± 192	n.a.	379 ± 58		Rn-222	Sadat-Noori & Glamore, 2019
Wetland-drained coastal canal	3.1 ± 1.5	841 ± 577	817 ± 528	--		Rn-222	Davis et al., 2020
Sandy Beach	30 ± 12	228	1225	--		Darcy	Chaillou et al., 2015
Sandy beach underlained by mud						Rn-222	Santos et al., 2009b
Summer	15.2	323.1			48.7		
Winter	17.2	227			61.3		
Sandy beach (Bay of Puck, Baltic Sea)	0.36 – 2.13	62.3 ± 5.0	793.9 ± 146.7			Various	Szymczycha et al. 2014

*Coastal peatland SGD and material fluxes were calculated using seepage meters (limited to the 0.25 m^2 area covered by seepage meters deployed up to 25 m from shoreline) and HYDRUS modeling (long-term total SGD mean for the first 100 m from shoreline but seepage face of 25 m to match with seepage meters). In addition, SGD-derived fluxes were calculated at -2 m from the shoreline, where the highest mean, long-term seepage rate along the transect was determined.

Table 3.7. Comparison of Upper Warnow River Load and SGD Load Normalized by Basin and Peatland Area

	Upper Warnow Load (mol d^{-1} km^2)	Hütelmoor SGD Load (mol d^{-1} km^{-2})	SGD: Upper Warnow (%)
DOC	4329	265	6
DIC	12563	1062	8
Ammonium	15	34	224
Phosphate	4	3	75

Notes: Solute loads from von Ahn et al., 2023; Upper Warnow Drainage Area (349 km^2) from Koch et al. 2018; Hütelmoor peatland area (3.5 km^2) from Toro et al., 2022.

3.5 Conclusions

Seasonal dynamics of submarine groundwater discharge from a diked, rewetted coastal peatland were assessed using a five-year soil hydrological model combined with seepage meter measurements. Our findings suggest that sea level primarily determines the hydraulic gradient and the ensuing total SGD from the coastal fen. Terrestrial SGD, nevertheless, follows seasonal variability of groundwater level which potentially affects solute concentrations and SGD-derived material fluxes. The SGD pathway from coastal peatlands could contribute substantially to dissolved carbon and nutrient inputs to coastal waters based on comparable estimated fluxes. Moreover, through velocity vectors, we were able to show the influence of the peat layer to SGD zone locations and that the biogeochemically important groundwater-seawater interface is restricted to the nearshore area. In addition, in similar brackish coastal environments, SGD could have salinities higher than ambient seawater as a consequence past seawater inundations. Expected increase in sea level and storm surge events will intensify seawater impacts to groundwater, i.e., higher salinity, increase in solute concentrations, and large SWI/ SGD fluxes during surge events. As a next step, linking hydrological and geochemical processes is required as, there is a definite need to understand these processes in light of the recent rewetting of coastal peatlands as a nature-based solution to combat climate change.

Supplementary Material to Chapter 3

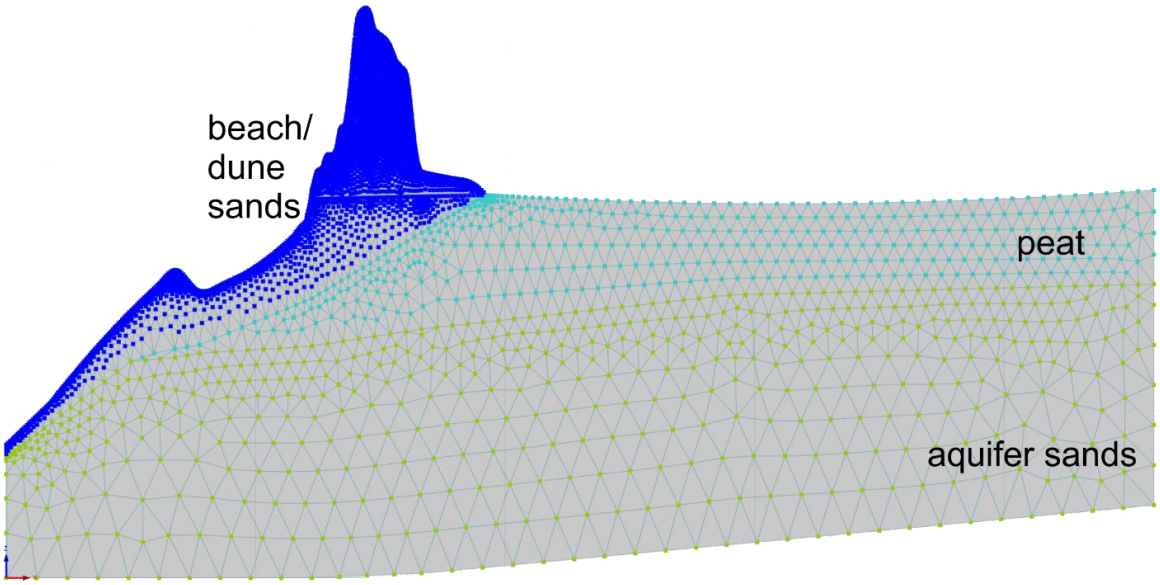

SM Figure 3.1. Modeling domain showing different geological layers and higher concentration of nodes of the finite element mesh at the unsaturated part of the dune dike.

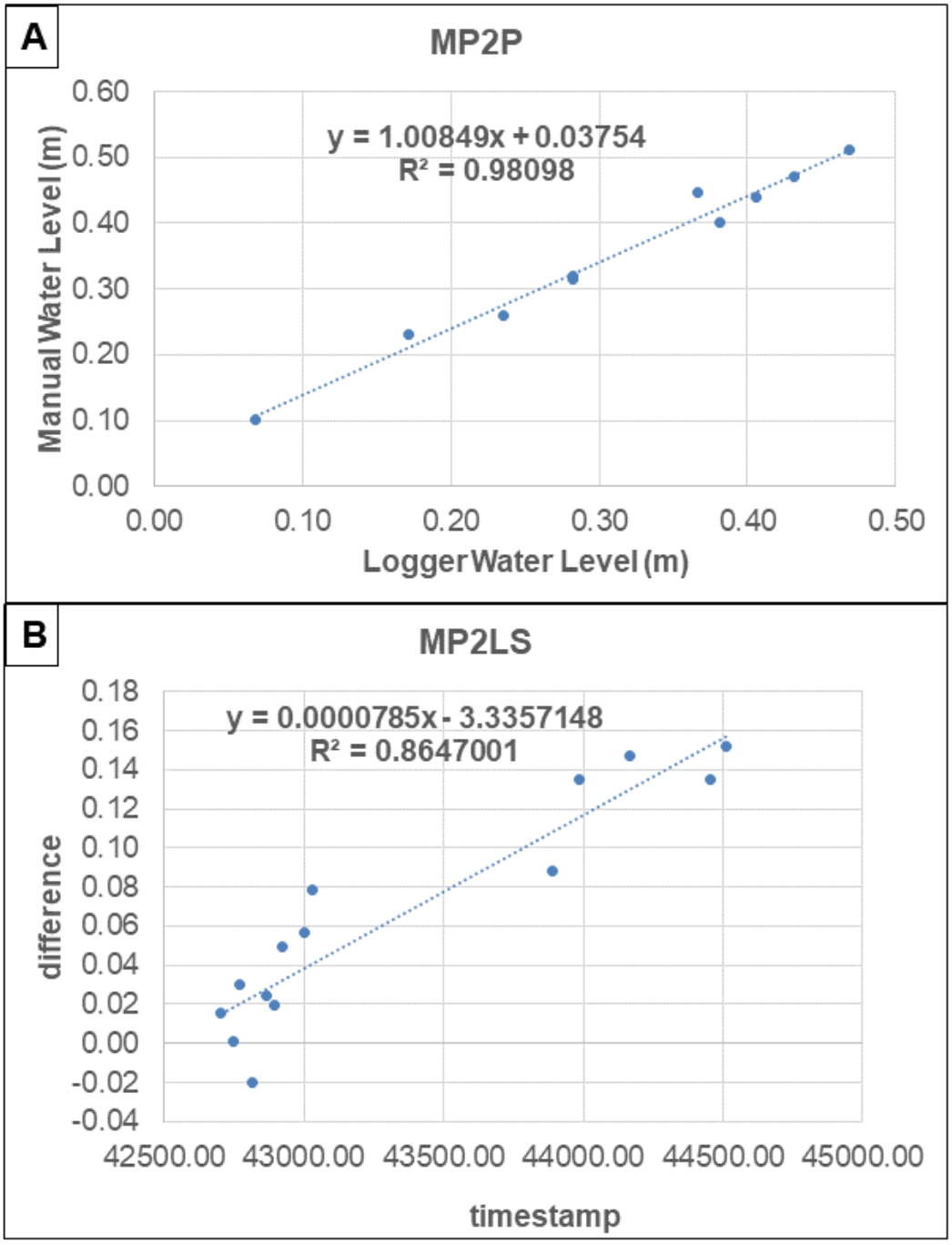

SM Figure 3.2. Examples of water level correction. Logger water levels were corrected by using linear regression of either A) logger measurements vs. manual measurements (MP6-peat, MP2-peat, MP2-dune sands) or B) measurement errors (difference between manual and logger measurements) vs time, if a drift was observed (MP2-aquifer sands). For the latter method, the measurement error was determined for a specific time using the linear regression equation for timestamp and difference in water levels. This measurement error was added to the logger measurement to get the final water level. The average difference between the manual measurements and the final water level was 0.00013 ± 0.02142 m (N = 14).

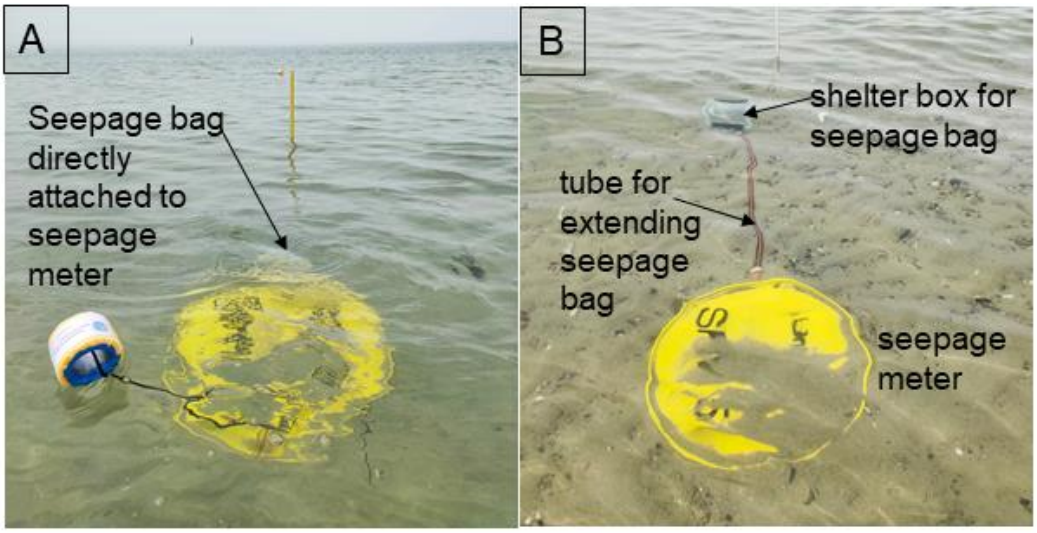

SM Figure 3.3. Two types of seepage meters used in the study: (A) the traditionally designed seepage meter based on Lee (1977) and (B) the modified seepage meter with a side hole, extended tubing, and shelter box for the seepage bag (Rosenberry et al., 2020; Duque et al., 2020). The latter is used for shallow water depths where waves may affect seepage bags and seepage measurements.

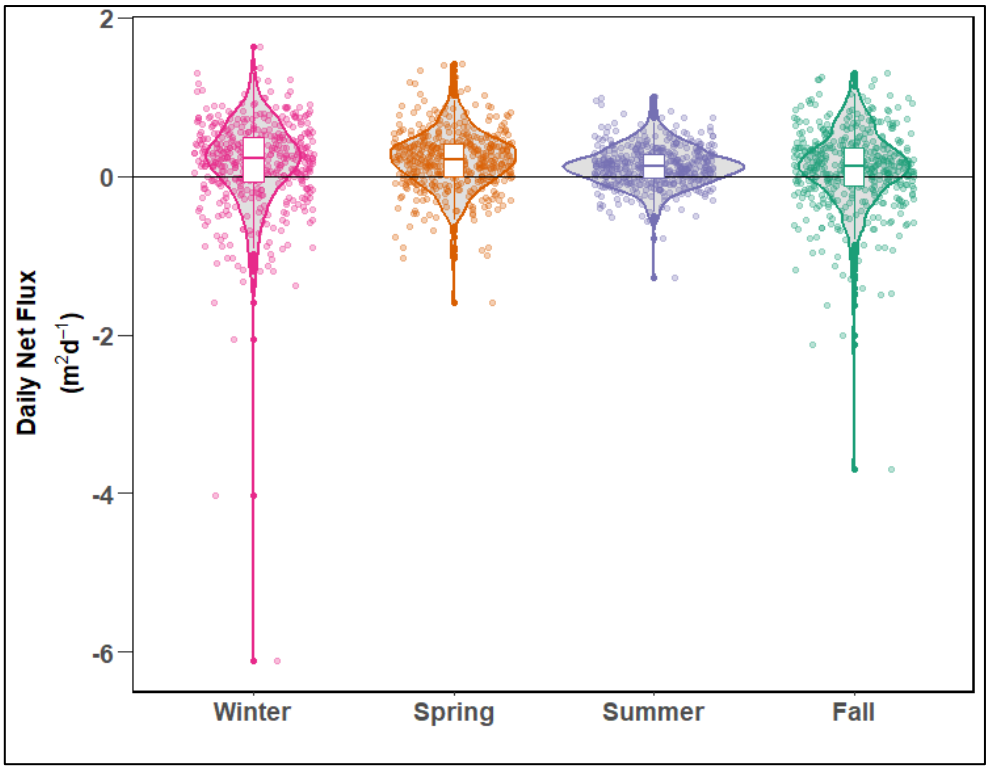

SM Figure 3.4. Probability distribution of daily net flux values showing extremes. Winter = Dec–Feb; spring = Mar–May; summer = Jun–Aug; fall = Sept–Nov.

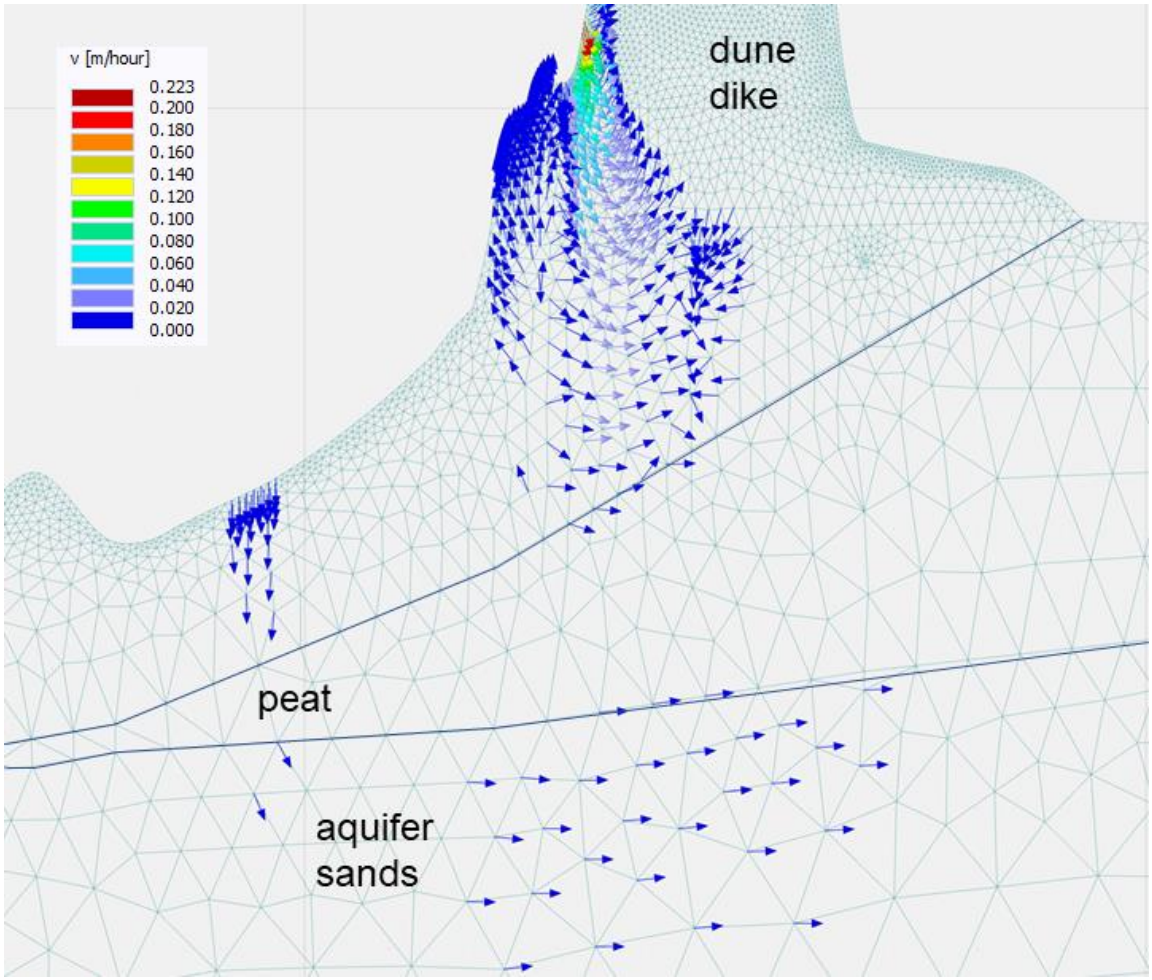

SM Figure 3.5. Seawater inflow into the narrow peat layer and the underlying aquifer sands during storm surge peak of Jan 2019.

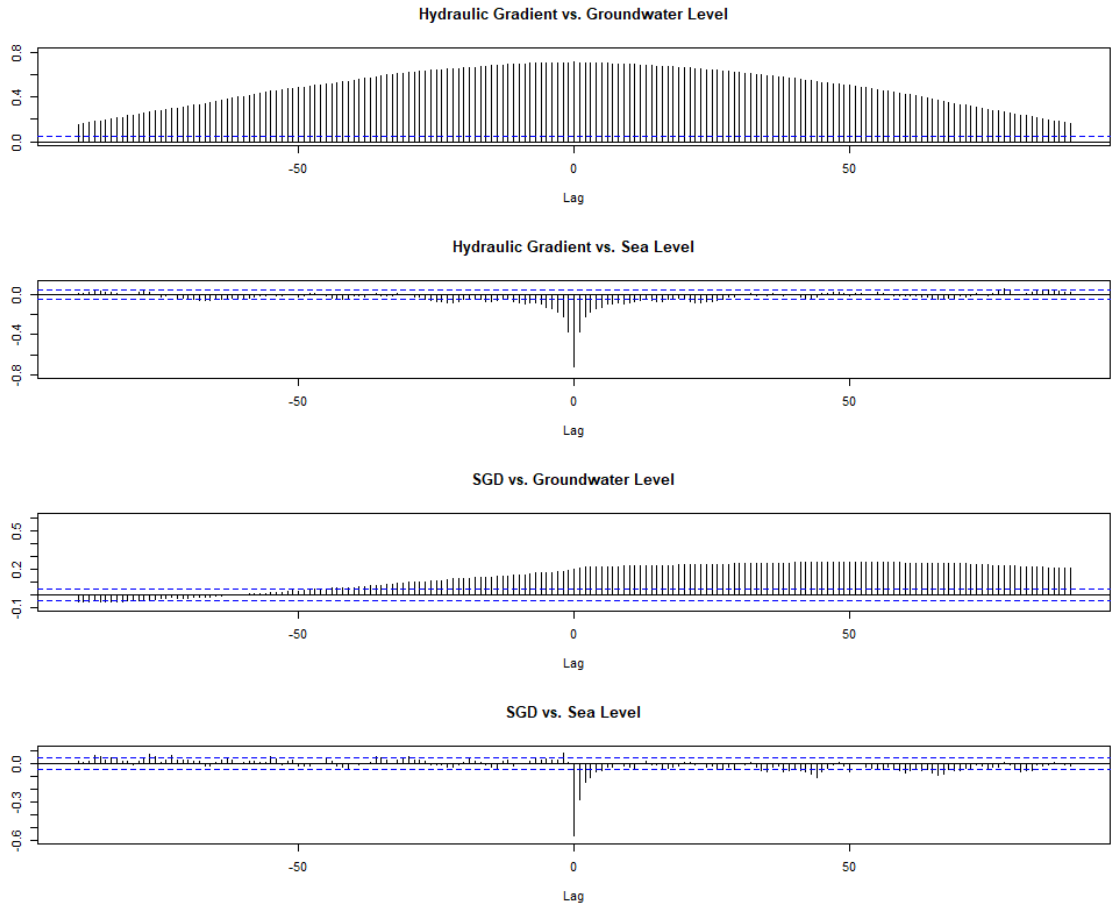

SM Figure 3.6. Cross-correlation plots of (from top to bottom) hydraulic gradient vs. groundwater level, hydraulic gradient vs. sea level, SGD vs. groundwater level, and SGD vs. sea level. Both sea level and groundwater level have high correlation at zero lag (r = 0.72 and r = 0.71, respectively; 95% confidence level) but only sea level has a moderate negative correlation with total SGD flux (r = -0.53; 95% confidence level). The cross-correlation plots were generated using the cross-correlation function (ccf) in RStudio (2022). The function determines the correlation coefficient between two time series at different time lags.

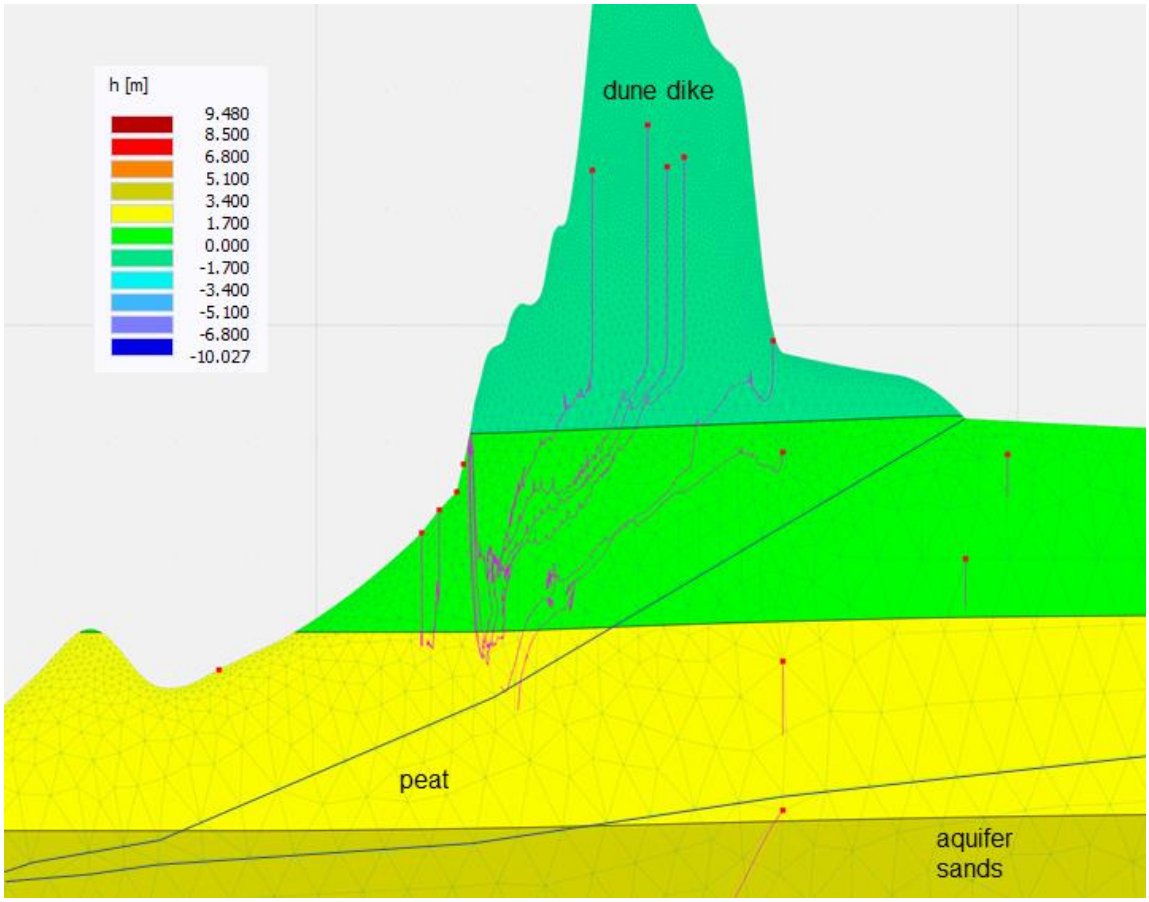

SM Figure 3.7. Particle trajectories after five years of simulations with particles at the initial position at T=0.

4. GROUNDWATER QUALITY IN TWO COASTAL FENS AND THE INFLUENCE OF STORM SURGE FLOODING AND REWETTING WITH SEAWATER

Abstract

Coastal peatlands are unique ecosystems situated at the interface of land and sea. In the past, these carbon-rich coastal regions were extensively diked and drained mainly for agriculture, turning them into carbon sources. Recent management strategies focus on restoring these coastal areas' natural connections with the adjacent sea. In this study, we aimed to characterize surface and groundwaters in two coastal fens and examine the impacts of seawater input caused by a storm surge and seawater rewetting. Surface and groundwater samples (from different depths and geological layers) were collected from a brackish-rewetted (2017–2022) and a seawater-rewetted fen (2019–2022) located in storm-surge-prone and brackish southern Baltic Sea. These samples were analyzed for major ions and dissolved carbon. Our findings reveal past variable marine influence on surface and groundwater of coastal peatlands which depend on distance from the coast, peat thickness, and possibly, drainage networks. Both storm surge and seawater rewetting affected surface waters most: increasing specific conductivity (SC) and pH. Significant and drastic changes in surface waters occurred in the seawater-rewetted fen since the peatland was transformed into a lagoon-like environment connected to its adjacent sea. While the groundwater of peat and aquifer sands did not change significantly, notable changes were observed. These included increased DOC concentrations in the brackish-rewetted fen under high SC and decreased pH conditions, contradicting laboratory studies. In the seawater-rewetted fen, initial DOC decreased, but later, additional sampling showed the same high SC, low pH, and high DOC concentration. Although we did not look at specific processes affecting DOC concentrations, its mobilization is likely related to anion exchange of organic acids with sulfate, but other processes should not be ignored. Excess strong base cations increased Acid Neutralizing Capacity (ANC) positively correlating with DOC. Cation exchange of ammonium adsorbed on peat soils with sodium probably occurred after seawater influx. Groundwater response to seawater rewetting is not fully understood. However, ongoing salinization of seawater-rewetted fens may lead to brackish-rewetted environments with higher concentrations of seawater salts and potentially create new biogeochemical reactive mixing zones of ground- and seawater.

Keywords: *coastal peatlands, rewetted fen, wetlands, dissolved organic carbon, ammonium*

4.1 Introduction

Coastal peatlands are important wetland ecosystems at the interface of land and sea. They play a vital role in storing and sequestering significant amounts of carbon (Limpens et al., 2008; Mitra et al., 2005) and, like other wetlands, provide a wide range of essential ecosystem services (Joosten & Clarke, 2002). Unfortunately, decades and centuries of anthropogenic activities, especially drainage, have caused substantial degradation to peatlands, turning them from carbon sinks into carbon greenhouse gas sources (Leifeld et al., 2019). To mitigate the release of greenhouse gas emissions from drained peatlands, restoration measures by rewetting to previous hydrological levels are being implemented. This process is considered the most cost-effective approach, as a nature-based solution, to reduce greenhouse gas emissions in the atmosphere (Leifeld & Menichetti, 2018).

While freshwater rewetting has successfully curbed carbon dioxide (CO_2) gas emissions from peatlands, it can also lead to an increase in methane (CH_4) gas emissions, a more potent greenhouse gas (Hahn et al., 2015). One solution being considered by restoration managers is restoring the natural connection of coastal peatlands with the sea by implementing seawater rewetting. Seawater rewetting can restore sulfate (SO_4^{2-}) pools in coastal peatlands and, thus, prevent CH_4 emissions by providing an alternative electron acceptor in the form of sulfate (Jørgensen, 1982; Miao et al., 2012). Sulfate deprivation can trigger high CH_4 production, and its replenishment can reverse the process (Koebsch et al., 2019; Pönisch and Breznikar et al., 2023; Gutekunst et al., 2022).

Storm surges can also bring in seawater, and therefore SO_4^{2-}, which could inundate several low-lying peatlands and wetlands that have been documented along the southern German Baltic coast (Jurasinski et al., 2018; Sterr, 2008). This Baltic Sea (BS) coastal region is particularly susceptible to storm surges due to prevailing northwestern and northeastern wind systems (Wolski & Wiśniewski, 2020). Further, sea level rise is predicted to affect Baltic coasts in the long term, with a mid-range scenario of 0.70 ± 0.30 m of sea level increase in the 21st century (BACC II Author Team, 2015).

The input of seawater may have large impacts on wetland ecosystems as well as surface and groundwater quality and quantity. In addition to SO_4^{2-}, seawater brings in salts such as sodium (Na^+) and chloride (Cl^-), which are important for re-establishing brackish or saline conditions necessary for the revival of diverse wetland ecosystems (Sinicrope et al., 1990), although adverse effects of increasing salinity have also been noted on some vegetation types (Batistel et al., 2022). Legacy salt effects from previous Baltic Sea floodings on groundwater have been recorded in a coastal peatland (Toro et al., 2022). In addition, ammonium (NH_4^+), dissolved organic carbon (DOC), and Dissolved Inorganic Carbon (DIC) may be exported to surface and groundwater after rewetting (Zak & Gelbrecht, 2007; Poenisch & Brezniker et al., 2023), as well as phosphate (Liu & Lennartz, 2019b; Linke & Gislason, 2018). Moreover, submarine groundwater discharge may be expected to increase as hydrological gradients increase from the peatlands to the sea (Racasa et al., 2021). With the combination of seawater rewetting, storm surges, and future sea level rise, the impacts of seawater on the peatland's biogeochemistry become even more complex. Additionally, there is a lack of field-based studies especially that laboratory experiments do not fully capture actual conditions and sometimes contradict field results (Tiemeyer et al., 2017; Kalbitz et al., 2000).

Thus, this study aims at characterizing surface and groundwater in two coastal fens and at understanding the impact of seawater on water quality (1) after a storm surge flooded a brackish-rewetted fen and (2) upon rewetting a drained fen with seawater. Specifically, the study will focus on the changes in the DOC, DIC, and ammonium concentrations after seawater impact.

4.2 Materials and Methods

4.2.1 Study Sites – Hütelmoor and Drammendorf

The two study sites, namely the nature reserve "Heiligensee und Hütelmoor" (hereinafter referred to as Hütelmoor/ HM) and the "Polder Drammendorf" (hereinafter referred to as Drammendorf/ DD), are situated in the northeastern state of Mecklenburg-Western Pomerania, Germany (Figure 4.1). Both sites are low-lying coastal peatlands with a history of anthropogenic activities. The Hütelmoor covers an area of 350 ha and is a paludification fen whose formation started around 7000 BP (Kreuzburg et al., 2018), surrounded by a forest and bordered by a man-made dune dike along the coastline of the Baltic Sea. The detailed geology and soil properties of the peatland is described in Kreuzburg et al. (2018) and Toro et al. (2022). The general geological stratification from the top is composed of peat, glaciofluvial sands, and the glacial till at the bottom (Figure 4.2A). The peat layer is thickest near the dune dike (up to 3 m). Saturated hydraulic conductivities (K_s) of the geological layers vary: 8.64 x 10^{-2} m d^{-1} (HM-7) to 10^{-4} m d^{-1} (HM-2) in the peat layers and 1.73 m d^{-1} in the aquifer sands (Toro et al., 2022). Similar to other peatlands in Europe, the Hütelmoor underwent initial drainage in the 18th century, followed by more extensive drainage during 1976 – 1991 to create grassland pasturage (Miegel et al., 2016). As a result of peat compaction and degradation, the peatland's surface elevation lowered. Although the ditches still exist today, the peatland has been rewetted since December 2009, following the construction of a 0.4 masl groundsill at its drainage outlet (HM-4, Figure 4.1). Seventeen wells were built in 2016 around the peatland with filter screens in the peat (n=4; abbrev.: P), aquifer sands (n=8; abbrev.: LS), dune sands (n=2; abbrev.: DS), and ditches (n=3; abbrev.: none) (Figure 4.1). Surface water level at the central peatland ranges from -0.26–0.88 masl (mean=0.42 masl; 09/2016–11/2021; measured from HM-6P).

In January 2, 2019, a 1.69 masl storm surge occurred which destroyed the northern part of the dune dike of the HM peatland in front of lake Heiligensee (Figure 4.1). This allowed seawater to flow into the peatland resulting to a rise in groundwater level at the central peatland (Figure 4.1 HM-6) by 37 cm. Specific conductivity measurements a few days after the storm surge showed that the seawater traveled into the peatland via the ditches (Gutekunst et al., 2022). Previous recorded seawater inundations in the peatland occurred in 1872, 1904, 1913/14, 1949, 1954, and 1995 (Toro et al., 2022).

Drammendorf is located on the island of Rügen, ~73 km from the Hütelmoor (Figure 4.1). The coastal peatland is protected from the open BS through the lagoon of Kubitzer Bodden. In contrast to the Hütelmoor, Drammendorf's subsurface geology has not been well described. As such, geological investigations were undertaken; methods and results are described in the next sections. Drammendorf peatland was diked and drained in the 1960s, which also resulted in peat degradation, compaction, and lowered elevation. The peatland's various agricultural uses were grassland (northwestern area), farming with

seasonal fertilizer application until the 1990s (northeastern), and cattle grazing (southern) (Pönisch and Breznikar et al., 2023). On 26 November 2019, a section of the dune dike was unearthed and opened, allowing seawater to flow in and rewet the peatland. At present, the peatland is hydrologically connected to the Kubitzer Bodden through the dike opening and to the larger BS. Most of the peatland has been rewetted with brackish seawater with surface water levels varying depending on the Bodden's sea level. Nine wells were built in 2019, before the peatland rewetting, in the peat (n=2; abbrev.: P), aquifer sands (n=3; abbrev.: LS), peat+aquifer sands (n=2; abbrev.: none; filter screen in both peat and aquifer sands), and ditches (n=2; abbrev.: none). Surface water level and specific conductivity measured at observation well 14 at the dune dike opening range -0.33–1.15 masl (mean = 0.15 masl; 08/2020–04/2022) and 2.0–19.9 mS/cm (mean=14.75 mS/cm; 08/2020–04/2022), respectively. During winter 2021, most of the wells were destroyed due to freezing of surface waters and subsequent movement of ice. Only the surface water well at the dune dike opening (DD-14, Figure 4.1) remains standing.

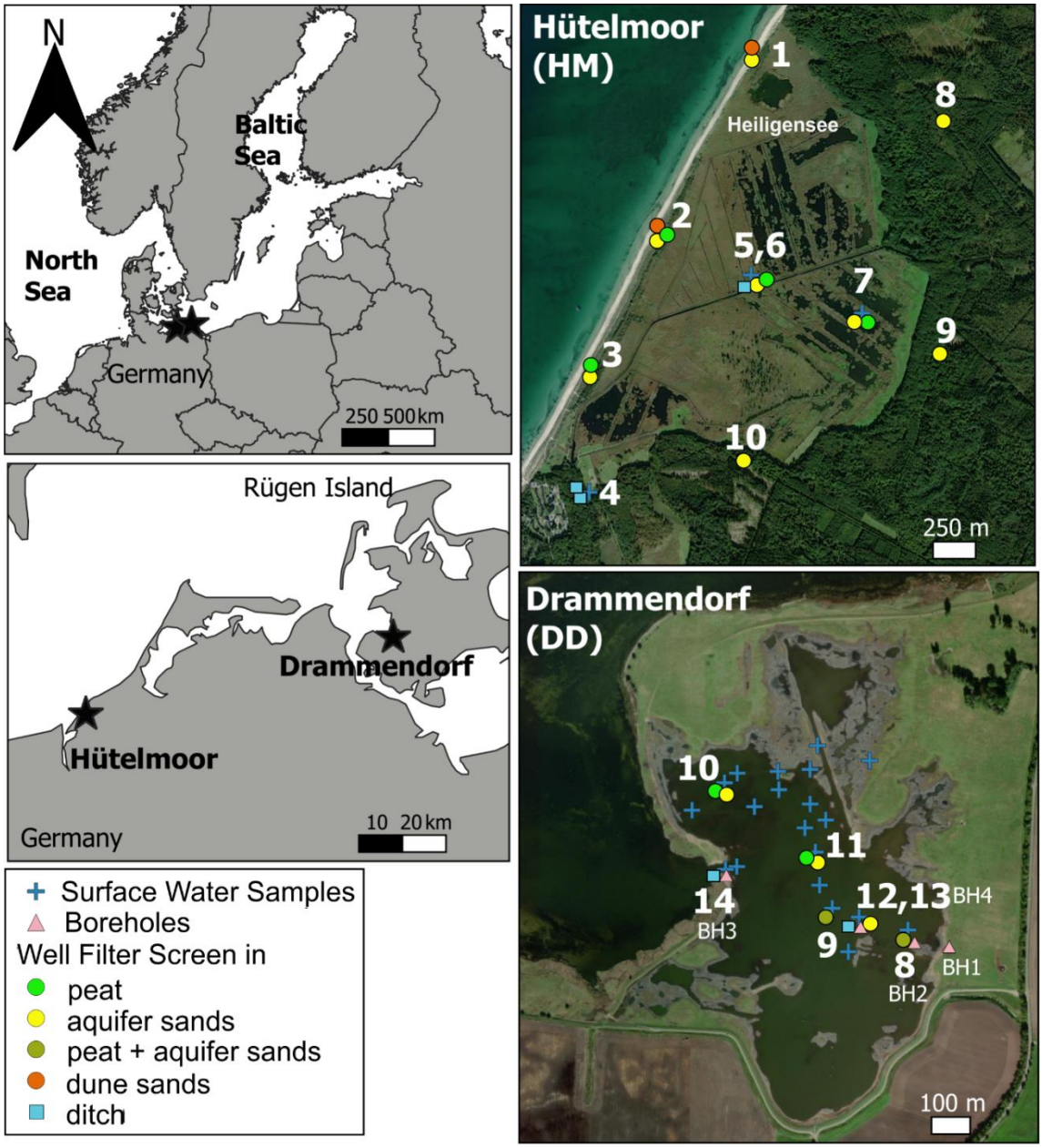

Figure 4.1. Heiligensee und Hütelmoor (Hütelmoor/ HM) and Polder Drammendorf (Drammendorf/ DD) study sites. Groundwater monitoring wells, ditch monitoring wells and surface water sampling locations are marked with circle, square and cross symbols, respectively. Borehole locations in Drammendorf are also displayed (pink triangles). Filter screens in the different geological layers are represented by different colors.

4.2.2 Core drilling and soil analyses for Drammendorf

Four sediment cores (boreholes) along an east-west transect were drilled down to a max. depth of -4.1 masl with a percussion driller and open metal rods of 4 cm diameter (Figures 4.1 & 4.2). Core logs were taken and samples were collected for grain size distribution analysis. In addition, core logs of observation wells DD-8,9,12 were utilized to describe the geological structure. The ground surface elevations of the sediment cores were levelled using a Leica CS20 with Leica GS07 GNSS receiver and Leica Captivate collecting software. Then, grain size analysis using the Sedimat 4-12 (Umwelt Geräte Technik,

Müncheberg, Germany; DIN ISO 1277) and soil organic matter content (SOM) through Loss on Ignition analysis (burning samples at a temperature of 550°C for 4 h; DIN EN 13039:2012-01) were performed on selected soil samples. Before rewetting in late 2019, measurements of hydraulic conductivity were carried out in observation wells following the borehole method (DIN 19682-8:2012-07).

4.2.3 Ground- and Surface Waters Sampling

For HM, sampling campaigns were conducted in 2019 (April, July, August, November), 2020 (February, June, November, December), September 2021, and April 2022 to collect ground- and surface water samples. Additional cation/ anion and DOC/DIC data for HM from August 2017 and April 2018 were adapted from Toro et al. (2022). Meanwhile, for DD, sampling campaigns were conducted on 18 November 2019, a week before the rewetting, and December 2019, 2020 (January, June, December), and 2022 (January and April). Harsh weather conditions and a variety of other technical problems have limited the samples collected during some of the campaigns. Physico-chemical parameters such as temperature, pH, specific conductivity (SC), total dissolved solids (TDS), and dissolved oxygen (DO) were determined *in situ* using a handheld multiparameter (smarTROLL, In-Situ Inc, Fort Collins, Colorado, USA) which was calibrated a day before each sampling campaign. Peat groundwater was collected after emptying out old waters in the wells. Due to low hydraulic conductivity of the peat layer, the recharge time for the wells took one to two hours. Groundwater from the aquifer sands with higher hydraulic conductivity was continuously pumped using a submersible pump until temperature and SC measurements stabilized before sampling was performed. The volume of the pumped groundwater from the aquifer wells was at least twice the volume of the wells. For DD, high sea level and harsh conditions prevented the use of the pump in later campaigns. Instead, wells were emptied using a bailer pipe. Surface water samples were taken from undisturbed waters a few meters from the wells. Water samples were also collected from the Baltic Sea HM campaigns. The samples from well DD-12LS from Jan and Apr 2022 were unusable since the bent well (a result of ice, wind, and wave actions) cannot be emptied prior to sampling. Collected samples were filtered on the field using 0.20 μm cellulose acetate membrane syringe filters (Rotilabo ®, Carl Roth, Karlsruhe, Germany) for major cations and anions analyses; and 0.45 μm polyethersulfone membrane syringe filters (Filtropur S, Sarstedt, Nümbrecht, Germany) for DOC/DIC/ total dissolved nitrogen (TDN) analysis. Cation and DOC samples were treated with 1 M nitric acid and concentrated hydrochloric acid, respectively. All samples were chilled during transport. Major ion samples were stored in a -20^{0}C freezer while DOC/DIC/TDN samples were temporarily stored at 4^{0}C and analyzed immediately.

4.2.4 Laboratory Analyses

Major cations (NH_4^+, K^+, Ca^{2+}, Mg^{2+}, Na^+) and anions (SO_4^{2-}, Cl^-, Br^-, F^-, NO_2^-, NO_3^-, PO_4^{3-}) were analyzed using ion chromatography (Metrohnm 930 Compact IC Flex; Herisau, Switzerland). F^-, NO_2^-, NO_3^-, and PO_4^{3-} concentrations were usually low and even beyond the limits of detection (0.5 mg L^{-1}) and thus, were not reported in this study. The DOC/DIC samples until November 2019 was analyzed using DIMATOC 2000 (DIMATEC Analysentechnik GmbH, Germany) while latter samples were analyzed using Analytik Jena Multi N/C 2100s analyzer (Jena, Germany), which additionally measures TDN. For

both instruments, DOC and DIC/TDN samples were analyzed separately since DOC samples were pre-treated with acid.

4.2.5 Calculations

No water analyses were undertaken for bicarbonate and carbonate contents which can be used to plot Piper diagrams, a useful tool to show relative compositions of cations and anions and determine groundwater facies (Appelo & Postma, 1993; Piper, 1944). However, their concentrations can be derived from DIC. The sum of all DIC species in water can be described by the following equation:

Equation 4.1

$$DIC = [CO_2] + [HCO_3^-] + [CO_3^{2-}]$$

where $[CO_2]$, $[HCO_3^-]$, and $[CO_3^{2-}]$ are the molar concentrations of the composite carbonic acid (sum of $CO_{2(aq)}$ + H_2CO_3), bicarbonate, and carbonate, respectively. Assuming that the majority of DIC species in water are in these forms and ignoring other carbonate complexes, e.g., $CaCO_3$, $MgCO_3$, etc., the equation can be rewritten using the equilibrium constants equations ($k_1 = \frac{[H^+][HCO_3^-]}{[CO_2]}$, $k_2 = \frac{[H^+][CO_3^{2-}]}{[HCO_3^-]}$) into:

Equation 4.2.

$$DIC = \frac{[H^+][HCO_3^-]}{k_1} + [HCO_3^-] + \frac{k_2\,[HCO_3^-]}{[H^+]}$$

The equilibrium constants can be calculated based on temperature (Appelo & Postma, 1993). Then, DIC, pH, and temperature can be used to determine the concentration of these inorganic carbon species. For the Piper diagram, only the samples with total anion/ total cation ratios of ± 20% error were included in the plots although 83% (HM) and 79% (DD) of the samples are within the ±10% error. The total anion and total cation were calculated by adding all the anion and cation species, respectively, in millequivalent (mEq L^{-1}) concentrations.

The Acid Neutralizing Capacity (ANC) is a reliable way to determine acidity of pore waters since it is unaffected by CO_2 degassing, aluminum reactions or organic species (Neal et al., 1999). In addition, it is a more consistent measure of acidification than relying solely on sulfate levels particularly in drought conditions (Clark et al., 2012). To calculate the ANC, the difference of the strong base cations (Ca^{2+}, K^+, Mg^{2+}, Na^+) and the strong acid anions (Cl^-, NO_3^-, SO_4^{2-}) (Equation 4.3) is determined using milliequivalent concentrations (Clark et al., 2012).

Equation 4.3.

$$ANC = ([Ca^{2+}] + [Mg^{2+}] + [Na^+] + [K^+]) - ([Cl^-] + [NO_3{}^-] + [SO_4{}^{2-}])$$

4.2.6 Statistical Analyses

To compare concentrations before and after storm surge/ rewetting in surface water, peat groundwater, and mineral soil groundwater (sands, silt and clay, marine sediments beneath peat layer), the non-parametric Kruskal-Wallis test was applied to the physico-chemical parameters. Likewise, the same test was used to compare the parameters between the two sites. The statistical test and the resulting boxplots were performed using the R program (R Core Team, 2022).

4.3 Results

4.3.1 Geological structure of the Drammendorf coastal peatland

In Drammendorf peatland, the typical sequence of sediments, in ascending order, comprises glacial till, glaciofluvial sands, locally shallow lacustrine sediments, and peat (Figure 4.2B). However, landwards from the new shoreline, a more straightforward sequence of glacial till overlain by sands was observed. The upper boundary of the glacial till layer has depths between 1.42 to -3.6 masl. The glaciofluvial sands, with a thickness of ~1.8 m near the coast, typically exhibit gravel near the till layer with slightly loamy/ silty sands on top. Meanwhile, the lacustrine sediments found in between the peat and the glaciofluvial sands has a thickness of 0.1 m. The peat layer, on the contrary, varies in thickness from 0.4 m inland to 1.3 m near the coast. Regarding peat decomposition, highly decomposed peat were found landwards (H8 and H9, von Post (1922); BH2 and BH4) while less decomposed peat (between H8 and H6, von Post (1922)) were discovered at the coast. The organic material is made of sedge-reed peat with identifiable *Phragmites* leaves. At the coast, particularly near the cleared dike, as well as at BH4 and BH1, there are clay and sand layer deposits suggesting a likely artificial deposition during the construction of the dike and drainage networks. On the land side, the glaciofluvial sands continue with silt and clay.

The formation of the coastal basal peat found at -1.70 masl depth perfectly corresponds to the Baltic Sea formation during the Littorina transgression wherein water level rose rapidly from -15 masl, starting 7.8 ky BP, up to a highstand of -1.5 - -2.0 masl at about 5.8 ky BP (Lampe, 2005). As for the saturated hydraulic conductivity, the magnitude varied by one order along the east-west transect (DD-8 to DD-9). Higher K_s was detected landwards (DD-8: 0.55 m d^{-1}; peat+sands) while lower K_s was observed in the middle (DD-12LS: 0.03 m d^{-1}; sands+lacustrine sediments), beside the north-south ditch. Other wells also exhibited low K_s both in the peat and underlying mineral soils layer (SM Figure 4.1).

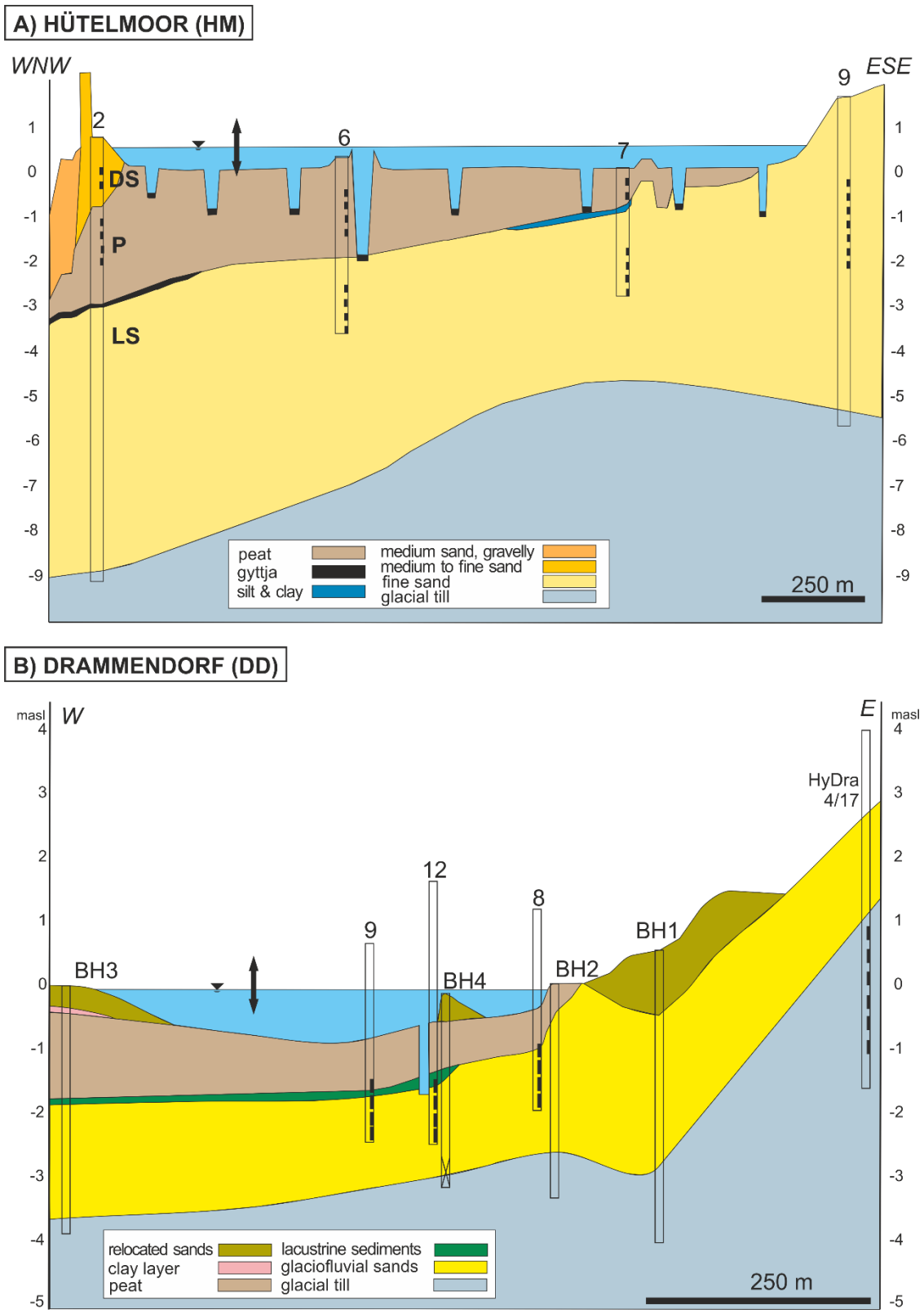

Figure 4.2. Geological profile of Hütelmoor and Drammendorf. A) Hütelmoor: cross-section modified from Toro et al. (2022) showing the geological layers and the location of filter screen of groundwater observation wells; heights of wells not shown. B) Drammendorf: geological layers, location of boreholes (BH) and filter screens of groundwater observation wells; core "HyDra 4/17' was taken from Hofmann (2017); a permanent hydrological connection to the Kubitzer Bodden exists through the dike opening on the western side, near BH3 (Figure 4.1). Note the difference in scale of the profiles of the two study sites.

4.3.2 General chemistry

Hütelmoor

Groundwater in the HM was slightly acidic to neutral with pH ranges of 6.0 – 7.2 (peat), 5.2 – 7.2 (aquifer sands) and 6.1 – 6.6 (dune sands) while surface waters fluctuated from slightly acidic to slight basic (6.4 – 7.7) (Table 4.1). A broad range of SC values were recorded from the different water samples (0.2 -13.7 mS cm^{-1}), with particularly large ranges in the aquifer sands and surface water (Table 4.1). The highest mean SC was observed in peat water. SC values measured in aquifer sands along the middle part of the peatland increased from the coast (2LS) to the peatland-forest border (7LS). High SC values were noted from the coastal side where the dune dike was breached (1LS, near Heiligensee) while the lower values were recorded from the dune and particularly the forest (<1 mS cm^{-1}). In terms of DO, as expected, surface water had the highest mean concentration (6.6 mg L^{-1}) although it dropped to 2.6 mg L^{-1}. Meanwhile, seawater had higher mean pH and mean SC values relative to ground- and surface waters (Table 4.1).

Generally, the distribution of major cations in sampled waters based on mean concentrations was $Na^+ > Ca^{2+} > Mg^{2+} > K^+ > NH_4^+$ except for surface waters where $Mg^{2+} > Ca^{2+}$. Highest mean groundwater Na^+ concentration (1037.5 mg L^{-1}) was recorded in the peat with moderate ranges when compared to Na^+ concentration ranges in the aquifer sands and surface water. In dune dike groundwater, lower Na^+ concentrations were measured while Ca^{2+} was twice that of Mg^{2+}. Potassium concentrations were higher in surface water than in groundwater. High NH_4^+ concentrations were recorded in the peat and aquifer sands (twice more in peat) while surface and dune groundwater had low concentrations.

For both groundwater and surface water, the dominant anions are chloride and sulfate followed by bicarbonate and bromide ($Cl^- > SO_4^{2-} > HCO_3^- > Br^-$) except for dune dike groundwater where SO_4^{2-} was mostly undetectable. The Cl^- distribution was similar to sodium where mean concentrations were measured in the following order: surface waters > peat > aquifer sands > dune waters. The highest mean SO_4^{2-} concentration was recorded in peat waters but high values were also recorded from the aquifer sands especially for 7LS. A wide range of SO_4^{2-} values were recorded in surface waters. Bicarbonate mean concentrations were in the same order of magnitude for peat, dune, and surface waters and slightly higher for aquifer sands. This was due to the very high DIC, hence bicarbonate, measured in the lower sands near lake Heiligensee.

The highest mean DOC concentration was measured in peat groundwater (204 mg DOC L^{-1}) with a range of 50–526 mg DOC L^{-1}. The TDN concentrations were also highest in peat with values reaching up to 108 mg L^{-1}. Meanwhile, DIC mean concentration was highest in aquifer sands (104 mg L^{-1}) with recorded values reaching 221 mg DIC L^{-1} and 330 mg DIC L^{-1} in HM-1 and -2, respectively (Figure 4.1).

Drammendorf

Groundwater pH in Drammendorf ranged from slightly acidic to slightly basic (pH=6.5-8.7) throughout the study period. A broad range of specific conductivity (1.5 – 14.2 mS cm^{-1}) and DO (0.1 -9.6 mg L^{-1}) were observed. Simultaneously, for surface waters, pH range

was more basic (6.1–9.1) while higher SC (1.0–18.1 mS cm^{-1}) and DO (4.8–15.0 mg L^{-1}) manifested.

The distribution of major cations in groundwater followed the order $Na^+ > Ca^{2+} > Mg^{2+} > K^+ > NH_4^+$ while $Mg^{2+} > Ca^{2+}$ in surface waters. Meanwhile, the major anion distribution in groundwater was dominated by sulfate and chloride and followed the order $SO_4^{2-} > Cl^- > HCO_3^- > Br^-$. For surface waters, however, Cl^- was much greater than SO_4^{2-}. Further, sulfate concentrations found in both ground- and surface waters were already in the higher range typical of natural groundwaters (Younger, 2007), even before the rewetting.

Comparison of HM-DD

Hütelmoor surface and groundwater were slightly acidic compared to more basic Drammendorf waters (SM Figure 4.2). In terms of SC levels, HM groundwater had higher values than DD while the reverse was true for surface waters. Mean Na^+ groundwater concentration (373 mg L^{-1}) in Drammendorf was half as low as HM concentration although values up to 1562 mg L^{-1} had been noted. The mean Na^+ groundwater concentration in DD resembled the mean Na^+ groundwater concentration recorded from the dune dike in HM. Mean Ca^{2+} in DD groundwater was comparable to HM concentrations (though broader concentration range) while groundwater Mg^{2+} DD values were in the lower end. Consistently high NH_4^+ values were measured from the HM, especially inside the peatland (HM-6 & -7). In DD, mean $SO_4^{2-} > Cl^-$ groundwater concentrations in contrast to HM which had more Cl^- in its groundwater. High HCO_3^- groundwater concentrations were recorded in DD though higher values were encountered in HM-aquifer sands, specifically from HM1 near the lake Heiligensee (Figure 4.1). In terms of DOC and TDN concentrations, groundwater in DD had lower concentrations compared to HM-peat groundwater but were similar to concentrations in dune and aquifer sands groundwater in the HM. The DD-DIC concentrations were comparable to their HM counterparts.

Table 4.1. Summary statistics showing physico-chemical parameters and major ions of water samples from ground, surface, and Baltic Sea water collected from Hütelmoor and Drammendorf.

		T (^{0}C)	pH	SC (mS cm^{-1})	DO (ppm)	Na^+ (mg L^{-1})	K^+ (mg L^{-1})	Ca^{2+} (mg L^{-1})	Mg^{2+} (mg L^{-1})	NH_4^+ (mg L^{-1})	Cl^- (mg L^{-1})	SO_4^{2-} (mg L^{-1})	HCO_3^- (mg L^{-1})	Br^- (mg L^{-1})	DOC (mg L^{-1})	DIC (mg L^{-1})	TDN (mg L^{-1})
HM-Surface Water	Ave	10.7	7.2	6.3	6.6	1098	40.9	103.7	128.4	1.4	1873	177.7	138.2	7.0	75.1	30.6	3.7
	Min	4.0	6.4	0.6	2.6	57	3.0	29.3	10.5	0.0	102	5.1	40.8	0.4	36.4	16.7	2.3
	Max	23.8	7.7	13.0	11.4	2199	69.5	217.1	242.1	7.0	4066	583.1	254.6	13.1	377.0	52.5	8.1
	SD	6.7	0.4	3.8	2.9	637	20.3	57.5	76.3	1.9	1134	207.5	67.9	3.5	84.7	11.8	1.8
	n	20	14	21	16	23	23	23	23	22	23	23	13	22	15	15	11
HM-Dune GW	Ave	11.3	6.4	3.0	4.4	408	17.3	102.8	48.1	1.9	797	1.0	154.2	4.0	59.6	66.8	4.5
	Min	6.0	6.1	0.5	3.9	65	10.1	13.0	7.4	1.0	95	1.0	36.1	1.8	31.8	22.9	3.5
	Max	15.6	6.6	4.6	5.4	618	23.1	171.3	79.8	2.8	1452	1.0	330.8	5.5	101.0	139.8	5.4
	SD	4.4	0.2	1.3	0.7	184	4.4	52.6	25.7	0.6	461	--	97.2	1.3	25.3	39.5	0.8
	n	8	8	8	4	8	8	8	8	5	8	1	6	6	6	6	4
HM-Peat GW	Ave	10.9	6.4	7.4	3.9	1038	32.1	248.2	207.7	31.9	1666	1143.7	157.4	8.1	203.8	64.0	52.0
	Min	5.3	6.0	4.4	0.6	660	15.0	19.7	68.9	12.7	940	9.6	17.3	4.6	50.4	12.7	14.0
	Max	22.4	7.2	10.1	7.1	1353	57.6	556.1	311.5	58.8	2194	2635.7	390.6	11.1	526.4	114.6	108.5
	SD	4.6	0.4	1.9	1.8	204	16.0	185.6	81.5	13.2	376	876.8	111.1	1.9	158.8	28.5	32.0
	n	23	18	23	15	24	24	24	24	24	24	24	16	20	17	17	12
HM-Aquifer Sands GW	Ave	10.2	6.5	5.9	2.5	815	23.0	198.4	119.6	14.9	1337	640.9	292.9	6.2	53.6	104.5	15.9
	Min	7.4	5.2	0.2	0.5	14	1.0	13.0	3.0	0.3	32	3.3	1.0	0.2	11.7	4.0	1.8
	Max	15.3	7.2	13.7	5.7	2117	58.8	472.0	281.0	34.1	3966	2216.0	959.4	21.4	132.9	330.2	40.0
	SD	1.9	0.4	3.7	1.5	556	16.4	146.3	83.7	7.9	969	810.6	230.4	3.8	27.9	73.4	11.8
	n	35	31	33	9	36	36	36	36	26	36	30	23	23	23	23	15
HM-Seawater	Ave	13.7	7.9	22.0	10.4	3924	145.3	172.2	472.0	1.1	6493	928.9	88.1	21.1	5.6	18.0	0.2
	Min	6.4	7.4	17.9	9.1	2960	110.9	137.4	361.6	0.0	3369	454.3	64.1	10.4	0.0	13.3	0.2
	Max	20.3	8.4	26.6	11.2	5141	183.2	214.3	617.4	2.2	8918	1259.2	103.3	28.3	11.7	21.0	0.3
	SD	6.8	0.4	3.3	0.9	852	27.5	29.2	101.5	1.0	1961	286.0	21.0	7.0	4.8	3.3	0.1
	n	5	4	6	4	6	6	6	6	5	6	6	3	5	4	4	3
DD-Surface Water	Ave	7.2	7.4	10.3	10.6	1636	60.2	118.8	199.4	1.6	2908	522.5	94.8	10.3	18.0	22.7	2.1
	Min	2.8	6.1	1.0	4.8	34	9.7	63.0	16.5	0.4	62	193.3	1.9	0.9	2.6	0.4	0.4
	Max	22.6	9.1	18.1	15.0	3332	115.3	185.3	374.7	9.3	5247	812.6	206.8	18.6	99.0	50.5	5.0
	SD	4.5	0.6	5.3	2.2	830	28.3	32.8	92.3	1.9	1451	138.1	41.8	4.2	18.4	10.3	1.2
	n	70	60	70	70	48	48	48	48	48	48	48	46	46	49	49	41
DD-GW	Ave	9.1	7.2	3.8	4.8	373	27.9	152.9	87.6	19.9	522	600.3	238.6	3.6	48.0	59.9	26.6
	Min	4.1	6.5	1.5	0.1	34	14.2	5.5	0.9	1.3	39	47.7	67.2	0.7	6.8	18.6	5.8
	Max	20.1	8.7	14.2	9.6	1562	58.8	258.1	247.1	44.1	2670	1488.6	445.8	10.4	191.5	122.9	53.3
	SD	4.1	0.6	3.1	2.8	351	10.7	71.9	63.1	12.8	618	350.0	102.2	2.4	47.7	24.6	15.6
	n	20	20	20	20	19	19	19	19	19	19	19	19	19	19	19	12

GW=groundwater; T=temperature; SC=specific conductivity; DO=dissolved oxygen; Na^+=sodium; K^+=potassium; Ca^{2+}=calcium; Mg^{2+}=magnesium; NH_4^+=ammonium; Cl^-=chloride; Br^-=bromide; SO_4^{2-}=sulfate; HCO_3^-=bicarbonate; DOC=dissolved organic carbon; DIC=dissolved inorganic carbon; TDN=total dissolved nitrogen; HM=Hütelmoor; DD=Drammendorf. Sulfate concentrations at HM-Dune are mostly below detection limits. 2017 and 2018 data for the HM were adapted from Toro et al., 2022.

4.3.3 Hydrochemical classification

Three groups of hydrochemical facies (Piper, 1944; Nazzal et al. 2014) were identified for the waters of HM and DD – Na-Cl (non-carbonate alkali), Ca-Cl (non-carbonate hardness), and mixed types (no dominating cation-anion pairs) (Figure 4.3). The majority of the sampled waters from the HM were classified as having Na-Cl facies with alkalis and strong acids dominating and exceeding 50% of the water composition characteristic of most ocean water (Piper, 1944). Only groundwaters from 7P, 7LS, 8LS, and 10LS had mixed water facies based on the Piper diagram and the cation/ anion ternary plots. Mixed water facies have no cation-anion pairs that exceed more than 50% (Piper, 1944). Unfortunately, groundwater samples from 9LS could not be included in the plots due to low anion/cation ratios.

Drammendorf water samples had more complex hydrochemical classifications. Pre-rewetting surface waters were distributed among Ca-Cl, Na-Cl, and mixed water facies while post-rewetting waters gravitated towards Na-Cl facies. Groundwaters from DD-10P (peat layer) and DD-12LS (aquifer sands) pre-rewetting were classified as having Ca-Cl facies or non-carbonate hardness with alkaline earth metals and strong acids exceeding 50% of water composition (Piper, 1944). Then, groundwater facies migrated to mixed and Na-Cl water types post-rewetting. This was also observed for the mixed peat+sand soils (DD-8). Meanwhile, pre-rewetting samples of DD-9 (closer to sea and on the other side of the north-south ditch), -11P, and -11LS (near the ditch perpendicular to the sea and close to DD-9) were classified as having Na-Cl facies. Unfortunately, post-rewetting sampling for DD-11P and DD-11LS was unsuccessful.

4.3.4 Hdyrochemical evolution

Groundwater chemistry of the majority of the surface and groundwater samples collected from HM and DD were likely controlled by evaporation-crystallization processes (Figure 4.4) based on the Gibbs' diagram (Gibbs, 1970). For the Hütelmoor, based on relative abundance of cationic facies, most groundwater exhibited evaporation dominance. Some groundwater samples showed evidence of higher Ca^{2+} content such as HM-7P and HM-7LS, which were clustered together, and HM-1DS and -2DS. Meanwhile, samples from HM-9LS and HM-10LS (wells located in aquifer sands of the adjacent forest) and one sample from HM-2DS showed rock weathering is the dominant factor controlling the chemistry of waters. This was also true for a HM-7 surface water sample taken in April 2018. Drastic changes among most groundwater samples were not observed after the storm surge inundation.

In Drammendorf, before the rewetting, surface and groundwater samples had higher Ca^{2+} concentrations than afterwards. Both rock weathering and evaporation crystallization processes can be assumed based on relative abundance of cationic facies. However, after rewetting, surface and groundwater samples revealed a migration from rock weathering to evaporation dominated waters, e.g., DD-8 and DD-12LS (labelled in Figure 4.4B). No water samples from either site exhibited rainfall dominance as the main process for controlling groundwater chemistry.

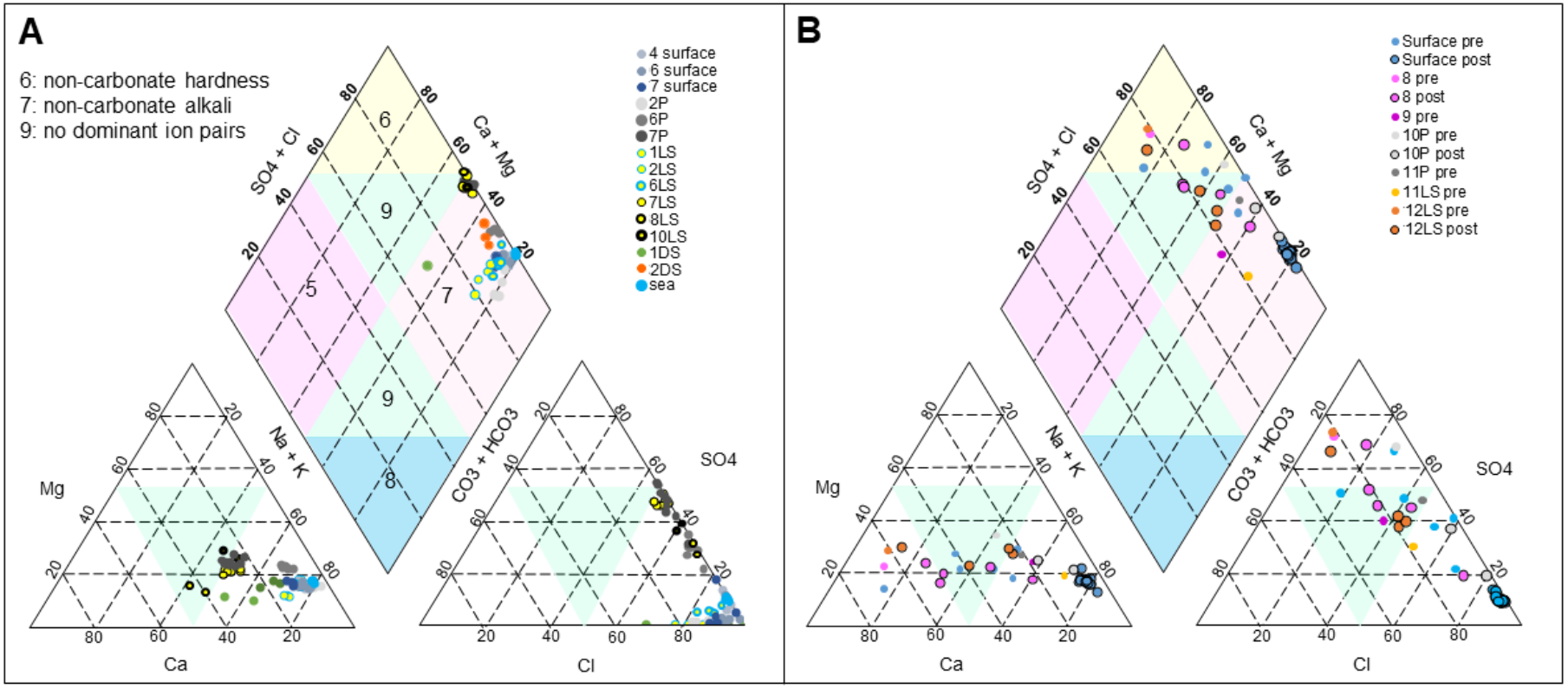

Figure 4.3. Piper plot for ionic types and groundwater facies classifications for Hütelmoor (A) and Drammendorf (B). The major groundwater facies based on the cations and anions are Ca-Cl (6), Na-Cl (7), and mixed types (9). Well filter screen in dune sands (DS), peat (P), aquifer sands (LS), peat+aquifer sands (no abbreviation). Pre and post for Drammendorf refer to pre-rewetting and post-rewetting, respectively. Hütelmoor campaigns: Aug 2017 and Apr 2018 (from Toro et al., 2022); Apr, Jul, Aug, Nov 2019; Feb, Jun, Nov, Dec 2020: Sept 2021; April 2022. Drammendorf campaigns: Nov 18, 2019 (one week before rewetting); Dec 2, 2019 (one week after rewetting); Jan, Jun, Dec 2020; Jan, Apr 2022.

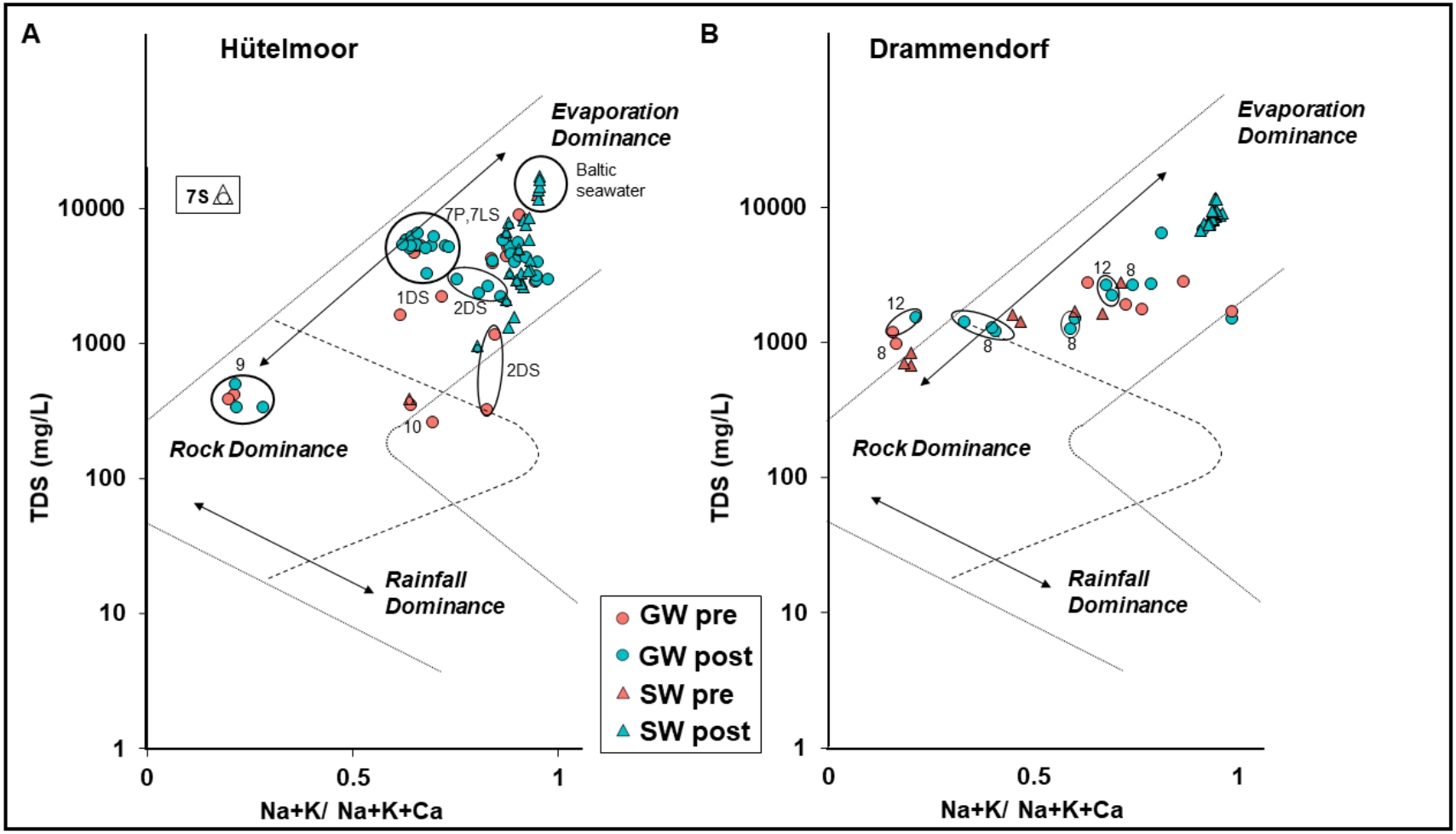

Figure 4.4. Major processes controlling groundwater chemistry in Hütelmoor (A) and Drammendorf (B). Labels refer to IDs of monitoring wells. Some of the samples are labelled and encircled. For Hütelmoor, surface samples at station 7 (7S) is represented by an empty circle enclosed in a triangle with colors corresponding to pre- or post-storm surge.GW=groundwater, SW=surface water.

4.3.5 Spatio-temporal distribution of specific conductivity, chloride, and sulfate along a transect

Hütelmoor
In terms of spatial distribution, it was generally observed that the specific conductivity and chloride concentrations exhibited higher magnitudes in the peat and aquifer sands located within the central peatland (HM-6,7), when compared to the forest (HM-9) and the dune dike (HM-2) stations (SM Figure 4.3). However, when considering sulfate concentrations, elevated values were recorded only from HM-7P, HM-7LS, and HM-6P. Conversely, low concentrations, including values that fell below detection limit, were noted from other HM stations.

With regard to temporal distribution, the investigated parameters display overall stability in the peat and aquifer sands groundwater while prominent changes were observed in surface waters and the shallow peat (7P) (SM Figure 4.2). The changes were characterized by a substantial rise in specific conductivity, chloride levels, DOC, and sulfate concentration subsequent to the flooding event. Notably, an increase in sulfate levels at 7P was observed following the storm surge flooding, which decreased again until towards the end of the study period. The DOC levels at 7P, in contrast, had a delayed but sustained increase until the end of the sampling in 2022. Remarkably, a slight increase in specific conductivity and chloride levels was also detected in the groundwaters of the dune dike (HM-2DS) one year after the storm surge.

Drammendorf
Immediate substantial changes in SC and Cl^- concentrations of surface waters were observed after the rewetting with seawater (SM Figure 4.4). Meanwhile, surface water sulfate concentrations were already elevated prior to rewetting and thus, experienced sustained increases subsequent to the rewetting. Likewise, before rewetting, the groundwater in observation wells along the east-west transect (DD-8,12LS) exhibited relatively high sulfate concentrations but low SC and low Cl^- (SM Figure 4.4). After rewetting, different responses were observed between the two wells: DD-8 exhibited an immediate impact, while a lag time was observed for DD-12. In DD-8, a week after the rewetting, a surge in Cl^- concentration was observed accompanied by an increase in SC. Conversely, the sulfate concentration decreased in concentration by up to 213 mg L^{-1}. In the case of the deeper DD-12 well, the increase in SC, the six-fold increase in Cl^-, and decrease in sulfate concentration by up to 287 mg L^{-1} were only recorded two months after the rewetting event.

4.3.6 Water quality parameters before and after storm surge: Hütelmoor

An increase in SC was generally observed in surface, peat and aquifer waters, although the changes were not statistically significant (Figure 4.5). However, a slight decrease in median SC was noted in the aquifer at HM-6 and HM-7. Furthermore, a general increase in pH was observed in HM waters, with a significant pH increase observed in the aquifer sands. An increase in pH was also recorded in aquifer waters of both HM-6 & HM-7, as well as the surface water of HM-7. In contrast, a decrease in pH was observed in HM-7. Pre-storm surge pH measurements were not available for surface and peat waters of HM-6. Ammonium concentrations decreased in both peat and aquifer waters, though not

significantly. Median DOC concentrations were similar before and after the storm surge for the entire HM area and HM-6. In the shallow HM-7, however, elevated DOC concentrations were observed for all water types, particularly for peat waters where the concentration increased more than threefold. For DIC, an increase in concentrations was observed in surface and aquifer waters for the entire HM, HM-6, and HM-7.

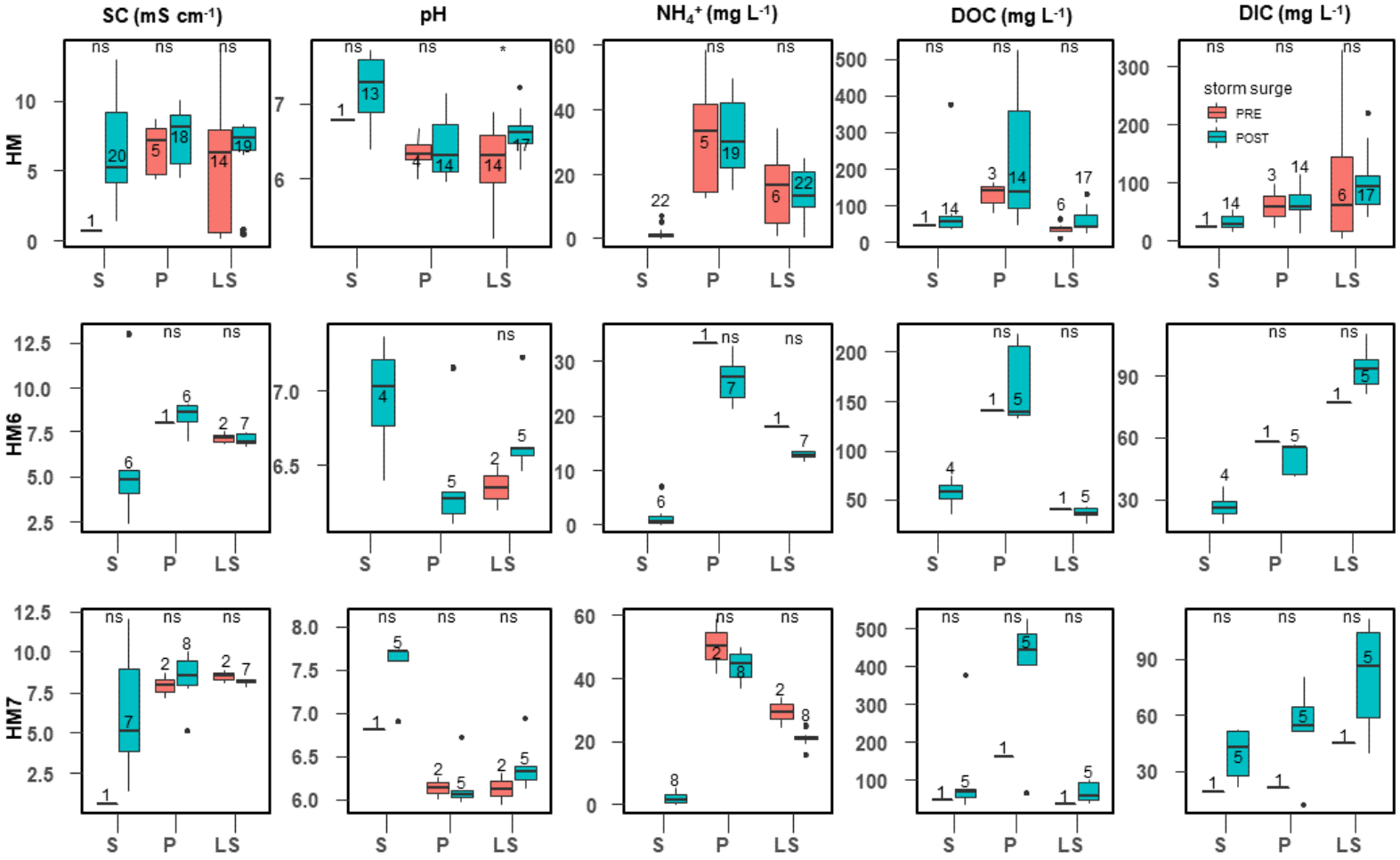

Figure 4.5. Water quality parameters (Specific Conductivity (SC), pH, ammonium (NH_4^+), Dissolved Organic Carbon (DOC), and Dissolved Inorganic Carbon (DIC)) in the Hütelmoor (A), HM6 (B), and HM7 (C) before (2017 & 2018 sampling from Toro et al., 2022) and after the storm surge (2019–2022 sampling). A grouped boxplot is labelled with '' if there is significant difference (95% confidence level) between the two groups while 'ns' denotes no significant difference. Numbers on each bar are the total number of water samples collected. S = surface water; P = peat groundwater; LS = lower sands/ aquifer sands groundwater.*

4.3.7 Water quality parameters before and after rewetting: Drammendorf

Notable changes were found post-rewetting following the rewetting event, with particularly significant variation in surface waters (Figure 4.6). In peat waters, although changes were not significant, evident shifts were observed in specific parameters: an increase in SC and pH, as well as decrease in NH_4^+, DOC, and DIC levels. Comparable trends in pH, NH_4^+, and DOC were also identified for the lower sands, mirroring the observations in peat waters, although SC median concentration decreased while ammonium concentration increased.

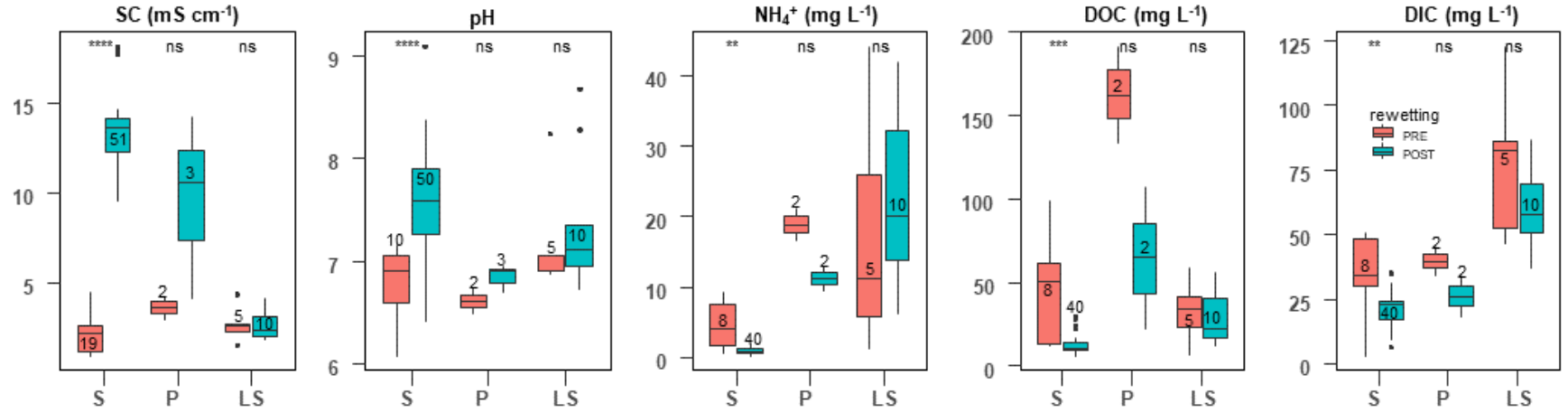

Figure 4.6. Water quality parameters (Specific Conductivity (SC), pH, ammonium (NH_4^+), Dissolved Organic Carbon (DOC), and Dissolved Inorganic Carbon (DIC)) in Drammendorf before and after the rewetting in 11/2019. A grouped boxplot is labelled with '' if there is significant difference between the two groups while 'ns' denotes no significant difference. Confidence level: '*'=95%, '**'=99%, '***'=99.9%. Numbers on each bar are the total number of water samples collected. S = surface water; P = peat groundwater; LS = lower sands/ aquifer sands water.*

4.3.8 Correlation Matrices

The subsequent subtopics present correlation matrices that examine the relationships between DOC, DIC, and NH_4^+ and other investigated parameters. The correlations were performed as a whole for both Hütelmoor and Drammendorf (Figure 4.6) and for specific sites within the Hütelmoor (HM-6 and HM-7; SM Figure 4.5). Furthermore, the correlation matrices are divided into the different surface and groundwaters (peat, aquifer sands).

Dissolved Organic Carbon
In surface waters in the Hütelmoor (Figure 4.7), HM-6 (SM Figure 4.5), and HM-7 (SM Figure 4.5), high to very high positive correlations between DOC and ANC have been observed with correlation coefficients of 0.77 ($p<0.001$), 0.88, and 0.95 ($p<0.01$), respectively. In Drammendorf, however, DOC and ANC were not correlated. Instead, DD correlations are: high positive between DOC and NH_4^+ ($r=0.88$; $p< 0.001$), moderate negative for SC ($r=-0.54$; $p<0.001$) and DO ($r=-0.67$, $p<0.001$), and moderate positive for Ca^{2+} ($r=0.52$, $p<0.001$).

In peat waters in HM, moderate negative correlations of DOC with pH ($r=-0.66$; $p<0.01$) and DO ($r=-0.61$; $p<0.05$) exist (Figure 4.7). Similarly, negative correlations of DOC and pH were observed for HM-6P ($r=-0.42$) and HM-7P ($r=-0.71$), respectively (SM Figure 4.5). Additionally, in HM-6P, very high negative correlation of DOC with DIC ($r=-0.97$, $p<0.01$) and sulfate ($r=-0.94$; $p<0.01$) were found. Although the general correlation between DOC and ANC in HM peat water showed no relationship, a high positive relationship was observed in HM-6P ($r=0.85$; $p<0.05$). In HM-7P, moderate negative relationships of DOC with EC ($r=-0.60$) and sulfate ($r=-0.55$) were identified. In DD peat waters, DOC very highly negatively correlated with Cl^- ($r=-0.95$; $p<0.05$), Na^+ ($r=-0.92$; $p<0.05$), water level above ground ($r=-1.00$; $p<0.01$), and DO ($r=-0.96$; $p<0.05$) but is very highly positively correlated with NH_4^+ ($r=0.97$; $p<0.05$) and DIC ($r=0.99$; $p<0.05$).

For aquifer sands waters, no strong correlations of DOC with parameters were observed for HM except for TDN which had a low positive correlation ($r=0.46$; $p<0.05$) (Figure 4.7). However, in HM-6, TDN ($r=0.88$), pH ($r=-0.73$), temperature ($r=0.57$), and water level ($r=0.57$) appear to be important parameters while in HM-7, ANC ($r=0.90$; $p<0.05$), chloride ($r=-0.85$; $p<0.05$), sulfate ($r=-0.86$; $p<0.05$), and TDN ($r=0.96$; $p<0.05$) have high to very high correlations with DOC (SM Figure 4.5). In Drammendorf, DOC is highly positively correlated with NH_4^+ ($r=0.83$; $p<0.001$) and TDN ($r=0.82$, $p<0.01$). In addition, DOC is moderately positively correlated with sulfate ($r=0.55$; $p<0.05$).

Dissolved Inorganic Carbon
In surface waters in HM, DIC is mainly correlated with pH ($r=0.77$; $p<0.01$), water level ($r=-0.76$; $p<0.001$), and Ca^{2+} ($r=0.73$; $p<0.01$) (Figure 4.7). Moreover, Cl^-, Na^+, NH_4^+, DOC, TDN, SC, and temperature are moderately correlated with DIC. In HM-6S (SM Figure 4.5), ANC ($r=0.97$, $p<0.05$), temperature ($r=0.92$; $p<0.05$) and Ca^{2+} ($r=0.96$; $p<0.05$) are very highly correlated with DIC while in HM-7S, water level above ground ($r=-0.94$; $p<0.01$), SC ($r=0.93$; $p<0.01$), DO ($r=-0.90$; $p<0.05$), and Cl^- ($r=0.90$, $p<0.05$) are the parameters very highly correlated with DIC. In DD surface waters, DIC moderate correlations with very high significance were recorded with Ca^{2+} ($r=0.51$; $p<0.001$) and SC ($r=-0.50$; $p<0.001$).

For HM peat waters, SC (r=-0.83; p<0.001) and water level above ground (r=-0.75; p<0.001) are correlated with DIC (Figure 4.7). The correlation of ANC on DIC for HM-6P and HM-7P contrasts each other since correlation coefficients are -0.79 (p<0.05) and 0.85 (p<0.05), respectively (SM Figure 4.5). In DD peat waters, water level above ground (r=-0.99; p<0.05) and DO (r=-0.95; p<0.05) are very highly correlated with DIC including SC (r=-0.82) although not significant. Other parameters that are highly correlated with DIC are Cl- (r=-0.90: p<0.05), NH4+ (r=0.94; p<0.05), and DOC (r=0.99; p<0.05).

In HM aquifer groundwater, DIC is moderately positively correlated with SC (r=0.62; p<0.01) overall (Figure 4.7). Meanwhile, pH is positively linearly correlated with DIC in HM6 (r=0.94; p<0.01) (SM Figure 4.5). Only moderate significant correlations of DIC with Mg^{2+} (r=0.64; p<0.01) and TDN (r=0.74; p<0.05) were recorded in Drammendorf lower sands groundwater.

Ammonium and Total Dissolved Nitrogen

Ammonium was very highly positively correlated with TDN in HM (all water types) and DD (aquifer sands) (Figure 4.7). With DOC, NH_4^+ was highly to very highly positively correlated with all water types in DD and moderately positively correlated with HM surface and peat waters. Correlations of NH_4^+ with DIC are variable from very highly positively correlated (DD-peat waters: r=0.94, p<0.05) to moderately negatively correlated (HM peat waters: r=-0.60, p<0.05) to negligible correlations (HM and DD aquifer sands).

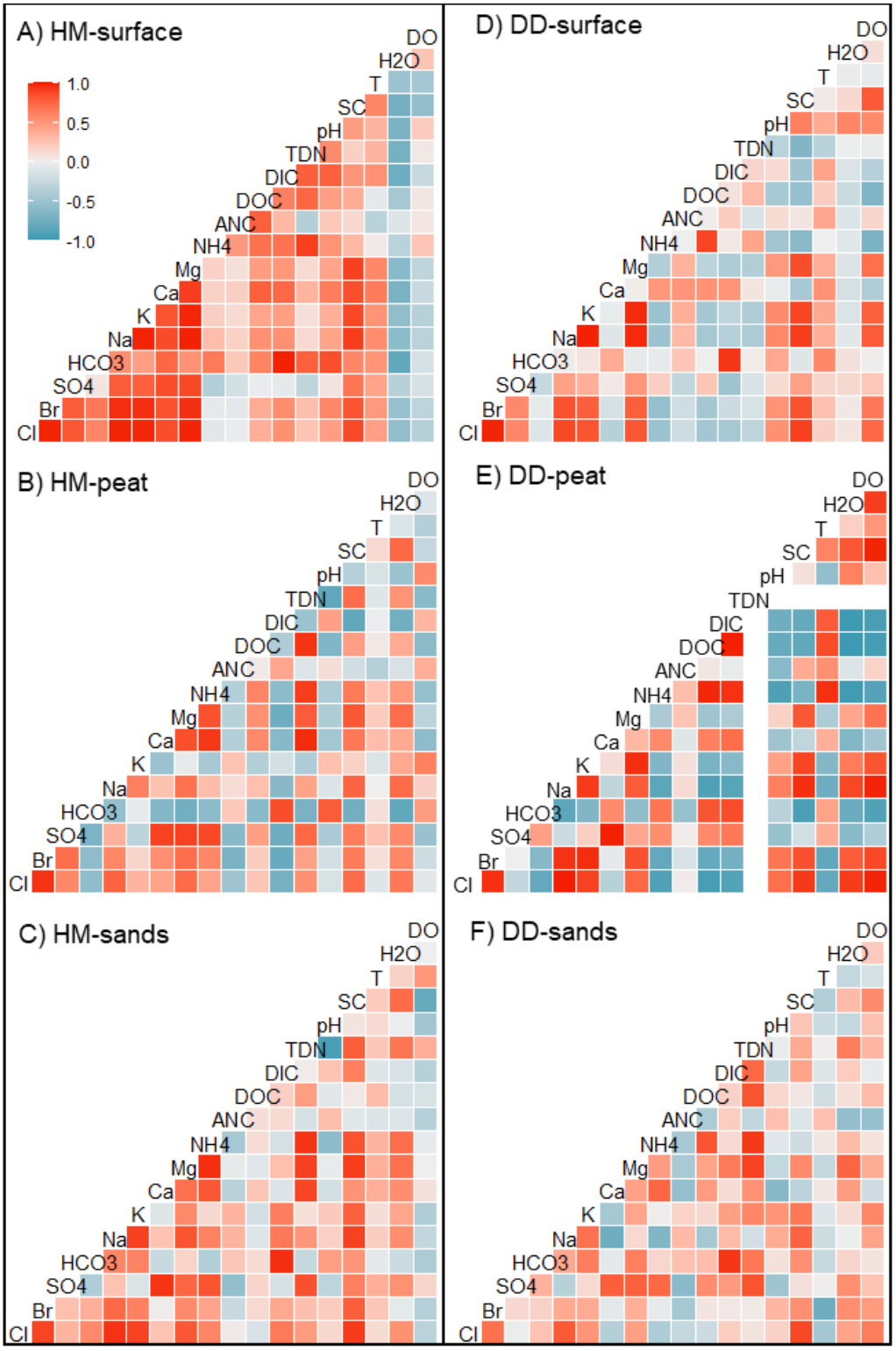

Figure 4.7. Correlation matrices between investigated parameters from Hütelmoor (A–C) and Drammendorf (D–F) from surface (A, D), peat (B,E), and aquifer sands (C,F) waters. Darker red and blue colors signify higher positive (red) and negative (blue) Pearson moment of correlation. HM=Hütelmoor; DRA=Drammendorf; Cl=chloride; Br=bromide; SO4=sulfate; HCO3=bicarbonate; Na=sodium; K=potassium; Ca=calcium; Mg=magnesium; NH4=ammonium; ANC=Acid Neutralizing Capacity; DOC=Dissolved Organic Carbon; DIC=Dissolved Inorganic Carbon; TDN=Total Dissolved Nitrogen; SC=Specific Conductivity; T=temperature; H2O=water level above the ground; DO=Dissolved Oxyge

4.4 Discussion

4.4.1 Hydrogeochemistry of Coastal Peatlands

The geochemical signatures of surface waters in the Hütelmoor and Drammendorf coastal peatlands before and after the storm surge inundation and the seawater rewetting indicate varying degrees of marine influence. The sole sample in pre-storm surge Hütelmoor (HM-7S) reveals rock-dominated processes (Figure 4.4A). However, after inundation, the evaporation-dominated surface water (7S marked in Figure 4.4A) could only be explained by the input of evaporation-dominated seawater. In Drammendorf, surface waters collected from ditches before the rewetting exhibited variable marine influences between rock-dominated and evaporation-dominated processes (Figure 4.4B). The ditch surface samples collected farther from the coast exhibited rock dominance while samples closer to the sea showed evaporation dominance reflecting the potential influence of seawater intrusion on water chemistry within the Drammendorf site. After rewetting, as expected, surface water samples displayed evaporation dominance with geochemical signatures similar to Baltic seawater. Interestingly, samples collected from 11S, located near the east-west ditch which was later connected to the Kubitzer Bodden, on 09.11.2019 and 18.11.2019 (dike opening already underway) showed rock- and evaporation-dominance, respectively. This further reveals the impact of seawater intrusion on the ditch surface water samples.

The legacy effects of past seawater inundations (six inundations since 1872; Toro et al., 2022) can be seen in Hütelmoor groundwater. The high chloride concentrations in the peat and aquifer sands (Table 4.1; SM Figure 4.3) indicate legacy effects from the frequent influence of seawaters in the past. Majority of the sampled groundwater in HM (2P, 6P, 1LS, 2LS, 6LS, 1DS, 2DS) (Figure 4.3A) are classified as having Na-Cl waters and controlled by evaporation (Figure 4.4A). There was no dike before to limit seawater inundation due to high sea levels and storm surges. Our results corroborate Toro et al. (2022), wherein it was shown using chloride concentrations that 24 ± 4% and 30 ± 3% of water in the peat and aquifer sands, respectively, originate from seawater when compared to the current Baltic Sea chloride concentrations. Seawater is thought to have come from inundations in the past and not from evapoconcentration or seawater intrusion (Toro et al., 2022; Koebsch et al., 2019). The seawater component of the groundwater explains the evaporation dominance of most groundwater in HM. Moreover, the peatland also gets flooded with seawater during high sea levels through the groundsill (Schreiber et al., 2021; Toro et al., 2022), which connects to the Warnow River and the eventual Baltic Sea.

In Drammendorf, the elevated Cl^- concentrations in groundwater before rewetting (Table 4.1; SM Figure 4.4) albeit at lower levels, is potentially from seawater intrusion rather than inundation. The peatland has no direct hydrological connection to the sea due to the dike. Seawater intrusion near the coast is highly likely due to the lowering of surface elevation and water level in the peatland as a result of draining. Pre-rewetting groundwater on the southwestern side (9, 11P, 11LS) closer to the coast are classified as having Na-Cl waters and governed by evaporation dominance. In contrast, groundwater farther away from the coast (8, 12) are Ca-Cl waters and dominated by rock weathering processes. Furthermore, storm surge inundations were expected less in the peatland because the site was protected by the islands surrounding the Kubitzer Bodden. Additionally, the artificial sandy dike also robustly protected the agricultural use peatland.

Dikes and drainage networks impact the groundwater facies and the controlling processes. For instance, in the Hütelmoor, dune dike groundwater (HM-2DS) is influenced by a relatively higher Ca^{2+} content but lower TDS/ SC (Figure 4.4) than groundwaters in the peatland. This freshening is indicative of surface waters infiltrating the dune dike mixing with precipitation. The role of precipitation in the dune to terrestrial submarine groundwater discharge has been investigated before, contributing about a third of the total terrestrial discharge to the HM coast (Racasa et al., 2021). Contrarily, the small, artificial dike belt of Drammendorf peatland is not expected to contribute to groundwater discharge to the coast. Meanwhile, the drainage networks established in the 1960's and 1970's may have profoundly affected peatland groundwaters. In HM, wells 6P and 6LS (central peatland closer to coast) and 7P and 7LS (central peatland closer to forest) are separated by a network of ditches with an east-west ditch that cuts across the entire peatland (Figure 4.1). While 6P and 6LS are Na-Cl types, 7P and 7LS are mixed types (Figure 4.3) with higher Ca^{2+} contents, as shown in the Gibbs diagram (Figure 4.4). Toro et al. (2022) elucidated that local flow fields exist near the ditches and that infiltration of ponded surface water is the main mechanism for water input into the peatland. Fresh groundwater input from the surrounding forest is diverted through the ditches. As such, the mixed water types at 7P and 7LS result from mixing old groundwaters and infiltration of fresh ponded surface waters, made possible by a thinner peat layer (0.9 m) at this site. In Drammendorf, wells 8, 12, and 9 are likewise separated by a north-south ditch (Figures 4.1, 4.2). Wells 8 and 12 (39 – 51 mg Cl^- L^{-1}) are distinctly fresher than well 9 (350 mg Cl^- L^{-1}) even though the distance between 12 and 9 is just 70 m and peat thickness are almost the same (0.81–0.88 m). Well 9 also has half Ca^{2+} level compared to wells 8 and 12. Localized flow fields as a result of the ditches could have isolated well 9 from the larger groundwater flow pathways, while wells 8 and 12 are still largely influenced by it. Seawater intrusion is more evident in well 9 (higher Cl^- concentration) with the north-south ditch acting possibly as a hydrological barrier to intruding seawater.

4.4.2 Impact of Storm Surge to a Brackish-Rewetted Coastal Peatland

Storm surges bring seawater and salts to the brackish Hütelmoor peatland, affecting its surface water quality. A general increase in SC of surface waters compared to pre-surge level of 0.60 mS cm^{-1} was observed months and years after the storm surge (Figure 4.5; SM Figure 4.3). The SC in surface waters increased up to 13 mS/cm during field sampling in Aug 2019, seven months after the Jan 2019 storm surge. However, SC values reached 22.4 mS/cm near the northern dune dike breach immediately after the storm event (Gutekunst et al., 2022). In addition, seawater entered the peatland via the groundsill, as described for the Jan 2017 storm surge (Toro et al., 2022). Further, a general increase in Cl^- (until end of 2020) and SO_4^{2-} (until spring 2020) concentrations persisted with variable increase in ammonium in surface waters (SM Figure 4.3). Although the general increase in SC, pH, DOC, and DIC is not significant (Figure 4.5), an increase in DOC (up by 330 mg L^{-1}) was notable in HM-7S in Nov 2019 (SM Figure 4.3). Based on correlation coefficients, Acid Neutralizing Capacity is the main factor affecting DOC concentrations in surface waters (HM: r=0.77; HM-6S: r=0.88; HM-7S: r=0.95). The positive correlation of ANC with DOC indicates that the excess strong base cations is related to increase in DOC concentrations in surface waters. This contradicts the known effects of polyvalent cations in reducing DOC leaching from soils, and eventually to surface waters, as a result of cation bridging (Kalbitz et al. 2000). Meanwhile, SO_4^{2-} is a well-established competitor for DOC

in adsorption sites, especially in mineral soils (Kalbitz et al., 2000). Though, SO_4^{2-} is not a reliable indicator of DOC concentration since it is nonconservative, especially in surface waters. Knorr (2013) showed that DOC can be positively or negatively correlated with SO_4^{2-} in stream water depending on the season probably due to changing hydrological flow pathways. The sulfate:chloride ratios increased in spring (>0.14–0.16 ratio of the Baltic Sea in front of HM) after the inflow and decreased significantly in succeeding field campaigns. Gutekunst et al. (2022) attribute this exhaustion of sulfate to microbial degradation. The contribution of fresh groundwater to DOC mobilization in surface waters could be observed with its highly positive correlation with Ca^{2+} (r=0.77). This is not surprising as DOC concentrations have been shown to increase when saline water is replaced with freshwater (Liu & Lennartz, 2019b; Kreuzburg et al., 2020).

The overall groundwater quality in the peat and aquifer sands layers is relatively stable throughout the study period since there are no significant differences in SC, pH, DOC, DIC, and NH_4^+ concentrations, except for pH of aquifer sands (Figure 4.5). This exception could be explained by the lack of sampling at HM-8 and HM-10 after the storm surge, which had pH values on the lower end. The groundwater facies – Na-Cl and mixed water types – remain the same before and after the storm surge (Figure 4.3A). Additionally, groundwater chemistry processes are similar before and after the surge event (Figure 4.4A). There are, however, obvious variations in the groundwater quality. Peat waters SC increased up to ~1.5 mS/cm after several months, but annual variance as a result of seasonal variability could not be discounted. The input of salts from seawater potentially flushes out ammonium ions from the peat leading to a slight decrease in concentration of 12 mg L^{-1} in HM-6 (2018–2022) and 21 mg L^{-1} in HM-7 (2017–2022) by the end of the study period (Figure 4.6). Ammonium may be replaced with sodium in fen peat (McCarter et al., 2018) through cation exchange and competitive adsorption. Zak and Gelbrecht (2007) reported the mobilization of ammonium during the initial stages of freshwater rewetting with a higher release of solutes in more degraded fen peat due to the formation of more mobile compounds through aerobic mineralization. Saltwater incursions during late summer droughts in a coastal plain doubled the annual export of NH_4^+ from a coastal wetland undergoing restoration (Ardon et al., 2013). Liu & Lennartz (2019b) additionally showed the increase and decrease in ammonium concentrations during saline-fresh water cycles in adjacent drained and rewetted peatlands, with an overall decreasing ammonium concentration trend. Higher ammonium concentrations were released from HM-7 than from HM-6, possibly due to a higher degree of degradation in the upper peat layer. In addition, higher sodium concentrations were recorded in HM-6P compared to HM-7P (>200 mg/L), probably due to higher amounts of sodium exchanged with ammonium in the soils in HM-7P. The HM-6P well screen is also deeper than HM-7P, and infiltration of salts could have taken longer.

Seawater salt inputs likely increased DOC mobilization in peat, possibly through anion exchange of organic acids with SO_4^{2-} and other anions. The massive input of seawater salts impacted the organic matter in the peat, particularly in the shallower HM-7P. During the first sampling with subsequent DOC analysis post-storm surge (Nov 2019), surface waters recorded 377 mg DOC L^{-1} while HM-7P was just 65 mg DOC L^{-1} (Figure 4.4). In the next sampling in Feb 2020, DOC concentration in HM-7P increased to 446 mg DOC L^{-1} while surface concentrations decreased to 56 mg DOC L^{-1}. A sustained increase in peat DOC concentrations was observed in succeeding samplings as recorded levels in Apr

2022 reached 526 mg DOC L^{-1} level (SM Figure 4.3). Though delayed, an increase in DOC concentrations was also observed in HM-6P, from 136 mg DOC/L in Nov 2019 to 207 mg DOC/L in Dec 2020 and 218 mg DOC L^{-1} in Apr 2022. The deeper peat layer at HM-6P showed a very high negative correlation between DOC and sulfate (r = -0.94), while the shallower well at HM-7P also revealed a moderate negative relationship (r = -0.55). The shallower well (HM-7P) could have been more affected by microbial sulfate reduction, exhausting the sulfate in pore waters in the top 30 cm, as Koebsch et al. (2019) documented. Similarly, for the top soil surface, sulfate concentrations are much more depleted closer to the Baltic Sea because of microbial sulfate reduction (Koebsch et al., 2019; Gutekunst et al., 2022). This anion exchange competition of DOC with sulfate on adsorption sites has been confirmed in mineral soils (Kalbitz et al. 2000) and has been previously documented by Gosch et al. (2019) in peat samples. Sulfate may displace DOC in acid forest soils if concentrations are larger than 480 mg L^{-1} (Kaiser & Zech, 1998; Kalbitz et al., 2000). Furthermore, the slight decrease in pH could not account for the three times increase of DOC in peat waters. Kang et al. (2018) have noted that DOC concentrations in pore waters increase with increasing pH due to the promotion of phenol oxidase activities and greater abundances in *Actinobacteria* and fungi. On the contrary, DOC has a low to high negative correlation with pH in our study (HM6P: -0.42; HM7P: -0.71). This agrees with Knorr (2013) who showed that DOC and pH in pore waters have a negative correlation in the presence of sulfate. Tiemeyer et al. (2017) suggested that high SC could lower pH by ion exchange and cation bridging. In terms of the DOC-ANC relationship, a high positive relationship has been noted at HM6P (r = 0.85) and a weak positive one at HM-7P (r = 0.28) which could also indicate potential sulfate reduction in the shallower HM-7P well. In addition, an increase in SC corresponding to an increase in DOC release supports Gosch et al. (2018; 2019) but contradicts other previous studies (Ardon et al., 2016; Tiemeyer et al., 2017; Liu & Lennartz, 2019b). In the same study by Tiemeyer et al. (2017), they showed contrasting DOC response to high SC in column experiments and field measurements. Field conditions reveal high DOC concentrations under high SC attributed to low pore water velocities and slightly higher soil organic carbon, and not because of pH. Unfortunately, iron which is highly correlated with DOC release in both peat and surface waters (Knorr, 2013) was not monitored during our field campaigns. Total iron measurements were taken by Ibenthal (2020) on Apr 2018 which showed extremely high concentrations at HM-7P (116 mg/L) and HM7LS (104 mg L^{-1}) compared to HM-6P (0.50 mg L^{-1}) and HM-6LS (0.40 mg L^{-1}). Moreover, Koebsch et al. (2019) suggested that high iron could have outcompeted sulfate as an electron acceptor leading to inhibition of sulfate reduction and thus, high sulfate observed in deeper peat layers. The relationship of DOC with iron is beyond the scope of this study but this could explain the difference in the magnitude of DOC released from HM-6P and HM-7P aside from the difference in the degree of the decomposition of the peat (Zak & Gelbracht., 2007). Altogether, the processes concerning DOC concentrations in the Hütelmoor after a storm surge flooding could be a combination of both physical and biological processes. Clark et al. (2012) have showed that the biological production of DOC is unlikely to entirely account for the observed increases in DOC concentrations during rewetting. Moreover, pH determines microbial-driven DOC increase (Kang et al., 2018) which is not the case for this study site. Microbial-driven dissimilatory sulfate reduction consumes hydrogen ions and produces bicarbonate which leads to an increase in pH (Miao et al., 2012). Hence, the abovementioned contribution of physico-chemical processes to the increase in DOC concentrations are also relevant.

Meanwhile, the impact of the storm surge to the aquifer sands is generally negligible. No discernable patterns of DOC and the factors studied in this paper could be observed for the whole of Hütelmoor. Although, very high positive DOC correlations have been noted in HM-7LS.

In terms of DIC relationships, various correlations were observed among the different types of waters. Contrasting correlations with pH and SC were noted, while water level generally exhibited an inverse correlation with DIC. Given these conflicting correlations, no overarching general relationship can be assumed.

The water quality changes in peatland surface waters can influence SGD along the coast. Racasa et al. (2021) have demonstrated that surface waters originating from the peatland infiltrate the base of the dune dike and subsequently discharge into the sea. Analysis of groundwaters at the dune dike (HM-2DS) between 2018 and 2021 revealed notable increases in SC by a factor of 8, Cl^- by a factor of 15, and ammonium, DOC, and DIC by a factor of 3. These elevated concentrations observed at the dune dike suggest horizontal flow from the peatland surface waters and their potential release into the coastal area through SGD. Toro et al. (2022) and Racasa et al. (2021) suggested surface water infiltration near the coast and subsequent flow as SGD to the Hütelmoor coast.

4.4.3 Impact of Seawater Rewetting on a Drained Coastal Peatland

In Drammendorf, rewetting flooded the peatland with seawater, drastically changing the surface water quality. Surface water prior to rewetting is mainly in the ditches and depressions where surface water ponding may occur. After rewetting, surface water resembled seawater in terms of groundwater facies (Na-Cl type, Figure 4.3B) and the major processes behind water chemistry (evaporation-dominated, Figure 4.4B). Significant changes in SC, pH, NH_4^+, DOC, and DIC have been noted in surface waters (Figure 4.6). No strong correlations could be observed for ammonium, DOC, DIC, and TDN except for the high positive correlation between DOC and ammonium. However, moderate negative correlations of DOC with SC and moderate positive correlations of DOC with Ca^{2+} might indicate the influence of groundwater on DOC concentration. These corroborate again the increase in DOC concentrations during the freshwater phase of a saline-freshwater leaching experiment by Liu & Lennartz (2019b).

Groundwater quality response to rewetting varies according to peat thickness and distance from the coast. Immediately after rewetting, the more landwards DD-8 initially changed from Ca-Cl to NaCl waters but eventually showed a mixed water type (Figure 4.3). Gibbs diagram shows a gradient between rock-water interaction and evaporation-dominance water processes (Figure 4.4). For 12LS, located at central peatland, groundwater exhibited a Na-Cl type only after two months of rewetting and then to a mixed type in subsequent sampling. The thinner peat and the higher K_s at DD-8 could be the reason for the faster infiltration of seawater, while thicker peat and lower K_s contributed to the delayed response to the rewetting of DD-12. The freshening of the groundwater in DD-8 could be potentially attributed to mixing with fresh groundwater inflowing from the landside. However, pumping at a nearby station could influence flow pathways here. Unfortunately, wells DD-9, -11P,

and -11LS could not be accessed post-rewetting (see Methods section on ground and surface water sampling).

Overall, water quality parameters in peat and aquifer sands did not change significantly (Figure 4.6), but noticeable changes were still observed. Considerable increase in SC and decrease in ammonium, DOC, and DIC concentrations were recorded. Seawater rewetting flushed out the ammonium ions in peat, lowering median concentrations (Figure 4.6). Although there are limited samples for comparison, ammonium could have migrated to the upper peat or the aquifer layer underneath through vertical water flow. Drammendorf's water level depends on the highly dynamic Baltic Sea level which causes the water-covered area in the peatland to vary from 0.08 to 0.7 km^2 (Pönisch and Breznikar et al., 2023). The pressure release from surface water level variation could cause this vertical flow reversals. Specific conductivity measured from Aug 2020 to Jan 2022 (SM Figure 4.5) from DD-8 showed a broad range of values between 1.4 to 12.7 mS/cm. These indicate the influence of freshwater from the larger groundwater catchment and the surface water mainly from seawater. Moreover, an additional well located a few meters near DD-12 with well screen -0.5 to -1.5 m below ground, was sampled 29 months after rewetting. High concentrations of ammonium (89 mg L^{-1}), extremely high DOC (862 mg DOC L^{-1}), and acidic waters (pH=4.4) were measured, indicating possible transport of ammonium and DOC to upper soil layers. These measurements were not included in the plots comparing water parameters before and after rewetting (Figure 4.6). The high NH_4^+ is expected since saltwater incursion to coastal wetlands lead to desorption of large quantities of NH_4^+, magnified by historical agricultural use (Ardon et al., 2013). The initial decrease in DOC concentrations after rewetting (Figure 4.6) could be due to polyvalent cation bridging (Kalbitz et al., 2000; Tiemeyer et al., 2017) and the later massive increase in DOC in the additional well could be a result of sulfate-mediated microbial organic matter degradation (Jørgensen, 1982), anion exchange of sulfate with organic acids (Gosch et al., 2019; Kalbitz et al., 2000) or localized effects of higher iron content (Knorr et al., 2013) or higher degree of decomposition (Zak & Gelbrecht, 2007). Further investigations are recommended to establish the connection between hydrology and the biogeochemistry of these waters.

4.5 Conclusion and Outlook

This study aimed at investigating surface and groundwaters (>50 cm below ground) in two coastal fens and examine the impact of seawater input resulting from storm surge and rewetting with seawater. Our results have revealed the past variable marine influence on surface and groundwater systems of coastal peatlands. The degree of marine impact depends on the distance from the coast, the thickness of the peat layer, and potentially, drainage networks that may serve as hydrological barriers or conduits for distributing seawater. The input of seawater in coastal peatlands can influence the hydrogeochemistry of both surface and groundwaters.

Surface waters of brackish-rewetted or drained peatlands exhibited the most pronounced changes due to recent storm surge inundation or seawater rewetting. For brackish-rewetted peatlands, increases in SC (including major ions such as sodium, chloride, and sulfate), pH, DOC, and DIC were recorded after seawater surge input, with elevated concentrations persisting for several months and years. Meanwhile, seawater rewetting of

drained peatlands led to drastic surface water changes as coastal peatlands can be turned into a lagoon-like environment. Significant increases (SC and pH) and decreases (NH_4^+, DOC, DIC) of specific parameters were recorded. A massive increase in DOC concentration was also recorded in an additional sample post-rewetting. In contrast to surface waters, the overall groundwater quality of peat and underlying sands are less affected. No statistically significant changes in groundwater quality were noted for peat and the underlying sands, albeit notable variations were observed.

Variable responses of groundwater DOC to seawater input were observed. We highlight the high DOC concentrations under high SC and decreasing pH in both study sites which contradict the results of laboratory experiments. Although we did not investigate the factors influencing the specific processes involved in DOC mobilization, we explored correlations with different parameters to explain the observed phenomenon. For instance, DOC mobilization was likely facilitated by anion exchange of organic acids with sulfate. However, microbial degradation, pH, pore water velocity, and localized effects, such as iron content or degree of peat decomposition, should not be ignored. The potential role of excess strong base cations, measured by ANC, to DOC concentration is ambiguous, but the observed cation exchange between ammonium and sodium is not.

The impact of seawater rewetting on groundwaters in a drained peatland is yet to be fully understood. However, ongoing salinization may lead to brackish-rewetted systems with high chloride, sodium, and sulfate concentrations. Groundwater response across the peatland may vary and may create new biogeochemical reactive zones at mixing zones of groundwater and seawater.

This field study provides valuable insights into seawater's effects on surface and groundwaters of coastal peatlands. Furthermore, this study highlights the potential export of elevated concentrations of DOC, DIC, NH_4^+, and other solutes from rewetted coastal peatlands to adjacent water bodies through direct channel connections or diffuse submarine groundwater discharge. As management strategies for increasing seawater input in rewetted coastal peatlands continue in response to climate change, further studies evaluating seawater effects on surface and groundwater systems should be pursued when considering benefits of wetland restoration.

Supplementary Material to Chapter 4

SM Table 4.1. Field-measured saturated hydraulic conductivity (K_s) from observation wells in Drammendorf using the borehole method.

Observation Well	Soil Type	Filter Screen Depth (masl)	Mean Saturated hydraulic conductivity (K_s) (m d^{-1})
DD-8	peat + sands	-0.91 to -1.91	0.55
DD-9	peat + sands + lacustrine sediments	-1.41 to -1.91	0.13
DD-10P	peat	-0.67 to -1.67	0.02
DD-10LS	sands	-1.82 to -2.82	0.01
DD-11P	peat	-1.16 to -1.65	0.05
DD-11LS	sands	-1.77 to -2.77	0.06
DD-12LS	sands + lacustrine sediments	-1.41 to -2.41	0.03

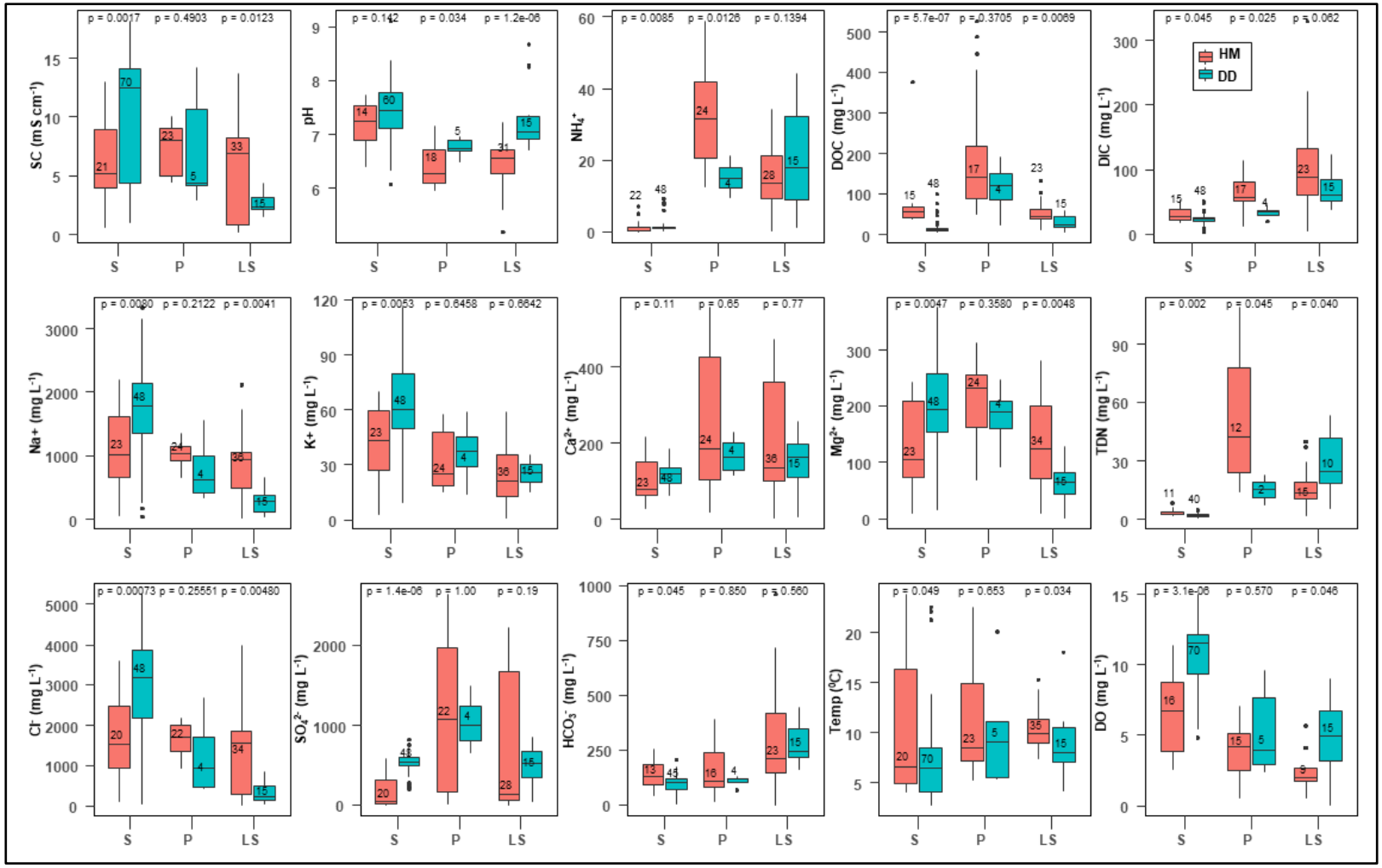

SM Figure 4.1. Comparison of water quality parameters of Hütelmoor (HM) and Drammendorf (DD). The bars represent mean concentrations and the numbers shown on/ near the boxes are the number of samples. The p-values are presented on top of each pair of boxplots. Specific conductivity (SC), pH, ammonium (NH_4^+), Dissolved Organic Carbon (DOC), Dissolved Inorganic Carbon (DIC) sodium (Na^+), potassium (K^+), calcium (Ca^{2+}), magnesium (Mg^{2+}), Total Dissolved Nitrogen (TDN), chloride (Cl^-), sulfate (SO_4^{2-}), bicarbonate (HCO_3^-), temperature (Temp), Dissolved Oxygen (DO). S=surface water; P=peat groundwater; LS=lower sands/ aquifer sands groundwater.

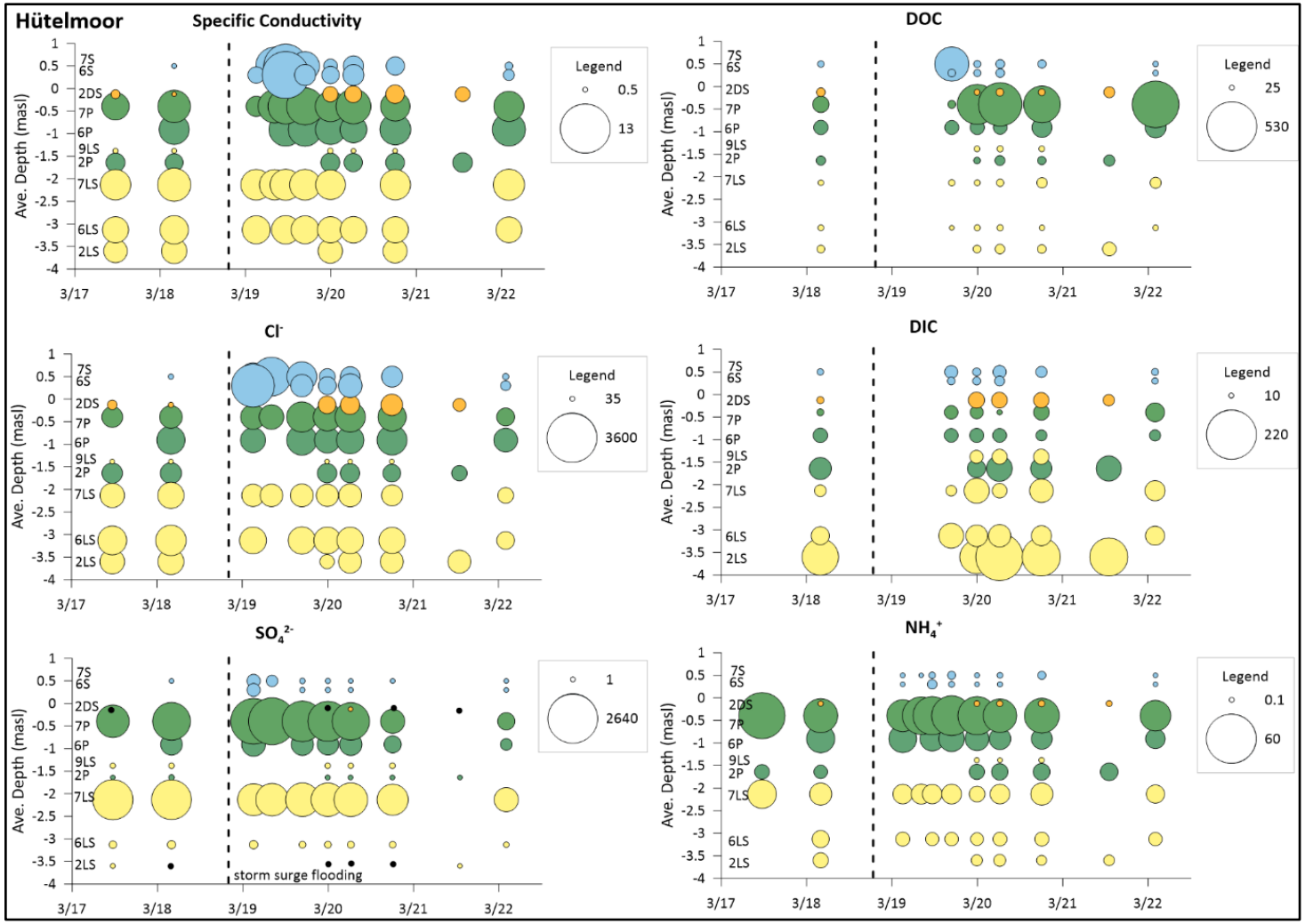

SM Figure 4.2. Specific conductivity, chloride, sulfate, DOC, DIC, and ammonium concentrations along a transect across the Hütelmoor peatland from different sampling campaigns from August 2017 to April 2022 (August 2017 and April 2018 data from Toro et al., 2022). Black dots correspond to samples with concentration below detection limit. The dashed line represents the storm surge on January 2, 2019 which flooded the peatland through a northern dune dike breach and through the groundsill.

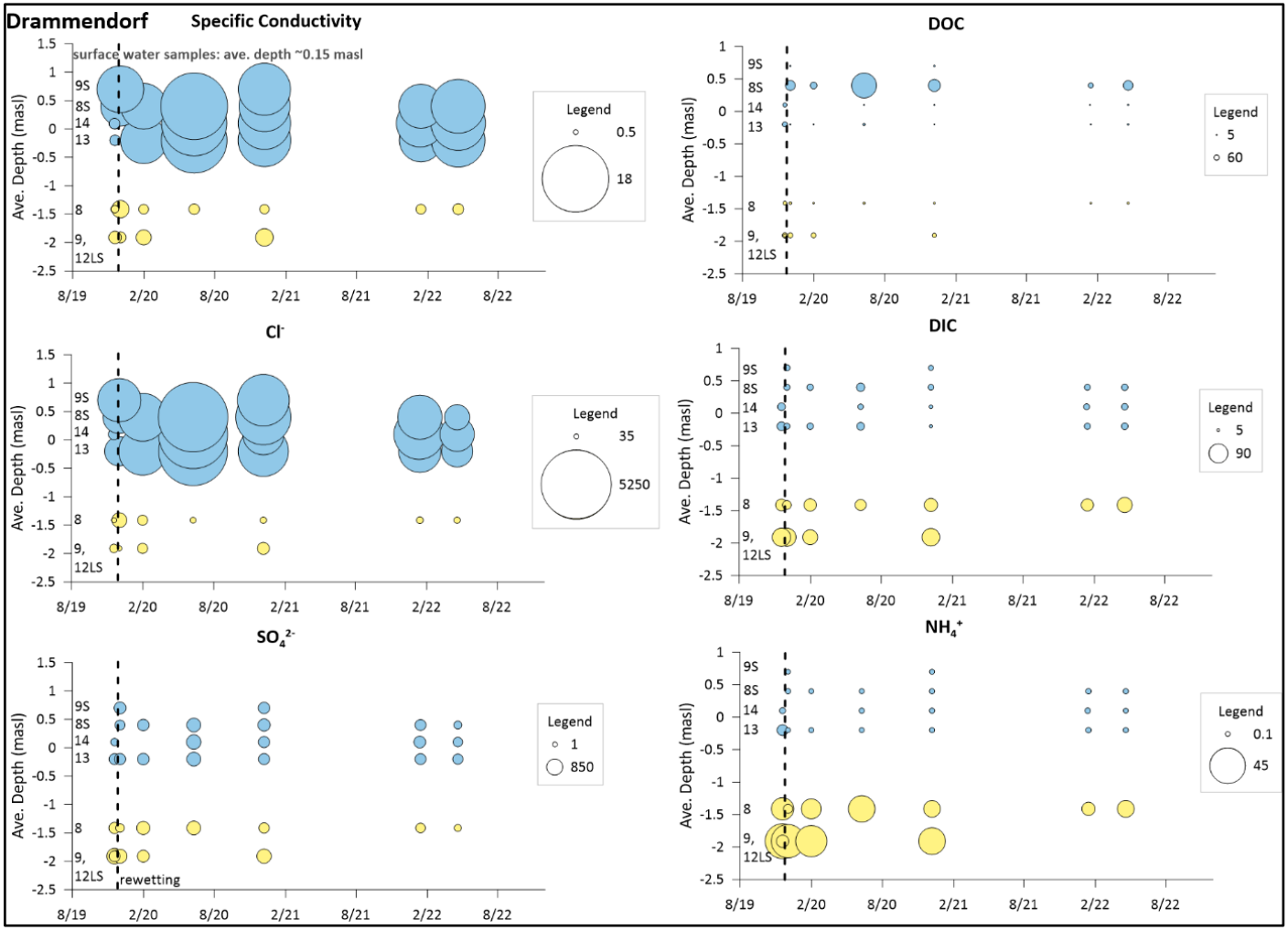

SM Figure 4.3. Specific conductivity (SC), chloride (Cl^-), sulfate (SO_4^{2-}), DOC, DIC, and ammonium (NH_4^+) concentrations along a transect across the Drammendorf peatland from November 2019 to April 2022. The dashed lines represent the creation of the dike opening and the rewetting of the peatland with brackish seawater on November 23, 2019. For surface water samples (blue bubbles), the average water depth is ~0.15 masl based on the average surface water level measured at the dike opening (DD-14). Majority of the wells from Drammendorf have been destroyed after winter 2021/22. S=surface, LS=aquifer sands.

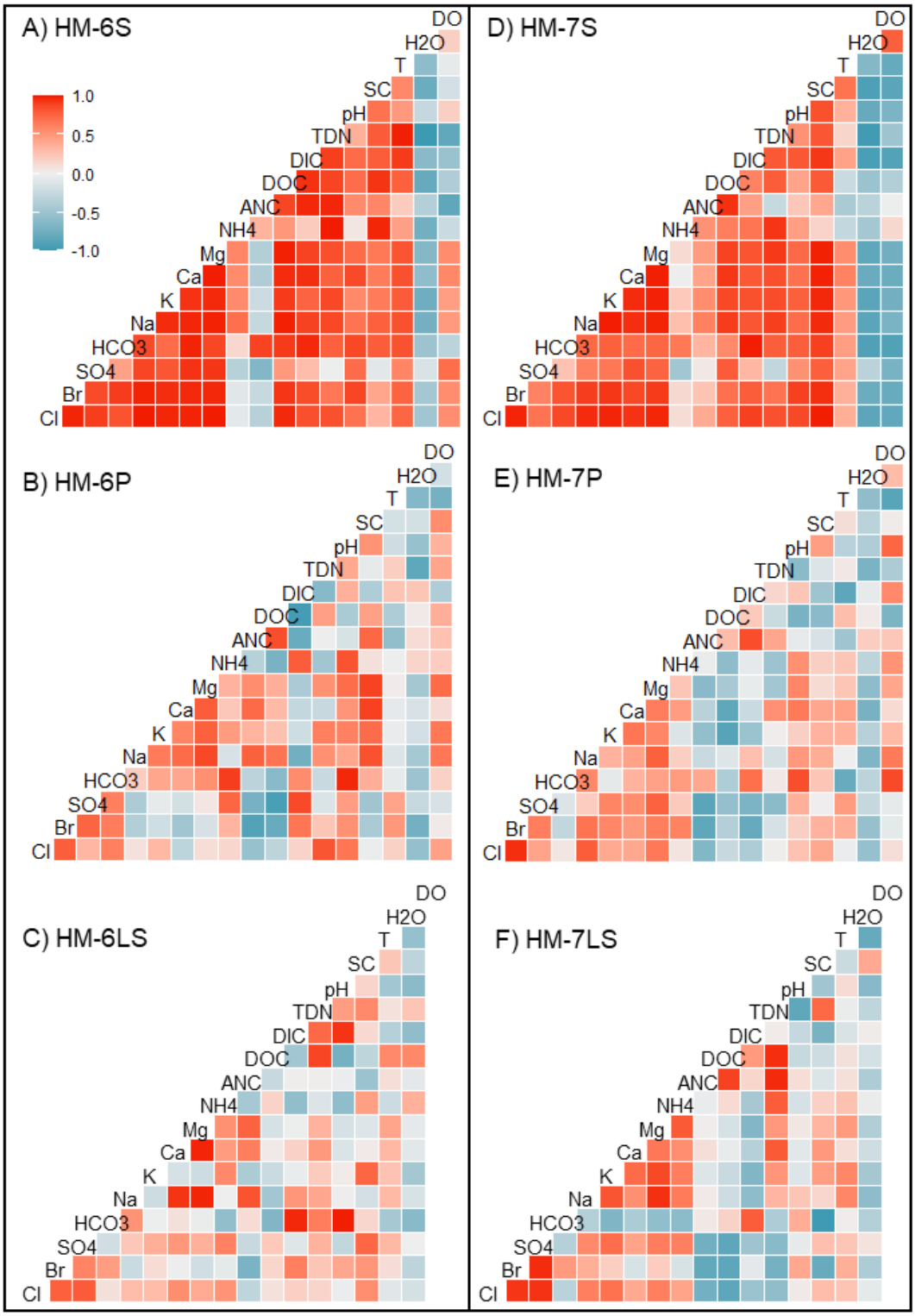

SM Figure 4.4. Correlation matrices for HM-6 and HM-7 surface (A, D), peat (B, E), and aquifer sands (C, F) waters. Darker red and blue colors signify higher positive (red) and negative (blue) Pearson moment of correlation. HM=Hütelmoor; Cl=chloride; Br=bromide; SO4=sulfate; HCO3=bicarbonate; Na=sodium; K=potassium; Ca=calcium; Mg=magnesium; NH4=ammonium; ANC=Acid Neutralizing Capacity; DOC=Dissolved Organic Carbon; DIC=Dissolved Inorganic Carbon; TDN=Total Dissolved Nitrogen; SC=Specific Conductivity; T=temperature; H2O=water level above the ground; DO=Dissolved Oxygen

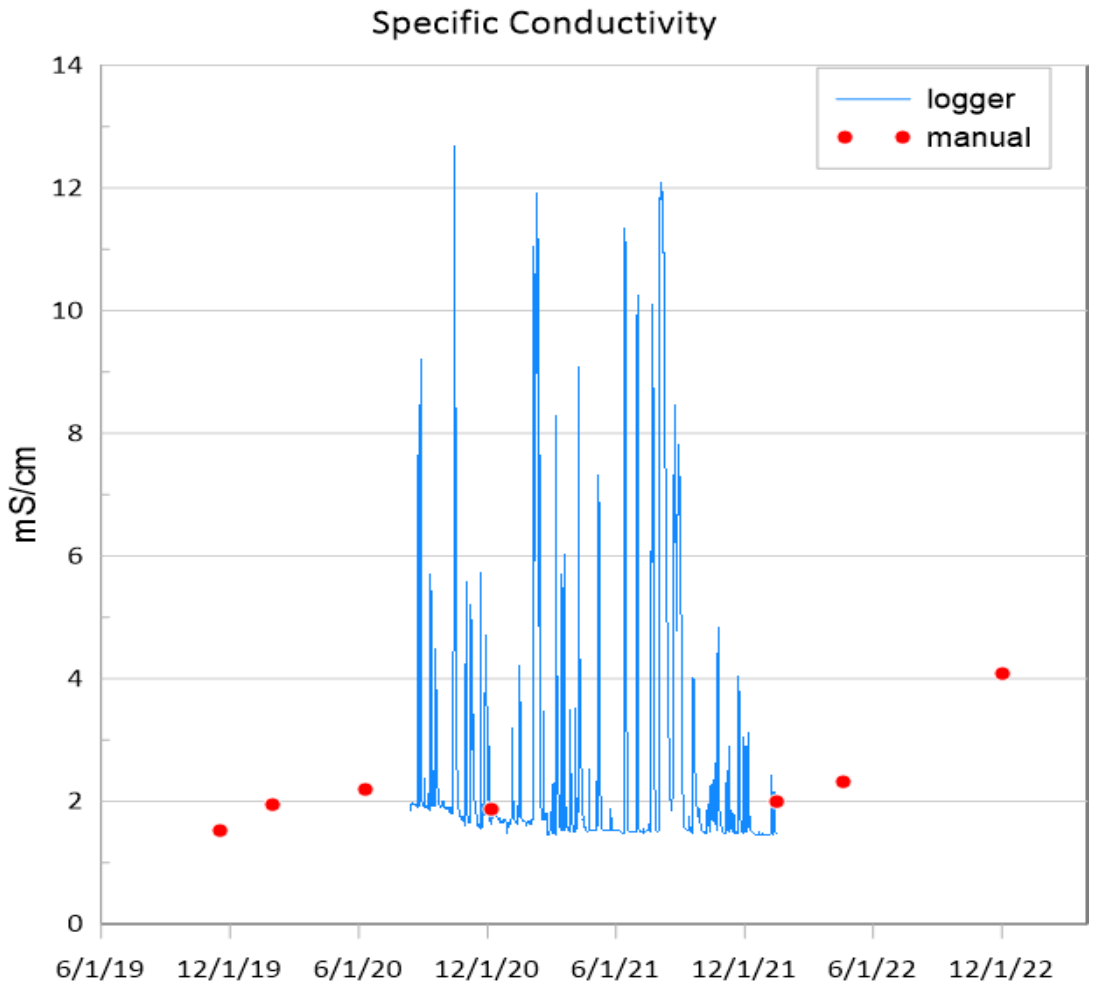

SM Figure 4.5. Specific Conductivity at DD-8 measured with a field probe (manual) and using a Dipper-PTEC logger.

5. SYNTHESIS

Most peatlands along the Baltic Sea have undergone various human alterations in the past. Submarine groundwater discharge from drained coastal peatlands is not expected because of water table drawdown resulting in land subsidence and landward-directed hydraulic gradient. Nevertheless, as hydrological restorations of coastal peatlands are pursued, the hydraulic gradient will shift towards the sea, accentuating the potential relevance of SGD in these environments. Groundwater discharge from a rewetted coastal peatland was previously thought to be negligible (Miegel et al., 2016), but it has been proven that SGD is not inconsequential but rather substantial (Racasa et al., 2021; Schreiber et al., 2021; Toro et al., 2022). Further, Racasa et al. (2021) and Chapter 3 unravel the processes behind terrestrial and total SGD from coastal peatlands of the Baltic Sea, including the impact of extreme storm surge events. Additionally, Chapter 4 examines the surface and groundwater quality of coastal peatlands that will eventually discharge to the Baltic Sea through SGD or old drainage networks. The enduring effects of seawater influx on drained and rewetted coastal peatlands were investigated in Chapter 4 as well. This final chapter synthesizes the interconnectivity of coastal peatlands at the interface of land and sea to both hydrological and marine processes, and human interventions.

5.1 SGD Occurs from Low-lying and Low-K_s Coastal Peatlands

Submarine groundwater discharge occurs even from low-lying, low-hydraulic conductivity coastal peatlands. In Racasa et al. (2021), the steady-state numerical modeling approach was employed to determine the long-term mean terrestrial SGD from the rewetted Hütelmoor coastal peatland. The estimated mean terrestrial SGD value was 0.080 $m^2\ d^{-1}$ (2.8 L s^{-1}; along the 3-km shoreline). Considering realistic scenarios, potential terrestrial SGD rates across various coastal peatlands could range from 0.008 – 0.293 $m^2\ d^{-1}$, with K_s of the geological layers and groundwater level identified as the most sensitive parameters. In Chapter 3, the mean terrestrial SGD estimate was refined by optimizing K_s, utilizing extended groundwater level data, and conducting daily transient simulations. The current long-term terrestrial SGD estimate is 0.15 $m^2\ d^{-1}$ (5.1 L s^{-1}) within a 100-m distance from the 3 km shoreline. This estimate surpasses the previous estimates (Racasa et al., 2021; Ibenthal, 2020; Miegel et al., 2016) but is within the range proposed by Schreiber et al. (2021).

Furthermore, the total SGD estimate from the Hütelmoor peatland, which includes recirculated SGD, is 0.47 $m^2\ d^{-1}$ (16.3 L s^{-1}). The maximal SGD and SWI fluxes are 2.7 $m^2\ d^{-1}$ (94.2 L s^{-1}) and -7.0 $m^2\ d^{-1}$ (243.6 L s^{-1}), respectively, underscoring the extent of the potential exchange of water fluxes. Importantly, marine drivers such as winds and waves are not factored into the model. These drivers are captured in regional SGD estimates using other techniques, e.g., isotope measurements (Burnett et al., 2006; Taniguchi et al., 2019). Consequently, the total SGD estimates presented here could be grossly underestimated.

In addition to numerical modeling, the occurrence of SGD from the Hütelmoor is corroborated by direct measurements and on-site observations. Chapter 3 provides the manual seepage meter measurements taken perpendicular to the shoreline (up to 3.86

cm d^{-1}). When normalized to the same seepage face, the measured mean seepage rate from summer and fall (0.62 cm d^{-1}; 0.62 m^2 d^{-1}; 21.5 L s^{-1}) is comparable to the mean total SGD of the numerical model. However, if the maximum seepage rate from the meters (3.86 cm d^{-1}) is used, the total SGD estimate would be 134 L s^{-1}. This could indicate that modeled total SGD estimates may be underestimated. Discrete seepage was also observed in the northern part of the coast where peat outcrops.

Through field sampling, it was also determined that SGD from coastal peatlands could be brackish and may have higher salinity than their receiving coastal areas because of legacy effects and long water flow residence time. One-third of the groundwater in the Hütelmoor is seawater from the Baltic Sea (Toro et al., 2022), and its discharge could take several months and years. The field-sampled, slightly higher salinity SGD reinforces the notion that density-driven effects may exert negligible influence, if any.

For decades, most SGD studies have focused on sandy shorelines (Taniguchi et al., 2019; Santos et al., 2021). Some muddy shoreline studies were conducted on mangroves, tidal marshes and other wetlands. This is the first time that total SGD has been quantified in detail from a rewetted coastal peatland in terms of temporal scale and spatial distribution.

5.2 Seasonal Dynamics; Factors and Drivers of Terrestrial and Total SGD

The magnitude of terrestrial SGD is primarily controlled by groundwater level and K_s. In Racasa et al., 2021, it was established that hydraulic gradient (mainly peatland groundwater level) and K_s are the most sensitive factors affecting the long-term magnitude of terrestrial SGD. The transient simulations in Chapter 3 accounted for the importance of K_s by optimizing the K_s of the geological layers, through inverse modeling against observed groundwater heads. These simulations provided broad temporal dimensions (daily to inter-annual) to terrestrial SGD (Figures 3.7 & 3.8; Table 3.3). It was revealed that seasonal terrestrial SGD fluctuations follow the seasonal variability of groundwater level and, to some extent, sea level. For example, despite lowering water levels in summer, the relative contribution of terrestrial SGD to total SGD is similar to spring, which has the highest absolute SGD magnitude. Calmer weather and sea conditions during summer facilitate groundwater discharges, while stormy conditions in fall and winter hinder them. The global coastal groundwater discharge depends on aquifer flow capacity, a function of permeability, thickness of permeable layers, and topographic gradient (Luijendijk et al., 2020). In rewetted coastal peatlands, the hydraulic gradient exceeds the topographic gradient (Racasa et al., 2021). Hydraulic conductivity also directly correlates with SGD rates, based on a study of four wetland types (Qu et al., 2017).

Sea level mainly determines the hydraulic gradient and the ensuing total SGD. While groundwater and sea levels are important to the hydraulic gradient, Chapter 3 shows that the dynamic sea level regulates the daily total SGD. The daily time series cross-correlation analyses between groundwater/ sea level with hydraulic gradient and total SGD unveiled that only sea level is moderately correlated with total SGD (SM Figure 3.6). Regarding seasonal dynamics, seasonal mean sea level fluctuations could be small but variability among different seasons influences the total SGD. Increased variability in sea level during fall and winter contributes to recirculated SGD and the total SGD. In contrast,

comparatively calmer and stable sea levels in spring and summer bring more terrestrial SGD, as described earlier. To illustrate, even though terrestrial SGD is lowest in September, more recirculated SGD were observed due to increasing sea level variability, leading to higher total SGD relative to summer discharges (Figure 3.8). These corroborate findings by Gonneea et al. (2013), wherein sea level dominated over groundwater heads as a contributor to hydraulic gradient variability. This dissertation extends the previous findings by encompassing a time-series of groundwater/ sea level correlation with total SGD.

The peat layer and its hydraulic properties play an immense role in determining the spatial distribution of both terrestrial and total SGD. The presence of an extended submerged peat layer, characterized by low K_s, creates a barrier for terrestrial groundwater discharge (Figure 2.3 & 3.6). A two-discharge region may occur (Racasa et al., 2021; Chapter 3), though most terrestrial SGD is concentrated at the shoreline. The observed discrete seepage where peat outcrops is physical proof of a second discharge region farther from the shoreline (Figure 3.1). This parallels offshore SGD from aquifers confined by a low permeability material (Kooi & Groen, 2001; Post et al., 2013). Similarly, the peat acts as a barrier to intruding seawater. Toro et al. (2022) did not document seawater intrusion or the formation of a saltwater wedge in the Hütelmoor peatland. Additionally, Chapter 3 suggests that the extending peat layer potentially limited the groundwater-seawater interface to the nearby beach area (Figure 3.6).

Despite its artificial nature, sandy dune dike belts can contribute to SGD. Approximately one-third of the terrestrial SGD is estimated to come from atmospheric inputs within the dune dike belt of the Hütelmoor peatland (Racasa et al., 2021). Hydrochemical analysis and SC data logger measurements reveal that dune dike groundwater exhibits slightly fresher water than its underlying peat and aquifer sands, indicating the mixing of precipitation and infiltrating ponded surface water from the peatland (Chapter 4).

Although not investigated directly, wind direction, aside from wind speed, may affect sea level and the hydraulic gradient. In the Hütelmoor, west-northwest winds directed towards the shore will increase sea level and reduce SGD, while southeasterly winds will decrease sea level and increase SGD. Wind direction and precipitation have increased SGD rates in the nearby Bay of Puck, Poland (Kłostowska et al., 2020).

The other factors that are not considered in this dissertation are the following: tides, density-driven convection, and wave set-up. The semi-enclosed, non-tidal Baltic Sea has a maximal tidal height of 23 cm (100-year estimate) for the whole region (Medvedev et al., 2016). Therefore, tidal pumping is expected to be limited. The Baltic's physiographic configuration leads to a brackish sea (HELCOM, 2018). With coastal peatlands exposed to the Baltic Sea, density-driven effects are projected to be minimal (SM Table 2.2). The brackish nature of the discharging groundwater could be potentially higher than receiving coastal areas (Chapter 3). Sea level predominantly affects daily SGD, but highly irregular and shorter temporal scales impact of wave set-up are not accommodated in our modeling, except to show the impact of the 2019 storm surge event. These factors either increase recirculated SGD (tidal or wave set up) or porewater fluxes (density-driven convection) (Santos et al., 2012).

Hypothesis (i), i.e., SGD occurs from coastal peatlands with groundwater level and hydraulic conductivity determining the magnitude of terrestrial SGD, is therefore accepted. Long-term, steady-state simulations showed the importance of groundwater level and hydraulic conductivity (Racasa et al., 2021). In addition, the hypothesis that more terrestrial SGD occurs at the coast is also accepted.

Hypothesis (ii). i.e., terrestrial and total SGD seasonal magnitudes depend on the hydraulic gradient, which is subject to the interaction of groundwater and sea level, is accepted. The seasonal variation of groundwater level primarily determines seasonal terrestrial SGD. However, it is also partly determined by sea level, which could hinder or stimulate the hydraulic gradient. On a daily temporal scale, the total SGD is governed by sea level, which dictates the hydraulic gradient. The seasonal changes in sea level affect the seasonal variations of total and terrestrial SGD.

5.3 Surface and Groundwater Quality of Coastal Peatlands

The surface and groundwater of coastal peatlands exhibit historical marine influence prior to the recent influx of seawater. Most of the groundwater from rewetted Hütelmoor was classified as Na-Cl water types. Conversely, groundwater proximate to the forest area displayed mixed water types. Roughly one-third of the groundwater from the peatland is estimated to originate from the Baltic Sea owing to historical seawater inundations rather than intrusion (Toro et al., 2022). In Drammendorf, a gradient of Ca-Cl, mixed types, and Na-Cl surface and groundwater facies was observed prior to rewetting, indicating seawater intrusion possibly resulting from a reversed hydraulic gradient directed inland (Figure 4.3B). Groundwater samples located farther from the shore exhibited Ca-Cl facies, whereas those near the shore showed Na-Cl types.

Coastal peatlands' surface and groundwater are enriched with organic carbon and remineralized chemical species. Throughout the sampling period in Hütelmoor and Drammendorf, high concentrations of DOC, DIC, NH_4^+, and other major ions were documented. In the Hütelmoor, DOC, DIC, and NH_4^+ concentrations peaked at 526 mg L^{-1}, 140 mg L^{-1}, and 59 mg L^{-1}, respectively. Likewise, in Drammendorf, additional analysis from peat groundwater revealed concentrations of 862 mg DOC L^{-1} and 89 mg NH_4^+ L^{-1}.

5.4 Extreme Events and Human Interventions: Storm Surges, Seawater Rewetting, Drainage Networks

The storm surge of 2 Jan 2019 brought about intrusion into the unsaturated beach area, along with inundation of the Hütelmoor peatland through overtopping of the northern dune dike and the groundsill. This event resulted in the exfiltration of intruded seawater and the elevation of groundwater level which eventually contributed to higher SGD fluxes (Chapter 3).

The introduction of seawater from storm surges influences both the surface and groundwater within coastal peatlands (Chapter 4). The input of salts such as Na^+, Mg^{2+}, Cl^-, and SO_4^{2-} can affect solute transport (McCarter et al., 2018) and microbial degradation processes (Gutekunst et al., 2022) in fen peat. Despite the apparent stability in

groundwater quality of the brackish-rewetted Hütelmoor peatland after seawater input, the leaching of DOC and ammonium could not be disregarded. The high concentrations of these materials are potentially attributed to anion (sulfate-organic acids; Gosch et al., 2019; Kalbitz et al., 2000) and cation (sodium-ammonium; McCarter et al., 2018; Liu & Lennartz, 2019b) exchanges. In surface waters, the impact of salts is more evident than in groundwater in terms of SC and pH.

Rewetting drained peatlands with seawater drastically changes surface water quality and impacts the underlying groundwater (Chapter 4). This change has been shown in Drammendorf by looking at water facies (Piper plot) and groundwater chemistry (Gibbs diagram). Surface waters changed significantly reflecting seawater quality. Post-rewetting, the changes in groundwater quality depend on the distance from the coast, which coincides with peat thickness. Immediately after rewetting, seawater strongly impacted groundwater farther from the coast, but groundwater quickly exhibited mixed-type waters two months later. Groundwater at the thicker peat layer revealed a delayed response to seawater impact due to low peat K_s. The changes in groundwater quality are not significant but noteworthy, where eventual increases in DOC and ammonium were observed.

The drainage networks still impact the peatlands' water flow dynamics and solute transport. Before seawater rewetting in Drammendorf, water facies showed potential seawater intrusion closer to the coast because of lowered ground elevation and water table. In Hütelmoor, Toro et al. (2022) showed groundwater flows to the nearby ditches. Similarly, within both coastal peatlands, these ditches could potentially divert larger groundwater flow pathways and act as hydrological barriers. This could explain the Ca-Cl and Na-Cl groundwater facies observed in Drammendorf despite the relative proximity of the monitoring well stations. Conversely, during higher sea levels, such as observed in the Hütelmoor, the ditches can also act as conduits for distributing seawater (Schreiber et al., 2021; Toro et al., 2022). These dynamics indicate inevitable impacts on groundwater flow patterns and solute transport.

Hypothesis (iii) is partially accepted, i.e., storm surge increases SWI fluxes and the eventual SGD fluxes. The storm surges of Jan 2019 (Chapter 3) led to increased SWI fluxes in the Hütelmoor. However, the succeeding increase in SGD fluxes is also due to the increase in hydraulic gradient because of increased groundwater level from seawater inundation and lowered sea level.

Hypothesis (iv), i.e., seawater input significantly changes the chemistry of surface and groundwater of coastal peatlands, is partially accepted. Only the surface waters of Drammendorf peatlands showed significant changes, which are expected because of drastic environmental changes. The groundwater in Drammendorf and both surface and groundwater in the Hütelmoor did not significantly change, but concentrations of DOC, DIC, and ammonium were notably affected.

The hypothesis that DOC/ DIC concentrations decrease with seawater is partially rejected. Results from Hütelmoor point to increasing DOC/ DIC despite lower pH and increasing SC. Localized effects such as iron concentration and peat decomposition should be considered. In Drammendorf, limited results point to

decreasing DOC/ DIC, but further sampling showed increasing DOC with low pH and high SC.

Lastly, the hypothesis that ammonium increases due to cation exchange is accepted. The decreasing trend in ammonium concentrations is evidence of continuous cation exchange in groundwater.

5.5 Implications to SGD and Peatland Research

This dissertation unraveled the processes governing terrestrial and total SGD from rewetted coastal peatlands. First, it was proven that SGD occurs from rewetted coastal peatlands based on numerical modelling, field measurements, and observations. This work adds to the limited research on SGD from muddy environments (Taniguchi et al., 2019). The factors affecting long-term terrestrial SGD (groundwater level and hydraulic conductivity) were determined (Racasa et al., 2021). The importance of sea level in determining the hydraulic gradient and total SGD on a daily temporal scale was highlighted. Seasonal weather variation of winds and waves determine the sea level which plays an important role to both terrestrial and total SGD. Furthermore, the critical role of the low K_s and extending peat layer to SGD and SWI has been established.

The surface and groundwater quality of both drained and brackish-rewetted peatlands were studied, as groundwater could eventually discharge as SGD to the coast. Unlike most peatland studies, surface and groundwater from deeper depths were sampled, including the deeper peat layers and the underlying aquifer sands. Groundwater chemistry showed historical marine influence, probably through seawater inundation or intrusion.

Human interventions – draining, diking, rewetting – play a central role in groundwater flow and solute transport in coastal peatlands. Ditches permanently altered flow fields in the rewetted Hütelmoor peatland (Toro et al., 2022) and may serve as conduits for seawater influx (Schreiber et al., 2021; Toro et al., 2022), still impacting the peatland up to the present. In addition to this, in drained peatlands, seawater intrusion may occur due to landward hydraulic gradients. The encompassing role of ditches remains to be fully understood, but results indicate that they may serve as hydrological barriers for seawater intrusion.

The removal or neglect of dikes allows seawater input by storm surges or seawater rewetting: these impact surface and groundwater, with surface waters being the most affected. Changes in surface water and groundwater chemistry were observed, increasing DOC, DIC, and ammonium concentrations. DOC mobilization was associated with high EC and low pH, which contradicts other studies (Ardon et al., 2016; Tiemeyer et al., 2017; Liu & Lennartz, 2019b). Iron, which was not considered in this study, is suggestive that it plays a role in local differences of DOC and other materials concentration. The results highlight the importance of conducting field-based research, which could differ greatly from laboratory studies.

Coastal peatlands are potential unaccounted sources of organic carbon and other materials. The high concentrations of DOC, DIC, NH_4^+, and other concentrations mark a

potential release of these materials either through SGD or the ditches. Restoring previous hydrological levels increases the likelihood of SGD. Regarding area-normalized flux estimates and the abundance of coastal peatlands, the results from this dissertation indicate the importance to local geochemical budgets in comparison to river systems.

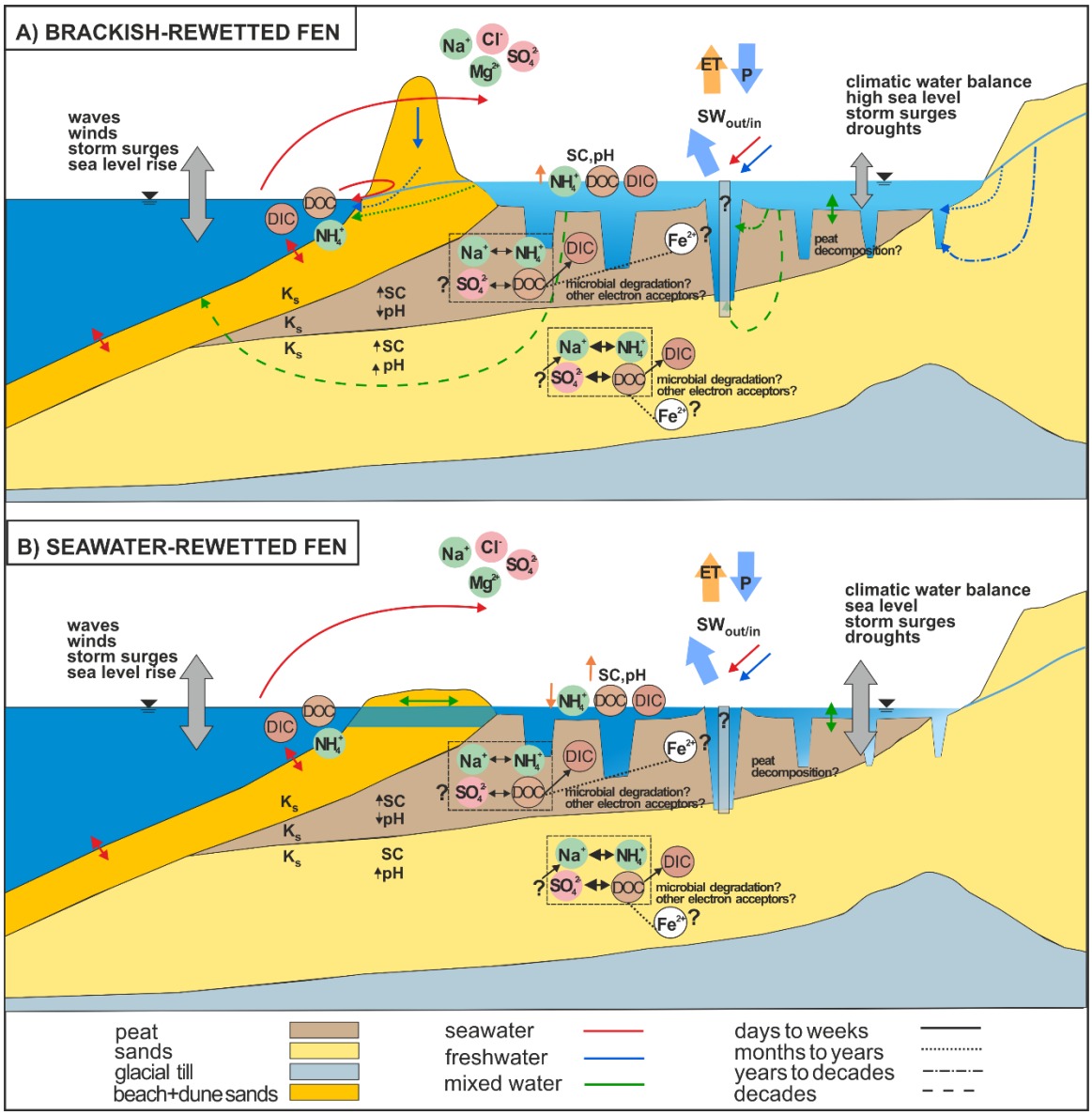

Figure 5.1. Simplified schematic diagram for water flow and solute dynamics for a brackish-rewetted fen (A) and a seawater-rewetted fen (B). Variables affecting groundwater and sea levels are shown and listed. Some flow pathways for the brackish-rewetted fen from Toro et al. (2022) are shown. Submarine groundwater discharge flow dynamics was only investigated in A and flow pathways in B (ditches) are not shown. Potential physical exchanges of solutes (in dashed rectangles) and resulting surface water quality are represented. The gray rectangle with the question mark indicates potential of ditches as hydrological barriers for groundwater flow or seawater intrusion (when drained). Impacts of distance-to-coast and peat thickness to solute transport are not represented.

5.6 Outlook

Upscaling local SGD estimates to regional fluxes remains a subject of investigation. The occurrence of SGD originating from rewetted coastal peatlands has been established. Likewise, the factors and temporal dynamics of SGD were analyzed. Given the abundance of coastal peatlands in the German state of Mecklenburg-Western Pomerania (Figure 5.2) and the larger Baltic Sea, SGD in the region increases in relevance. The potential of SGD for transporting high organic matter and other remineralized materials from the peatlands to the sea through the SGD pathway could be far-reaching.

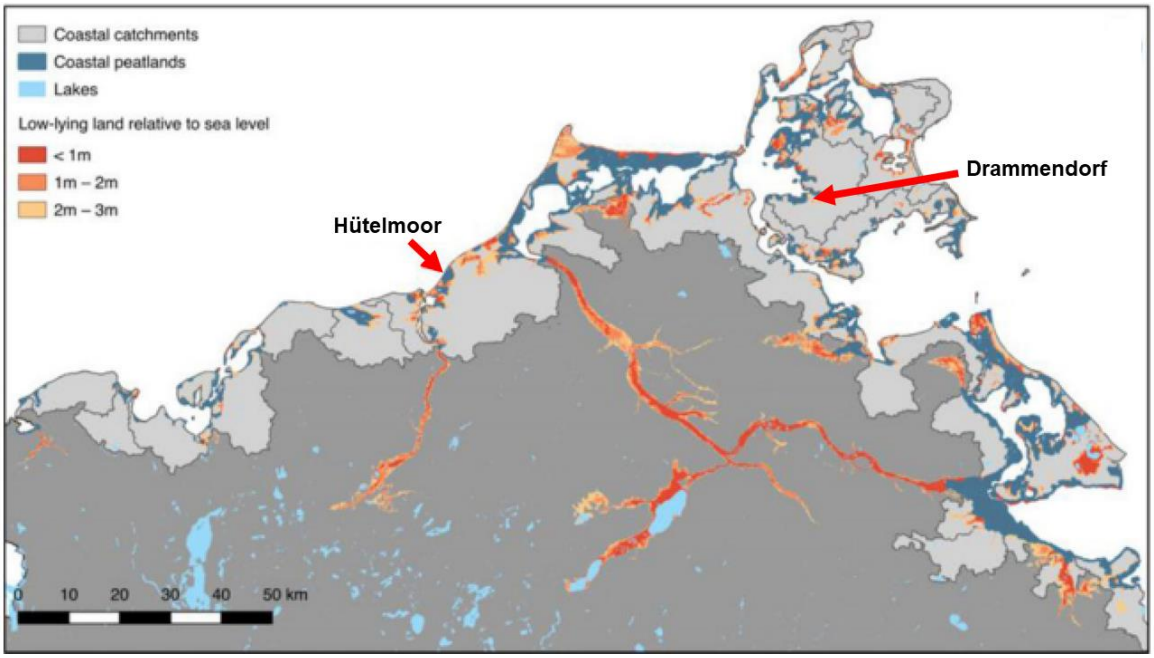

Figure 5.2. Coastal peatlands (dark blue shaded areas) along the German state of Mecklenburg-Western Pomerania (modified from Jurasinski et al., 2018).

Anticipated sea level rise will continue, along with more intense and higher frequency of storm surges attributable to continued climate change impacts. These will amplify wave-driven SGD while decreasing hydraulic gradients, except if the groundwater level is elevated due to the mass influx of seawater from winter storm surges. Solute dynamics will be affected as more seawater input may leach out DOC, DIC, NH_4^+, and other materials from groundwater. Consequently, seawater input may intensify material exports through SGD or ditches. Moreover, the lack of comprehensive understanding of SGD impacts on local ecosystems necessitates further investigation. Whether rewetting coastal peatlands and re-establishing SGD will benefit or harm coastal ecosystems remains to be seen.

Rewetting with seawater and increasing natural sea connections may create potential biogeochemical hotspots at newly created coastlines. Where seawater meets with groundwater could be particularly interesting, especially if dynamic changes in salinity distribution are observed in shallower peat layers. These areas could become sources of high organic matter, nutrients, metals, and other material fluxes. Further studies linking hydrology, marine processes, and biogeochemical processes should be pursued to

understand the temporal extent of seawater's impact on groundwater quality and the salinization of coastal groundwater systems in rewetted peatlands.

On the landside, our understanding of the impacts of peatland rewetting on the water quality of rivers and streams remains incomplete. Rise in DOC concentrations in temperate catchments have been reported (Knorr, 2013), with peatland rewetting as one of the proposed causes. In addition to previous studies (Zak & Gelbrecht, 2007; Pönisch & Breznikar et al., 2022), the results of this dissertation point to an increase in DOC mobilization in ground and surface waters likely through anion exchange processes with seawater salts. The high carbon concentrations in ground and surface waters of peatlands will eventually discharge to downstream rivers and streams. Although studies have shown that rewetting peatlands is beneficial for preventing GHG emissions, the study of its impact on river water quality is understated despite decades of peatland restoration. In regions where rivers serve as a source of drinking water, e.g., the city of Rostock gets its water from the Warnow River, the rise in DOC concentrations may contribute to water quality challenges. Historically, massive peatland drainage for agricultural expansion has led to various ecosystem problems, including rising GHG emissions. The unforeseen impacts of large scale draining of peatlands in the past underscore the need for a thorough investigation of the potential environmental impacts of peatland rewetting that may not be apparent at the present time.

6. RERENCES

Ahmad, S., Hörmann, G., Zantout, N., Schrautzer, J. (2020). Quantifying actual evapotranspiration in fen ecosystems: Implications of management and vegetation structure. Ecohydrology & Hydrobiology, 20 (3), 382–396. https://doi.org/10.1016/j.ecohyd.2020.04.001

Allen, R. G., Pereira, L. S., Raes, D., & Smith, M. (1998). *FAO Irrigation and Drainage Paper No. 56 - Crop Evapotranspiration*. *56*.

Anderson, W. P., Jr., & Lauer, R.M. (2008), The role of overwash in the evolution of mixing zone morphology within barrier islands, Hydro- geol. J., 16(8), 1483–1495, doi:10.1007/s10040-008-0340-z.

Anderson, M. P., Woessner, W. W., & Hunt, R. J. (2015). *Applied Groundwater Modeling: Simulation of Flow and Advective Transport* (2nd ed.). Elsevier.

Appelo, C.A.J., & Postma, D. (1993). *Geochemistry, groundwater, and pollution*. A.A. Balkema.

Ardón, M., Helton, A. M., & Bernhardt, E. S. (2016). Drought and saltwater incursion synergistically reduce dissolved organic carbon export from coastal freshwater wetlands. *Biogeochemistry*, *127*(2–3), 411–426. https://doi.org/10.1007/s10533-016-0189-5

BACC II Author Team. (2014). Second Assessment of Climate Change for the Baltic Sea Basin. Regional climate studies. In *Second Assessment of Climate Change for the Baltic Sea Basin. Regional climate studies.* https://doi.org/10.1007/978-3-319-16006-1

Baird, A. J. (1997). Field estimation of macropore functioning and surface hydraulic conductivity in a fen peat. *Hydrological Processes*, *11*(3), 287–295. https://doi.org/10.1002/(SICI)1099-1085(19970315)11:3<287::AID-HYP443>3.0.CO;2-L

Baird, A. J., & Gaffney, S. W. (2000). Solute movement in drained fen peat: A field tracer study in a Somerset (UK) wetland. *Hydrological Processes*, *14*(14), 2489–2503. https://doi.org/10.1002/1099-1085(20001015)14:14<2489::aid-hyp110>3.0.co;2-q

Batistel, C., Porsche, C., Jurasinski, G., & Schubert, H. (2022). Responses of Four Peatland Emergent Macrophytes to Salinity and Short Salinity Pulses. *Wetlands*, *42*(7), 67. https://doi.org/10.1007/s13157-022-01592-0

Beckwith, C. W., Baird, A. J., & Heathwaite, A. L. (2003). Anisotropy and depth-related heterogeneity of hydraulic conductivity in a bog peat. II: Modelling the effects on groundwater flow. *Hydrological Processes*, *17*(1), 103–113. https://doi.org/10.1002/hyp.1117

Beyer, W. (1964). Zur Bestimmung der Wasserdurchlassigkeit von Kieson und Sanduen aus der Kornverteilung, Wasserwirt. Wassertech 14, 165–169.

Boergens, E., Güntner, A., Dobslaw, H., Dahle, C. (2020). Quantifying the Central European droughts in 2018 and 2019 with GRACE Follow-on. Geophysical Research Letters 47 (14). https://doi.org/10.1029/2020GL087285

Bokuniewicz, H. J. (1992). Analytical Descriptions of Subaqueous Groundwater Seepage. *Estuaries*, *15*(4), 458. https://doi.org/10.2307/1352390

Bollmann, Bosch, C. et al. (2010). World ocean review. *Physical Review E*, *67*.

Bratton, J. F. (2010). The three scales of submarine groundwater flow and discharge across passive continental margins. *Journal of Geology*, *118*(5), 565–575. https://doi.org/10.1086/655114

Burnett, W. C., Aggarwal, P. K., Aureli, A., Bokuniewicz, H., Cable, J. E., Charette, M. A., Kontar, E., Krupa, S., Kulkarni, K. M., Loveless, A., Moore, W. S., Oberdorfer, J. A., Oliveira, J., Ozyurt, N., Povinec, P., Privitera, A. M. G., Rajar, R., Ramessur, R. T., Scholten, J., … Turner, J. V. (2006). Quantifying submarine groundwater discharge in the coastal zone via multiple methods. In *Science of the Total Environment*. https://doi.org/10.1016/j.scitotenv.2006.05.009

Burnett, W. C., Bokuniewicz, H., Moore, W. S., & Taniguchi, M. (2003). Groundwater and pore water inputs to the coastal zone. *Biogeochemistry*, *66*, 3–33. https://doi.org/10.1023/B:BIOG.0000006066.21240.53

Burnett, W. C., Taniguchi, M., & Oberdorfer, J. (2001). Measurement and significance of the direct discharge of groundwater into the coastal zone. *Journal of Sea Research*, *46*, 109–116.

BSH (Bundesamt fuer Seeschifffahrt und Hydrographie) (2021). Hourly (1953-2020) and per minute (2021) tide gauge data from Rostock-Warnemünde. Requested November 2021 thru Mr. Daniel Melchert.

Cardenas, M. B., Bennett, P. C., Zamora, P. B., Befus, K. M., Rodolfo, R. S., Cabria, H. B., & Lapus, M. R. (2015). Devastation of aquifers from tsunami-like storm surge by Supertyphoon Haiyan. *Geophysical Research Letters*, *42*(8), 2844–2851. https://doi.org/10.1002/2015GL063418

Chaillou, G., Lemay-Borduas, F., & Couturier, M. (2016) Transport and transformations of groundwater-borne carbon discharging through a sandy beach to a coastal ocean. Canadian Water Resources Journal / Revue canadienne des ressources hydriques, 41:4, 455-468. doi: 10.1080/07011784.2015.1111775

Charette, M. A., & Sholkovitz, E. R. (2002). Oxidative precipitation of groundwater-derived ferrous iron in the subterranean estuary of a coastal bay. *Geophysical Research Letters*, *29*(10), 85-1-85–4. https://doi.org/10.1029/2001gl014512

Charette, M. A., Sholkovitz, E. R., & Hansel, C. M. (2005). Trace element cycling in a subterranean estuary: Part 1. Geochemistry of the permeable sediments. *Geochimica et Cosmochimica Acta*, *69*(8), 2095–2109. https://doi.org/10.1016/j.gca.2004.10.024

Chen, X., Zhang, F., Lao, Y., Wang, X., Du, J., & Santos, I. R. (2018). Submarine Groundwater Discharge-Derived Carbon Fluxes in Mangroves: An Important Component of Blue Carbon Budgets? *Journal of Geophysical Research: Oceans*, *123*(9), 6962–6979. https://doi.org/10.1029/2018JC014448

Cho, H. M., Kim, G., Kwon, E. Y., Moosdorf, N., Garcia-Orellana, J., & Santos, I. R. (2018). Radium tracing nutrient inputs through submarine groundwater discharge in the global ocean. *Scientific Reports*. https://doi.org/10.1038/s41598-018-20806-2

Church, T. M. (1996). An underground route for the water cycle. *Nature*, *380*(6575), 579–580. https://doi.org/10.1038/380579a0

Clark, J. M., Heinemeyer, A., Martin, P., & Bottrell, S. H. (2012). Processes controlling DOC in pore water during simulated drought cycles in six different UK peats. *Biogeochemistry*, *109*(1–3), 253–270. https://doi.org/10.1007/s10533-011-9624-9

Correa, R. E., Xiao, K., Conrad, S. R., Wadnerkar, P. D., Wilson, A. M., Sanders, C. J., & Santos, I. R. (2022). Groundwater Carbon Exports Exceed Sediment Carbon Burial in a Salt Marsh. *Estuaries and Coasts*, *45*(6), 1545–1561. https://doi.org/10.1007/s12237-021-01021-1

Costall, A. R.,Harris, B. D., Teo,B., Schaa, R.,Wagner, F. M., and Pigois,J. P. (2020). Groundwater Throughflow and Seawater Intrusion in High Quality Coastal Aquifers. Sci. Rep. 10 (1), 1–33. doi:10.1038/s41598-020- 75736-9

Davis, K., Santos, I. R., Perkins, A. K., Webb, J. R., & Gleeson, J. (2020). Altered groundwater discharge and associated carbon fluxes in a wetland-drained coastal canal. *Estuarine, Coastal and Shelf Science*, *235*, 106567. https://doi.org/10.1016/j.ecss.2019.106567

de Sieyes, N. R., Yamahara, K. M., Paytan, A., & Boehm, A. B. (2011). Submarine Groundwater Discharge to a High-Energy Surf Zone at Stinson Beach, California, Estimated Using Radium Isotopes. *Estuaries and Coasts*, *34*(2), 256–268. https://doi.org/10.1007/s12237-010-9305-2

Dettmann, U., Bechtold, M., Frahm, E., & Tiemeyer, B. (2014). On the applicability of unimodal and bimodal van Genuchten-Mualem based models to peat and other organic soils under evaporation conditions. *Journal of Hydrology*, *515*, 103–115. https://doi.org/10.1016/j.jhydrol.2014.04.047

DIN 19685-8:2012-07. Bodenbeschaffenheit - Felduntersuchungen - Teil 8: Bestimmung der Wasserdurchlässigkeit mit der Bohrlochmethode. 2012.

DIN EN 13039:2012-01. Bodenverbesserungsmittel und Kultursubstrate - Bestimmung des Gehaltes an organischer Substanz und Asche; Deutsche Fassung EN 13039:2011

DIN ISO 11277. Soil quality — Determination of particle size distribution in mineral soil material — Method by sieving and sedimentation.

Duque, C., Russoniello, C. J., & Rosenberry, D. O. (2020). History and evolution of seepage meters for quantifying flow between groundwater and surface water: Part 2 – Marine settings and submarine groundwater discharge. *Earth-Science Reviews*, *204*, 103168. https://doi.org/10.1016/j.earscirev.2020.103168

DWD (Deustcher Wetterdienst) (2020). Warnemünde. Available at: https://cdc. dwd.de/portal/201912031600/mapview (Accessed July 20, 2020)

DWD-CDC (Deutscher Wetterdienst-Klima und Umwelt) (2021a). Daily station measurements Precipitation height in mm. Downloaded November 2021.

DWD-CDC (Deutscher Wetterdienst-Klima und Umwelt) (2021b). Daily average of the station measurements of the average wind speed at approx. 10 m height in m/s. Downloaded November 2021.

DWD-CDC (Deutscher Wetterdienst-Klima und Umwelt) (2021c). Daily station measurements of the maximum air temperature at a height of 2 m in °C. Downloaded November 2021.

DWD-CDC (Deutscher Wetterdienst-Klima und Umwelt) (2021d). Daily station measurements of the minimum air temperature at a height of 2 m in °C. Downloaded November 2021.

Ferone, J. M., & Devito, K. J. (2004). Shallow groundwater-surface water interactions in pond-peatland complexes along a Boreal Plains topographic gradient. *Journal of Hydrology*, *292*(1–4), 75–95. https://doi.org/10.1016/j.jhydrol.2003.12.032

Forster, S., & Zettler, M. L. (2004). The capacity of the filter-feeding bivalve Mya arenaria L. to affect water transport in sandy beds. *Marine Biology*, *144*(6), 1183–1189. https://doi.org/10.1007/s00227-003-1278-2

Fukuo, Y., & Kaihotsu, I. (1988). A theoretical analysis of seepage flow of the confined groundwater into the lake bottom with a gentle slope. *Water Resources Research*, *24*(11), 1949–1953. https://doi.org/10.1029/WR024i011p01949

Gibbs, R.J. (1970). Mechanisms Controlling World Water Chemistry. *Science*, *170*(3962), 1088–1090.

Gonneea M. E., Mulligan A. and Charette M. A. (2013) Climate- driven sea level anomalies modulate coastal groundwater dynamics and discharge. Geophys. Res. Lett, http:// dx.doi.org/10.1002/grl.50192

Goodridge, B. M. (2018). The influence of submarine groundwater discharge on nearshore marine dissolved organic carbon reactivity, concentration dynamics, and offshore export. *Geochimica et Cosmochimica Acta*, *241*, 108–119. https://doi.org/10.1016/j.gca.2018.08.040

Gosch, L., Janssen, M., & Lennartz, B. (2018). Impact of the water salinity on the hydraulic conductivity of fen peat. *Hydrological Processes*. https://doi.org/10.1002/hyp.11478

Gosch, L., Townsend, H., Kreuzburg, M., Janssen, M., Rezanezhad, F., & Lennartz, B. (2019). Sulfate Mobility in Fen Peat and Its Impact on the Release of Solutes. *Frontiers in Environmental Science*, *7*(November), 1–13. https://doi.org/10.3389/fenvs.2019.00189

Grinsted, A., Jevrejeva, S., Riva, R. E. M., & Dahl-Jensen, D. (2015). Sea level rise projections for Northern Europe under RCP8.5. *Climate Research*, *64*(1), 15–23. https://doi.org/10.3354/cr01309

Grolemund G, Wickham H (2011). “Dates and Times Made Easy with lubridate.” *Journal of Statistical Software*, **40**(3), 1–25. https://www.jstatsoft.org/v40/i03/.

Günther, A., Barthelmes, A., Huth, V., Joosten, H., Jurasinski, G., Koebsch, F., & Couwenberg, J. (2020). Prompt rewetting of drained peatlands reduces climate warming despite methane emissions. *Nature Communications*, *11*(1), 1–5. https://doi.org/10.1038/s41467-020-15499-z

Gupta, H. V., Kling, H., Yilmaz, K. K., & Martinez, G. F. (2009). Decomposition of the mean squared error and NSE performance criteria: Implications for improving hydrological modelling. *Journal of Hydrology*, *377*(1–2), 80–91. https://doi.org/10.1016/j.jhydrol.2009.08.003

Gutekunst, C. N., Liebner, S., Jenner, A. K., Knorr, K. H., Unger, V., Koebsch, F., Racasa, E. D., Yang, S., Böttcher, M. E., Janssen, M., Kallmeyer, J., Otto, D., Schmiedinger, I., Winski, L., & Jurasinski, G. (2022). Effects of brackish water inflow on methane-cycling microbial communities in a freshwater rewetted coastal fen. *Biogeosciences*, *19*(15), 3625–3648. https://doi.org/10.5194/bg-19-3625-2022

Habicht, H.-L., Rosentau, A., Jõeleht, A., Heinsalu, A., Kriiska, A., Kohv, M., et al. (2017). GIS-based Multiproxy Coastline Reconstruction of the Eastern Gulf ofRiga,BalticSea,duringthe StoneAge. Boreas 46, 83–99. doi:10.1111/ bor.12157

Hahn, J., Köhler, S., Glatzel, S., & Jurasinski, G. (2015). Methane Exchange in a Coastal Fen in the First Year after Flooding - A Systems Shift. *PLOS ONE*, *10*(10), e0140657. https://doi.org/10.1371/journal.pone.0140657

Heiss, J. W., and H. A. Michael (2014). Saltwater-freshwater mixing dynamics in a sandy beach aquifer over tidal, spring-neap, and seasonal cycles. Water Resour. Res., 50, 6747–6766. doi:10.1002/2014WR015574.

HELCOM. (2009). Eutrophication in the Baltic Sea. *Baltic Sea Environment Proceedings No. 115B*, 148. https://doi.org/10.1016/b978-0-444-89990-3.50058-4

HELCOM. (2018). State of the Baltic Sea- Second HELCOM holistic assessment, 2011-2016. *Baltic Sea Environment Proceedings 155*, *155*, 4–7. http://stateofthebalticsea.helcom.fi/pressures-and-their-status/hazardous-substances/

HELCOM, 2022. HELCOM Pollution Load Compilation Database. Accessed from https://helcom.fi/baltic-sea-trends/data-maps/databases/. Accessed 14.07.2023.

Hofmann, 2017. Renaturierung Polder Drammendorf (Company Report on the Renaturation of Polder Drammendorf).

Holden, J. (2005). Peatland hydrology and carbon release: Why small-scale process matters. *Philosophical Transactions of the Royal Society A: Mathematical, Physical and Engineering Sciences*, *363*(1837), 2891–2913. https://doi.org/10.1098/rsta.2005.1671

Hsu, F.-H., Su, C.-C., Wang, P.-L., and Lin, I.-T. (2020). Temporal Variations of Submarine Groundwater Discharge into a Tide-Dominated Coastal Wetland (Gaomei Wetland, Western Taiwan) Indicated by Radon and Radium Isotopes. Water 12, 1806. doi:10.3390/w12061806

Hwang, D., Kim, G., Lee, W., & Oh, H. (2010). The role of submarine groundwater discharge (SGD) in nutrient budgets of Gamak Bay , a shellfish farming bay , in Korea. *Journal of Sea Research*, *64*(3), 224–230. https://doi.org/10.1016/j.seares.2010.02.006

Hwang, D., Lee, Y., & Kim, G. (2005). Large submarine groundwater discharge and benthic eutrophication in Bangdu Bay on volcanic Jeju Island , Korea. *Limnoloogy and Oceanography*, *50*(5), 1393–1403.

Ibenthal, M. (2020). Marine and Terrestrial Influence on Submarine Groundwater Discharge in Coastal Waters Connected to a Peatland. E dissertation. Göttingen, Germany: Georg-August-Universität Göttingen. Avaialble at: https://ediss.uni-goettingen.de/handle/21.11130/00-1735-0000-0005-13C2-A.

Idczak, J., Brodecka-Goluch, A., Łukawska-Matuszewska, K., Graca, B., Gorska, N., Klusek, Z., Pezacki, P. D., & Bolałek, J. (2020). A geophysical, geochemical and microbiological study of a newly discovered pockmark with active gas seepage and submarine groundwater discharge (MET1-BH, central Gulf of Gdańsk, southern Baltic Sea). *Science of the Total Environment*, *742*. https://doi.org/10.1016/j.scitotenv.2020.140306

IOW (Leibniz Institute for Baltic Sea Research Warnemünde) (2020). Environmental Long-Term Data Programme, Station TFO5 - Oceanographic Database Search with Interactive Navigation - ODIN2. Avaialble at: https://odin2.io-warnemuende.de/#/(Accessed December 12, 2020).

ITZBund. (2020). *Stammdaten – Warnemünde*. https://www.pegelonline.wsv.de/gast/stammdaten?pegelnr=9640015

Jakobsson, M., O'Regan, M., Mörth, C. M., Stranne, C., Weidner, E., Hansson, J., Gyllencreutz, R., Humborg, C., Elfwing, T., Norkko, A., Norkko, J., Nilsson, B., & Sjöström, A. (2020). Potential links between Baltic Sea submarine terraces and groundwater seeping. *Earth Surface Dynamics*, *8*(1), 1–15. https://doi.org/10.5194/esurf-8-1-2020

Jiao, J., & Post, V. (2019). *Coastal Hydrogeology*. Cambridge University Press. https://doi.org/10.1017/9781139344142

Johannes, R. (1980). The Ecological Significance of the Submarine Discharge of Groundwater . *Marine Ecology Progress Series*, *3*, 365–373. https://doi.org/10.3354/meps003365

Joosten, H., & Clarke, D. (2002). Wise Use of Mires and Peatlands. In *International Mire Conservation Group and International Peat Society, Helsinki* (Issue November 2003). http://www.gret-perg.ulaval.ca/fileadmin/fichiers/fichiersGRET/pdf/Doc_generale/WUMP_Wise_Use_of_Mires_and_Peatlands_book.pdf

Joosten, H., Sirin, A., Couwenberg, J., Laine, J., & Smith, P. (2016). The role of peatlands in climate regulation. In *Peatland Restoration and Ecosystem Services* (pp. 63–76). Cambridge University Press. https://doi.org/10.1017/CBO9781139177788.005

Joosten, H., Tanneberger, F., & Moen, A. (Eds.). (2017). *Mires and Peatlands of Europe: Status, Distribution, and Conservation*. E. Schweizerbart'sche Verlagsbuchhanglung (Nagele u. Obermiller).

Jørgensen, B. B.: Mineralization of organic matter in the sea bed-the role of sulphate reduction, Nature, 296, 643–645, https://doi.org/10.1038/296643a0, 1982.

Jurasinski, G., Janssen, M., Voss, M., Böttcher, M. E., Brede, M., Burchard, H., Forster, S., Gosch, L., Gräwe, U., Gründling-Pfaff, S., Haider, F., Ibenthal, M., Karow, N., Karsten, U., Kreuzburg, M., Lange, X., Leinweber, P., Massmann, G., Ptak, T., … Lennartz, B. (2018). Understanding the Coastal Ecocline: Assessing Sea–Land Interactions at Non-tidal, Low-Lying Coasts Through Interdisciplinary Research. *Frontiers in Marine Science*. https://doi.org/10.3389/fmars.2018.00342

Kaiser, K., & Zech, W. 1998. Soil dissolved organic matter sorption as influenced by organic and sesquioxide coatings and sorbed sulfate. Soil Sci. Soc. Am. J. 62: 129-136

Kalbitz, K.; Solinger, S.; Park, J.-H.; Michalzik, B.; Matzner, E.. CONTROLS ON THE DYNAMICS OF DISSOLVED ORGANIC MATTER IN SOILS: A REVIEW. Soil Science 165(4):p 277-304, April 2000.

Kang, H., Kwon, M. J., Kim, S., Lee, S., Jones, T. G., Johncock, A. C., Haraguchi, A., & Freeman, C. (2018). Biologically driven DOC release from peatlands during recovery from acidification. *Nature Communications*, *9*(1), 1–7. https://doi.org/10.1038/s41467-018-06259-1

Kimmel, K., & Mander, Ü. (2010). Ecosystem services of peatlands: Implications for restoration. *Progress in Physical Geography: Earth and Environment*, *34*(4), 491–514. https://doi.org/10.1177/0309133310365595

Kłostowska, Ż., Szymczycha, B., Lengier, M., Zarzeczańska, D., & Dzierzbicka-Głowacka, L. (2020). Hydrogeochemistry and magnitude of SGD in the Bay of Puck, southern Baltic Sea. *Oceanologia*, *62*(1), 1–11. https://doi.org/10.1016/j.oceano.2019.09.001

Knoben, W. J. M., Freer, J. E., & Woods, R. A. (2019). Technical note: Inherent benchmark or not? Comparing Nash-Sutcliffe and Kling-Gupta efficiency scores. *Hydrology and Earth System Sciences*, *23*(10), 4323–4331. https://doi.org/10.5194/hess-23-4323-2019

Knorr, K. H. (2013). DOC-dynamics in a small headwater catchment as driven by redox fluctuations and hydrological flow paths - Are DOC exports mediated by iron reduction/oxidation cycles? *Biogeosciences*, *10*(2), 891–904. https://doi.org/10.5194/bg-10-891-2013

Knorr, K. H., & Blodau, C. (2009). Impact of experimental drought and rewetting on redox transformations and methanogenesis in mesocosms of a northern fen soil. *Soil Biology and Biochemistry*, *41*(6), 1187–1198. https://doi.org/10.1016/j.soilbio.2009.02.030

Koch, S., Kahle, P., Lennartz, B. (2018). Spatio-temporal analysis of phosphorus concentrations in a North-Eastern German lowland watershed. *J. Hydrol. Reg. Stud.* 15, 203-216. https://doi.org/10.1016/j.ejrh.2018.02.001

Koebsch, F., Winkel, M., Liebner, S., Liu, B., Westphal, J., Schmiedinger, I., Spitzy, A., Gehre, M., Jurasinski, G., Köhler, S., Unger, V., Koch, M., Sachs, T., & Böttcher, M. E. (2019). Sulfate deprivation triggers high methane production in a disturbed and rewetted coastal peatland. *Biogeosciences*, *16*(9), 1937–1953. https://doi.org/10.5194/bg-16-1937-2019

Kolp, O., 1957. Die Nord¨ostliche Heide Mecklenburgs (The Northeastern Heath of Mecklenburg). Deutscher Verlag der Wissenschaften, Berlin, Germany.

Kooi, H., & Groen, J. (2001). Offshore continuation of coastal groundwater systems; predictions using sharp-interface approximations and variable-density flow modelling. *Journal of Hydrology*, *246*(1–4), 19–35. https://doi.org/10.1016/S0022-1694(01)00354-7

Kotwicki, L., Grzelak, K., Czub, M., Dellwig, O., Gentz, T., Szymczycha, B., & Böttcher, M. E. (2014). Submarine groundwater discharge to the Baltic coastal zone: Impacts on the meiofaunal community. *Journal of Marine Systems*. https://doi.org/10.1016/j.jmarsys.2013.06.009

Kreuzburg, M., Ibenthal, M., Janssen, M., Rehder, G., Voss, M., Naumann, M., & Feldens, P. (2018). Sub-marine Continuation of Peat Deposits From a Coastal Peatland in the Southern Baltic Sea and its Holocene Development. *Frontiers in Earth Science*. https://doi.org/10.3389/feart.2018.00103

Kreuzburg, M., Rezanezhad, F., Milojevic, T., Voss, M., Gosch, L., Liebner, S., Van Cappellen, P., & Rehder, G. (2020). Carbon release and transformation from coastal peat deposits controlled by submarine groundwater discharge: a column experiment study. *Limnology and Oceanography*, *65*(5), 1116–1135. https://doi.org/10.1002/lno.11438

Kreuzburg, M., Scholten, J., Hsu, F.-H., Liebetrau, V., Sültenfuß, J., Rapaglia, J., & Schlüter, M. (2023). Submarine Groundwater Discharge-Derived Nutrient Fluxes in Eckernförde Bay (Western Baltic Sea). *Estuaries and Coasts*. https://doi.org/10.1007/s12237-023-01202-0

Kreyling, J., Tanneberger, F., Jansen, F., van der Linden, S., Aggenbach, C., Blüml, V., Couwenberg, J., Emsens, W. J., Joosten, H., Klimkowska, A., Kotowski, W., Kozub, L., Lennartz, B., Liczner, Y., Liu, H., Michaelis, D., Oehmke, C., Parakenings, K., Pleyl, E., … Jurasinski, G. (2021). Rewetting does not return drained fen peatlands to their old selves. *Nature Communications*, *12*(1), 1–8. https://doi.org/10.1038/s41467-021-25619-y

Kwon, Devries, T., Sarmiento, J. L., Charette, M. A., & Cho, Y. (2014). Global estimate of submarine groundwater discharge based on an observationally constrained radium isotope model. *Geophysical Research Letters*, 8438–8444. https://doi.org/10.1002/2014GL061574.Received

Lampe, R. (2005). Lateglacial and Holocene water-level variations along the NE German Baltic Sea coast: Review and new results. *Quaternary International*, *133–134*(1 SUPPL.), 121–136. https://doi.org/10.1016/j.quaint.2004.10.005

Lee, D. R. (1977). A device for measuring seepage flux in lakes and estuaries. In *Limnology and Oceanography* (Vol. 22, Issue 1, pp. 140–147). https://doi.org/10.4319/lo.1977.22.1.0140

Lee, Y. W., & Kim, G. (2007). Linking groundwater-borne nutrients and dinoflagellate red-tide outbreaks in the southern sea of Korea using a Ra tracer. *Estuarine, Coastal and Shelf Science*. https://doi.org/10.1016/j.ecss.2006.08.004

Leifeld, J., & Menichetti, L. (2018). The underappreciated potential of peatlands in global climate change mitigation strategies. *Nature Communications*, *9*(1), 1071. https://doi.org/10.1038/s41467-018-03406-6

Leifeld, J., Wüst-Galley, C., & Page, S. (2019). Intact and managed peatland soils as a source and sink of GHGs from 1850 to 2100. *Nature Climate Change*, *9*(12), 945–947. https://doi.org/10.1038/s41558-019-0615-5

Li, X., Hu, B. X., Burnett, W. C., Santos, I. R., & Chanton, J. P. (2009). Submarine ground water discharge driven by tidal pumping in a heterogeneous aquifer. *Ground Water*, *47*(4), 558–568. https://doi.org/10.1111/j.1745-6584.2009.00563.x

Linke, T., & Gislason, S. R. (2018). Stability of iron minerals in Icelandic peat areas and transport of heavy metals and nutrients across oxidation and salinity gradients - A

modelling approach. *Energy Procedia*, *146*, 30–37. https://doi.org/10.1016/j.egypro.2018.07.005

Limpens, J., Berendse, F., Blodau, C., Canadell, J. G., Freeman, C., Holden, J., Roulet, N., Rydin, H., & Schaepman-Strub, G. (2008). Peatlands and the carbon cycle: from local processes to global implications – a synthesis. *Biogeosciences*, *5*(5), 1475–1491. https://doi.org/10.5194/bg-5-1475-2008

Liu, H., Forsmann, D. M., Kjaergaard, C., Saki, H., and Lennartz, B. (2017). Solute Transport Properties of Fen Peat Differing in Organic Matter Content. J. Environ. Qual. 46 (5), 1106–1113. doi:10.2134/jeq2017.01.0031

Liu, H., Janssen, M., & Lennartz, B. (2016). Changes in flow and transport patterns in fen peat following soil degradation. *European Journal of Soil Science*, *67*(6), 763–772. https://doi.org/10.1111/ejss.12380

Liu, H., & Lennartz, B. (2019a). Hydraulic properties of peat soils along a bulk density gradient—A meta study. *Hydrological Processes*, *33*(1), 101–114. https://doi.org/10.1002/hyp.13314

Liu, H., & Lennartz, B. (2019b). Short term effects of salinization on compound release from drained and restored coastalwetlands. *Water (Switzerland)*, *11*(8). https://doi.org/10.3390/w11081549

Luijendijk, E., Gleeson, T., & Moosdorf, N. (2020). Fresh groundwater discharge insignificant for the world's oceans but important for coastal ecosystems. *Nature Communications*, *11*(1). https://doi.org/10.1038/s41467-020-15064-8

Lupia, F. (2013). ETo-PM. doi: 10.13140/RG.2.1.3359.1286

Malone, T. C., & Newton, A. (2020). The Globalization of Cultural Eutrophication in the Coastal Ocean: Causes and Consequences. *Frontiers in Marine Science*, *7*(August), 1–30. https://doi.org/10.3389/fmars.2020.00670

McBride, M. S., & Pfannkuch, H. O. (1975). Distribution of seepage within lakebeds. *J Res US Geol Surv*, *3*(5), 505–512.

McCarter, C. P. R., Weber, T. K. D., & Price, J. S. (2018). Competitive transport processes of chloride, sodium, potassium, and ammonium in fen peat. *Journal of Contaminant Hydrology*, *217*(August), 17–31. https://doi.org/10.1016/j.jconhyd.2018.08.004

Medvedev, I. P., Rabinovich, A. B., & Kulikov, E. A. (2016). Tides in Three Enclosed Basins: The Baltic, Black, and Caspian Seas. *Frontiers in Marine Science*, *3*. https://doi.org/10.3389/fmars.2016.00046

Miao, Z., Brusseau, M.L., Carroll, K.C., Carreon-Diazconti, C., Johnson, B. (2012). Sulfate reduction in groundwater: characterization and applications for remediation. Eviron. Geochem. Health. 34(4):539-550. Doi: 10.1007/s10653-011-9423-1

Michael, H. A., Mulligan, A. E., & Harvey, C. F. (2005). *Seasonal oscillations in water exchange between aquifers and the coastal ocean*. *436*(August), 1145–1148. https://doi.org/10.1038/nature03935

Miegel, K., Graeff, T., Selle, B., Salzmann, T., Franck, C., & Bronstert, A. (2016). Investigation of a renatured fen on the Baltic Sea coast of Mecklenburg - Part I:

System description and basic hydrological characterisation. *HYDROLOGIE UND WASSERBEWIRTSCHAFTUNG*. https://doi.org/10.5675/HyWa_2016.4_1

Millero, F. J., and Poisson, A. (1981). International One-Atmosphere Equation of State of Seawater. Deep Sea Res. A. Oceanographic Res. Pap. 28 (6), 625–629. doi:10.1016/0198-0149(81)90122-9

Mitra, S., Wassman, R., & Vlek, P. L. G. (2005). An appraisal of global wetland area and its organic carbon stock. *Current Science*, *88*(1), 25–34.

Mohawesh, O., Janssen, M., Maaitah, O., and Lennartz, B. (2017). Assessment the Effect of Homogenized Soil on Soil Hydraulic Properties and Soil Water Transport. Eurasian Soil Sci. 50 (9), 1077–1085. doi:10.1134/ s1064229317090046

Moore, W. S. (1996). Large groundwater inputs to coastal waters revealed by 226Ra enrichments. *Nature*, *380*(6575). https://doi.org/10.1038/380612a0

Moore, W. S. (1999). *The subterranean estuary : a reaction zone of ground water and sea water*.

Moore, W. S. (2010). The effect of submarine groundwater discharge on the ocean. *Annual Review of Marine Science*, *2*, 59–88. https://doi.org/10.1146/annurev-marine-120308-081019

Moosdorf, N., & Oehler, T. (2017). Societal use of fresh submarine groundwater discharge: An overlooked water resource. *Earth-Science Reviews*, *171*(August 2016), 338–348. https://doi.org/10.1016/j.earscirev.2017.06.006

Müller, H., von Dobeneck, T., Nehmiz, W., & Hamer, K. (2011). Near-surface electromagnetic, rock magnetic, and geochemical fingerprinting of submarine freshwater seepage at Eckernförde Bay (SW Baltic Sea). *Geo-Marine Letters*, *31*(2), 123–140. https://doi.org/10.1007/s00367-010-0220-0

Mulligan, A. E., & Charette, M. A. (2006). Intercomparison of submarine groundwater discharge estimates from a sandy unconfined aquifer. *Journal of Hydrology*. https://doi.org/10.1016/j.jhydrol.2005.11.056

Nash, J. E., & Sutcliffe, J. V. (1970). River flow forecasting through conceptual models part I - A discussion of principles. *Journal of Hydrology*, *10*(3), 282–290. https://doi.org/10.1016/0022-1694(70)90255-6

Nazzal, Y., Ahmed, I., Al-Arifi, N.S.N., Ghrefat, H., Zaidi, F.K., El-Waheidi, M.M., Batayneh, A., Zumlot, T. (2014). A pragmatic approach to study the groundwater quality suitability for domestic and agricultural usage, Saq aquifer, northwest of Saudi Arabia. Environ. Monit. Assess. DOI: 10.1007/s10661-014-3728-3.

Neal, C., Reynolds, B., Robson, A.J. (1999). Acid neutralization capacity measurements within natural waters: towards a standardized approach. *Sci. Tot. Env.* 23(244), 233-241. https://doi.org/10.1016/S0048-9697(99)00385-X

Nordio, G., Frederiks, R., Hingst, M., Carr, J., Kirwan, M., Gedan, K., Michael, H., & Fagherazzi, S. (2023). Frequent Storm Surges Affect the Groundwater of Coastal Ecosystems. *Geophysical Research Letters*, *50*(1), 1–10. https://doi.org/10.1029/2022GL100191

Paerl, H.W., Hall, N.S., Peierls, B.L. et al. Evolving Paradigms and Challenges in Estuarine and Coastal Eutrophication Dynamics in a Culturally and Climatically Stressed World. Estuaries and Coasts 37, 243–258 (2014). https://doi.org/10.1007/s12237-014-9773-x

Peña-Haro, S., Pulido-Velazquez, M., and Llopis-Albert, C. (2011). Stochastic Hydro-Economic Modeling for Optimal Management of Agricultural Groundwater Nitrate Pollution under Hydraulic Conductivity Uncertainty. Environ. Model. Softw. 26, 999–1008. doi:10.1016/j.envsoft.2011.02.010

Piper, A.M. (1944) A Graphic Procedure in the Geochemical Interpretation of Water-Analyses. Eos, Transactions American Geophysical Union, 25, 914-928. http://dx.doi.org/10.1029/TR025i006p00914

Pönisch, D., & Breznikar, A. (2004). Nutrient release and flux dynamics of CO2, CH4, and N2O in a coastal peatland driven by actively induced rewetting with brackish water from the Baltic Sea. *Biogeosciences*, *37*(12), 1960–1965.

Pörtner, H.-O., Roberts, D. C., Adams, H., Adelekan, I., Adler, C., Adrian, R., Aldunce, P., Ali, E., Ara Begum, R., Bednar-Friedl, B., Bezner Kerr, R., Biesbroek, R., Birkmann, J., Bowen, K., Caretta, M. A., Carnicer, J., Castellanos, E., Cheong, T. S., Chow, W., … Zaiton Ibrahim, Z. (2022). Climate Change 2022 - Impacts, Adaptation and Vulnerability - Summary for Policymakers. In H.-O. Pörtner, D. C. Roberts, E. S. Poloczanska, K. Mintenbeck, M. Tignor, A. Alegria, M. Craig, S. Langsdorf, S. Löschke, V. Möller, & A. Okem (Eds.), *Ipcc*. https://doi.org/10.1017/9781009325844.002

Post, V. E. A., Groen, J., Kooi, H., Person, M., Ge, S., & Edmunds, W. M. (2013). Offshore fresh groundwater reserves as a global phenomenon. *Nature*, *504*(7478), 71–78. https://doi.org/10.1038/nature12858

Post, V., Kooi, H., & Simmons, C. (2007). Using hydraulic head measurements in variable-density ground water flow analyses. *Ground Water*, *45*(6), 664–671. https://doi.org/10.1111/j.1745-6584.2007.00339.x

Qu, W., Li, H., Huang, H., Zheng, C., Wang, C., Wang, X., & Zhang, Y. (2017). Seawater-groundwater exchange and nutrients carried by submarine groundwater discharge in different types of wetlands at Jiaozhou Bay, China. *Journal of Hydrology*, *555*, 185–197. https://doi.org/10.1016/j.jhydrol.2017.10.014

Quillet, A., Larocque, M., Pellerin, S., Cloutier, V., Ferlatte, M., Paniconi, C., et al. (2017). The Role of Hydrogeological Setting in Two Canadian Peatlands Investigated through 2D Steady-State Groundwater Flow Modelling. Hydrological Sci. J. 62 (15), 2541–2557. doi:10.1080/02626667.2017.1391387

R Core Team (2022). R: A language and environment for statistical computing. R Foundation for Statistical Computing, Vienna, Austria. URL https://www.R-project.org/.

Racasa, E. D., Lennartz, B., Toro, M., & Janssen, M. (2021). Submarine Groundwater Discharge From Non-Tidal Coastal Peatlands Along the Baltic Sea. *Frontiers in Earth Science*, *9*(July), 1–17. https://doi.org/10.3389/feart.2021.665802

Ramsar Convention Secretariat. (2014). *Wetlands: Why Should I Care?* https://www.ramsar.org/sites/default/files/documents/library/factsheet1_why_should_i_care_0.pdf

Rau, G. C., Post, V. E. A., Shanafield, M., Krekeler, T., Banks, E. W., & Blum, P. (2019). Error in hydraulic head and gradient time-series measurements: A quantitative appraisal. *Hydrology and Earth System Sciences*, *23*(9), 3603–3629. https://doi.org/10.5194/hess-23-3603-2019

Rezanezhad, F., Price, J. S., Quinton, W. L., Lennartz, B., Milojevic, T., & Van Cappellen, P. (2016). Structure of peat soils and implications for water storage, flow and solute transport: A review update for geochemists. *Chemical Geology*. https://doi.org/10.1016/j.chemgeo.2016.03.010

Richter, D. (1995). Ergebnisse methodischer Untersuchungen zur Kor- rektur des systematischen Messfehlers des Hellmann-Niederschlags- messers. – Berichte des Deutschen Wetterdienstes 194, Offenbach a.M.

Robinson, C. E., Xin, P., Santos, I. R., Charette, M. A., Li, L., & Barry, D. A. (2018). Groundwater dynamics in subterranean estuaries of coastal unconfined aquifers: Controls on submarine groundwater discharge and chemical inputs to the ocean. *Advances in Water Resources*, *115*(April 2017), 315–331. https://doi.org/10.1016/j.advwatres.2017.10.041

Robinson, C., Gibbes, B., & Li, L. (2006). Driving mechanisms for groundwater flow and salt transport in a subterranean estuary. *Geophysical Research Letters*, *33*(3), L03402. https://doi.org/10.1029/2005GL025247

Robinson, C., Li, L., & Barry, D. A. (2007). Effect of tidal forcing on a subterranean estuary. *Advances in Water Resources*, *30*(4), 851–865. https://doi.org/10.1016/j.advwatres.2006.07.006

Rosenberry, D. O., Duque, C., & Lee, D. R. (2020). History and evolution of seepage meters for quantifying flow between groundwater and surface water: Part 1 – Freshwater settings. *Earth-Science Reviews*, *204*(March), 103167. https://doi.org/10.1016/j.earscirev.2020.103167

Röper, T., Kröger, K. F., Meyer, H., Sültenfuss, J., Greskowiak, J., and Massmann, G. (2012). Groundwater Ages, Recharge Conditions and Hydrochemical Evolution of a Barrier Island Freshwater Lens (Spiekeroog, Northern Germany). J. Hydrol. 454-455, 173–186. doi:10.1016/j.jhydrol.2012.06.011

RStudio (2022). RStudio 2022.07.2 Build 576. https://www.rstudio.com.

Sadat-Noori, M., Santos, I. R., Sanders, C. J., Sanders, L. M., and Maher, D. T. (2015). Groundwater Discharge into an Estuary Using Spatially Distributed Radon Time Series and Radium Isotopes. J. Hydrol. 528, 703–719. doi:10.1016/j.jhydrol.2015.06.056

Sadat-Noori M, Glamore W. (2019). Porewater exchange drives trace metal, dissolved organic carbon and total dissolved nitrogen export from a temperate mangrove wetland. J Environ Manage. 248:109264. doi: 10.1016/j.jenvman.2019.109264.

Santos, I. R., Burnett, W. C., Chanton, J., Dimova, N., & Peterson, R. N. (2009a). Land or ocean?: Assessing the driving forces of submarine groundwater discharge at a

coastal site in the gulf of mexico. *Journal of Geophysical Research: Oceans*, *114*(4), 1–11. https://doi.org/10.1029/2008JC005038

Santos, I. R., Burnett, W. C., Chanton, J., Mwashote, B., Suryaputra, I. G. N. A., & Dittmar, T. (2008). Nutrient biogeochemistry in a Gulf of Mexico subterranean estuary and groundwater-derived fluxes to the coastal ocean. *Limnology and Oceanography*, *53*(2), 705–718. https://doi.org/10.4319/lo.2008.53.2.0705

Santos, I. R., Burnett, W. C., Dittmar, T., Suryaputra, I. G. N. A., & Chanton, J. (2009b). Tidal pumping drives nutrient and dissolved organic matter dynamics in a Gulf of Mexico subterranean estuary. *Geochimica et Cosmochimica Acta*, *73*(5), 1325–1339. https://doi.org/10.1016/j.gca.2008.11.029

Santos, I. R., Chen, X., Lecher, A. L., Sawyer, A. H., Moosdorf, N., Rodellas, V., Tamborski, J., Cho, H. M., Dimova, N., Sugimoto, R., Bonaglia, S., Li, H., Hajati, M. C., & Li, L. (2021). Submarine groundwater discharge impacts on coastal nutrient biogeochemistry. *Nature Reviews Earth and Environment*, *2*(5), 307–323. https://doi.org/10.1038/s43017-021-00152-0

Santos, I. R., Eyre, B. D., & Huettel, M. (2012). The driving forces of porewater and groundwater flow in permeable coastal sediments: A review. *Estuarine, Coastal and Shelf Science*, *98*, 1–15. https://doi.org/10.1016/j.ecss.2011.10.024

Schaap, M. G., Leij, F. J., & Van Genuchten, M. T. (2001). Rosetta: A computer program for estimating soil hydraulic parameters with hierarchical pedotransfer functions. *Journal of Hydrology*, *251*(3–4), 163–176. https://doi.org/10.1016/S0022-1694(01)00466-8

Schlüter, M., Sauter, E. J., Andersen, C. E., Dahlgaard, H., & Dando, P. R. (2004). Spatial distribution and budget for submarine groundwater discharge in Eckernförde Bay (Western Baltic Sea). *Limnology and Oceanography*, *49*(1), 157–167. https://doi.org/10.4319/lo.2004.49.1.0157

Schreiber, L., Munz, M., Salzmann, T., & Oswald, S. E. (2021). Coupled simulation of groundwater and drainage dynamics in a coastal fen. *Grundwasser*, *26*(3), 289–304. https://doi.org/10.1007/s00767-021-00486-y

Schuerch, M., Spencer, T., Temmerman, S., Kirwan, M. L., Wolff, C., Lincke, D., McOwen, C. J., Pickering, M. D., Reef, R., Vafeidis, A. T., Hinkel, J., Nicholls, R. J., & Brown, S. (2018). Future response of global coastal wetlands to sea-level rise. In *Nature*. https://doi.org/10.1038/s41586-018-0476-5

Schwieger, S., Kreyling, J., Couwenberg, J., Smiljanić, M., Weigel, R., Wilmking, M., & Blume-Werry, G. (2021). Wetter is Better: Rewetting of Minerotrophic Peatlands Increases Plant Production and Moves Them Towards Carbon Sinks in a Dry Year. *Ecosystems*, *24*(5), 1093–1109. https://doi.org/10.1007/s10021-020-00570-z

Selle, B., Graeff, T., Salzmann, T., Oswald, S. E., Walther, M., & Miegel, K. (2016). Investigation of a renatured fen catchment on the Baltic Sea coast of Mecklenburg - Part II: Salt dynamics and water balance. *Hydrologie Und Wasserbewirtschaftung*.

Šimůnek, J., M., van Genuchten, Th., & Šejna, M. (2018). *The HYDRUS Software Package for Simulating Two- and Three Dimensional Movement of Water, Heat, and Multiple Solutes in Variably- Saturated Porous Media, Technical Manual* (Version 3.). PC Progress.

Sinicrope, T. L., Hine, P. G., Warren, R. S.. Niering, W. A. (1990). Restoration of an impounded salt marsh in New England. Estuaries, 13, 25-30.

Slomp, C. P., & Van Cappellen, P. (2004). Nutrient inputs to the coastal ocean through submarine groundwater discharge : controls and potential impact. *Journal of Hydrology*, *295*, 64–86. https://doi.org/10.1016/j.jhydrol.2004.02.018

Smith, A. J., & Nield, S. P. (2003). Groundwater discharge from the superficial aquifer into Cockburn Sound Western Australia: Estimation by inshore water balance. *Biogeochemistry*, *66*(1–2), 125–144. https://doi.org/10.1023/B:BIOG.0000006152.27470.a9

Smith, V. H., Tilman, G. D., & Nekola, J. C. (1999). Eutrophication: Impacts of excess nutrient inputs on freshwater, marine, and terrestrial ecosystems. *Environmental Pollution*, *100*(1–3), 179–196. https://doi.org/10.1016/S0269-7491(99)00091-3

Sterr, H. (2008). Assessment of Vulnerability and Adaptation to Sea-Level Rise for the Coastal Zone of Germany. *Journal of Coastal Research*, *242*(242), 380–393. https://doi.org/10.2112/07a-0011.1

Stieglitz, T. (2005). Submarine Groundwater Discharge into the Near-Shore Zone of the Great Barrier Reef, Australia. Mar. Pollut. Bull. 51 (1–4), 51–59. doi:10.1016/j.marpolbul.2004.10.055

Sugimoto, R., Honda, H., Kobayashi, S., Takao, Y., Tahara, D., Tominaga, O., & Taniguchi, M. (2016). Seasonal Changes in Submarine Groundwater Discharge and Associated Nutrient Transport into a Tideless Semi-enclosed Embayment (Obama Bay, Japan). *Estuaries and Coasts*, *39*(1), 13–26. https://doi.org/10.1007/s12237-015-9986-7

Szymczycha, B., Kłostowska, Ż., Lengier, M., & Dzierzbicka-Głowacka, L. (2020). Significance of nutrient fluxes via submarine groundwater discharge in the Bay of Puck, southern Baltic Sea. *Oceanologia*, *62*(2), 117–125. https://doi.org/10.1016/j.oceano.2019.12.004

Szymczycha, B., Maciejewska, A., Winogradow, A., & Pempkowiak, J. (2014). Could submarine groundwater discharge be a significant carbon source to the southern Baltic Sea? *Oceanologia*, *56*(2), 327–347. https://doi.org/10.5697/oc.56-2.327

Szymczycha, B., Kroeger, K. D., and Pempkowiak, J. (2016a). Significance of Groundwater Discharge along the Coast of Poland as a Source of Dissolved Metals to the Southern Baltic Sea. Mar. Pollut. Bull. 109, 151–162. doi:10.1016/ j.marpolbul.2016.06.008

Szymczycha, B., & Pempkowiak, J. (2016b). *The Role of Submarine Groundwater Discharge as Material Source to the Baltic Sea*. https://doi.org/10.1007/978-3-319-25960-4

Szymczycha, B., Vogler, S., & Pempkowiak, J. (2012). Nutrient fluxes via submarine groundwater discharge to the Bay of Puck, southern Baltic Sea. *Science of the Total Environment*, *438*, 86–93. https://doi.org/10.1016/j.scitotenv.2012.08.058

Tait, D. R., Maher, D. T., Sanders, C. J., & Santos, I. R. (2017). Radium-derived porewater exchange and dissolved N and P fluxes in mangroves. *Geochimica et Cosmochimica Acta*, *200*, 295–309. https://doi.org/10.1016/j.gca.2016.12.024

Tamborski, J. J., Cochran, J. K., & Bokuniewicz, H. J. (2017). Submarine groundwater discharge driven nitrogen fluxes to Long Island Sound, NY: Terrestrial vs. marine sources. *Geochimica et Cosmochimica Acta*, *218*, 40–57. https://doi.org/10.1016/j.gca.2017.09.003

Taniguchi, M., Burnett, W. C., Christopher, F., Paulsen, R. J., Rourke, D. O., Steve, L., & Christoff, J. L. (2003). *Spatial and temporal distributions of submarine groundwater discharge rates obtained from various types of seepage meters at a site in the Northeastern Gulf of Mexico*. *Burnett 1999*, 35–53.

Taniguchi, M., Dulai, H., Burnett, K. M., Santos, I. R., Sugimoto, R., Stieglitz, T., Kim, G., Moosdorf, N., & Burnett, W. C. (2019). Submarine Groundwater Discharge: Updates on Its Measurement Techniques, Geophysical Drivers, Magnitudes, and Effects. *Frontiers in Environmental Science*, *7*(October), 1–26. https://doi.org/10.3389/fenvs.2019.00141

Tanneberger, F., Appulo, L., Ewert, S., Lakner, S., Ó Brolcháin, N., Peters, J., & Wichtmann, W. (2021). The Power of Nature-Based Solutions: How Peatlands Can Help Us to Achieve Key EU Sustainability Objectives. *Advanced Sustainable Systems*, *5*(1), 2000146. https://doi.org/10.1002/adsu.202000146

Tiemeyer, B., Pfaffner, N., Frank, S., Kaiser, K., & Fiedler, S. (2017). Pore water velocity and ionic strength effects on DOC release from peat-sand mixtures: Results from laboratory and field experiments. *Geoderma*, *296*, 86–97. https://doi.org/10.1016/j.geoderma.2017.02.024

Toro, M., Ptak, T., Massmann, G., Sültenfuß, J., & Janssen, M. (2022). Groundwater flow patterns in a coastal fen exposed to drainage, rewetting and interaction with the Baltic Sea. *Journal of Hydrology*, *615*(October), 128726. https://doi.org/10.1016/j.jhydrol.2022.128726

Trepel, M., Pfadenhauer, J., Zeitz, J., and Jeschke, L. (2017). Mires and Peatlands of Europe: Status, Distribution, and Conservation. Editors H. Joosten, F. Tanneberger, and A. Moen (Stuttgart, Germany: Schweizerbart Science Publishers)

Turner, R. E., & Lewis, R. R. (1996). Hydrologic restoration of coastal wetlands. *Wetlands Ecology and Management*. https://doi.org/10.1007/bf01876229

United Nations. (2018, September 10). *Secretary-General's remarks on Climate Change*.

United Nations. (2023). *Global Issues: Climate Change*. https://www.un.org/en/global-issues/climate-change

United Nations Climate Change. (2023). *The Paris Agreement*. https://unfccc.int/process-and-meetings/the-paris-agreement

von Ahn, C. M. E. (2023). Spatial and temporal variations in the isotope hydrobiogeochemistry of a managed river draining towards the southern Baltic Sea. *Geochemistry*, *125979*, 1–33.

von Ahn, C. M. E., Scholten, J. C., Malik, C., Feldens, P., Liu, B., Dellwig, O., Jenner, A.-K., Papenmeier, S., Schmiedinger, I., Zeller, M. A., & Böttcher, M. E. (2021). A Multi-Tracer Study of Fresh Water Sources for a Temperate Urbanized Coastal Bay (Southern Baltic Sea). *Frontiers in Environmental Science*, *9*(October), 1–20. https://doi.org/10.3389/fenvs.2021.642346

von Post, L., 1922. Sveriges Geologiska Undersöknings torvinventering och några av dess hittills vunna resultat. Sven. Mosskulturfören. Tidskr. 36, 1–27.

Vilumaa, K., Ratas, U., Tõnisson, H., Kont, A., and Pajula, R. (2017). Multidisciplinary Approach to Studying the Formation and Development of beach-ridge Systems on Non-tidal Uplifting Coasts in Estonia. Boreal Env. Res. 22, 67–81.

Virtasalo, J. J., Schröder, J. F., Luoma, S., Majaniemi, J., Mursu, J., and Scholten, J. (2019). Submarine Groundwater Discharge Site in the First Salpausselkä Ice-Marginal Formation, South Finland. Solid Earth. 10, 405–423. doi:10.5194/se- 10-405-2019

Wang, M., Liu, H., and Lennartz, B. (2021). Small-scale Spatial Variability of Hydro-Physical Properties of Natural and Degraded Peat Soils. Geoderma 399, 115123. doi:10.1016/j.geoderma.2021.115123

Wang, M., Liu, H., Zak, D., & Lennartz, B. (2020). Effect of anisotropy on solute transport in degraded fen peat soils Miaorun. *Hydrological Processes*, *34*, 2128–2138.

Waska, H., & Kim, G. (2011). Submarine groundwater discharge (SGD) as a main nutrient source for benthic and water-column primary production in a large intertidal environment of the Yellow Sea. *Journal of Sea Research*, *65*(1), 103–113. https://doi.org/10.1016/j.seares.2010.08.001

Wickham H, François R, Henry L, Müller K (2022). *dplyr: A Grammar of Data Manipulation*. https://dplyr.tidyverse.org, https://github.com/tidyverse/dplyr.

Wilson, A. M., T. B. Evans, W. S. Moore, C. A. Schutte, and S. B. Joye (2015), What time scales are important for monitoring tidally influenced submarine groundwater discharge? Insights from a salt marsh, Water Resour. Res., 51, 4198–4207, doi:10.1002/2014WR015984.

Wolski, T., & Wisniewski, B. (2020). *Geographical diversity in the occurrence of extreme sea levels on the coasts of the Baltic Sea*. *159*(May 2019). https://doi.org/10.1016/j.seares.2020.101890

Wolski, T., & Wisniewski, B. (2021). *Characteristics and Long-Term Variability of Occurrences of Storm Surges in the Baltic Sea*. https://doi.org/https://doi.org/ 10.3390/atmos12121679

Xin, P.,S.S.J. Wang, C. Robinson,L. Li, Y.-G.Wang, and D.A.Barry (2014), Memory of past randomwave conditions in submarine groundwater discharge, Geophys. Res. Lett., 41, 2401–2410, doi:10.1002/2014GL059617.

Younger, P.L. (2007). *Groundwater in the environment: An introduction*. Blackwell Publishing.

Zak, D., & Gelbrecht, J. (2007). The mobilisation of phosphorus, organic carbon and ammonium in the initial stage of fen rewetting (a case study from NE Germany). *Biogeochemistry*, *85*(2), 141–151. https://doi.org/10.1007/s10533-007-9122-2

Zauft, M., Fell, H., Glasser, F., Rosskopf, N., & Zeitz, J. (2010). Carbon storage in the peatlands of Mecklenburg-Western Pomerania , north-east Germany. *Mires and Peat*, *6*, 1–12. http://www.mires-and-peat.net/map06/map_06_04.pdf

Zhang, J., & Mandal, A. K. (2012). Linkages between submarine groundwater systems and the environment. In *Current Opinion in Environmental Sustainability*. https://doi.org/10.1016/j.cosust.2012.03.006

Curriculum Vitae of Erwin Don R. Racasa

Personal Information	
Birth	7 April 1989 in Lucban, Quezon, Philippines
Contact Details	erwin.racasa@uni-rostock.de; racasaerwin@gmail.com
Current Address	Platz der Freundschaft 1, 18059, Rostock, Germany
ResearchGate Profile	https://www.researchgate.net/profile/Erwin-Don-Racasa
Education	
02.2019 – present	**Ph.D. Candidate;** University of Rostock, Faculty of Agricultural and Environmental Sciences, Soil Physics *Dissertation: Groundwater quality and submarine groundwater discharge from rewetted coastal fen peatlands*
2015	**M.Sc. Environmental Science;** University of the Philippines–Diliman, College of Science, Institute of Environmental Science and Meteorology Thesis: *Submarine Groundwater Discharge and Its Associated Nutrient Fluxes in Harmful Algal Blooms-Prone Sorsogon Bay, Philippines*
2009	**B.Sc. Chemistry;** University of the Philippines–Diliman, College of Science, Institute of Chemistry Thesis: *Fabrication and Testing of a CO_2 Gas Sensing Probe Based on a Combination pH Electrode*
Research Experience	
02.2019 – present	**Wissenschaftlicher Mitarbeiter;** University of Rostock, Faculty of Agricultural and Environmental Sciences, Soil Physics Project: Baltic TRANSCOAST Program Key Tasks: Determination of water and material fluxes via submarine groundwater discharge from coastal peatlands using HYDRUS-2D numerical modeling and field methods
07.2017 – 02.2019	**Science Research Specialist II;** Mines and Geosciences Bureau, Department of Environment and Natural Resources (Philippines) Key Tasks: Determination of water quality (physico-chemical properties and trace metals) of groundwater, surface waters, and sediments
04.2016 – 06.2017	**Senior Science Research Specialist;** National Research Council of the Philippines, Department of Science and Technology Key Tasks: Writing of policy briefs from completed scientific researches for local government units, policy makers, and other stakeholders

07.2012 –03.2016 **Senior Research Assistant;** Geological Oceanography Laboratory, Marine Science Institute, University of the Philippines – Diliman

Key Tasks: water quality analysis of Laguna de Bay, Philippines water quality analysis of submarine groundwater discharge and rivers on Sorsogon Bay, Philippines; collection of sediments from rivers and coastal areas of Manila Bay for the establishment of the first sediment quality standards in the Philippines

Publications

Racasa, EDR., Lennartz, B., Toro, M., Janssen, M., 2021. Submarine groundwater discharge from non-tidal coastal peatlands along the Baltic Sea. Frontiers in Earth Science. https://doi.org/10.3389/feart.2021.665802

Gutekunst, CN, Liebner, S., Jenner, AK., Knorr, KH., Unger, V. Koebsch, F., **Racasa, EDR.**, et al., 2022. Effects of brackish inflow on methane-cycling microbial communities in a freshwater rewetted coastal fen. Biogeosciences. 19:3625–3648. https://doi.org/10.5194/bg-19-3625-2022

Racasa, EDR., Lloren, R., Manglicmot, M., Jago-on, KAB., Balangue, MIRD., Taniguchi, M., Siringan, FP. 2018. Lacustrine groundwater discharge in Southern Laguna de Bay, Philippines. In: Endo, A. & Oh, T. The Water-Energy-Food Nexus. Global Environmental Studies. Springer, Singapore. https://doi.org/10.1007/978-981-10-7383-0_7

Siringan, FP., **Racasa, EDR.***, David, CPC., Saban, RC. 2018. Increase in dissolved silica of rivers due to a volcanic eruption in an estuarine bay (Sorsogon Bay, Philippines). Estuaries and Coasts. 41(8):2277-2288. https://doi.org/10.1007/s12237-018-0428-1

Publication in review

Gutekunst, CN., Liebner, S., Jenner, A-K., **Racasa, EDR.**, et al., ***in review***. Brackish water rewetting of a temperate coastal peatland: Effects on biogeochemistry, microorganisms and greenhouse gas emissions. Science of the Total Environment.

Publications in preparation

Racasa, EDR., Kienzler, J., Lennartz, B., Janssen, M. et al. ***in preparation***. Seasonal dynamics of submarine groundwater discharge from a rewetted coastal peatland.

Racasa, EDR., Liu, H., Janssen, M. ***in preparation***. Groundwater quality in two coastal fens and the influence of storm surge flooding and rewetting with seawater.

Policy Briefs written for the National Research Council of the Philippines

A pollutant on the rise: Its implications to fisheries in Laguna de Bay. Michelle Paraso and ***Erwin Don Racasa***. NRCP Policy Brief Series. Issue 1, Q4, 2016.

Fish parasites detect heavy metal pollution in lakes. Vachel Gay Paller, Michelle Paraso, ***Erwin Don Racasa***. NRCP Policy Brief Series. Issue 2, Q4, 2016.

Scholarships/ Grants

- Conference Grant Awardee:
  - 3rd PICES/ ICES Early Career Scientist Conference. Busan, Korea. 2016

- 16th International Conference on Harmful Algae. Wellington, New Zealand. 2016
- 11th Annual Meeting of Asia Oceania Geosciences Society. Sapporo, Japan. 2014

- Philippine Department of Science and Technology Scholarship Awardee – M.Sc. Environmental Science, 2010–2012
- Chevron Geothermal and Dr. Tengonciang Scholarship Awardee – B.Sc. Chemistry, 2007–2009

Declaration of Authorship

I hereby declare that I have written the submitted dissertation independently and that I did not use any other sources or aids other than those indicated and cited properly. Moreover, I declare that the figures presented are prepared by myself or are clearly cited otherwise.

Rostock, 15.09.2023

Erwin Don R. Racasa